A NEW MULTI-CURVE INTERACTION METHOD FOR THE PLASTIC ANALYSIS AND DESIGN OF UNBRACED AND PARTIALLY-BRACED FRAMES

H E SCHOLZ

A NEW MULTI-CURVE INTERACTION METHOD FOR THE PLASTIC ANALYSIS AND DESIGN OF UNBRACED AND PARTIALLY-BRACED FRAMES

Hans Erich Scholz

A Thesis Submitted to the Faculty of Engineering
University of the Witwatersrand, Johannesburg
for the Degree of Doctor of Philosophy

Johannesburg 1981

A B S T R A C T

A NEW MULTI-CURVE INTERACTION METHOD FOR THE PLASTIC ANALYSIS AND DESIGN OF UNBRACED AND PARTIALLY-BRACED FRAMES

SCHULZ, Hans Erich, Ph.D. University of the Witwatersrand, Johannesburg, 1981

This thesis describes the development of an alternative approximate technique for the elasto-plastic analysis of unbraced and partially-braced rigid frames.

The proposed technique, which allows for the treatment of simple portal frames as well as for multi-storey and multi-bay structures, is not confined to steel to which it has been applied in this research but could also be developed for other materials such as reinforced concrete.

In essence, the method represents a refinement and extension of the Merchant-Rankine interaction formula. The proposed concept makes use of a multi-curve interaction principle placing the failure load of the actual frame between its plastic collapse load on the one hand and a load related to the elastic buckling load on the other hand. The failure curves in the inelastic range are empirical. The plastic collapse load is obtained using the standard first-order approach. The required elastic parameters are evaluated from an elastic buckling analysis and a second-order elastic

load analysis, both performed on suitable subassemblages for the general frame. The mathematical derivations are based on the slope-deflection equations including stability functions.

For the elastic analyses a purpose-made computer program has been developed. This program makes allowance for transverse column loads, patterned beam loadings and the special case of sway buckling including bending, termed "Symmetry-Buckling".

In this thesis the proposed method has been applied to the structure as a whole. In this case the plastic collapse load of the entire frame is determined, whereas the corresponding elastic parameters are evaluated from as many subassemblages as are contained in the structure. The combination of plastic collapse load and elastic parameters which gives the lowest failure load is significant.

It is also possible to calculate failure loads for individual sections of a framework. The plastic collapse load and the salient elastic parameters would then both be examined on matching subassemblages.

Furthermore, it has been demonstrated that a graphical presentation of the elastic results is possible, thus allowing a "manual" evaluation of the failure load, i.e. without the need of a computer, once the plastic collapse load is known. The derivation of the plastic collapse load is not included in the scope of this thesis.

In addition, an approximate analytical procedure, using established computer methods, has been formulated for the calculation of the elastic values.

A number of frames have been evaluated by the proposed method and the results have been compared both, to the Merchant-Rankine solutions and to mathematical solutions obtained using an elasto-plastic, computer analysis. The accuracy of the new method has also been tested against published laboratory results of other researchers. In addition, ten small-scale model frames were analysed and tested for this research to confirm the validity of the empirically evolved interaction curves.

It has been concluded that the proposed method is in good agreement with test results and discrete mathematical solutions, and thus represents a satisfactory substitute for the more complex approaches, without the loss in accuracy and the restriction in usage which applies to the Merchant-Rankine formula.

Some other related aspects such as the application of the proposed method to other materials and structures, deflections at the working load level, in-plane member instability, lateral torsional buckling and additional $P - \Delta$ effects have been identified as areas recommended for future research.

ACKNOWLEDGEMENT

I would like to express my gratitude to Professor A R Kemp who has been my supervisor during the course of this research. Without his guidance, support and constructive criticism this thesis may not have been completed.

My thanks are also due to Professors G E Blight and A R Kemp for initiating the financial support received from the Council's Faculty of Engineering Research Grant of the University of the Witwatersrand. For the financial assistance of the Council, during the latter part of the thesis, I wish to express my sincere appreciation.

I wish to extend my thanks to Dr D Anderson and Dr D Nethercot for their invaluable comments on the chosen topic of research and to Mr A G A Hofmeyr for his beneficial suggestions after reading through the manuscript.

I am also indebted to the Department of Civil Engineering and the Computer Centre of the University of the Witwatersrand for allowing me the use of their laboratory and computer facilities respectively.

Finally, I wish to record my sincerest gratitude to my wife, who typed the manuscript, for her patience, understanding and unfailing support during the course of the research programme.

DECLARATION

I declare that this thesis is my own, unaided work. It is being submitted for the degree of Doctor of Philosophy in the University of the Witwatersrand, Johannesburg. It has not been submitted before for any degree or examination in any other University, nor has it been prepared under the aegis or with the assistance of any other body or organisation or person outside the University of the Witwatersrand, Johannesburg.

TABLE OF CONTENTS

LIST OF ILLUSTRATIONS

LIST OF TABLES

LIST OF MAJOR SYMBOLS

A	= area of section
a_i, b_i, c_i	= load and force ratios for differential equation method in Appendix IV/1
ad M	= additional moment defined in Equations 38, 64a-d, 65a-e,
$\bar{B}, \bar{B}_1, \bar{C}$	= stiffness matrices
$\bar{B}_{ij}$	= elements of stiffness matrix $\bar{B}$
BM1...BM6	= designation of test beams
b	= width of section
$\bar{C}_{ij}$	= elements of stiffness matrix $\bar{C}$
C_i	= constant of integration
C,N,O,S	= stability functions
D, D_1	= displacement vectors
DET $\bar{B}$, DET $\bar{C}$	= symbol for determinants of stiffness matrices $\bar{B}$ and $\bar{C}$
d	= depth of section
E	= modulus of elasticity
$F, \bar{F}$	= parameters for linear elastic rotational restraint
F_7, $\bar{F}_7$	= lateral bracing restraint
f_{max}	= stress at extreme fibre of section
f_Y	= specified yield stress
f_{PC}, f_{PB}	= effective stress at onset of yield for column and beam
H	= ultimate horizontal load or lateral storey shear

h	= storey height or height of structure
h_ℓ	= height of storey for "limiting frame"
I	= second moment of area (moment of inertia)
i	= storey number parameter
i_O	= parameter in straight-line Equation 11
K	= I/L = member stiffness
$\bar{K}_S$	= non-dimensional base stiffness
L	= length of member
L_ℓ	= length of beam for "limiting frame"
L_V	= load vector
M	= bending moment
M_i	= ultimate applied joint moment
M_ℓ	= bending moment of "limiting frame"
M_m	= member-end moment
M_P	= plastic moment capacity of section
M_{PC}	= plastic moment capacity of section reduced by effect of axial forces
M_Y	= yield moment of section
M1...M5	= designation of test frames (double-storey frames)
M_f	= fixed-end moment
mag M	= magnified moment defined in Equation 48
m	= parameter associated with axial member forces defined in Equation 15c
m_O	= $L\sqrt{P_O/EI}$ = buckling load parameter
n	= $(I_C/I_B)(L/h)$ = stiffness ratio of column to beam
n_i	= load ratios relating other loads to P_O or Q
P	= axial force

P1...P5	= designation of test frames (single-storey frames)
P_F	= failure load
P_E	= Euler load of column
P_e	= elastic buckling load of column
P_{cr}	= ultimate axial column load in the absence of moment
P_P	= plastic collapse load of frame
P_{PC}	= ditto, accounting for the effects of axial forces
P_O	= elastic buckling load of frame
$P_{O\ell}$	= elastic buckling load of "limiting frame"
$P_{P\ell}$	= plastic collapse load of "limiting frame"
$(P_O/P_P)_\ell$	= ratio of elastic buckling load to plastic collapse load for "limiting frame"
P_Y	= yield load of member
Q	= total ultimate load applied between joints 2 and 3
q	= uniformly distributed ultimate load intensity
r	= radius of gyration
R_5,R_6	= reactions at joints 5 and 6
S_S	= spring stiffness of lateral restraint defined in section 4.1.7
S_P	= stiffness matrix for axial forces
SC,NO	= stiffness abbreviations defined in Appendix II/1
U,U_1,U_2,U_3	= ultimate dual-point load
V	= shear force
W	= working load
x_1,x_2,x_3	= co-ordinates of distance
y	= distance from centroid of section to extreme fibre

$\sigma_1, \sigma_2, \sigma_3$ [illegible]

E_s [illegible]

Z_p plastic section modulus

F_i [illegible] quantities defined [illegible] equation 18

y_1, y_2, y_3 = member deflection

Z_P = plastic section modulus

Z_Y = elastic section modulus

z_i = moment magnifier defined for Equation 48

α	= reduction factor defined in Equation 39
α_i	= stiffness coefficients for infinitesimally displaced frame, Appendix III
β, β_1, β'	= sway correlation factors defined in Equations 25a, 25b and 25c
β_2, β_3	= rotation correlation factors
γ_f	= load factor
γ_P	= load factor relating to plastic collapse load P_P
γ_O	= load factor relating to elastic buckling load P_O
γ_m	= safety factor for material
γ_A, γ_B	= end rotation of simply supported member A-B
Δ	= sway
$\delta M, \delta M_F, \delta V, \delta S, \delta C, \delta P, \delta D$	= incremental form of equivalent basic parameters M, M_F, V, S, C, P, D
$\delta\Delta$	= incremental sway
$\delta\Theta$	= incremental rotation
ε_i	= moment parameters defined in Appendix IV/2
η, ξ	= non-dimensional length coefficients
Θ	= member-end or joint rotation
κ_1	= shape factor
κ_2	= ratio d/r
λ	= slenderness ratio of actual member
λ_ℓ	= slenderness ratio of member in "limiting frame"
$\lambda_{HO,4}$	= slenderness ratio of member if frame is subjected to non-symmetry loading related to 0,4 P_O
μ_{ij}	= Kani distribution factor defined in Appendix IV/2
ν	= non-dimensional shear distribution coefficient

Σ = symbol for summation

ϕ $\sim \Delta/L$ = sway index of storey

ϕ_L $\sim \Delta_L/L_L$ = sway index of lower storey

ϕ_U $\sim \Delta_U/L_U$ = sway index of upper storey

Ω = angle describing slope P_O/P_P of actual frame

Ω_ℓ = angle describing slope $(P_O/P_P)_\ell$ of "limiting frame"

CHAPTER 1

INTRODUCTION

1.1 General

Plastic design of unbraced frames is complicated by the need to make adequate allowance for the loss in load carrying capacity induced by in-plane instability effects of which the P-Δ moments are the most prominent. Initially, in section 1.1 of this chapter, an overview is provided of existing P-Δ approaches, a detailed literature survey of the various methods will follow in sections 1.3 and 1.6.

In general, past research has attempted to solve the problem of instability in three ways, namely

a) By using rigorous analysis techniques taking the exact moment-curvature characteristic into account.

b) By using an elasto-plastic iteration procedure on the frame as a whole or on suitable subassemblages.

c) By using interaction formulae applied to the entire framework.

Exact rigorous methods of analysis have so far only been applied to simple structures or to individual beam-columns. Some relevant research is mentioned in section 1.3.2 of this study.

Elasto-plastic analysis procedures, for which various computer programs have been developed, are most suitable fo: the investigation of larger frameworks. A detailed literature survey of elasto-plastic methods follows in sec 1 1.3.2.

Approximate subassemblage approaches, which use the true moment-curvature relationship of the column members, have been introduced to facilitate the plastic analysis of multi-storey structures. Similar techniques have been developed on an idealised elasto-plastic basis. Reference literature related to representative subassemblage methods is presented in section 1.3.3 of this introductory chapter. Although the subassemblage techniques may be regarded as "manual" methods, incorporating a semi-graphical approach, they appear cumbersome. They usually involve plotting the load-deflection or load-stiffness history for each column and its restraining beams. Thereby, all possible hinge permutations of the particular subassemblage have to be considered. This procedure has to be extended over the entire storey for each storey of the framework.

On the other hand, interaction formulae predicting the approximate failure load of unbraced frames are simple in their application when compared to other methods of analysis. The two most important developments in this field have been the Merchant-Rankine formula[1,2] and its modification by Wood[3] and the design rule based on research by Lu[4]. The modified Merchant-Rankine formula has been proposed by the European Convention for Constructional Steelwork[5,6] (ECCS) and is intended for inclusion in the new British Steel Design Code, B20[7]. However, the Merchant-Rankine formula and Lu's design rule, although extremely useful in practical design, have a number of shortcomings. A detailed discussion of the interaction methods is presented in section 1.6 of this chapter.

1.2 Present design code requirements and provisions for the plastic design of unbraced frames

Plastic analysis and design of unbraced frames, as covered by design specifications, has been regulated by the following three provisions:

a) A number of current design codes[8-10], recommendations for steel construction[5] and draft specifications[7] all call for a second-order, elasto-plastic analysis for the general unbraced multi-storey framework in order to account for the P-Δ effects.

b) At the same time, most major codes[5,7-9] make allowances to dispense with this overall stability check provided certain requirements are met.

c) The ECCS Recommendations[5] and the British Draft Code B20[7] contain an approximate second-order technique based on the Merchant-Rankine principle which may be followed in cases where the structural parameters satisfy certain specific conditions.

In the subsequent sections of this chapter the above provisions will be examined in some more detail, making reference to the various analysis techniques. Special emphasis will be placed on the evaluation of the interaction methods, since this research project falls into this category.

In addition, in order to formulate the objectives of this research, it was necessary to analyse briefly the P-Δ provisions of the "stress-controlled" design approaches. In this context, a great deal of criticism has been voiced in connection with the use of the traditional moment-magnification concept incorporated in various design codes[1-10]. A number of deficiencies have been discussed in the literature, the most important of which will be presented in section 1.7 of this study. The plastic and elastic analyses are also closely interrelated by certain design requirements. Firstly, a plastically designed structure has to perform adequately at working loads. Secondly, in order to control the sway deflections of unbraced frames, the stiffness of structures is often modified to such a degree that plastic analysis and the P-Δ provisions become irrelevant as the principal criteria. In fact, sway limitations are used to justify the omission of the overall-stability check[5,7].

1.3 Rigorous and second-order, elasto-plastic analysis methods

1.3.1 General

These methods predict the failure load of a frame by using loss of stiffness as the failure criterion. Rigorous and second-order, elasto-plastic analysis techniques may be subdivided into full-frame approaches and subassemblage methods.

1.3.2 Full-frame methods

Full-frame analyses, using the exact moment-curvature relationships of all members, are rare and have only been performed for limited structures. In the solutions by Oxfort[11,12] a single beam and column arrangement with rectangular member sections was considered. Chu & Pabacius[13], Moses[14], Yura & Galambos[15] and Adams[16] investigated simple portal frames with pinned bases and flanged members and included the effects of residual stresses. The demands on the computer are formidable and the compilation of the enormous amount of data becomes a time-consuming task.

More commonly, designers resort to the so-called second-order, elasto-plastic methods of analysis, which assume that plastic hinges form at discrete points whereas other portions of the members remain elastic. A second-order analysis is performed at loads between the formation of consecutive hinges. A detailed survey on computer based methods for plastic analysis and design was published by Grierson[17]. Massonet[18], writing about the ECCS Recommendations, referred to the minimum-weight computer programs by Horne & Morris[19] and Emkin & Litle[20,21] which consider strength and sway requirements at the same time in a step by step procedure.

A frame collapse method using the tangent stiffness was proposed by Tranberg et al[22]. This method can also include strain-hardening.

The benefits of strain-hardening were first examined by Horne[23,24], who suggested that for many structures strain-hardening will be sufficient to overcome the tendency for the carrying capacity to be reduced by frame instability. For this purpose, Horne proposed a concept termed rigid-plastic-rigid theory. This theory was examined by Medland [25,26], who conducted experiments on pitched-roof portal frames which to some extent confirmed the rigid-plastic-rigid theory for particular frames. Davies[27] discovered additional limitations of the rigid-plastic-rigid theory associated with mode changes due to frame instability. He concluded that, because of frame instability, plastic theory must lose a good deal of its basic simplicity when applied to tall slender structures.

Parikh[28] considered axial deformations and residual stresses, Davies[29] included for hinge reversal effects and Korn & Galambos[30] allowed for the reduction in plastic moment capacity due to the presence of axial loads. For symmetrical frames subjected to symmetrical vertical dations, referred to the minimum-weight computer programs by Horne & Morris[19] and Emkin & Litle[20,21] which consider strength and sway requirements at the same time in a step by step procedure.

A frame collapse method using the tangent stiffness was proposed by Tranberg et al[22]. This method can also include strain-hardening.

The benefits of strain-hardening were first examined by Horne[23,24], who suggested that for many structures strain-hardening will be sufficient to overcome the tendency for the carrying capacity to be reduced by frame instability. For this purpose, Horne proposed a concept termed rigid-plastic-rigid theory. This theory was examined by Medland [25,26], who conducted experiments on pitched-roof portal frames which to some extent confirmed the rigid-plastic-rigid theory for particular frames. Davies[27] discovered additional limitations of the rigid-plastic-rigid theory associated with mode changes due to frame instability. He concluded that, because of frame instability, plastic theory must lose a good deal of its basic simplicity when applied to tall slender structures.

Parikh[28] considered axial deformations and residual stresses, Davies[29] included for hinge reversal effects and Korn & Galambos[30] allowed for the reduction in plastic moment capacity due to the presence of axial loads. For symmetrical frames subjected to symmetrical vertical loading, McNamee & Lu[31] published a solution known as the limit-load technique or small-lateral-load approach. Wood[32] developed the concept of the deteriorated critical load. Other elasto-plastic computer methods were published by Driscoll et al[33], Majid[34], Jennings & Majid[35], Majid & Anderson[36], Cheong Siat Moy[37] and Cohn & Franchi[38]. A "manual" preliminary design method based on the equilibrium concept was put forward by Driscoll et al[39].

1.3.3 Subassemblage methods

Subassemblage techniques were developed in an attempt to undertake a second-order, elasto-plastic analysis of multistorey structures without the aid of computers. Solutions described by Chu & Pabacius[13], Lu[4], Moses[14] and Ojalvo & Lu[40] seem to be more appropriate to single-storey frames.

Two representative methods suitable for a general frame are:

a) The subassemblage technique suggested by Daniels & Lu[41] based on the research by Levi et al[42] for combined loading.

b) The storey-stiffness concept by Cheong Siat Moy[43,44] applied to plastic analysis, for vertical and combined loading.

Both methods consider a subassemblage consisting of a column and its restraining beams. At the formation of plastic hinges, either in the column or in the beams, reductions in the restraining functions are introduced.

In the method by Daniels [illegible] a shear-displacement curve is constructed for the entire storey. For a specified applied column load and column slenderness and for a given beam restraining function, the moment at the top of the column is determined. From the corresponding rotation, the compatible sway-displacement is computed, which in turn is related to the shear force. The maximum acceptable horizontal shear for a given vertical load corresponds to the apex of the resulting combined displacement curve constructed for the entire storey.

In the method by Cheong Siat Moy [illegible] instability failure is interpreted as the occurrence of zero or negative storey stiffness. When horizontal loading is involved an incremental load analysis is required relating the storey stiffness, the change in sway and the variation in the beam and column moments to the load increment. The moment changes are added successively to give the total moment acting on the beam and on the columns. When plastic hinges occur the storey stiffness is reduced accordingly. In this way a load-storey stiffness curve is obtained.

Cheong Siat Moy has pointed out that five possible types of failure mechanisms may apply for each individual subassemblage. Hence, despite the fact that both subassemblage approaches can be performed "manually", it appears that they are cumbersome. It must be expected that a number of different hinge locations will have to be investigated, that moment calculations for beams and columns are required

In the method by Daniels & Lu[41] a shear-displacement curve is constructed for the entire storey. For a specified applied column load and column slenderness and for a given beam restraining function, the moment at the top of the column is determined. From the corresponding rotation, the compatible sway-displacement is computed, which in turn is related to the shear force. The maximum acceptable horizontal shear for a given vertical load corresponds to the apex of the resulting combined displacement curve constructed for the entire storey.

In the method by Cheong Siat Moy[43,44] instability failure is interpreted as the occurrence of zero or negative storey stiffness. When horizontal loading is involved an incremental load analysis is required relating the storey stiffness, the change in sway and the variation in the beam and column moments to the load increment. The moment changes are added successively to give the total moment acting on the beam and on the columns. When plastic hinges occur the storey stiffness is reduced accordingly. In this way a load-storey stiffness curve is obtained.

Cheong Siat Moy has pointed out that five possible types of failure mechanisms may apply for each individual subassemblage. Hence, despite the fact that both subassemblage approaches can be performed "manually", it appears that they are cumbersome. It must be expected that a number of different hinge locations will have to be investigated, that moment calculations for beams and columns are required for load increments, and that a shear-displacement or load-stiffness path has to be constructed for each sub-assemblage and storey. The lowest load factor for any one storey is adopted as the overall failure load factor of the frame. It must be recognised that this procedure can only result in an approximate failure load for the general structure, since effectively no parameter is used which is representative of the frame as a whole.

1.4 Omission of stability check in plastic design

The purpose of a second-order, elasto-plastic analysis is to account adequately for the in-plane instability effects. The P-Δ moments of unbraced frames have been identified as the most important contributory factor to reduce the overall strength and to change the failure mode from plastic collapse to inelastic instability. The need to consider the P-Δ effect in the design of steel frames has generally been acknowledged[45,46]. This is even more relevant in the case of plastic design because sway displacements will increase rapidly once inelastic action has commenced. Since any second-order, elasto-plastic analysis is time-consuming and laborious, the designer would be interested to know whether such an analysis is required in the first place.

Parameters have therefore been extracted from research which categorise the class of frames for which the P-Δ effect is small enough to be ignored. These parameters have been described in the design codes and indicate to the designer which frames can be proportioned by a first-order analysis, without the risk of failure below the desired load level.

1.4.1 Low-rise buildings

The ECCS Recommendations[5] and the British Draft Code B20[7] give simple safeguards in terms of stiffness and sway limits for single-storey frames and pitched-roof portals. If these limits are satisfied, stability is guaranteed.

The American Design Specifications[8] , AISC November 1978, do not require a stability check for single or double-storey frames with rigid joints.

The Australian Standard, AS 1250-1975[9] , has based its recommendations on the research by Lu[4] and dispenses with stability checks for frames not exceeding three storeys, provided the ratio of elastic-buckling load to plastic-collapse load is at least equal to 3,0.

1.4.2 High-rise buildings

On the basis of Wood's modification of the original Merchant-Rankine rule, the full plastic-collapse load may be realised, when the ratio of elastic-buckling load to plastic-collapse load exceeds a value of 10. This is justified by strain-hardening and sundry composite action in buildings. If composite action is included in explicit ways, the ratio should be taken as 20. Wood's proposals were incorporated in the

ECCS Recommendations and the British Draft Code B20.

1.5 Provisions for cladding

It is of interest to note that Massonnet[46] queried the omission of stability effects for low-rise buildings without further safeguards, and the lack of provisions in other codes[8,9] for cladding or bracing effects. These aspects have been covered to some extent in the ECCS Recommendations.

Considerable research has been undertaken to establish the interaction behaviour between steel frames and their cladding[47-54]. A more rational approach to account for this beneficial influence was suggested by Wood[3] and Wood & Roberts[55]. They recommended that this effect should be incorporated by an equivalent elastic restraint at the beam levels. This reduces the sway of the structure and enhances the elastic buckling load of the system. Goldberg[56] demonstrated that out-of-plane horizontal bracing can fulfil a similar function.

1.6 The interaction methods

Two interaction methods are mentioned in recent design specifications as an approximation to the second-order, elasto-plastic failure load of unbraced frames. Firstly, the Merchant-Rankine formula[1,2] and its modification by Wood[3] and, secondly, the design rule based on the research by Lu[4]. However, both approaches are severely restricted in their application in the codes. Furthermore, results obtained by the Merchant-Rankine formula are generally considered as too conservative.

1.6.1 The Merchant-Rankine method[1,2] and Wood's modification[3]

In this interaction method the failure load of the frame, P_F, is obtained using the value of the plastic collapse load P_P and the elastic buckling load P_O.

Wood has slightly modified the original Merchant-Rankine formula to account for a minimum amount of strain-hardening and restraining action due to composite behaviour. This modification would not be applicable when comparisons are being made with bare frame solutions and when strain-hardening is neglected.

The interaction curves proposed by Merchant-Rankine and Wood are illustrated in Figure 1, which also shows the results of theoretical studies on single-storey and two-storey frames by Salem[57]. In Figure 2 these curves are compared with the theoretical solutions by Salem[57] and Moses[14] and the experimental results by Low[13]. A further comparison is contained in Massonnet's paper[16] on the ECCS Recommendations.

The ECCS Recommendations and the British Draft Code B20 have limited the use of Wood's modified version of the Merchant-Rankine method to ratios of $P_P/P_O \leq 0,25$. This boundary is also marked on both figures.

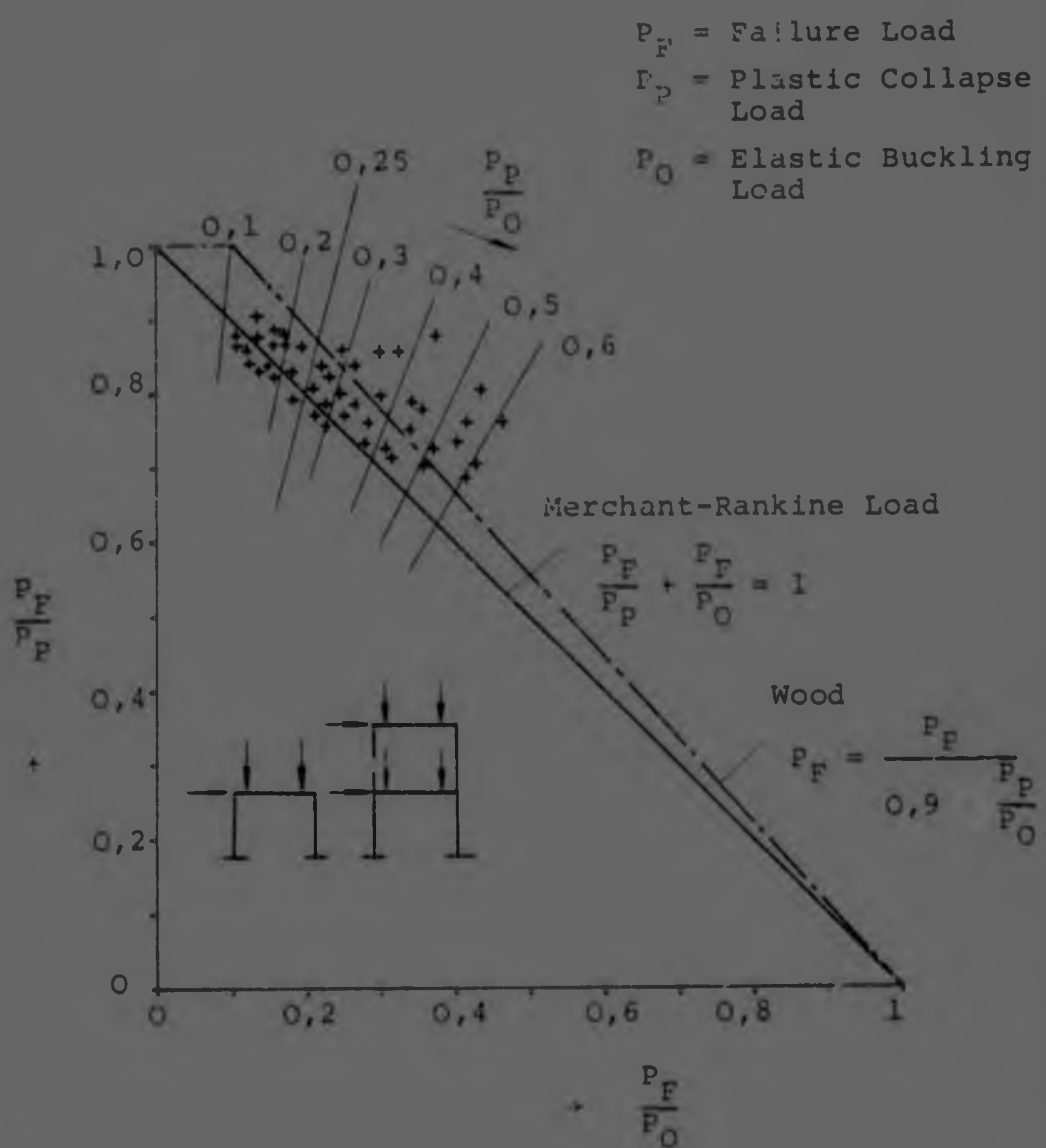

FIGURE 1: The Merchant-Rankine load and Wood's proposal compared with theoretically obtained failure loads

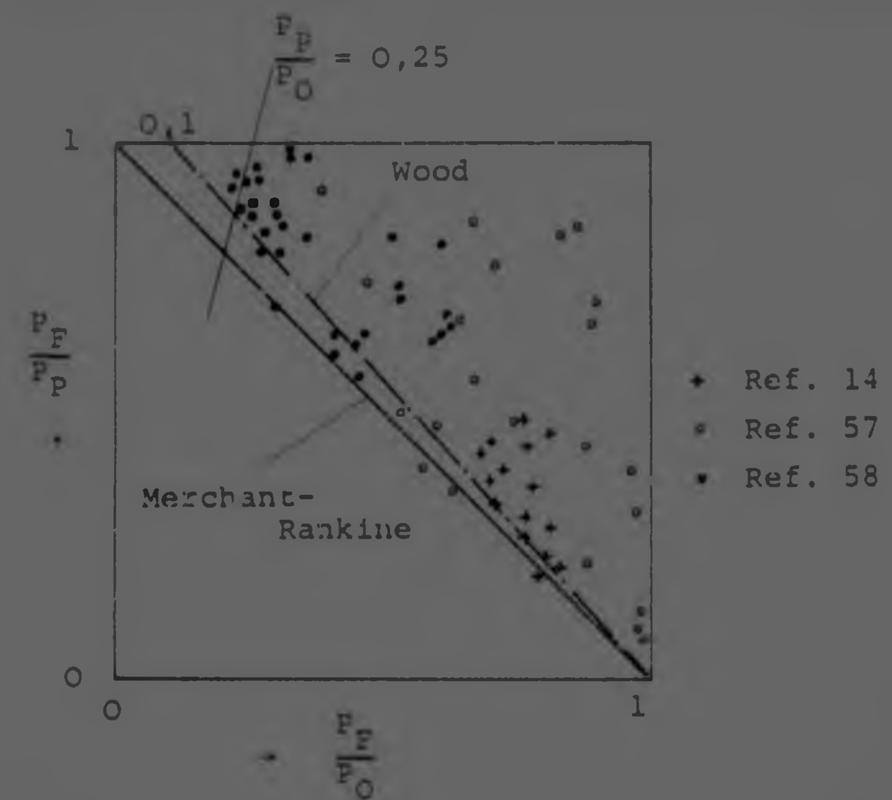

FIGURE 2: The Merchant-Rankine formula and Wood's modification compared with tests and theoretical results

The reservations which exist in regard to the use of the Merchant-Rankine formula are apparent from these comparisons. It is clear that the results are generally too conservative, thereby requiring unnecessary strengthening of members. In addition, the representation of frames subjected to a multitude of different load arrangements can hardly be justified by a mere combination of the plastic collapse load and the elastic buckling load. Moreover, the implication that a frame at the elastic buckling load level, when $P_F/P_O = 1$, has a zero failure load ratio in terms of its corresponding plastic collapse load ($P_F/P_P = 0$) can at best lead to a lower-bound solution.

Because of its increasing inadequacy in the case of more slender and flexible frameworks, the use of the Rankine-based approximations have been limited to frames for which P_P/P_O does not exceed a value of 0,25. Frame solutions falling above this ratio of 0,25 should be analysed by more exact second-order procedures.

A more refined formulation of the Merchant-Rankine method was suggested by Ligtenberg[illegible]. He proposed to use the buckling load of the structure after the formation of all plastic hinges but one, in place of the elastic buckling load. However, the evaluation of this condition is in itself a tedious task and not easily identified for a frame of practical importance.

The research project described in this thesis attempts to eliminate some of the shortcomings of the Merchant-Rankine methods without increasing the complexity of the procedure unduly. The study will in particular focus on an improved representation of the frame behaviour in the region where the failure load approaches the elastic buckling load, i.e. at high values of the ratios P_F/P_O and P_P/P_O. To achieve this, the nature of the applied loading has to be observed and not just the elastic buckling load as in the case of the Merchant-Rankine methods.

1.6.2 Lu's design approximation

Lu has evolved an approximate second-order, elasto-plastic design rule from a rigorous full-scale analysis of a symmetrical portal frame with pinned bases and subjected to symmetrical vertical loading. He subsequently suggested that these results were also suitable for double-storey and three-storey frames.

Lu's design graph is depicted in Figure 3 which also shows the results of some theoretical calculations and model frame tests for simple portal frames. Results for the failure load P_F are obtained from the elastic buckling load P_O and the ultimate load P_U. The term P_U is not the plastic collapse load P_P used in the Merchant-Rankine formula. P_U is defined as the ultimate load of the frame, determined by assuming that the frame is prevented from swaying, and that failure occurs as a result of instability of the column members. Conveniently, P_U is obtained by making reference to prepared tables or graphs, which relate axial force and column-end moments for a particular column slenderness ratio. The applied column-end moments and the corresponding axial forces must not exceed the permissible values of the relevant beam-column curves. Hence, the computation of P_U will usually result in an iterative procedure. By using the ultimate load P_U rather than the plastic collapse load P_P, allowance is made for member instability on a direct basis since the occurrence of plastic hinges between the nodes is recognized.

1.6.2 Lu's[4] design approximation

Lu has evolved an approximate second-order, elasto-plastic design rule from a rigorous full-scale analysis of a symmetrical portal frame with pinned bases and subjected to symmetrical vertical loading. He subsequently suggested that these results were also suitable for double-storey and three-storey frames.

Lu's design graph is depicted in Figure 3 which also shows the results of some theoretical calculations and model frame tests for simple portal frames. Results for the failure load P_F are obtained from the elastic buckling load P_O and the ultimate load P_U. The term P_U is not the plastic collapse load P_p used in the Merchant-Rankine formula. P_U is defined as the ultimate load of the frame, determined by assuming that the frame is prevented from swaying, and that failure occurs as a result of instability of the column members. Conveniently, P_U is obtained by making reference to prepared tables or graphs[60], which relate axial force and column-end moments for a particular column slenderness ratio. The applied column-end moments and the corresponding axial forces must not exceed the permissible values of the relevant beam-column curves. Hence, the computation of P_U will usually result in an iterative procedure. By using the ultimate load P_U rather than the plastic collapse load P_P, allowance is made for member instability on a direct basis since the occurrence of plastic hinges between the nodes is recognised.

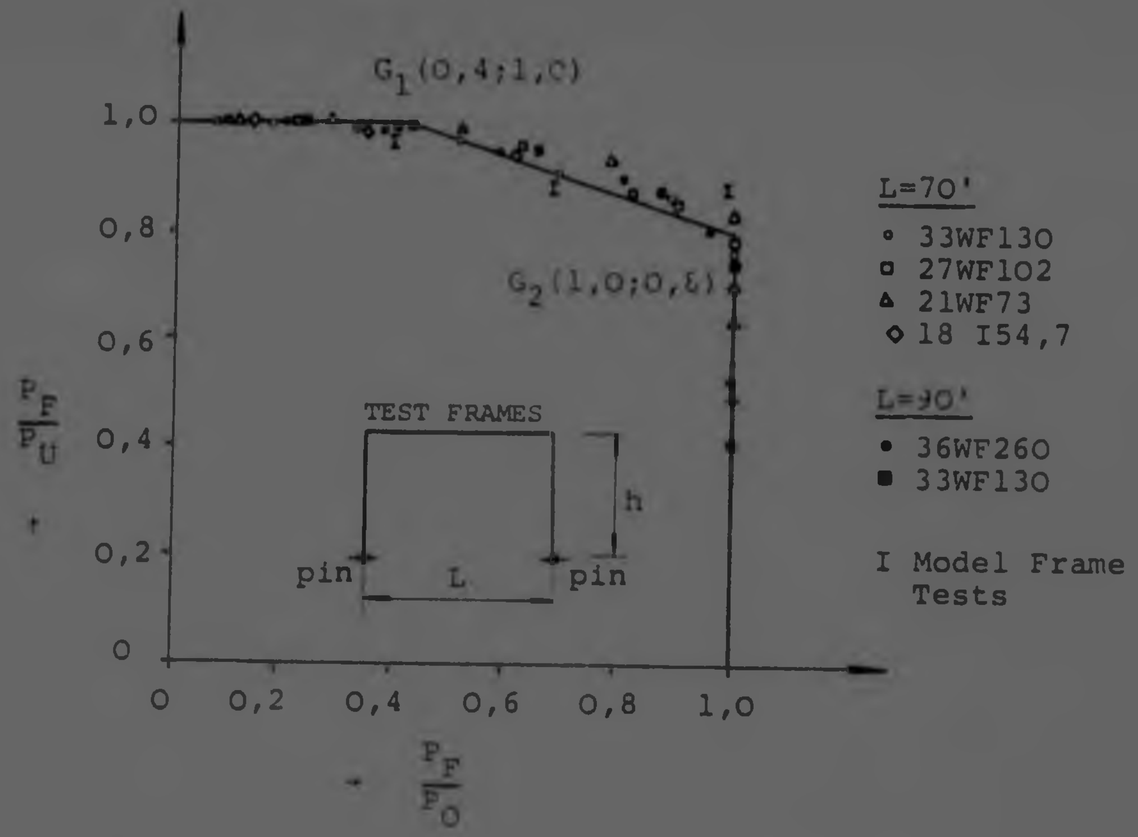

FIGURE 3: Lu's design rule compared with tests and theoretical results

The straight line passing through G_1 and G_2 in Figure 3 is given by

$$\frac{P_F}{P_O} + 3\,\frac{P_F}{P_U} = 3{,}4$$

Where P_F/P_O is less than 0,4, the failure load P_F will equal P_U and for conditions $P_F/P_U \leq 0{,}8$ the strength of the frame is determined by the elastic buckling load P_O. For cases $0{,}4 < P_F/P_O < 1{,}0$, the failure load is calculated from the linear expression given above. The resulting value for P_F must at least equal the factored working loads.

It can be seen that theoretical results and model tests plotted in Figure 3 are in good agreement with the proposed design rule.

However, the following comments can be made:

a) The graph is only applicable to vertical loading.

b) The graph is based on a theoretical analysis of a portal frame with pinned bases and different curves may be required for other base conditions and for multi-bay and multi-storey structures.

c) The rule does not apply to any deviation from full symmetry. This includes geometry, stiffness, loading and imperfections.

d) The evaluation of the failure load necessitates the knowledge of P_U, the ultimate load of the frame. This may require the calculation of the full bending moment diagram for the frame and may result in an iterative procedure.

1.7 P-Δ effects in "stress-controlled" design

The reason for covering the P-Δ aspect in the context of "stress-controlled" design is twofold. Firstly, in this research project, as well as in traditional P-Δ provisions in "stress-controlled" design, use is made of the elastic buckling load as a principal parameter. Secondly, a study of present elastic P-Δ techniques would be helpful in formulating an approximate analytical procedure as a complementary alternative to the computer and graphical solutions developed for this research.

The origin of "stress-controlled" design, as it is used in various design specifications[8-14], is found in the ultimate-strength, interaction curves of beam-columns analysed into the plastic range. These codes propose the following equations in ultimate strength form for the design of a beam-column. Equivalent expressions can be formulated in terms of working loads.

$$M = M_{PC} = M_P \qquad \text{for } 0 \leq \frac{P}{P_Y} \leq 0{,}15 \qquad |\text{EQN. } 1|$$

$$M = M_{PC} = 1{,}18\, M_P \left(1 - \frac{P}{P_Y}\right) \quad \text{for } 0{,}15 \leq \frac{P}{P_Y} \leq 1{,}0 \qquad |\text{EQN. } 2|$$

$$\frac{P}{P_{cr}} + \frac{C_m \; M}{M_P\left(1 - \frac{P}{P_e}\right)} \leq 1{,}0 \qquad |\text{EQN. } 3|$$

The various terms in Equations 1, 2 and 3 are:

P and M = Axial load and end moment defining a point on the ultimate strength interaction curve.

P_{cr} = Ultimate axial load that can be supported in the absence of moment. Based on a safety factor and an allowable stress related to the relevant effective length.

P_e = Elastic buckling load for the member in the plane of M, usually derived on the basis of the effective length.

$\frac{1}{1-\frac{P}{P_e}}$ = Amplification factor for moment.

M_P = Fully plastic moment capacity of section.

M_{PC} = Reduced plastic moment capacity to account for axial load effects (Equation 2).

P_Y = A f_Y = Yield load of a member with cross-sectional area A and yield stress f_Y.

C_m = Factor, used to allow for the shape of the bending moment diagram along the length of the member.

The mechanics and implications of "stress-controlled" P-Δ design are best demonstrated by comparing a first-order and a second-order analysis with the relevant provisions of Equations 1, 2 and 3. For this purpose reference has been made to the graphs of Figures 4, 5 and 6, which were derived by Wood et al[61, 62]. These figures give the results of various analyses for columns subjected to an axial load, P, and a transverse load, H. The column, which is pinned at the base and restrained by a rotational spring at the top, is shown in the inset to Figures 4, 5 and 6. The spring represents the restraining action of beams as the column undergoes a sway Δ. In the deformed position the c[illegible]n-end moment is $M_C = Hh + P\Delta$. The value G represents the ratio of column to beam stiffness and r is the radius of gyration of the column section in the plane of bending. Three different combinations of column slenderness $\lambda = h/r$ and stiffness ratio G are considered.

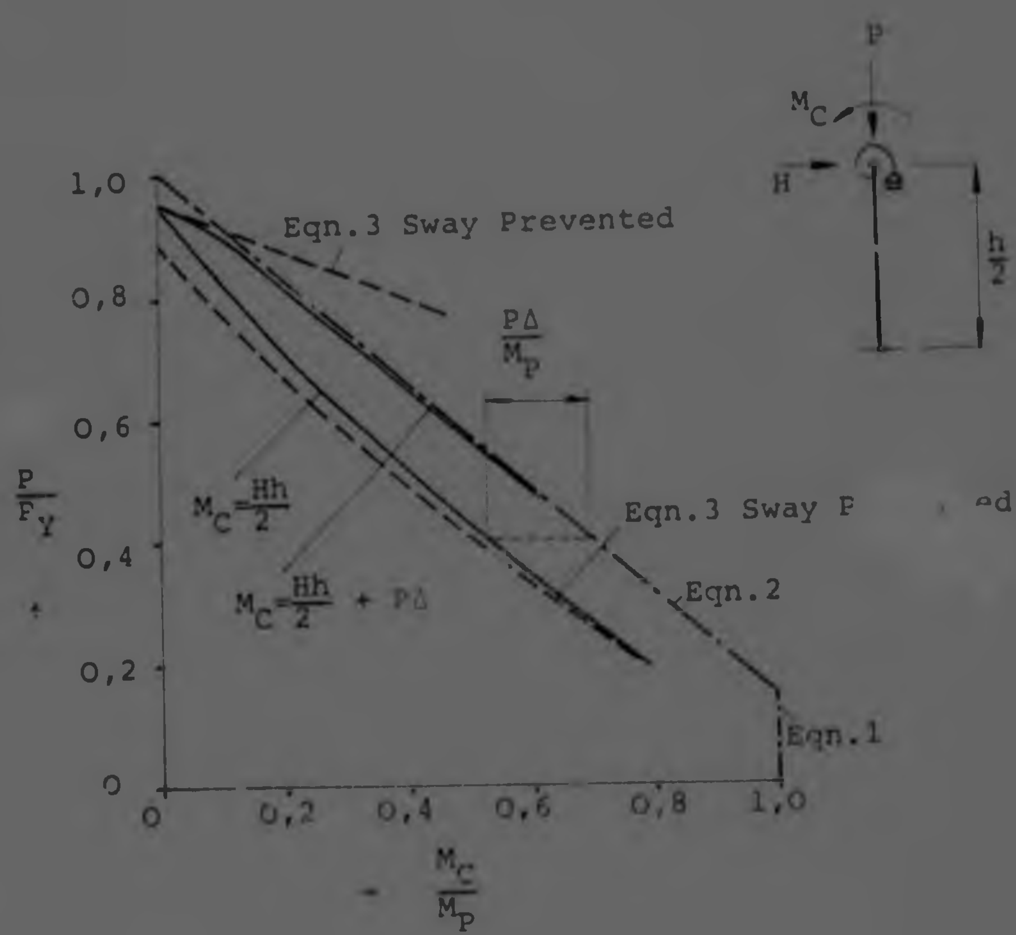

FIGURE 4: Interaction relationship, h=40r, G=2
(Reference 62)

the column-end moment is $M_C = Hh + P\Delta$. The value G represents the ratio of column to beam stiffness and r is the radius of gyration of the column section in the plane of bending. Three different combinations of column slenderness $\lambda = h/r$ and stiffness ratio G are considered.

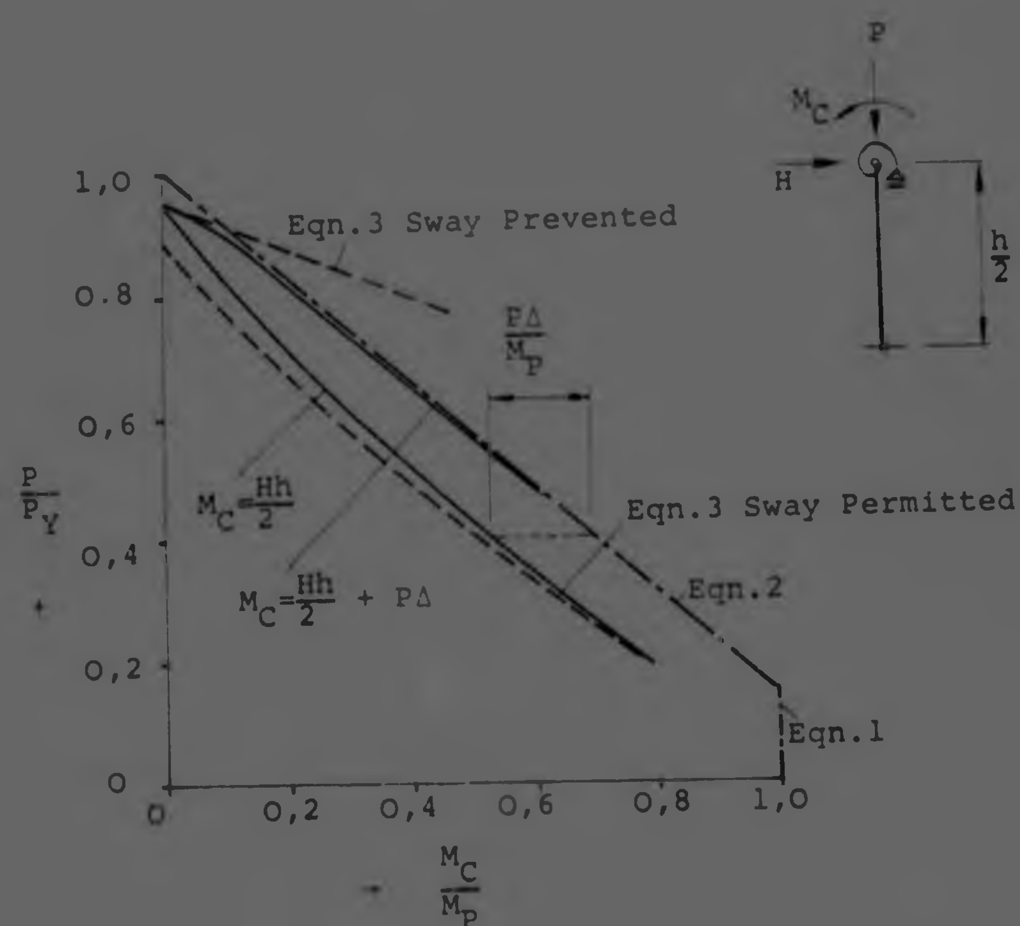

FIGURE 4: Interaction relationship, h=40r, G=2
(Reference 62)

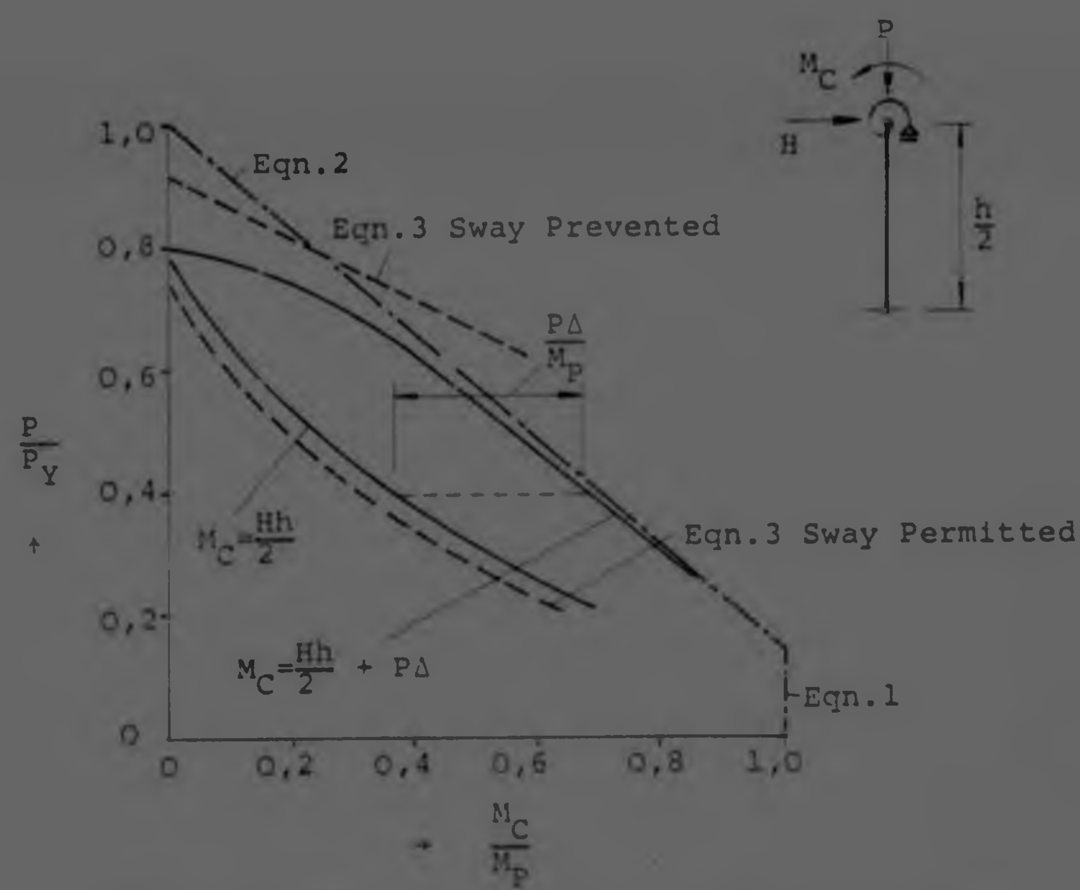

FIGURE 5: Interaction relationship, h=60r, G=2 (Reference 62)

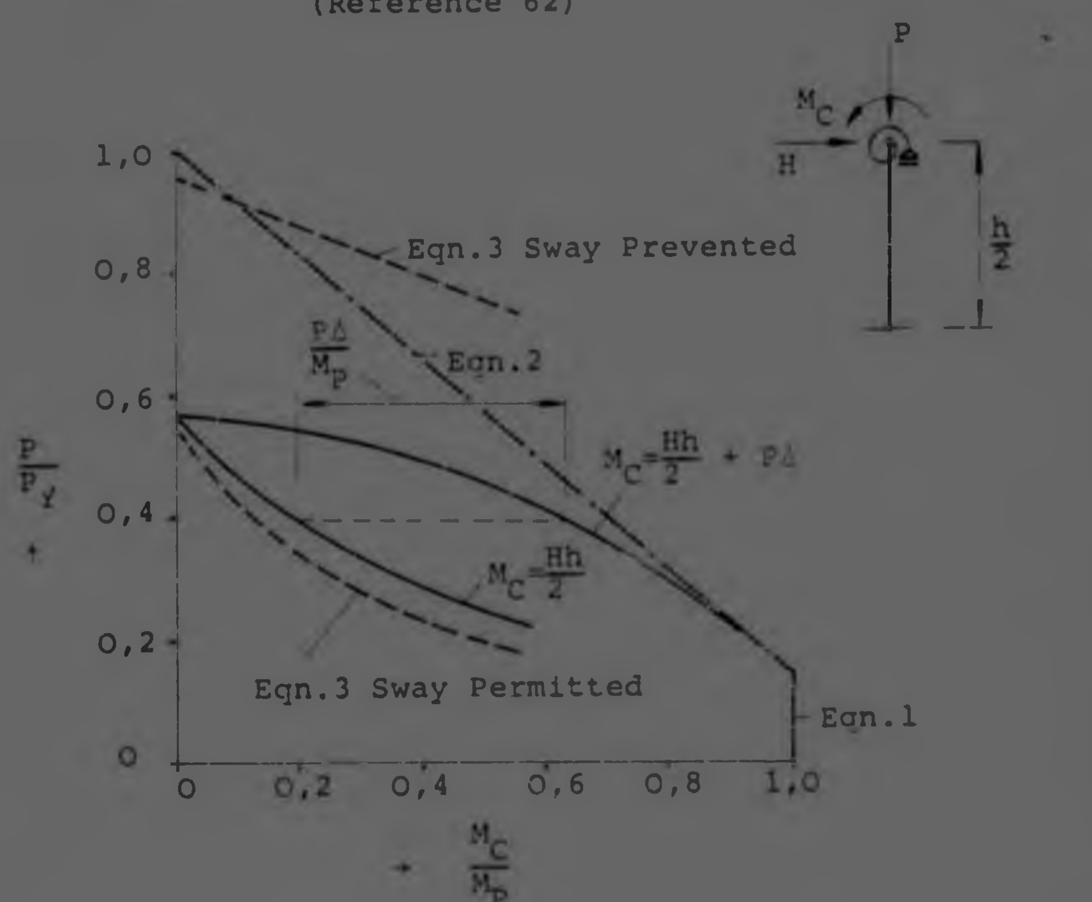

FIGURE 6: Interaction relationship, h=40r, G=10 (Reference 62)

The upper solid lines in Figures 4, 5 and 6 represent the carrying capacity of the three subassemblages based on a second-order, elasto-plastic analysis. The lower solid lines indicate the permissible corresponding axial force and moment ratios in terms of first-order principles. Thus, the difference between the two solid lines is a measure of the actual P-Δ effect. The results of Equations 1, 2 and 3 are also shown in Figures 4, 5 and 6. The upper dashed lines in the diagrams represent the solutions of Equations 1, 2 and 3, the latter incorporating an amplification factor applicable to the sway-prevented case. The lower dashed curve represents Equation 3 evaluated on the basis of the sway-permitted model.

The following findings with respect to the P-Δ provisions are self-evident from the diagrams of Figures 4, 5 and 6:

a) A second-order analysis provides directly for the P-Δ moments. In this instance, Equations 1, 2 and 3 (the latter based on the sway-prevented case), will usually predict the failure behaviour adequately, provided the column slenderness is moderate and the restraining beams are substantial such as in Figure 4. In fact, this approach is slightly unsafe since the capacity predicted by the interaction equations exceeds the actual capacity represented by the upper solid line.

b) For more flexible subassemblages (Figures 5 and 6) and higher load ratios, P/P_Y, the same procedure may overestimate the member capacity by a considerable margin, since the full strength of the section cannot be utilised.

c) If the structure is analysed on a first-order basis, the P-Δ moments are initially ignored. Compensation for overall-stability is then provided by sizing the column on the basis of the effective length factor applicable to the sway-permitted model (lower dashed lines in Figures 4, 5 and 6). The relevant curves suggest a conservative result. The first-order moment M_C permitted on the structure (lower dashed line) is less than the moment $M_C = Hh/2$ which could be accepted for a given ratio of P/P_y.

d) If a first-order analysis is used as a basis for design, no recognition is given to the fact that the P-Δ effect increases the beam moments as well as the column moments. This may lead to a reduction in safety for structures in which the P-Δ effect is significant. The designer is also misled in believing that an increase in column size is the best remedy in order to improve the structural efficiency. However, in the general case, a stiffer beam would be more helpful. This was confirmed for numerical examples by Cheong Siat Moy[63,64] and Liapunov[65], who also warned that the use of high strength steel would have a particularly adverse effect on sway and ultimate strength.

e) Actual columns in rigid multi-storey frames are converted into equivalent pin-ended struts using their elastic buckling load as the reference parameter. A wrong assessment of the elastic buckling load may lead to a considerable error in evaluating the strength of such a member.

The above points are amplified by a number of research findings. Based on comparisons of seven representative frames, designed in a number of different ways, Cheong Siat Moy et al[66,67] in two studies and Lu et al[68] in a further investigation concluded that instability may be ignored for "stress-controlled" designs according to the AISC Specifications[44], provided the following conditions are satisfied for the case of uniformly distributed loading:

i) The storey stiffness is such that $\Delta/h \leq \Sigma H/9\Sigma P_S$, in which,

   h = Storey height

   ΣP_S = Total vertical load on storey at working loads

   ΣH = Total shear on storey at working loads

   Δ = First-order relative sway of storey due to ΣH

ii) At working loads, the bending moment due to distributed loads w on a beam, taken conservatively as the fixed-end moment $wL^2/12$, must be greater than 25 per cent of the beam moment due to lateral load.

iii) The column stress ratio is such that $f_a/p_a \leq 0,75$, where,

f_a = Average axial compression stress due to vertical loads

p_a = Allowable compressive axial stress in the absence of moment, based on h/r

iv) The maximum in-plane column slenderness $h/r \leq 35$.

If conditions i) and ii) are satisfied, designs based on the AISC Specifications will result in frames which have failure load factors for combined loading greater than the specified value of 1,30. The other two constraints prevent premature hinge formation in the column members. Similar recommendations were subsequently proposed by Cheong Siat Moy[63] when he investigated the relevant design method of the Australian Standard, AS1250-1975.

The above limitations are possible due to the intrinsic conservatism of "stress-controlled" design approaches. It lies in the nature of Equations 1, 2 and 3, that practically the attainment of a plastic hinge at one location in the critical member is assumed to correspond to failure of the complete structure.

Cheong Siat Moy[66,67] and Lu et al[68] designed a number of frames in accordance with "stress-controlled" methods and subsequently analysed the same frames on a second-order, elasto-plastic analysis basis. These studies revealed that the particular frames had a further strength reserve of between 15 and 35 per cent, with an average excess of 20 per cent. Cheong Siat Moy[66,67] and Lu et al[68] concluded that frames of the nature investigated, which meet the limitations above, will develop P-Δ effects which can be absorbed by this extra strength margin. The omission of the P-Δ moments, and a first-order analysis procedure would then suffice.

Where the above limitations are exceeded two approaches are possible:

v) An elastic second-order analysis. This may be done by making use of a full-scale computer analysis, by employing the concept of storey-stiffness advocated by Cheong Siat Moy[44] or by modifying the results of a first-order analysis as demonstrated by Wood et al[61] and McGregor & Hage[69].

vi) A first-order analysis and implicit P-Δ provisions on the basis of the effective length concept applicable to the sway-permitted case. Cheong Siat Moy et al[66,67] and Lu et al[68] confirmed for seven representative frames that this approach is usually safe.

The strength margin and safety scatter identified for "stress-controlled" design methods would not be relevant to second-order, elasto-plastic analysis techniques, which provide a more economical structure with a consistent factor of safety against failure. However, in this context it should be noted that design provisions based on a sway limit at working loads were found to govern the design of the structure when compared with either "stress-controlled" or plastic design procedures[64,60].

Cheong Siat Moy[63] demonstrated on a frame designed to the Australian Standard, AS1250-1975, that the approach outlined in point vi) is not always conservative. He concluded that the P-Δ effect may be underestimated from a first-order analysis when axial forces are large enough to influence the frame stiffness significantly. He subsequently proposed a revised design interaction formula, directly incorporating the actual second-order moments[63,67].

A further magnification effect to the P-Δ moments can be attributed to member yielding[62]. Theoretically, the P-Δ forces should thus be based on deflections that exceed those calculated by elastic analysis. However, because of the conservative nature of the column design procedure (Daniels[71]) and since elastic beam action does not seem to reduce the overall frame stiffness significantly (Ramirez[72]), Wood et al[62] concluded that this effect may be ignored in "stress-controlled" design.

A fair amount of criticism has recently been voiced in connection with the implicit P-Δ provisions based on the effective length concept or the elastic buckling load. This arises firstly, because of the inability of representing the true behaviour of a frame by its elastic buckling load. In addition, there are the problems involved in finding correct effective length values from alignment graphs or equivalent formulae. For a number of sway frames Kuhn[73] and Kuhn & Lundgren[74] have compared the results of typical effective length charts as used in various design codes[1-10] with rigorous elastic stability solutions. They noted that the chart solutions often deviate by as much as 20 per cent from exact solutions and identified several instances of variations as large as 50 per cent, and in one case even 74 per cent. They concluded that modifications to the basic effective length, as suggested by the Structural Stability Research Council (SSRC)[75,76], had no effect on these results and advised a cautious use of the alignment charts. The implications of a 50 per cent error in the effective length on the P-Δ effect may be assessed by comparing Figure 4 and Figure 5 for a given ratio P/P_y. For the more slender column of Figure 5, the P-Δ moments are approximately doubled.

In another publication Lind[77] demonstrated that different analysis techniques may lead to vastly different results for the elastic buckling load. He recommended that current design methods should be adjusted to include for selfweight and load redistribution.

Cheong Siat Moy[11] maintained that effective length factors will never be able to account properly for such effects as semi-rigid connections, partial yielding, initial storey eccentricities, axial beam loads, foundation settlement, non-uniform temperature and strain-hardening which all have a direct influence on the sway and thus the P-Δ moments. On these premises, and referring to the essays on the effective length by Grier[78], he developed his proposals for a frame design without the use of the effective length concept to account for the P-Δ effect[70]. In a further study, Cheong Siat Moy[79], utilising his own storey-stiffness approach[80], showed that secondary effects such as those mentioned above can be included in a rational way.

In discussions on Cheong Siat Moy's design of frames without the effective length, v.d.Woude, Johnston and Zweig[81] agreed that limitations exist but argued that the effective length concept nevertheless fulfills a useful role in many other ways, e.g. in selecting the relevant factor of safety and in accounting for member instability. Johnston[76], writing about the Third SSRC Guide, referred to the five possible modifications offered by the SSRC Guide to provide for unsymmetrical frames, unsymmetrical loads, column base conditions, semi-rigid connections and inelastic action. Inelastic effective length factors were pioneered by Yura[82] and further investigated by Disque[83].

Iffland[84] pointed out that the effective length concept has an extremly weak theoretical and empirical justification when used to account for the influence of the P-Δ effect of the entire frame on a single member. This statement has been confirmed by the results of exact second-order analyses of frames designed in accordance with the effective length approach. Wood et al[61] and Cheong Siat Moy et al[66] clearly exposed the erratic nature of the effective length provisions.

In a further study, Liapunov[65] emphasised the importance of assessing the correct conditions at the column bases. In this context he demonstrated the effects of an incorrect assumption on the analysis of a 32-storey, three-bay frame.

It is obvious from the above literature survey that the effective length concept is unreliable in certain cases. Moreover, it appears that the elastic buckling load is better evaluated from first principles, when required in a design situation. Many techniques are available for this purpose. A simple and apparently very successful method, based on the first-order storey sway or storey stiffness respectively, was suggested by Rosenblueth[85], Goldberg[86], Stevens[87] and lately by Cheong Siat Moy[illegible]. A similar approach, using the sway deflection of frames initially proportioned to satisfy a sway limit, was recently endorsed by Anderson[88] for use in the Merchant-Rankine formula.

1.8 Choice of research and objectives

1.8.1 Choice of problem

The preceding sections give an insight into the provisions for frame stability in plastic and "stress-controlled" design. It becomes apparent that a need exists for a more accurate and comprehensive approximate second-order, elasto-plastic analysis procedure for unbraced and partially-braced rigid frames.

The only codified method presently available is the Merchant-Rankine interaction approach of the ECCS Recommendations and the British Draft Code, B20. This approach is known to be conservative and only covers frames for which the elastic buckling load is at least four times the plastic collapse load. This requirement, in many cases, compels the designer to resort to more complex analysis techniques.

Another interaction procedure, developed by Lu, has only been proven for unbraced symmetrical portal frames with pinned bases and subjected to symmetrical vertical loading. Lu allowed for the pre-buckling bending moments caused by loading applied between the ends of members. This is a case corresponding to the special condition of "Symmetry Buckling". In this thesis, the term "Symmetry-Buckling" refers to frames which are characterised by symmetry in regard to geometry and loading and which fail in a sway mode when analysed elastically for buckling.

Other approximate second-order, elasto-plastic analysis techniques published in the literature are based on the subassemblage concept. They require a step-wise approach and the plotting of load-displacement or load-stiffness diagrams and appear to be lengthy in comparison with the interaction methods.

In developing the objectives of this research project, recognition had to be given to the following points:

a) An interaction method based on estimating the failure load by the loss-of-stiffness principle and similar in procedure to the Merchant-Rankine rule would be desirable. This approach promises to be simple and dispenses with moment and/or stress calculations in the plastic range in establishing structural stability.

b) A consistent and generalised approach covering all types of unbraced rigid frames would be essential.

c) Accuracy would be of prime importance to improve on the results obtained from the Merchant-Rankine formula. However, this should be achieved with little increase in the complexity of the method in general.

d) It would be untenable to make implicit provisions for the P-Δ effect in the elastic or inelastic range by using a concept based on the effective length, such as the moment-magnifier approach in "stress-controlled" design.

e) Where the elastic buckling load is required in the analysis, an evaluation based on first principles or the storey-stiffness approach would be superior to results derived from effective length or related charts.

f) A computer analysis should remain simple and should therefore be performed on a limited frame, provided the necessary accuracy is maintained. A subassemblage approach would facilitate a graphical presentation of results for "manual" use, i.e. a method without the need of the computer.

g) A subassemblage technique would enable the designer to concentrate on critical portions of a frame which can often be identified by inspection of the practical structure. Repetitive or less critical sub-sections of the same framework are then covered by one sub-assemblage analysis. This will reduce data compilation and computer time and will speed up a "manual" assessment.

h) Recognition should be given to the restraining effects of cladding and allowance should be made for different types of base restraint.

i) For symmetrical structures and loadings cognisance should be given to the special case of "Symmetry-Buckling".

j) It would be desirable to outline an alternative, approximate analytical procedure to cover cases which have not been presented in graphical form. Where possible, this technique should be based on established analytical concepts.

1.8.2 Objectives of this research

The principal objective of this research project has been to develop an alternative, approximate second-order, elasto-plastic analysis procedure for the plastic design of un-braced and partially-braced, rigid steel frames.

Suitable mathematical formulations have been derived and a relevant computer program has been developed and tested. A graphical presentation of certain solutions has been prepared and an analytical approximation outlined. The method of analysis proposed in this research has been compared with research results of other studies. A series of purpose-made, small-scale model frames has been tested to confirm the proposed design curves.

The investigational procedure followed in the accomplishment of the various research objectives is briefly outlined below:

1.9 Investigational procedure

a) Description of principles and derivation of proposed design curves.

b) Choice of suitable subassemblages for analysis purposes.

c) Mathematical analysis of subassemblages covering conventional buckling, "Symmetry-Buckling" and the second-order elastic state of stress corresponding to loading related to the elastic buckling load.

d) Development of the computer program.

e) Description of the design process.

f) Comparison of the proposed method with previous theoretical results and experimental work by other researchers.

Suitable mathematical formulations have been derived and a relevant computer program has been developed and tested. A graphical presentation of certain solutions has been prepared and an analytical approximation outlined. The method of analysis proposed in this research has been compared with research results of other studies. A series of purpose-made, small-scale model frames has been tested to confirm the proposed design curves.

The investigational procedure followed in the accomplishment of the various research objectives is briefly outlined below:

1.9 Investigational procedure

a) Description of principles and derivation of proposed design curves.

b) Choice of suitable subassemblages for analysis purposes.

c) Mathematical analysis of subassemblages covering conventional buckling, "Symmetry-Buckling" and the second-order elastic state of stress corresponding to loading related to the elastic buckling load.

d) Development of the computer program.

e) Description of the design process.

f) Comparison of the proposed method with previous theoretical results and experimental work by other researchers.

g) Confirmation of the design curve shape by comparison with results obtained from the testing of purpose-made model frames.

h) Derivation of parameters and design aids for a "manual" design technique.

i) Outline of an approximate analytical procedure.

j) Conclusions and some recommendations for future research.

CHAPTER 2

THE PROPOSED ANALYSIS TECHNIQUE

2.1 General Principles

The proposed method is based on a multi-curve, interaction approach, incorporating the plastic collapse load on the one hand and certain elastic failure parameters on the other hand. They are combined in empirical curves in order to cover the inelastic instability range of the structure.

For a specific frame and loading, it will be necessary to identify the relevant curve on the interaction diagram. Each curve represents the behaviour of an infinite number of frames, all of which have the same value of a parameter which is referred to in this thesis as the "limiting slenderness ratio". The "limiting slenderness ratio" is based on the elastic response of the frame to loading which is related to the elastic buckling load. The position on this curve of a particular frame within this group of frames is identified by the ratio of the plastic collapse load, P_p, to a load related to the elastic buckling load of the frame, αP_O.

For the general case of a multi-storey, multi-bay framework, the plastic collapse load is calculated from a full-scale analysis of the complete structure, whereas the corresponding elastic buckling parameters are evaluated for each of the relevant subassemblages contained in the structure. The combination of plastic collapse load and elastic parameters leading to the lowest failure load is then identified. This is the way the method is used in this thesis.

In addition, it is also possible to employ the principles of the method developed in this study to determine the failure load of the various subassemblages contained in the framework. For this purpose, the plastic collapse load and the elastic parameters would both be evaluated on matching subassemblages. The significance of this approach will briefly be referred to in section 3.2, paragraph c).

2.2 Interaction curve

2.2.1 General

Initially, the underlying principles and theory of the proposed interaction curves will be developed. A detailed description of how to derive the individual curve shape will follow in the next section of this study. A typical interaction curve applicable to a specific group of frames is shown in Figure 7.

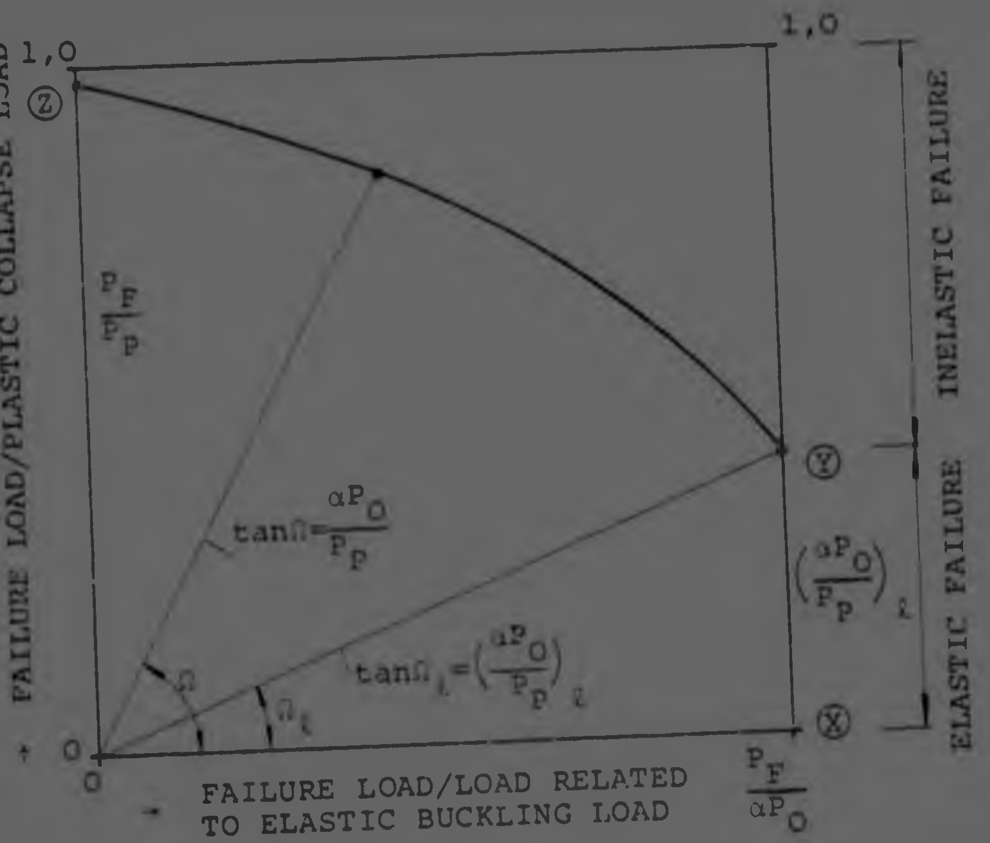

FIGURE 7: Interaction curve

In Figure 7, the failure load P_F of a frame is presented as a function of the plastic collapse load P_P and a load αP_O, in which P_O is the elastic buckling load of the frame and α a reduction factor. The purpose and significance of the reduction factor α will be explained at a later stage.

Section X-Y of the interaction diagram of Figure 7 signifies elastic failure, for which the ratio $P_F/\alpha P_O$ must be equal to 1,0. For failure unaffected by instability, the ratio P_F/P_P reaches a maximum value at point Z as the ratio $P_p/\alpha P_O$ approaches zero. A value somewhat lower than P_p may be reached near point Z if the reduction in fully plastic load due to the presence of axial forces and initial imperfections is allowed for. The inelastic failure behaviour between these two extremes is represented by the curve between points Y and Z. The curve shape, which is empirical, will be further discussed when the detailed derivation of the interaction curves is examined. Point Y at the right end of the curve marks the transition between elastic failure and inelastic instability. Furthermore, a point on the curve between Y and Z is identifiable by the radial line of slope $\alpha P_O/P_P$ through the origin of Figure 7. It will be shown that a curve such as that given in Figure 7 applies to a specific group of frames, characterised by common intersection points Y and Z.

Initially, a failure curve will be examined in more detail for the special case of "Symmetry-Buckling". Subsequently, the findings will be extended to cover the general framework.

2.2.2 Symmetrical conditions

For demonstration purposes the symmetrical pinned-base portal frame of Figure 8 is investigated. The frame is subjected to symmetrical beam loading and has uniform beam and column properties. The given loading, Q, refers to the ultimate limit state; i.e. factored working loads are considered.

The following sections of this chapter, up to section 2.3.4, only refer to structures in which the beam and columns have the same inertias. Equations 4 to 9 are applicable to this case. The implications of a difference in the inertias of columns and beam will be examined in section 2.3.4.

Because of the symmetrical geometry and loading, the behaviour of the frame given in Figure 8 would be that of "Symmetry-Buckling". When considering the case of "Symmetry-Buckling", the pre-buckling deformations due to the applied loading are allowed for. The value μ applicable to this condition (see Figure 7) is equal to 1,0.

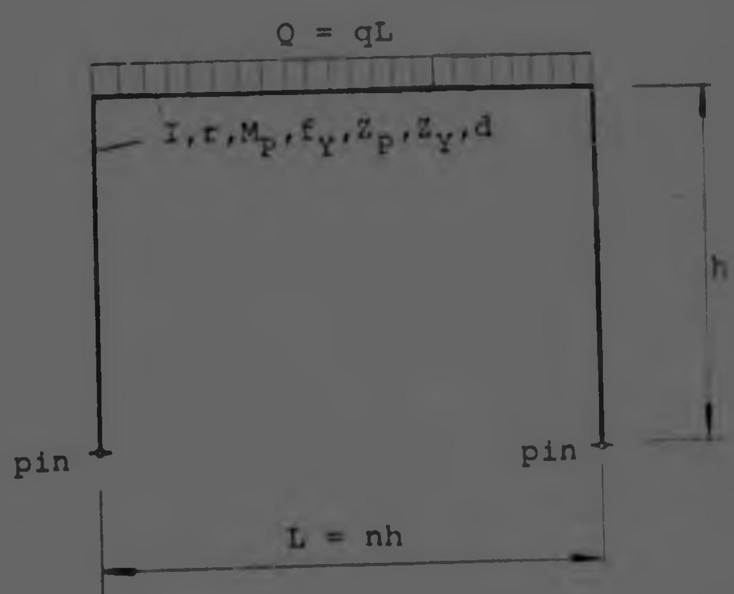

FIGURE 8: Frame example

Ignoring the influence of axial member forces, the frame of Figure 8 has a plastic collapse load P_P of

$$P_P = \frac{16M_P}{nh} = \frac{16f_Y Z_P}{nh}$$

where M_P is the plastic moment capacity of the section.

The moment M_P can be related to the yield stress, f_Y, and the plastic section modulus Z_P, which in turn can be expressed as the elastic section modulus Z_Y multiplied by the shape factor κ_1. For symmetrical sections it follows that:

$$Z_P = \kappa_1 Z_Y = \kappa_1 \frac{2I}{d}$$

where I is the second moment of area and d the depth of the section.

The depth of the section is related to the radius of gyration, r, about the axis of bending by the factor κ_2.

$$d = \kappa_2 r$$

Hence, the following expression for P_P is obtained:

$$P_P = \frac{32f_Y I\kappa_1}{\kappa_2 r\ nh}$$

The elastic buckling load P_O of the frame is evaluated from basic principles. This load will have the same arrangement and location as the applied ultimate load, Q, i.e.

uniformly distributed for the example of Figure 8. The buckling load P_O may be expressed as follows:

$$P_O = \frac{m_O^2}{h^2} EI$$

where m_O, and the buckling load itself, is a function of the beam and column stiffness, the conditions at the column bases and, to a lesser extent, the load arrangement.

For given base and loading conditions, m_O is simplified to a function of the ratio of beam to column length, provided the inertias, I, are uniform.

$$m_O = f\ (n = \frac{L}{h})$$

The ratio P_O/P_P of the given frame assumes the following form, if $\lambda = h/r$ is substituted as the column slenderness ratio:

$$\frac{P_O}{P_P} = \frac{E\kappa_2 m_O^2 n}{32 f_Y \kappa_1} \frac{1}{\lambda} \qquad |\text{EQN. 4}|$$

It has been mentioned that one such interaction curve as shown in Figure 7 applies to a certain group of frames, and that this group is identified by a common intersection point Y. The particular frame corresponding to the transition point Y will be designated as the "limiting frame" within a specific group of frames. This "limiting frame" is characterised by a column slenderness which is called the "limiting slenderness ratio", λ_ℓ. The "limiting frame" is similar to the actual frame in regard to the frame configuration and the load arrangement. Moreover, if subjected to its elastic buckling load $P_{O\ell}$, it will develop a stress corresponding to first-yield at a particular critical section.

If Equation 4 is relevant to frames falling on the curve of Figure 7, it also applies to the "limiting frame" corresponding to point Y. For the "limiting frame" Equation 5 is obtained from the expression given in Equation 4. All parameters specifically referring to the "limiting frame" will be given the additional suffix (ℓ).

$$\frac{P_{O\ell}}{P_{P\ell}} = \left(\frac{P_O}{P_P}\right)_\ell = \frac{E\kappa_2 m_O^2 n}{32 f_Y \kappa_1} \frac{1}{\lambda_\ell} \qquad |\text{EQN. } 5|$$

In Equation 5 the plastic collapse load of the "limiting frame" has been assumed as

$$P_{P\ell} = \frac{32 f_Y I \kappa_1}{\kappa_2 r n h_\ell}$$

This expression presumes that plastic failure occurs in the same mode for both, the actual and the "limiting frame", that the hinge locations are identical and that the effects of axial forces on the plastic moment capacity of the section are negligible. These assumptions, which are satisfied for the problem of Figure 8, will be further examined in sections 2.2.5 and 2.3.4 of this chapter.

A group of frames represented by a specific curve as shown in Figure 7 will have the same ratio $(P_O/P_P)_\ell$. This is generally accomplished by keeping the "limiting slenderness ratio", λ_ℓ, as well as the first term in Equation 5, constant for all frames of a particular group. Thus, Equation 5 defines the parameters of a specific group of frames. Furthermore, frames other than the "limiting frame", but lying on the same interaction curve, are then related to their "limiting frame" by Equation 6.

$$\frac{P_O}{P_P} = \left(\frac{P_O}{P_P}\right)_\ell \frac{\lambda_\ell}{\lambda} \qquad |\text{EQN. } 6|$$

By varying the column slenderness ratio from $\lambda=0$ to $\lambda=\lambda_\ell$, the whole range of frames is considered in terms of the radial lines of slope, P_O/P_P. The relationship between the actual and limiting frames as defined by Equations 4, 5 and 6 is further illustrated in Figures 9a and 9b for the problem of Figure 8.

As required by the previous definition, none of the parameters contained in the first term of Equation 5 has been altered in the transition from the actual frame to the "limiting frame" and, in addition, Equation 6 is satisfied.

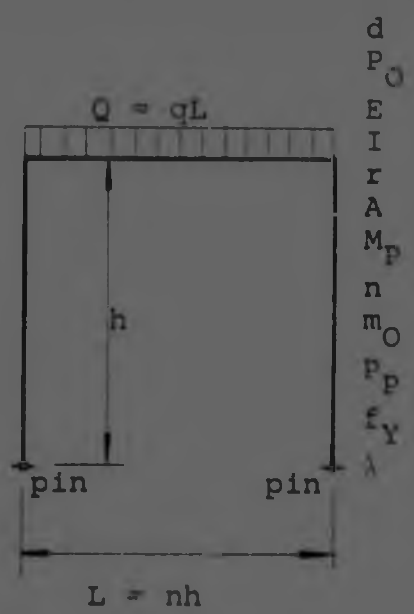

FIGURE 9a: Actual frame

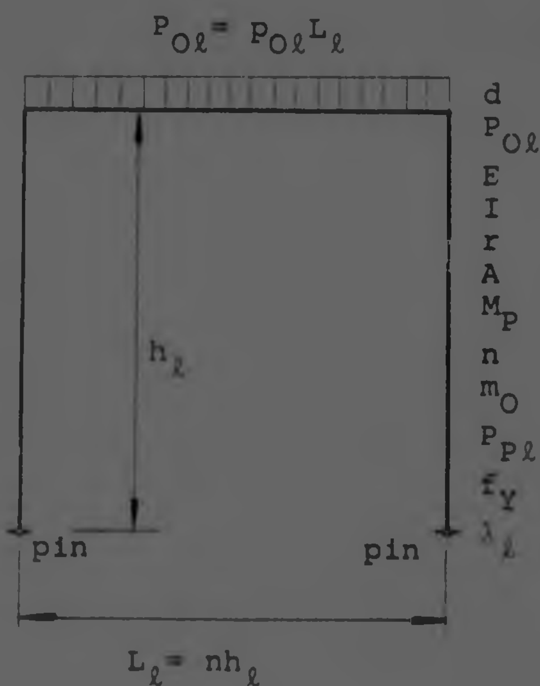

FIGURE 9b: "Limiting frame"

A further requirement, namely that of constant λ_ℓ for a particular group of frames, is demonstrated for the frame of Figure 10 using the results of second-order stress computations.

Example:

A symmetrical pinned-base, portal frame is subjected to a uniformly distributed beam loading of intensity q. All other salient parameters are given in Figure 10.

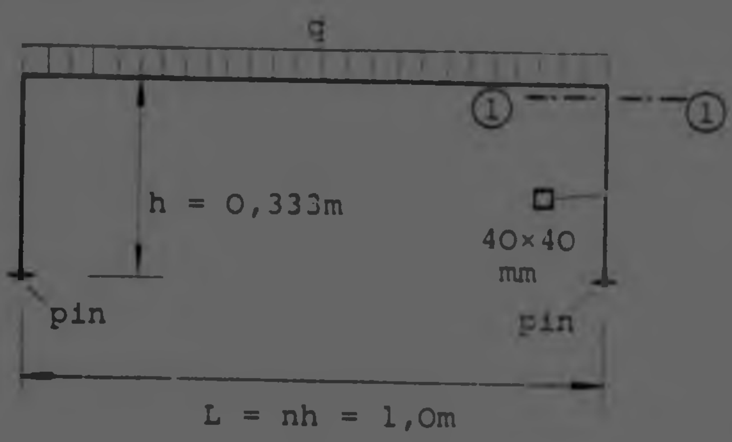

f_Y = 250 MPa

d = 40mm

m_O = 1,48

$n = \frac{L}{h} = 3$

A = $1{,}6\times10^{-3}m^2$

r = 11,55mm

$\lambda = \frac{h}{r} = 28{,}83$

I = $0{,}2133\times10^{-6}m^4$

E = $2{,}06\times10^5$ MPa

FIGURE 10: Demonstration of "limiting slenderness ratio"

The buckling parameter m_O=1,48 has been obtained from a computer analysis for a frame with a ratio of beam to column length n=3. From this follows the buckling load of the actual frame

$$P_O = p_O L = \left(\frac{m_O}{h}\right)^2 EI = 868 \text{ kN}$$

The critical section of the frame is section 1-1 of Figure 10. Loading the frame of Figure 10 with P_O=868 kN results in the following bending moment for the critical section using a second-order elastic analysis:

M_{1-1} = 69,5 kNm

The formula for the "limiting slenderness ratio", λ_ℓ, is derived in a later chapter of this thesis (section 6.2), and will be used here without further verification. At this stage, it is sufficient to point out that the "limiting slenderness ratio" can be expressed as a function of the properties and forces of the actual frame when subjected to loading related to its elastic buckling load P_O.

$$\lambda_\ell = \frac{M}{I}\,\frac{h}{f_Y}\,\frac{d}{2r}$$

$$\lambda_\ell = 752$$

The "limiting frame" will have the properties and configuration of the actual frame, with the only difference that

$$h_\ell = h\,\frac{\lambda_\ell}{\lambda} = 8,69 \quad \text{m}$$

$$L_\ell = L\,\frac{\lambda_\ell}{\lambda} = 26,08 \ \text{m}$$

This result is now put to the test. It needs to be shown that the "limiting frame" attains a stress of 250 MPa at section 1-1, when subjected to its own elastic buckling load $P_{O\ell}$. The buckling load for the "limiting frame" amounts to

$$P_{O\ell} = P_{O\ell}L_\ell = \left(\frac{m_O}{L_\ell}\right)^2 EI = 1,28 \ \text{kN}$$

The value m_O=1,48 is also applicable to the "limiting frame".

The bending moment at section 1-1 of the "limiting frame" due to $P_{O\ell}$=1,28 kN has been calculated as

$$M_{\ell,1-1} = 2,66 \text{ kNm}$$

For this moment, the corresponding stress at section 1-1 becomes

$$f_{\ell,1-1} = \frac{M_{\ell,1-1}\, d}{2I} + \frac{P_{O\ell}}{2A}$$

$$f_{\ell,1-1} \simeq 250 \text{ MPa}$$

It can easily be verified that other frames, similar to the portal frame of Figure 10, would yield the same "limiting slenderness ratio" of λ_{ℓ}= 752, e.g. retaining n=3 but changing the length L to 0,75m, or keeping L at 1,0m but changing the cross-section to 50×50mm, will also result in λ_{ℓ}= 752. All these frames will have a different P_O/P_P - ratio as λ changes. At the same time, the two terms of Equation 5 and thus the ratio $(P_O/P_P)_{\ell}$ of the corresponding "limiting frames" remain unaltered. This proves that an infinite number of frames with a common "limiting frame" may be accommodated on a particular interaction curve, such as that given in Figure 7. Furthermore, a specific frame of a certain group of frames is distinguishable by its ratio P_O/P_P, which in turn is proportional to the inverse of the column slenderness λ. The easiest way to generate a specific group of frames is to modify the absolute member lengths L and h but keeping their ratio n constant so that the frames are geometrically similar.

2.2.3 Non-symmetrical conditions

For the case of "Symmetry-Buckling" a specific "limiting slenderness ratio" λ_ℓ and load ratio $(P_O/P_p)_\ell$ can be identified at point Y of Figure 7. This is only possible because "Symmetry-Buckling" is characterised by true load bifurcation at the elastic buckling loads P_O and $P_{O\ell}$. This is further illustrated in section 6.1 of this thesis which deals in detail with the derivation of the "limiting slenderness ratio" for this case.

For conditions not qualifying for the case of "Symmetry-Buckling", the "limiting slenderness ratio" λ_ℓ would tend to infinity for loading corresponding to the elastic buckling load P_O. The reason for this can be found in the nature of the associated load-displacement curve which is not characterised by load bifurcation. To obtain a finite stress and slenderness ratio corresponding to elastic failure, a reduced load αP_O and $\alpha P_{O\ell}$ $(\alpha < 1,0)$ will be nominated as the fictitious "elastic buckling load". The detailed derivation of the "limiting slenderness ratio" λ_ℓ and the factor α will be discussed in section 6.1 of this thesis. At this stage, it is sufficient to point out that α will be related to the "limiting slenderness ratio", λ_ℓ.

The reduction of the elastic buckling loads P_O and $P_{O\ell}$ to αP_O and $\alpha P_{O\ell}$ for non-symmetrical cases has been found to be a safe approximation as illustrated in Figure 11. This manipulation of nominating a fictitious "elastic buckling load" below the actual elastic buckling load would qualitatively change the failure curve from the dashed curve X-Z to the solid curve Y-Z in Figure 11.

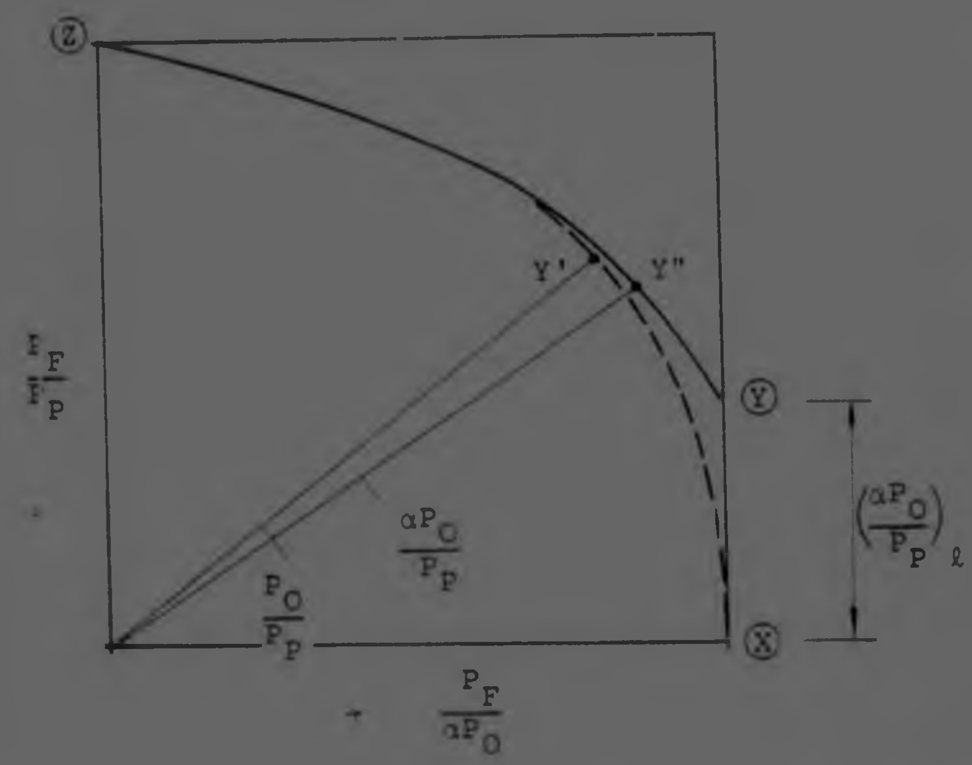

FIGURE 11: Effect of reduced buckling load

The failure load corresponding to a point Y' for the full P_O will be greater than the failure load for a point Y" which belongs to a reduced load αP_O. This has been confirmed by computer evaluations for progressively increased values of α. It has also been observed that for frames of practical proportions the consequences of using slightly different values of α for a given problem is not significant. In the same context, it must be remembered that the assumption of infinite displacements and thus infinite slenderness ratios at the instance of elastic buckling is not a realistic one. This is only due to the linearised mathematical approach usually adopted to solve the problem of elastic buckling. If the effects of axial member shortening and large displacements were allowed for, a finite stress and deformation state corresponding to the full buckling load could also be identified for non-symmetrical cases.

Thus, except for the reduction factor α, non-symmetrical cases may be treated in the same way as the special case of "Symmetry-Buckling". The fact that curves such as shown in Figure 7 are relevant for both cases has also been confirmed by comparisons with results from other research (Tables 6/1 and 6/2).

The frames and loadings applicable to the actual and limiting conditions of non-symmetrical cases are illustrated in Figures 12a and 12b.

It is of interest to recognise that the "limiting frame" is subjected to the same arrangement of loading as the actual frame and that the load ratios, n_i, are retained.

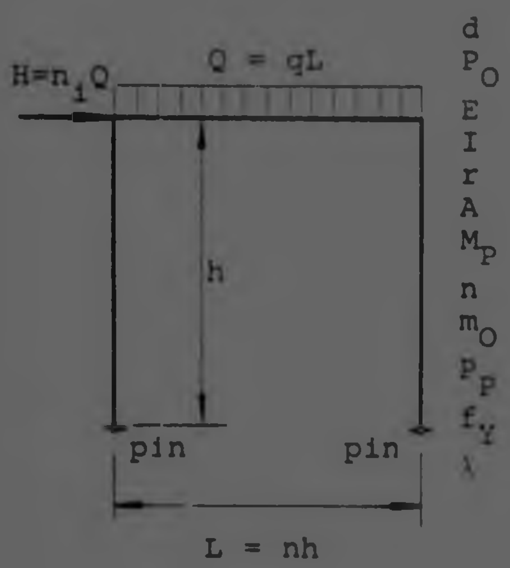

FIGURE 12a: Actual frame

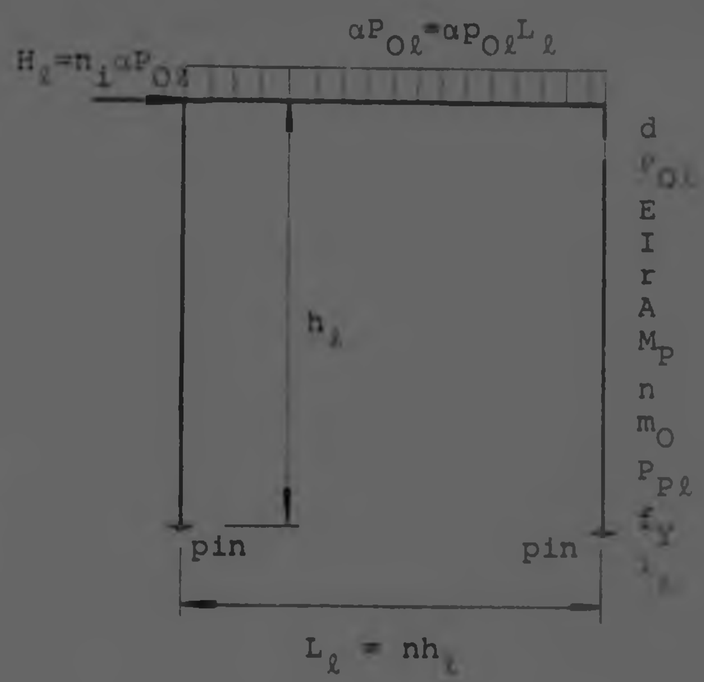

FIGURE 12b: "Limiting frame"

As for the case of "Symmetry-Buckling", the fictitious "elastic buckling load" αP_O can be related to the plastic collapse load P_P. For the frames of Figures 12a and 12b the following expression is valid:

$$\frac{\alpha P_O}{P_P} = \frac{\alpha E \kappa_2 m_O^2 (n+4n_i)}{32 f_Y \kappa_1} \quad \frac{1}{\lambda} \qquad |\text{EQN. } 7|$$

and for the "limiting frame", assuming a mode of collapse identical to the actual frame and ignoring the effect of axial forces.

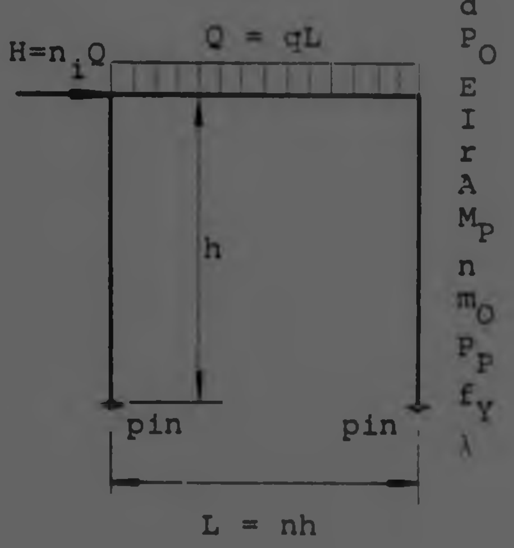

FIGURE 12a: Actual frame

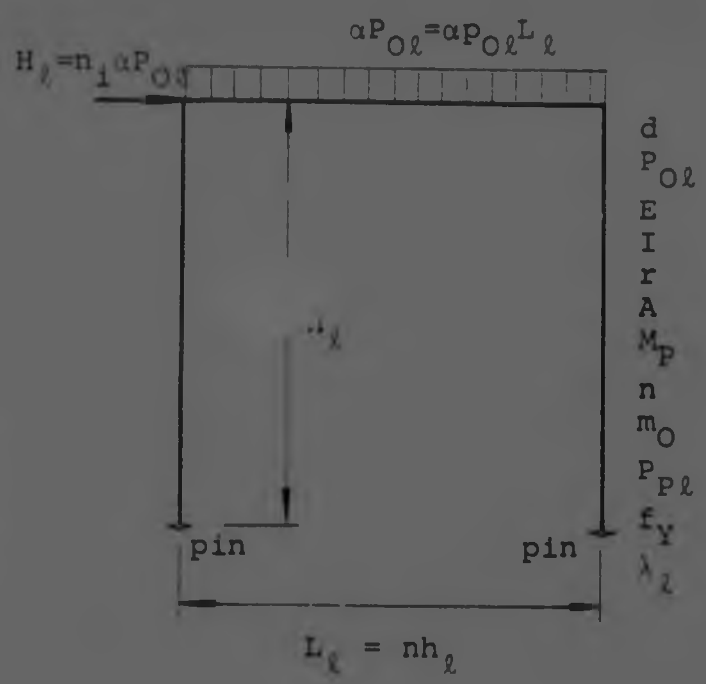

FIGURE 12b: "Limiting frame"

As for the case of "Symmetry-Buckling", the fictitious "elastic buckling load" αP_O can be related to the plastic collapse load P_P. For the frames of Figures 12a and 12b the following expression is valid:

$$\frac{\alpha P_O}{P_P} = \frac{\alpha E\kappa_2 m_O{}^2(n+4n_i)}{32f_Y\kappa_1} \quad \frac{1}{\lambda} \qquad |\text{EQN. 7}|$$

and for the "limiting frame", assuming a mode of collapse identical to the actual frame and ignoring the effect of axial forces.

$$\frac{\alpha P_{O\ell}}{P_{P\ell}} = \left(\frac{\alpha P_O}{P_P}\right)_\ell = \frac{\alpha E\kappa_2 m_O^{\,2}(n+4n_1)}{32 f_Y \kappa_1} \; \frac{1}{\lambda_\ell} \qquad |\text{EQN. } 8|$$

Actual and "limiting" frames are then related by the following expression:

$$\frac{\alpha P_O}{P_P} = \left(\frac{\alpha P_O}{P_P}\right)_\ell \frac{\lambda_\ell}{\lambda} \qquad |\text{EQN. } 9|$$

For frames falling on a particular interaction curve Equation 8 must furnish the same numerical value. This is achieved by keeping the first term of Equation 8 constant for identical "limiting slenderness ratios" λ_ℓ. Since the factor α is indirectly related to λ_ℓ, it will also remain unchanged as long as λ_ℓ is constant. The easiest way to generate a specific group of frames is to alter the column slenderness ratio λ in Equation 7, whilst maintaining the dimensional ratio $n=L/h$ and the load ratio n_1. This will neither influence the factor α nor the "limiting slenderness ratio", λ_ℓ, nor the elastic buckling load parameter, m_O. This has been confirmed by a computer analysis, the results of which appear in a later chapter of the thesis (Table 9 of chapter 10).

2.2.4 Multi-curve diagram

In the preceding sections a particular interaction curve was defined by its intersection point Y on the right axis of the interaction graph. The position of this intersection

$$\frac{\alpha P_{O\ell}}{P_{P\ell}} = \left(\frac{\alpha P_O}{P_P}\right)_\ell = \frac{\alpha E\kappa_2 m_O{}^2(n+4n_i)}{32f_Y\kappa_1} \frac{1}{\lambda_\ell} \qquad |\text{EQN. } 8|$$

Actual and "limiting" frames are then related by the following expression:

$$\frac{\alpha P_O}{P_P} = \left(\frac{\alpha P_O}{P_P}\right)_\ell \frac{\lambda_\ell}{\lambda} \qquad |\text{EQN. } 9|$$

For frames falling on a particular interaction curve Equation 8 must furnish the same numerical value. This is achieved by keeping the first term of Equation 8 constant for identical "limiting slenderness ratios" λ_ℓ. Since the factor α is indirectly related to λ_ℓ, it will also remain unchanged as long as λ_ℓ is constant. The easiest way to generate a specific group of frames is to alter the column slenderness ratio λ in Equation 7, whilst maintaining the dimensional ratio $n=L/h$ and the load ratio n_i. This will neither influence the factor α nor the "limiting slenderness ratio", λ_ℓ, nor the elastic buckling load parameter, m_O. This has been confirmed by a computer analysis, the results of which appear in a later chapter of the thesis (Table 9 of chapter 10).

2.2.4 Multi-curve diagram

In the preceding sections a particular interaction curve was defined by its intersection point Y on the right axis of the interaction graph. The position of this intersection point is a function of the ratio $(\alpha P_O/P_P)_\ell$ as given by Equations 5 and 8 respectively. It is obvious, that any variation of the parameters contained in these equations can lead to a different numerical result for $(\alpha P_O/P_P)_\ell$. In terms of the proposed method, this signifies that an infinite number of different interaction curves, with respect to the intersection point Y, could be generated. It is for this reason, that a multi-curve interaction diagram is proposed for the purposes of this research. The tendency of having more than one design curve for columns and beam-columns has been given ample attention in literature [75, 89-96]; however, so far this approach has not been attempted for entire frameworks.

The evaluation of a problem requires three steps:

a) The curve relevant to the particular problem has to be selected from the array of possible curves. This is achieved by calculating the ratio $(\alpha P_O/P_P)_\ell$ for the "limiting frame".

b) On the relevant curve, which represents a whole group of related frames, the particular frame under consideration has to be identified. This is accomplished by calculating the ratio $\alpha P_O/P_P$ for the actual frame. This ratio appears as a radial line of this slope through the origin of Figure 7. The intersection point of the radial line with the curve selected in a) above will locate the specific frame on its failure curve.

c) The distance from the intersection point to the upper ceiling (P_F/P_P=1,0) of Figure 7 is the measure by which the plastic collapse load P_P is reduced due to instability.

2.2.5 The ratios $\alpha P_O/P_P$ and $(\alpha P_O/P_P)_\ell$

The purpose of the two ratios was outlined at the end of the previous section, and their functional relationship was expressed in Equations 6 and 9 respectively. Thus, once the α-values are known, it will suffice to compute the elastic buckling load P_O and the plastic collapse load P_P for the actual frame. The ratio $\alpha P_{O\ell}/P_{P\ell}$ for the "limiting frame" can then be calculated by factoring $\alpha P_O/P_P$ by the ratio of the actual to "limiting slenderness ratio", i.e. $\frac{\lambda}{\lambda_\ell}$. The expressions given in Equations 6 and 9 are valid for all cases in which the effect of axial forces on the plastic moment capacity of the section can be ignored. Two other conditions may occur:

a) The hinge locations in the actual frame and the "limiting frame" are identical, but the plastic moment capacity of the section is influenced by the presence of axial forces. Since the plastic collapse load of the "limiting frame" is usually much smaller than that of the actual frame, the reduction of the plastic moment M_P due to axial load will be different for the two frames.

b) The plastic capacity of the column section is affected by the presence of axial forces, and certain column hinges in the actual frame are replaced by beam hinges in the analysis of the "limiting frame" because of a gain in the plastic capacity of the column section due to the lower axial forces of the "limiting frame". This is especially relevant for cases in which the plastic capacity of the column section is different from that of the beam section.

Both these aspects can be accounted for by establishing the plastic collapse load of the "limiting frame" from first principles. Alternatively, the ratio $(\alpha P_O/P_P)_\ell$ for these conditions may be evaluated on the basis of the "limiting slenderness ratio", λ_ℓ, as given in Equation 10, i.e. using a correction factor R. This factor would have to make provision for the variation in the influence of the axial forces on the plastic collapse load of the actual frame and the "limiting frame".

$$\left(\frac{\alpha P_O}{P_{PC}}\right)_\ell = \frac{\alpha P_O}{P_{PC}} \; \frac{\lambda}{\lambda_\ell} \; R \qquad |\text{EQN. 10}|$$

The additional suffix (C) in Equation 10 signifies that the plastic collapse load has been calculated giving due consideration to the presence of axial forces. In many cases it is possible to estimate the size of R. The factor α, which is concerned with the elastic analysis of the structure, is not affected by the abovementioned considerations.

2.3 Evolution of design curve shape

2.3.1 Procedure

Initially, the load-slenderness curves for a number of frames will be drawn for regular increments of the slenderness ratio λ. Subsequently, these curves will be converted into plots fitting a non-dimensional graph such as presented in Figure 7.

The principle is first demonstrated on the uniform symmetrical portal frame of Figure 10. For this frame the graph development procedure will comprise four consecutive stages. The frame of Figure 10 will be identified within each of the four stages and the status of the various parameters will be defined at the beginning of each stage. Thereafter, the method will be extended to include for horizontal loading and other changes.

The following two hypotheses need to be confirmed:

a) A group of frames as defined by Equation 5 can be presented on a common curve in a non-dimensional interaction diagram as shown in Figure 7.

b) On a particular failure curve, a frame of lower slenderness will have a higher failure load as related to its actual plastic collapse load than a more slender frame.

2.3.2 Vertical loading - "Symmetry-Buckling"

Stage 1

Constant parameters for the purpose of the example:

I, A, r, E, f_Y.

Constant parameters for any one curve:

$(m_O{}^2EA)$ for a particular EA and base fixity, n, $P_{O\ell}$.

Variable parameters for any one curve:

λ, P_O, h, $L=nh$.

These parameters apply to Figure 13 and to a problem such as given in Figure 10.

Following the Euler principle, the elastic buckling load of frames can be expressed as $P_O=m_O{}^2EA/\lambda^2$ where m_O, which is a function of L/h for the given problem, reflects the elastic buckling load of the complete frame. This hyperbolic function is presented in Figure 13 for frames of different geometry. Each curve corresponds to a certain ratio $n=L/h$, which is given as a ringed number next to the point on the relevant curve marked thus ✦. For a particular value of slenderness ratio, λ, the curves only differ by the factor m_O, which in turn remains unchanged for any one curve when λ varies. The variation in λ is then achieved by modifying the member lengths h and L. Hence each curve of Figure 13 represents a whole group of frames. For any one group of frames with a specific geometry factor $n=L/h$, the buckling load, axial member forces, bending moments and thus stresses can be expressed as a function of the term $m_O{}^2EA/\lambda^2$. Recognising that for given base and

2.3.2 Vertical loading - "Symmetry-Buckling"

Stage 1

Constant parameters for the purpose of the example:

I, A, r, E, f_Y.

Constant parameters for any one curve:

$(m_O{}^2EA)$ for a particular EA and base fixity, n, $P_{O\ell}$.

Variable parameters for any one curve:

λ, P_O, h, $L=nh$.

These parameters apply to Figure 13 and to a problem such as given in Figure 10.

Following the Euler principle, the elastic buckling load of frames can be expressed as $P_O=m_O{}^2EA/\lambda^2$ where m_O, which is a function of L/h for the given problem, reflects the elastic buckling load of the complete frame. This hyperbolic function is presented in Figure 13 for frames of different geometry. Each curve corresponds to a certain ratio n=L/h, which is given as a ringed number next to the point on the relevant curve marked thus ✦. For a particular value of slenderness ratio, λ, the curves only differ by the factor m_O, which in turn remains unchanged for any one curve when λ varies. The variation n λ is then achieved by modifying the member lengths h and L. Hence each curve of Figure 13 represents a whole group of frames. For any one group of frames with a specific geometry factor n=L/h, the buckling load, axial member forces, bending moments and thus stresses can be expressed as a function of the term $m_O{}^2EA/\lambda^2$. Recognising that for given base and

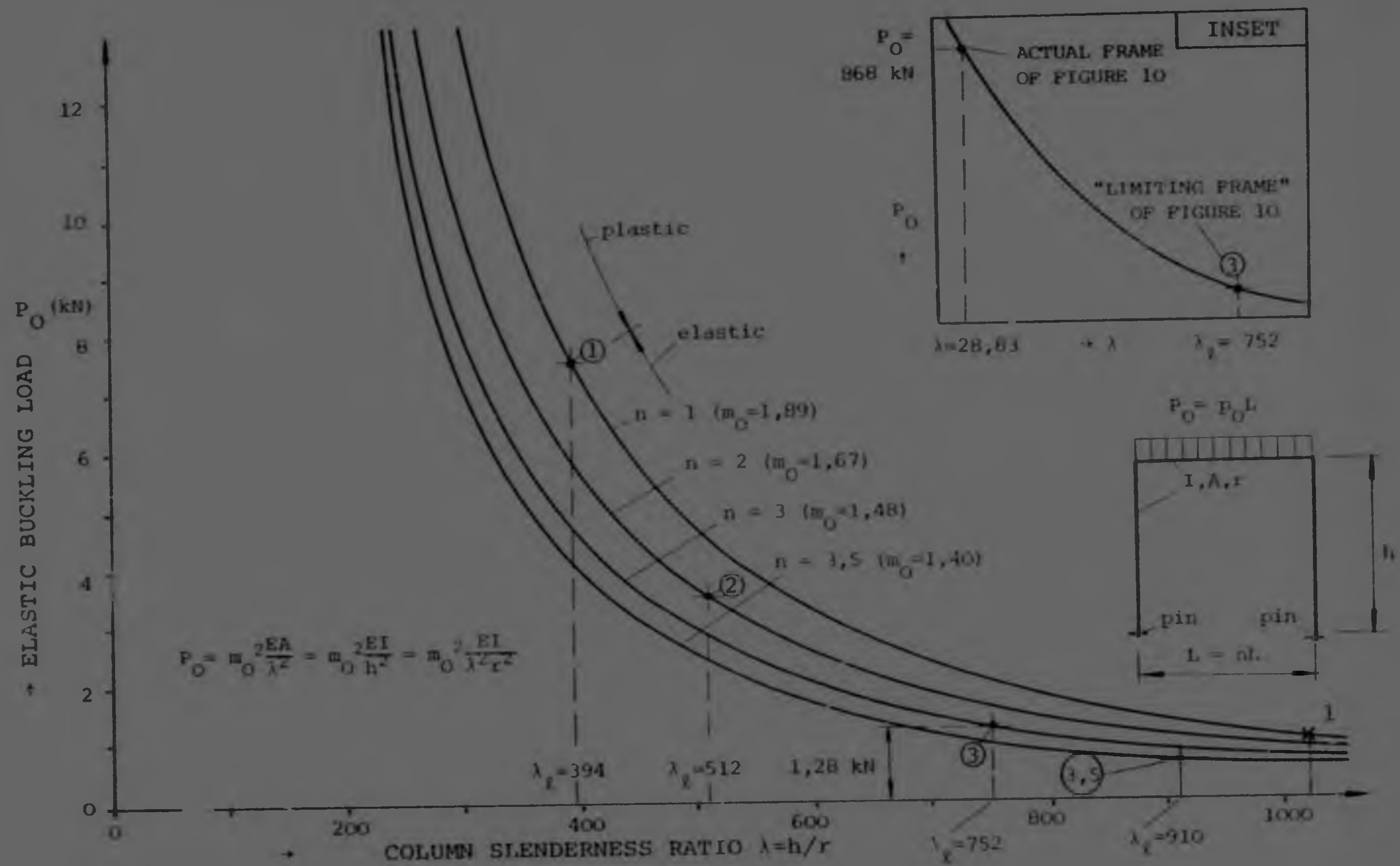

FIGURE 13: Elastic buckling load of frames

loading conditions, m_O is solely a function of n, the stress function can be expressed as follows:

$$\text{stress} = f\left(n; \frac{EA}{\lambda^2}\right)$$

If the frame geometry n and its parameters E and A are known and if, furthermore, the stress is equated to the stress value at the onset of yield, the above expression can be solved for a specific value λ, called the "limiting slenderness ratio" λ_ℓ. This parameter is well known in individual column design and has here been applied to frames in a similar way.

The slenderness ratios λ_ℓ and the corresponding points on the buckling curve are marked thus ✦ in Figure 13. They indicate the transition from elastic to inelastic failure, and the associated failure load would equal $P_{O\ell} = m_O^2\ EA/\lambda_\ell^2$. The corresponding frame has been defined as the "limiting frame".

<u>Example frame of Figure 10</u>

The "limiting slenderness ratio" λ_ℓ for this frame (n=3) was calculated in section 2.2.2 as λ_ℓ = 752. With m_O=1,48 follows:

actual frame: $P_O = m_O^2 \frac{EA}{\lambda^2}$ = 868 kN

"limiting frame": $P_{O\ell} = m_O^2 \frac{EA}{\lambda_\ell^2}$ = 1,28 kN

The latter result, together with the limiting slenderness λ_ℓ, is marked on Figure 13. The buckling load P_O of the actual frame would fall outside the graph for the scale chosen in Figure 13. The relevant curve is therefore shown again in the inset to Figure 13.

<u>Stage 2</u>

Constant parameters for the purpose of the example:

I, A, r, E, f_Y, M_P.

Constant parameters for any one curve:

$L_\ell=L$, L/r, λ_ℓ, h_ℓ, $P_P=P_{P\ell}$, $P_{O\ell}$, $m_{O\ell}$, r

Variable parameters for any one curve:

h, λ, m_O, P_O, P_F, $n=L/h$.

These parameters apply to Figures 14 and 15 and to a problem such as given in Figure 10.

From stage 1, only the transition points, again shown thus ✦, have been transferred to another diagram depicting the frame failure load P_F on the vertical axis (Figure 14). These transition points correspond to the "limiting frame" which is characterised by a dimension ratio $n_\ell=L_\ell/h_\ell$, given ringed next to the points marked thus ✦ in Figure 14, and the "limiting slenderness ratio", λ_ℓ. A particular curve of Figure 14 is obtained by keeping the beam length constant at a size corresponding to that of the "limiting frame", i.e. $L=L_\ell = n_\ell\lambda_\ell r$. At the same time, the column height is allowed to vary from zero to infinity. As a result, L is different for different curves since n_ℓ and λ_ℓ changes and, in addition, for any one curve the ratio L/h varies from

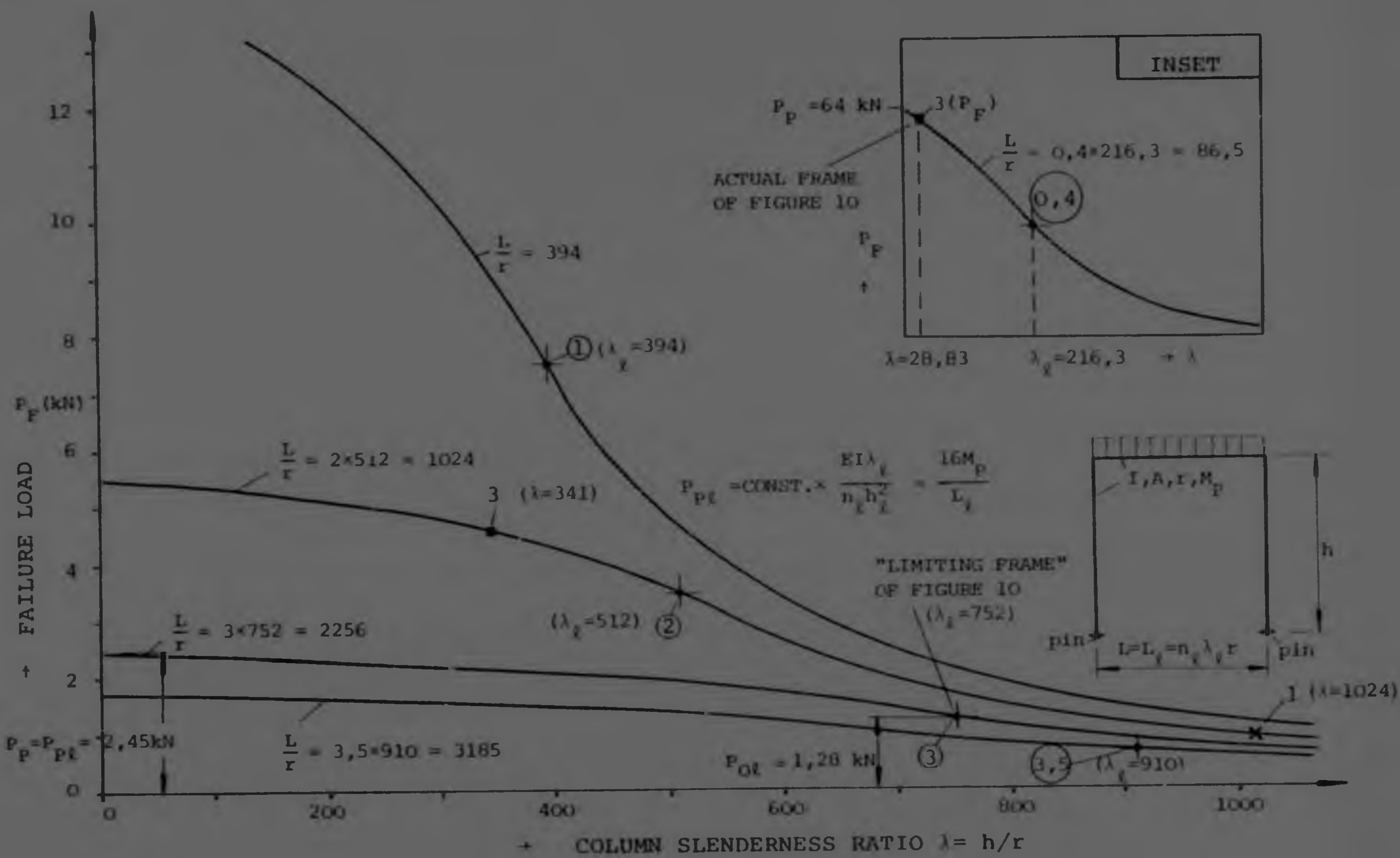

FIGURE 14: Failure loads of frames

zero to infinity because of the height change.

With reference to the constant parameters stipulated for this stage, individual curves will have a constant ratio L/r and plastic collapse load $P_p=16M_p/L$. Due to the variation in L, different curves will show proportionally different P_p values on the vertical axis. At the limiting conditions the plastic collapse load would be $P_{p\ell}=P_p$, and the elastic buckling load would equal $P_{O\ell}=m^2_{O\ell}EA/\lambda^2_\ell$, as already derived for stage 1.

The curve section between the "limiting slenderness ratio" λ_ℓ and $\lambda=0$, represents frames failing by inelastic instability. In this region the curve shapes of Figure 14 are empirical. For this research it has been assumed that the curves branch-off tangentially from the exact elastic buckling curves, applicable to frames with slenderness ratios greater than the "limiting slenderness ratio" λ_ℓ. At the other end, near $\lambda=0$, the failure curves of frames would gradually reach the plastic collapse load in a near-tangential approach. Similar curve shapes were suggested by Lu[4] based on an exact elasto-plastic analysis for pinned-base portal frames. Scholz[37] confirmed the general curve shapes by testing four small-scale portal frames with constant beam length but varying column height.

Curves of the nature assumed in Figure 14 will eventually lead to the final interaction graph proposed in this research. These interaction curves were compared with a number of discrete theoretical solutions and results of various laboratory tests. A good agreement was obtained.

It needs to be mentioned that frames falling on a particular curve of Figure 14 correspond to different "limiting frames" by definition of Equation 5. In fact, in simple terms, Figure 14 represents a series of curves for frames with different beam and column stiffnesses in which each curve represents all the frames with the same beam length and fully plastic collapse load, but not the same λ_ℓ or $P_{O\ell}$.

Points on the curves of Figure 14 other than the transition points can be identified by referring to the relevant "limiting slenderness ratio". This is demonstrated by obtaining some points on the curve passing through the transition point marked 2 +, for which L/r=1024.

Elastic range

To find a point 1 × on the curve of Figure 14, corresponding to a slenderness ratio λ=1024, it is necessary that the column height is double that of the "limiting frame", for which λ_ℓ=512 and n_ℓ=2. The modified frame column will thus attain a slenderness ratio of 1024 and n would change to 1. Returning to Figure 13, the corresponding point for λ=1024 is found on the curve for n=1 and has been marked thus 1 ×. The relevant failure load, which is elastic, will equal $m_O^2 EA/1024^2$, where m_O refers to a frame with n=1.

Inelastic range

Points in the inelastic range such as 3 ■ can be related to column heights by simple proportion from the limiting condition, i.e. the column height and slenderness ratio corresponding to point 3 ■ (n=3) would have to be $n_\ell/n=2/3$ times those at the limiting condition, i.e. $\lambda=341$ applies. The failure load P_F applicable to the frame with $\lambda=341$ is evaluated from empirical curves, as discussed previously in this section.

Example frame of Figure 10

Frames with the same ratio $n=L/h$ of Figure 14 are found on different curves. By definition of Equation 5 such frames have the same "limiting frame" and "limiting slenderness ratio". For the frame of Figure 10, n=3 and $(L/r)_\ell=n\lambda_\ell=2256$, the corresponding "limiting frame" with $\lambda_\ell=752$ is marked thus ③ ✦ in Figure 14.

A summary of results applicable to this "limiting frame" is given below:

$$M_P = f_Y \frac{d^3}{4} = 4 \text{ KNm}$$

$$L_\ell = n_\ell \lambda_\ell r = 26{,}08 \text{ m}$$

$$P_{P\ell} = \frac{16 M_P}{L_\ell} = \frac{16 \times 4}{26{,}08} = 2{,}45 \text{ kN}$$

$$m_{O\ell} = 1{,}48$$

$$P_{O\ell} = \left(\frac{m_{O\ell}}{\lambda_\ell r}\right)^2 EI = 1{,}28 \text{ kN}$$

$$\left(\frac{P_O}{P_P}\right)_\ell = 0,52$$

The plastic collapse load for the actual frame of Figure 10 is given by

$$P_P = \frac{16M_P}{L} = 64 \text{ kN}$$

To identify the failure load of this actual frame on curves such as given in Figure 14, it is argued that a curve will exist for which L/r=86,5. In this instance, the beam length and the plastic collapse load will both coincide with that of the actual frame of Figure 10. The condition described above may come about for a curve such as shown in the inset to Figure 14. On this particular curve the actual frame with λ=28,83 can be located by proportional reference to the relevant transitional slenderness ratio of 216, which corresponds to a value n=0,4. The failure load P_F of the actual frame is indicated on the same curve.

Stage 3

For stage 3, the same definition of parameters applies as for stage 2.
This stage involves the simple transfer of all curves and the points marked on the curves of Figure 14 to a new plot giving the non-dimensional ratio P_F/P_P on the vertical axis rather than the absolute failure load P_F (Figure 15). As a result, all curves of Figure 15 run into the common intersection point P_F/P_P=1,0 on the vertical axis. The

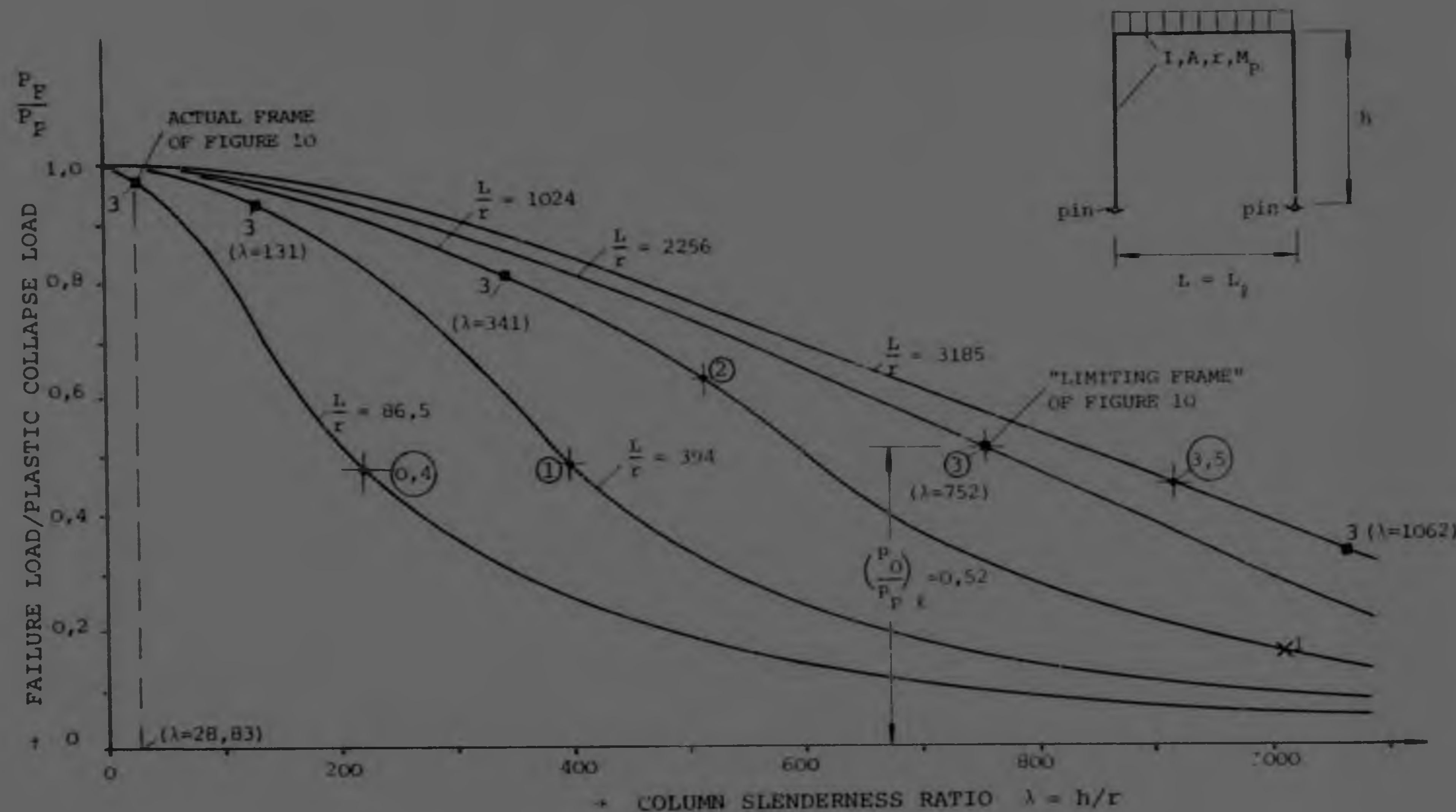

FIGURE 15: Failure load to plastic collapse load

constraint of constant beam length for the individual curve of Figure 14 throughout the λ-range still applies.

For the example frame of Figure 10 the position of the actual frame with L/r=86,5 as well as the ratio $(P_O/P_P)_\ell$ are indicated on the relevant curves of Figure 15. It must be reiterated that by definition of Equation 5 the actual and "limiting" frames are not located on the same curve. This will only be accomplished in the final interaction graphs.

Stage 4

Constant parameters for the purpose of the example:

I, A, r, E, F_Y, M_P.

Constant parameters for any one curve:

$\lambda_\ell, h_\ell, L_\ell, L_\ell/h_\ell, L/h, m_O, n, P_{O\ell}, P_{P\ell}, (P_O/P_P)_\ell$

Variable parameters for any one curve:

$\lambda, P_O, h, P_F, P_P, L=nh$.

These parameters apply to Figure 16 and a problem such as given in Figure 10.

In stage 4 the construction of the final interaction plot of Figure 16 will be explained for frames with a common dimensional ratio n . For this purpose, it is necessary to identify the points on the different L/r curves of Figure 15 which correspond to the same value of n=L/h=3, i.e. points corresponding to $\lambda=h/r=(1/n)(L/r)$. Hence point 3 ■ on the curve for L/r=1024 corresponds to $\lambda=1/3\times1024$.

Likewise, other points 3 ■ have been indicated on all curves of Figure 15. The relevant point on the curve for L/r=3185 is found on the elastic curve section. For the curve applicable to L/r=2256, the transitional point is directly valid. Points on the curves for L/r less than 2256 will fall in the inelastic region.

It is possible to change the horizontal axis to represent the dimensionless ratio P_F/P_O in Figure 16, by noting that the slope of any radial line through the origin, $\tan \Omega = (P_F/P_P)/(P_F/P_O) = P_O/P_P$. Thus any point on Figure 15, corresponding to a specific value of n, can be transferred onto Figure 16 by recording the relevant value of P_F/P_P (vertical axis of Figure 15) and calculating the magnitude of P_O/P_P for the associated value of λ (horizontal axis of Figure 15). The scale of the slope of the radial line through the origin is determined from the slope of the line through the limiting value $(P_O/P_P)_{\lambda}$. The ratio of these slopes is inversely proportional to the relevant slenderness ratios for frames with the same geometric parameters. In this way points 3' ■ on the curve of Figure 16 can be developed from equivalent points 3 ■ of Figure 15.

The resulting plot is taken as the common locus of all frames with a dimensional ratio n=3 for portal frames with a uniformly distributed beam loading, pinned bases, equal column and beam properties I, A, κ_1 and κ_2. For such frames, the buckling parameter m_0 remains unaltered

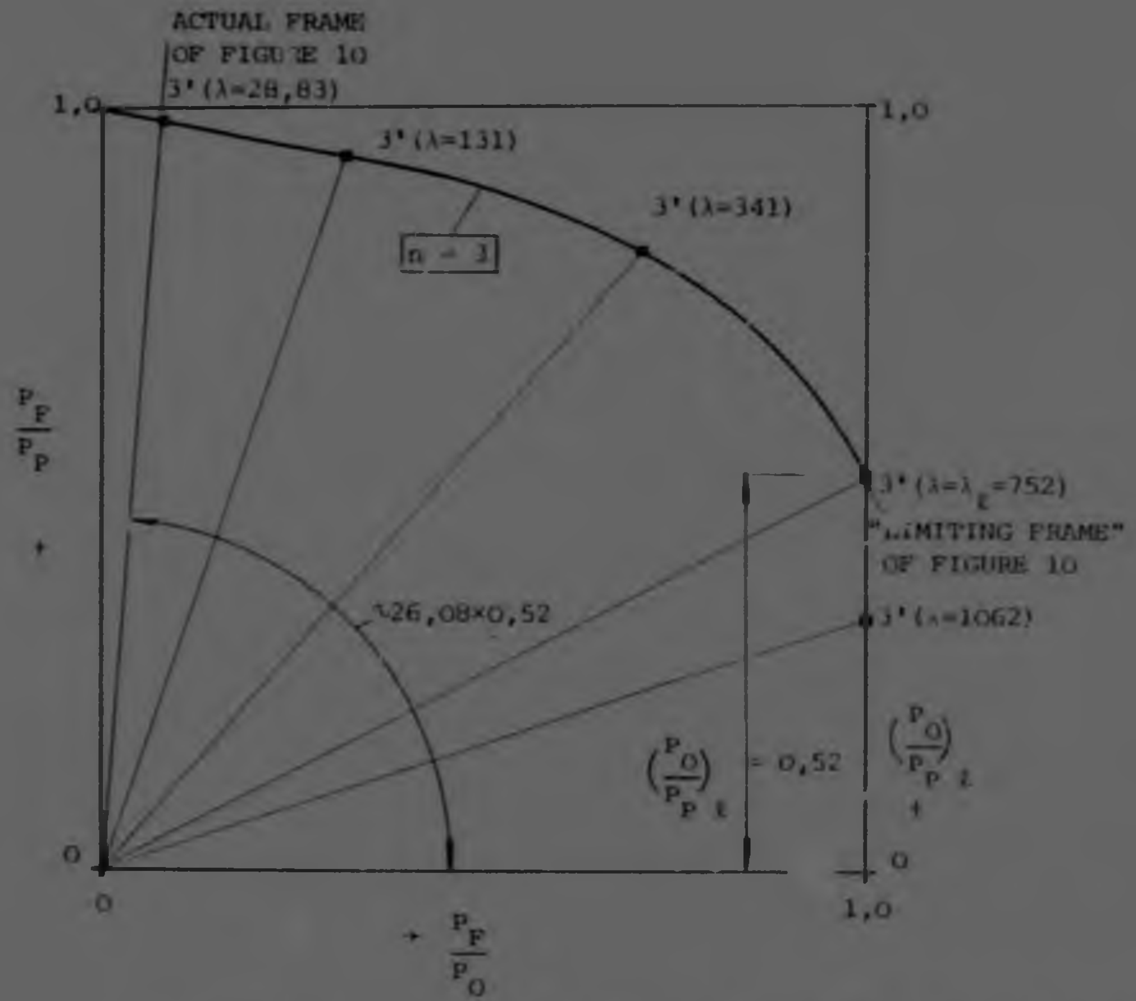

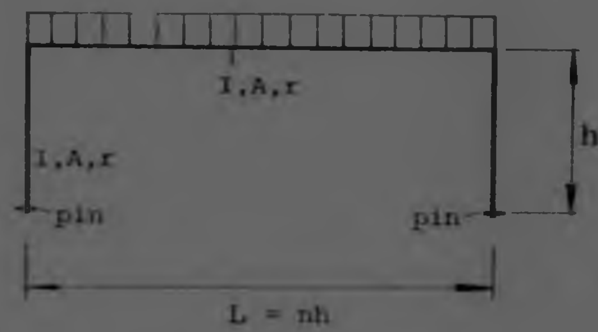

P_F = Failure Load

P_P = Plastic Collapse Load

P_O = Elastic Buckling Load

FIGURE 16: Interaction curve derived from load-slenderness relationship

despite the variation in the absolute length of the members.

Within the slenderness range $0<\lambda<\lambda_\ell$ the curve represents inelastic failure, with a load P_F/P_P or P_F/P_O, and for $\lambda>\lambda_\ell$, failure would be elastic with $P_F=P_O$. A specific frame on the curve of Figure 16 is located by plotting the radial line of slope P_O/P_P from its actual parameters.

It is important to recognise that in the process of constructing the curve of Figure 16, the previous constraint of constant beam length L, applicable to Figures 14 and 15, has been removed since different points 3' stem from different curves of Figures 14 and 15. Similarly, different plastic collapse load values P_P correspond to different points on the curve of Figure 16.

<u>Example frame of Figure 10</u>

Once a curve, such as that in Figure 16, is derived for a specific value of n, all one needs to identify for the frame of Figure 10 is the ratio P_O/P_P or λ. Using as the scale of the slope of the line through the origin, the slope of the line through the limiting point, the actual frame can be located. Thus, for a frame of constant geometric proportions such as the frame of Figure 10 follows:

$$\frac{P_O/P_P}{(P_O/P_P)_\ell} = \frac{868/64}{0,52} \approx 26,08 \text{ or } \frac{\lambda_\ell}{\lambda} = \frac{752}{28,83} \approx 26,08$$

Both slopes, i.e. P_O/P_P and $(P_O/P_P)_\ell$, and the failure load ratio P_F/P_P have been entered in Figure 16.

Conclusion

With the development of the curve in Figure 16 for n=3 for the special case of "Symmetry-Buckling" it has been shown that a specific group of frames, characterised by a constant "limiting slenderness ratio" λ_ℓ and particular values E, f_Y, κ_1, κ_2, n and m_c, can be presented on one interaction curve. Furthermore, frames falling on a particular interaction curve would progressively reach a higher failure load ratio P_F/P_P as their slenderness diminishes.

The behaviour summarised in this conclusion confirms the two hypotheses formulated in section 2.3.1. It is also easy to verify that in Figure 16 different curves would be obtained for different dimensional ratios n. The principal difference between these curves is the ratio $(P_O/P_P)_\ell$ of their "limiting frames".

2.3.3 Non-symmetrical conditions

In many ways a frame subjected to arbitrary loading behaves similarly to a frame subjected to vertical, symmetrical loading. As mentioned in section 2.2.3, for cases involving general loading (e.g. horizontal loading) a fictitious "elastic buckling load" αP_O, below the actual elastic buckling load P_O, will be selected, with the reduction factor α closely related to the "limiting slenderness ratio". Hence, for combined loading elastic failure curves would deviate by a factor α from the hyperbolic curves of Figure 13.

For the general load case, failure curves such as shown in Figures 14 and 15 cannot be plotted since individual curves were based on a constant beam length L throughout the λ-range. As a result, the plastic collapse load P_P remained unaltered as the column height was changed. If a horizontal load were added, the plastic collapse load P_P would increase as the column height diminishes. However, the constraint of constant beam length was finally removed for the interaction graph of Figure 16. In fact, the intermediate plots of Figures 14 and 15 were only presented here to facilitate the understanding of the development process behind the final interaction curves.

The supposition that a curve, such as that in Figure 16, is also applicable to combined loading is based on the following two conditions:

Firstly, that frames with the same dimensional properties $n=L/h$, particular geometric properties I, A, E and subjected to a specific load arrangement could be classified into a common group of frames at the limiting conditions. This would satisfy Equation 8 for specific values m_O, E, f_Y, κ_1 and κ_2.
Secondly, that frames on a particular interaction curve would display a progressively increasing failure load P_F as their slenderness reduces.

Both these points have been confirmed by elastic second-order computer solutions, which were processed in a similar way as described for the case of "Symmetry-Buckling". The second statement has also been checked by appropriate laboratory testing and the relevant results are published in a later chapter of this thesis (Table 9 of chapter 10).

2.3.4 The extended n-ratio to cover variations in sectional properties and strength

If the ratio $n=L/h$ is extended to include sectional variations between the members, e.g. n becomes $(L/h)(I_C/I_B)$, or allowance is being made for a difference in beam to column depth or beam to column strength, this will not be reflected in the elastic buckling loads P_C and $P_{O\ell}$. It must be remembered that the inertia ratio is in itself not significant since the ratios L/h and I_C/I_B are interchangeable with respect to the elastic buckling loads as well as the corresponding parameters m_O and $m_{O\ell}$.

However, the above variations will influence the plastic collapse loads P_P and $P_{P\ell}$, the reduction factor α and the "limiting slenderness ratio" λ_ℓ. The change in the plastic collapse load P_P is absorbed by the non-dimensional axis parameter P_F/P_P in graphs such as given in Figure 16. The other variations can only produce a deflection from the basic curve shape which is shown as a solid line in Figure 17. The dashed lines in Figure 17 represent possible curve modifications to account for sectional or strength variations.

A similar effect occurs, when different subassemblages or load arrangements are compared. In fact, these influences can also change the elastic buckling parameters m_C and $m_{O\ell}$.

Notwithstanding these modifications, the two principal hypotheses of section 2.3.1 are confirmed.

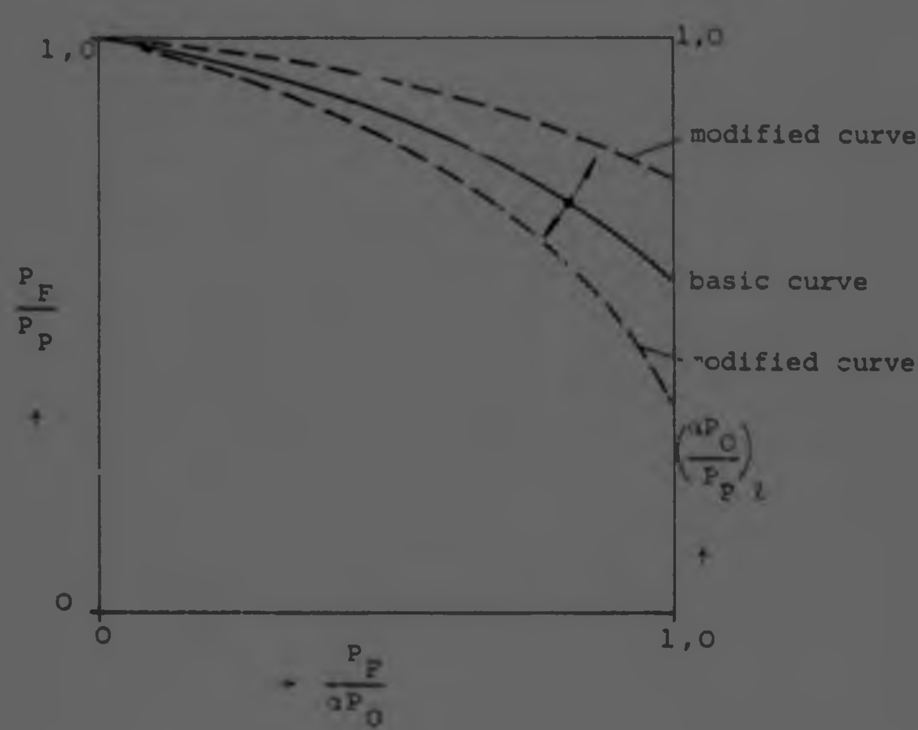

FIGURE 17: Influence of sectional and strength variations

The phenomena described above, together with the wide variety of possible load applications, base conditions and subassemblage shapes makes it impractical to present curves such as that in Figure 16 as a function of the dimensional ratio n. A vast number of different curve shapes would be necessary to cover all these eventualities for a given value of n. Hence, more conveniently, the ratio $(\alpha P_O/P_P)_\ell$ at the limiting conditions is proposed as the dominant variable. This ratio appears on the right, vertical axis of the non-dimensional diagram of Figure 16. Thus, for a particular frame $(\alpha P_O/P_P)_\ell$ has to be evaluated to select the curve applicable to the problem. Conveniently, the ratio $(\alpha P_O/P_P)_\ell$ can be determined in the way as already shown in Equations 6, 9 and 10 and as outlined in section 2.2.5. The value α, which is related to the "limiting slenderness ratio", will be derived in section 6.1 of this thesis.

2.4 Some general applications

The mechanics of using interaction curves such as that in Figure 16 and the implications of the fictitious "elastic buckling load" αP_O are briefly outlined in a general way. Some cases are examined in this context, exposing the shortcomings of the Merchant-Rankine approach and demonstrating the improvements achieved by this research at the same time.

If the Merchant-Rankine rule is used to compare two identical frames, one subjected to vertical loading and one to vertical and horizontal loading, it would appear on first sight that the addition of a horizontal loading, such as shown in Figure 18, would have a favourable influence on the behaviour of the frame in regard to instability. However, by intuition, one would expect the opposite to be true.

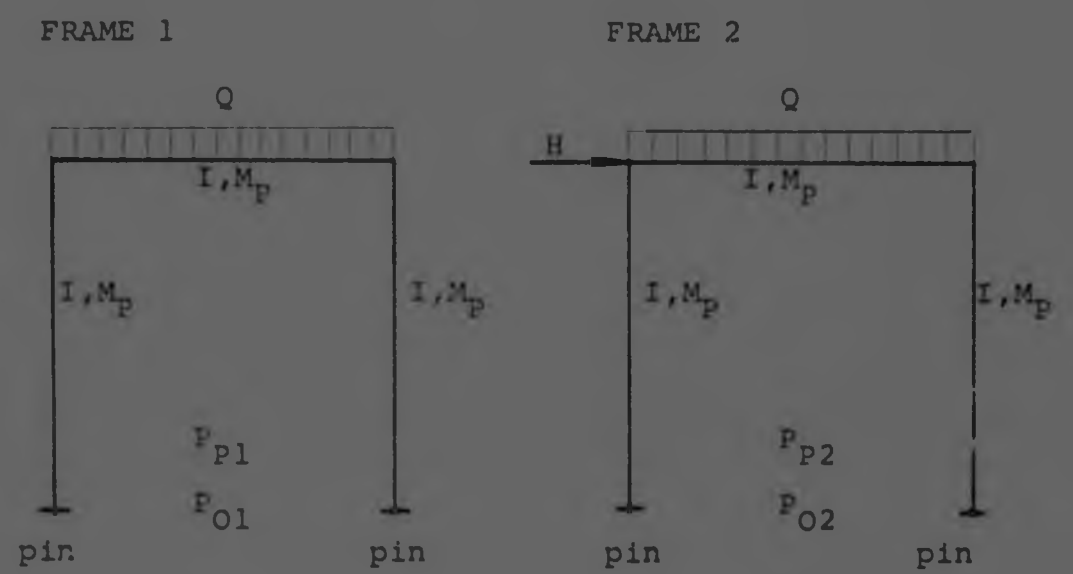

FIGURE 18: Frames subjected to vertical or combined loading

For otherwise identical frames, the plastic collapse load P_P reduces when a horizontal load is added, whereas the elastic buckling load P_O remains constant, i.e. for the conditions of Figure 18, the following applies:

$$P_{P1} > P_{P2}$$

$$P_{O1} = P_{O2} = P_O$$

and thus, $\tan\Omega_1 < \tan\Omega_2$ for the Merchant-Rankine rule.

The two slopes $\tan\Omega_1$ and $\tan\Omega_2$, both referring to actual conditions, have been entered in Figure 19 for comparison. The distance from the curve intersection points S_1, S_2, R_1 and R_2 to the load level $P_F/P_P=1,0$ represents the reduction to the plastic collapse load due to frame instability.

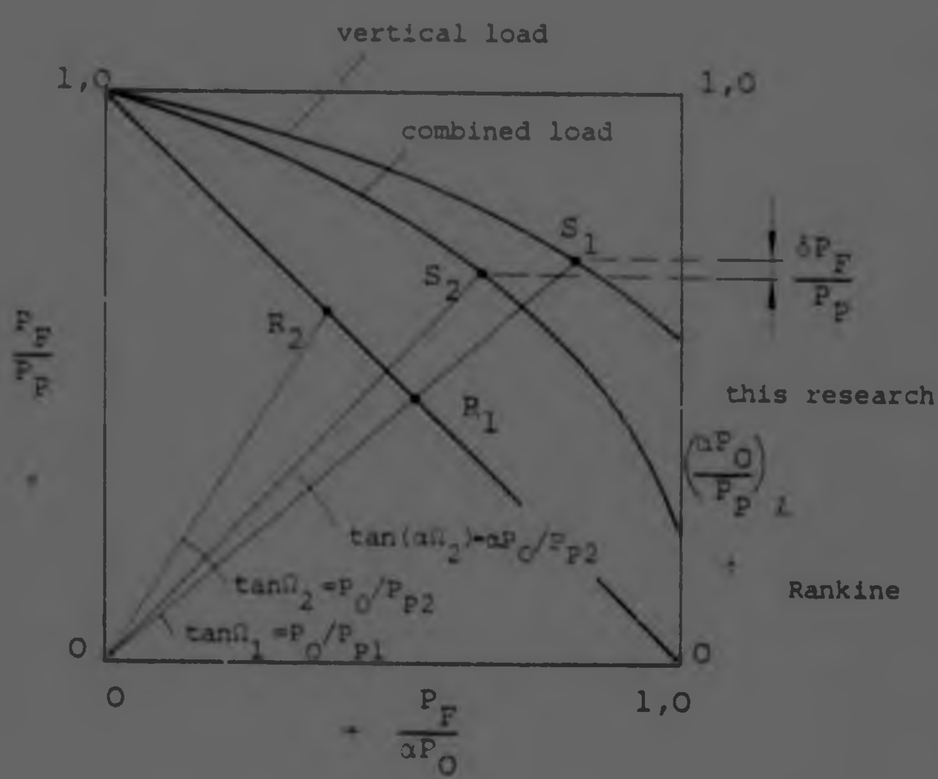

FIGURE 19: Effect of combined loading

The Merchant-Rankine rule assigns a higher relative loss in load carrying capacity due to instability to frame 1 since the intersection point R_1 lies below R_2. This effectively equates instability to the magnitude of the applied load, whereas it should rather be a function of applied load and corresponding sway.

Using the proposals developed in this research, intersection points S_1 and S_2 may be obtained for frame 1 and frame 2 respectively. A different curve, at a level below that for vertical load, would be applicable to combined loading due to an increase in the "limiting slenderness ratio". The slope $\tan\Omega$ is not presented as P_O/P_p but rather as $\frac{1}{[illegible]}$ (Equations 4 and 7). In addition to that, for cases other than "Symmetry-Buckling", a nominated fictitious "elastic buckling load" αP_O, less than P_O, will contribute to conservatism in the evaluation of $\tan\Omega$.

The intersection points S_1 and S_2 are thus brought into the correct perspective, i.e. S_2 falls below S_1. It has been speculated earlier that the Merchant-Rankine formula is conservative. Hence, if the failure loads pertaining to S_1 and S_2 are taken as being correct, then R_1 should fall below S_1 and R_2 below S_2 in Figure 19. This requirement, together with the fact that R_1 is less than R_2, whereas it should be greater than R_2, shows that methods based on the ratio of the elastic buckling load P_O to plastic collapse load P_p can be little better than just a safe lower bound.

In this context it is opportune to emphasise and illustrate the following further shortcomings of the Rankine-based methods:

a) No real distinction is being made between a difference in the type of the beam loading.

This is demonstrated on a pin-based portal frame subjected to different types of vertical beam loading, but otherwise identical conditions, as shown in Figure 20.

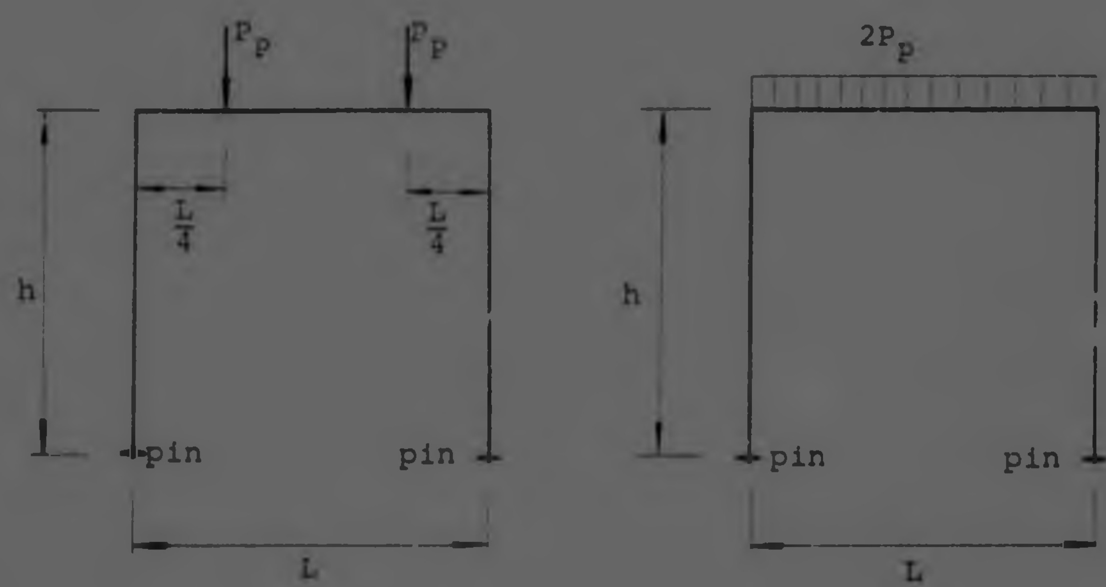

FIGURE 20: Frames subjected to different beam loading

The plastic collapse load P_P and the elastic buckling load P_O are the same for both frames of Figure 20. Hence, Rankine-based methods would predict identical failure loads P_F. However, it can be verified that the given loadings would impose different deformed shapes on the structure in the elastic and post-elastic range. The different curvatures would correspond to different second-order forces.

This behaviour, which is ignored by other methods, is reflected in the method developed in this research by considering the actual load arrangement when determining the curve intersection points Y on the axis for $(P_O/P_P)_F$.

Different failure loads P_F are thus obtained for the portal frames of Figure 20, since different failure curves will be evaluated, as illustrated in Figure 21.

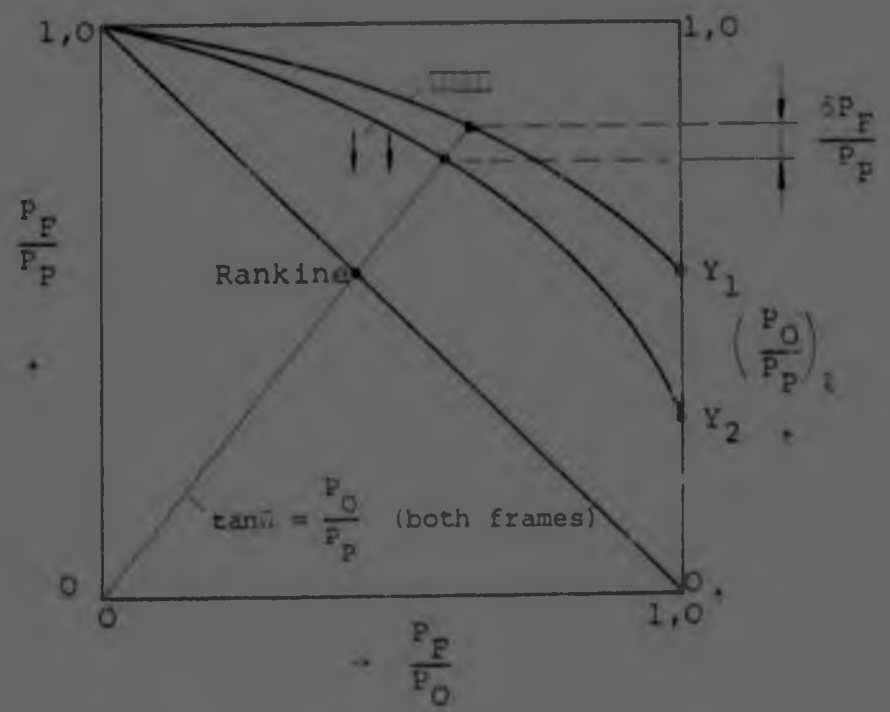

FIGURE 21: Non-dimensional failure diagram for different beam loading

b) A gradual transition between and within failure mechanisms is not fully recognised.

This is demonstrated on a fixed-base portal frame with given geometric properties. The frame of Figure 22 would give rise to unchanged failure loads P_F for the entire range of either collapse mode i) or iii) when analysed by the Merchant-Rankine rule, despite differences in the magnitudes of the applied loads.

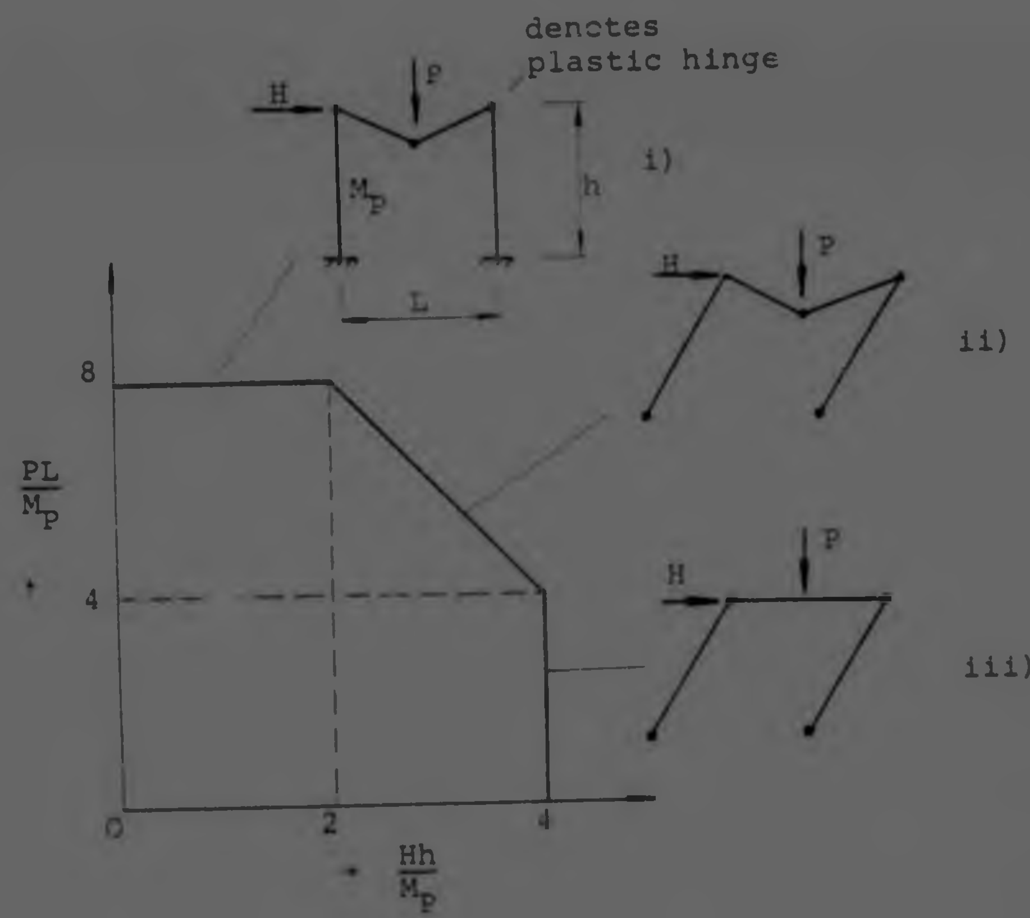

FIGURE 22: Failure modes of fixed-base portals

For collapse mode i), for example, the plastic collapse load, P_p, for a given frame, would result in the constant value $P_p=8M_p/L$ despite the variation in H from zero to $2M_p/h$. For practical purposes, the same frame would also be characterised by a constant elastic buckling load, P_O. Therefore, the ratio P_p/P_O and thus the failure load P_F remain unaltered for mode i). Similarly, for mode iii), the elastic buckling load, P_O, and the plastic collapse load, $P_p=H_p=4M_p/h$, stay constant when the vertical load P changes from P=0 to $P=4M_p/L$. Model frame M2, investigated for vertical and combined loading, serves to amplify the aspect described in this paragraph (see section 10.5 and Table 9).

The multi-curve interaction method developed in this research differentiates between such cases of varying load, providing a gradual change in failure load between and within collapse modes.

c) For cases of pure vertical loading proper cognisance is not taken of the fact that the unbraced frame may approach the braced frame capacity for finite values of P_F/P_O.

This has been amply illustrated in publications by Lu[4] and Scholz[illegible]. It suffices to note that certain unbraced frames display a failure load which very nearly equals the failure load of a braced but otherwise identical frame. The difference, in fact, is so small that it may be ignored, and a "braced" treatment would be allowed for the actual unbraced frame. A considerable economic penalty may be imposed on such structures if this aspect is neglected.

2.5 Proposed interaction curves

2.5.1 Basic curves

Based on the theory outlined in the preceding sections of this chapter the design graph of Figure 23 has been proposed. The curve shapes, which are empirical, will be

P_F = Failure Load
P_P = Plastic Collapse Load
P_O = Elastic Buckling Load
α = Reduction Factor

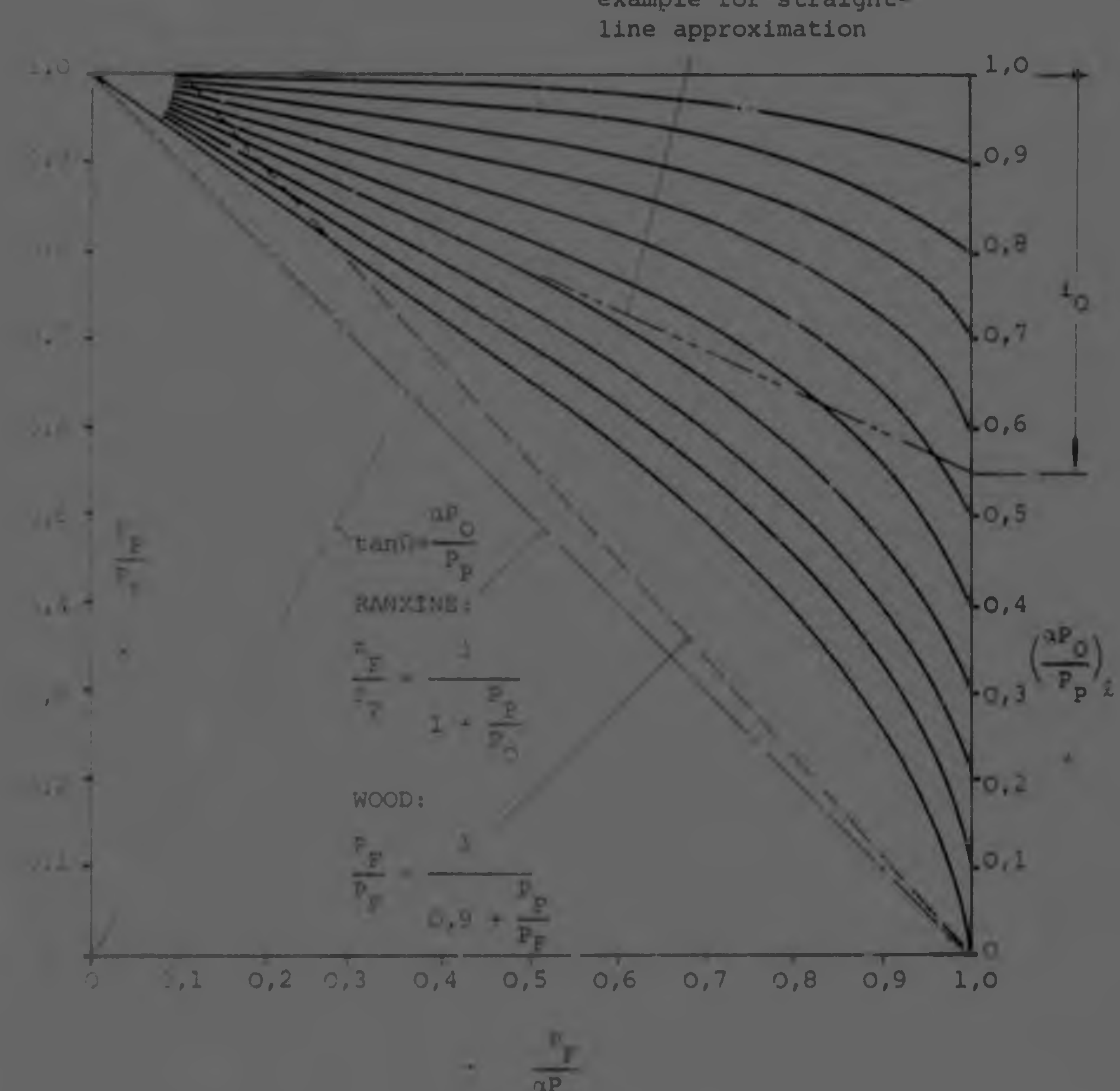

FIGURE 23: Basic interaction curves

compared with a number of exact theoretical solutions and results of laboratory tests in a later chapter of this thesis. The formulations by Merchant-Rankine and Wood are also entered in Figure 23.

The curves of Figure 23 together with the elastic parameters αP_O and λ_ℓ, which are typically obtained by computer analysis, are the fundamental components of the proposed method. It will also be demonstrated at a later stage that the required computer results can be presented in graphical form (chapter 11 and Appendix VI). Moreover, a simplified analytical procedure to obtain the elastic parameters will be described in chapter 12.

2.5.2 Straight-line approximation

A satisfactory straight-line approximation to the curves of Figure 23 has also been formulated within the $P_F/\alpha P_O$ range of 0 to 0,60. The straight-line Equation 11 has been derived from the curved $(\alpha P_O/P_P)_\ell$ -values of Figure 23 by utilising the intersection points i_O of straight lines through $P_F/P_P = 1,0$.

An approximate expression for the intersection points is compared with the actual values in Figure 24.

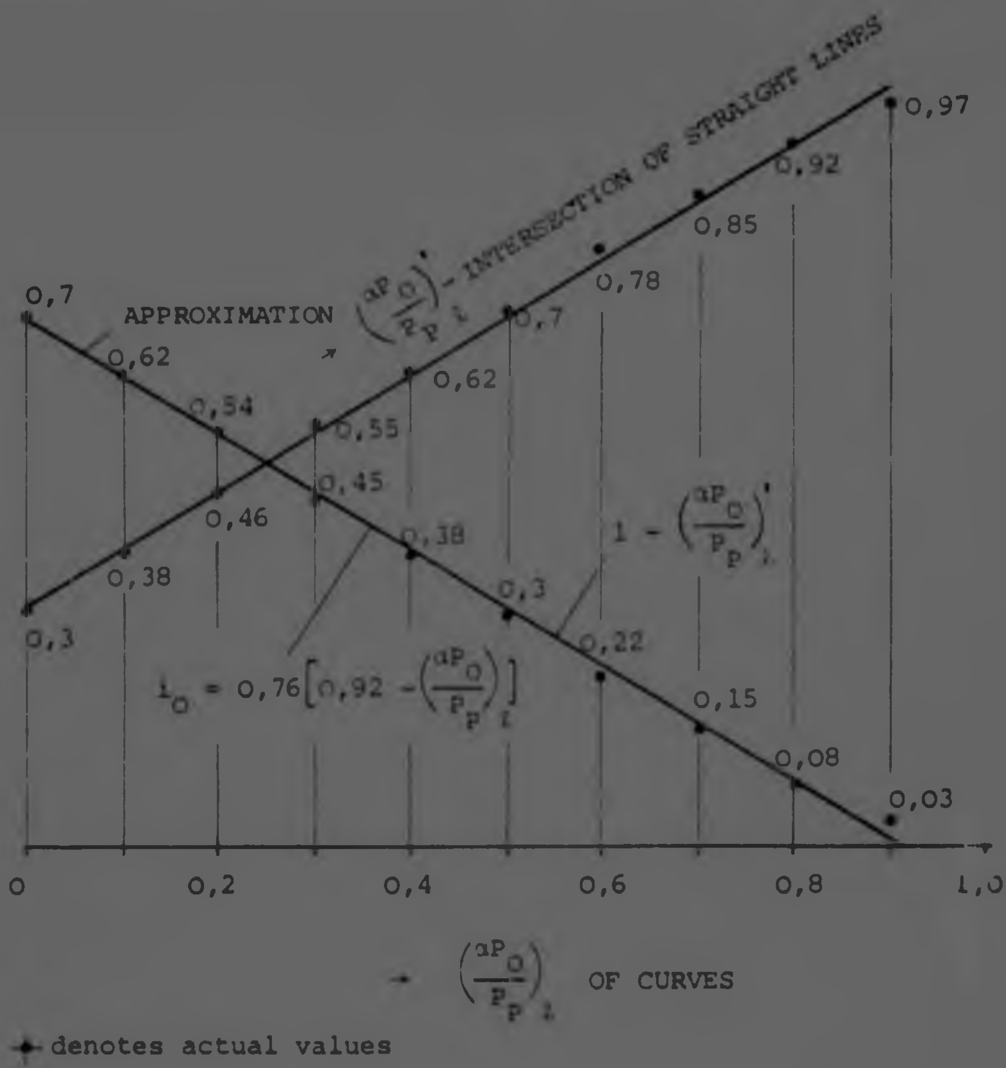

FIGURE 24: Intersection points for straight-line approximation

Using the information given in Figure 24, the straight-line approximation i_O can be incorporated into an interaction formula for the failure load as shown in Equation 11.

$$\frac{P_F}{P_P} = \frac{1}{1 + \frac{i_O P_P}{\alpha P_O}} \qquad |\text{EQN. } 11|$$

with

$$i_O = 0,76 \left[0,92 - \left(\frac{\alpha P_O}{P_P} \right)_{\ell} \right]$$

The ratio $(\alpha P_O/P_P)_\ell$ in the expression for i_O refers to limiting conditions, i.e. to $\lambda=\lambda_\ell$.

In Equation 11 the resulting value of P_F should not exceed 0,60 of αP_O to maintain good correlation with the actual failure curves. The approximation of Equation 11 has also been incorporated in the computer program.

2.5.3 Design parameters

In summary, it can be concluded that for design purposes all the designer needs to know is the plastic collapse load P_P, the fictitious "elastic buckling load" αP_O and the relevant "limiting slenderness ratio" λ_ℓ. By comparison, the Rankine-based methods only require the knowledge of the plastic collapse load P_P and the elastic buckling load P_O.

In the proposed method, the elastic buckling load is restricted to

a) being the failure load in the case of "Symmetry-Buckling", as long as all parts of the structure remain elastic,

b) being the failure load in the case of conventional buckling in conjunction with the reduction factor α, as long as all parts of the structure remain elastic,

c) being the indicator for locating the actual frame on the inelastic failure curve.

Since the proposed second-order, elasto-plastic analysis technique and the basic Merchant-Rankine formula are both applicable to bare frames, results obtained from these methods are directly comparable. The term bare frames refers to structures comprising column and beam members, disregarding the effect of any composite action such as from cladding, infill panels or masonry.

CHAPTER 3

CHOICE OF SUBASSEMBLAGE

3.1 Purpose of analysis

It has been mentioned in the preceding chapters that the proposed method requires an elastic buckling analysis and an elastic analysis for loading related to the elastic buckling load of the structure. The elastic buckling load P_O is obtained from the buckling analysis. Subjecting the actual frame to a loading arrangement the same as that for the ultimate load, but in magnitude related to the elastic buckling load P_O, the outstanding terms λ_ℓ and α are evaluated from a second-order, elastic load analysis. In principle, this procedure has already been demonstrated in section 2.2.2, where the "limiting slenderness ratio", λ_ℓ, was obtained for the frame of Figure 10. For the special case of "Symmetry-Buckling" the factor α is generally 1,0.

Ideally, the required elastic analysis would be performed on the entire framework to achieve optimum accuracy. However, in the approach described in this thesis a subassemblage method was given preference. The computation of the plastic collapse load P_p is amply illustrated in many textbooks and has not been included in the scope of this work.

3.2 Reasons for subassemblage approach

The following considerations led to the choice of a subassemblage method:

a) A subassemblage analysis would lend itself more readily to a "manual" design procedure, i.e. a method without the need to use a computer. One of the primary objectives of this study has been to demonstrate that results may be presented in graphical form for "manual" use. This can only be achieved successfully by keeping the number of variables to a minimum.

b) An elastic solution by computer of the entire frame would require the compilation and processing of a large amount of data for a single analysis, which may only be a first trial in a series of attempts to obtain the optimum solution. Although computer time for an elastic analysis would be less than that for a full elasto-plastic analysis, from the designer's viewpoint, there would not be a great deal to choose between the proposed method when applied to an entire frame and established elasto-plastic approaches.

c) The failure load calculation for portions of a frame is possible. By combining the plastic collapse load P_P and the relevant elastic parameters αP_O and λ_l of corresponding subassemblages, the failure load of the subassemblage can be determined. In this way, the method developed in this research functions exactly as the subassemblage methods by Daniels & Lu[41] and Cheong Siat Moy[43,44], which were outlined in section 1.3.3. However, much less calculation work is required for the proposed interaction procedure since only αP_O, λ_ℓ and P_p for the subassemblage need to be determined.

d) A subassemblage approach would enable the designer to focus attention on critical portions of a frame. These can often be identified by inspection of the practical structure. Repetitive or less critical sub-sections of the same framework are then covered by one subassemblage analysis.

e) The special case of "Symmetry-Buckling" requires a complex mathematical approach for the computation of the elastic buckling load and the corresponding stresses. Furthermore, for the stress calculations, the axial member forces appear in the arguments of trigonometric functions. For larger structures, the mathematics involved becomes prohibitive and there are no simplifying computer algorithms.

f) Results obtained on a subassemblage basis have been found to be in good agreement with full-scale second-order, elasto-plastic solutions.

When using a subassemblage approach certain simplifications are inevitable. However, in this context it must be borne in mind that the method developed in this research is not very sensitive with respect to a moderate error in the elastic buckling load. The corresponding state of stress will have a compensating effect. The accuracy of the solution, therefore, should be assessed in terms of the final results of the complete procedure.

This is demonstrated for an arbitrary case using the design graph of Figure 23 in conjunction with Equation 6. A frame is investigated with a column slenderness ratio $\lambda=50$ and qualifying for the special condition of "Symmetry-Buckling", i.e. $\alpha=1,0$. The ratio $P_O/P_P=2,5$ and $\lambda_\ell=250$.

actual frame: $$\tan\Omega = \frac{P_O}{P_P} = 2,5$$

"limiting frame": $$\tan\Omega_\ell = \frac{P_O}{P_P}\frac{\lambda}{\lambda_\ell} = 0,5$$

For these two ratios follows from Figure 23:

$$\frac{P_F}{P_P} = 0,89$$

It is now assumed that a 25 per cent error has been made in the assessment of P_O, i.e. P_O becomes 1,25 P_O. From the equation for the "limiting slenderness ratio" a value of $\lambda_\ell=1,40\times250$ would be obtained using the results of a second-order, elastic load analysis for the example. Hence, the above ratios are modified by a factor of 1,25 and a factor of 1,40 respectively.

actual frame: $$\tan\Omega = 2,5\times1,25 = 3,125$$

"limiting frame": $\tan\Omega_{\ell} = 0{,}5 \times \frac{1{,}25}{1{,}40} = 0{,}45$

If entered in Figure 23, the two slopes result in a failure load of

$$\frac{P_F}{P_P} = 0{,}90$$

This compares with $P_F/P_P = 0{,}89$. The difference is in the order of 1 per cent and could even be less for non-symmetry buckling, where the factor α contributes to conservatism.

3.3 Objectives of subassemblage analysis

The principal objective of the subassemblage analysis is to obtain adequate results for the elastic buckling load and the second-order stresses for loading related to the elastic buckling load, pertaining to the same portion of the structure. The stress calculations may involve vertical and combined loading of a nature typical for buildings. It should also be possible to transfer the chosen subassemblage laterally within a storey and vertically from storey to storey throughout the height of the structure. For the general multi-storey, multi-bay frame the relevant elastic parameters for the various subassemblages are to be combined with the plastic collapse load of the total structure. That combination of plastic load and elastic parameters giving the lowest failure load is significant.

In choosing a suitable subassemblage certain recognition has to be given to the remainder of the frame, where the frame size exceeds the subassemblage size. The subassemblage must also be feasible for smaller structures such as single-storey portal frames.

3.4 The investigated subassemblages

3.4.1 General

On the basis of the foregoing considerations it was decided to investigate the subassemblage shown in Figure 25. It comprises information on up to three storeys and a maximum of five bays. The subassemblage of Figure 25 is applicable to the buckling analysis and the analysis of vertical loading, as will be illustrated in more detail in sections 3.5 and 3.6 respectively. It was felt that the general subassemblage of Figure 25 could be further simplified for the analysis of horizontal loading. This will be examined in section 3.7 of this chapter.

In the derivation of the various subassemblages, it was endeavoured to keep the size of the subassemblages as small as possible without reducing the accuracy of the final result unduly. This objective was also of importance in view of a graphical representation of results for which the number of variables should be kept small. A number of frames investigated for the purpose of this study (chapters 9 and 10) have all been analysed on the basis of the subassemblages derived in this chapter. A good agreement with exact full-scale solutions has been obtained.

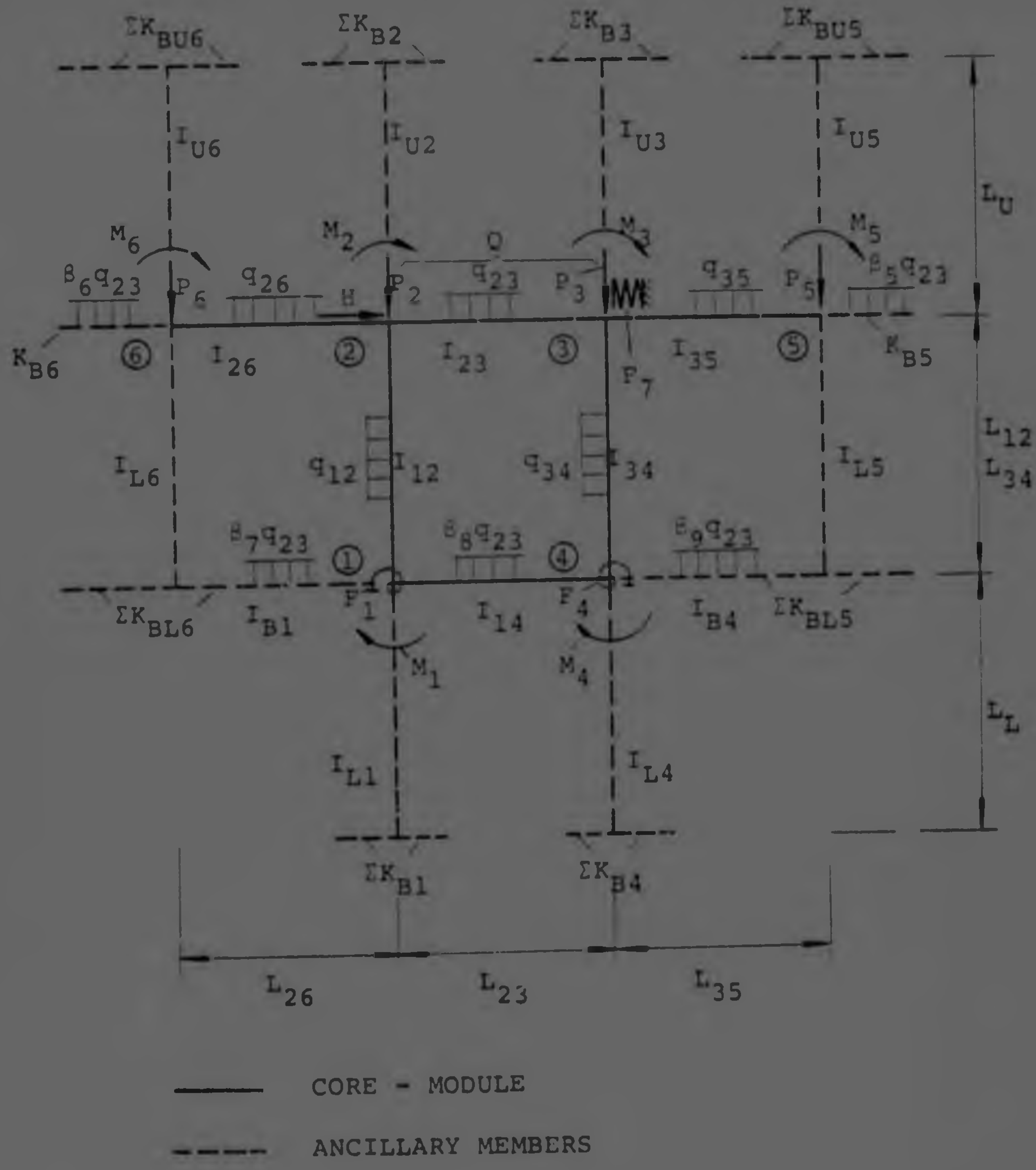

FIGURE 25: General subassemblage

The section of the subassemblage shown in solid lines in Figure 25 has been designated as the core-module. Satisfactory results with respect to the elastic buckling load and the state of stress corresponding to loading related to the elastic buckling load are sought for the two columns and the upper three beams of the core-module. By transferring the core-module laterally throughout the storey, and vertically from storey to storey, the total framework can be investigated. The dashed lines in Figure 25 represent ancillary members. They have been added to improve the accuracy of the results of the buckling and load analyses, considering that the core-module may be part of a larger structure.

In the mathematical analysis of the subassemblage, the members shown as solid lines will be represented on an exact basis, whereas various simplifications will be allowed for the dashed ancillary members. The approximations in regard to the axial forces in the ancillary column members are discussed in section 4.1.4.1. Simplifications concerning the rotational behaviour at the remote ends of ancillary columns and beams are presented in sections 4.1.5, 4.1.8, 4.2.2 and 4.2.4. Furthermore, the sway-displacement of ancillary columns is allowed for on an approximate basis as demonstrated in section 4.2.3 of the thesis.

3.4.2 Notation and symbols

The salient parameters of Figure 25 are explained below. A suffix has been added to the basic symbol for further identification. This suffix usually refers to the nearest significant joint(s) of the core-module.

I_{ij} = moment of inertia of member

L_{ij} = length of member

K_{ij} = stiffness of member

F_1, F_4 = linear elastic rotational restraint

F_7 = lateral bracing restraint

$$\left.\begin{array}{l} q_{ij} = \\ M_i = \\ P_i = \\ H = \\ Q = \end{array}\right\} \text{applied loading referring to the ultimate limit state}$$

$\beta_5 \ldots \beta_9$ = coefficients for loading

3.4.3 Loading

The loading shown in Figure 25 covers the typical loading encountered in buildings. Allowance has been made for an applied lateral load H, for joint moments M_i and for transverse loading acting on the columns between the joints.

Furthermore, the uniformly distributed beam loading shown in Figure 25 may be replaced by a set of dual-point loads which can be reduced to a single central beam load. Particulars referring to this case are set out below in Figure 26.

The beam load between joints 2 and 3, whether uniformly distributed or po.. load, will henceforth be referred to as Q. This term has been used as the reference parameter, to which all other loading will be related.

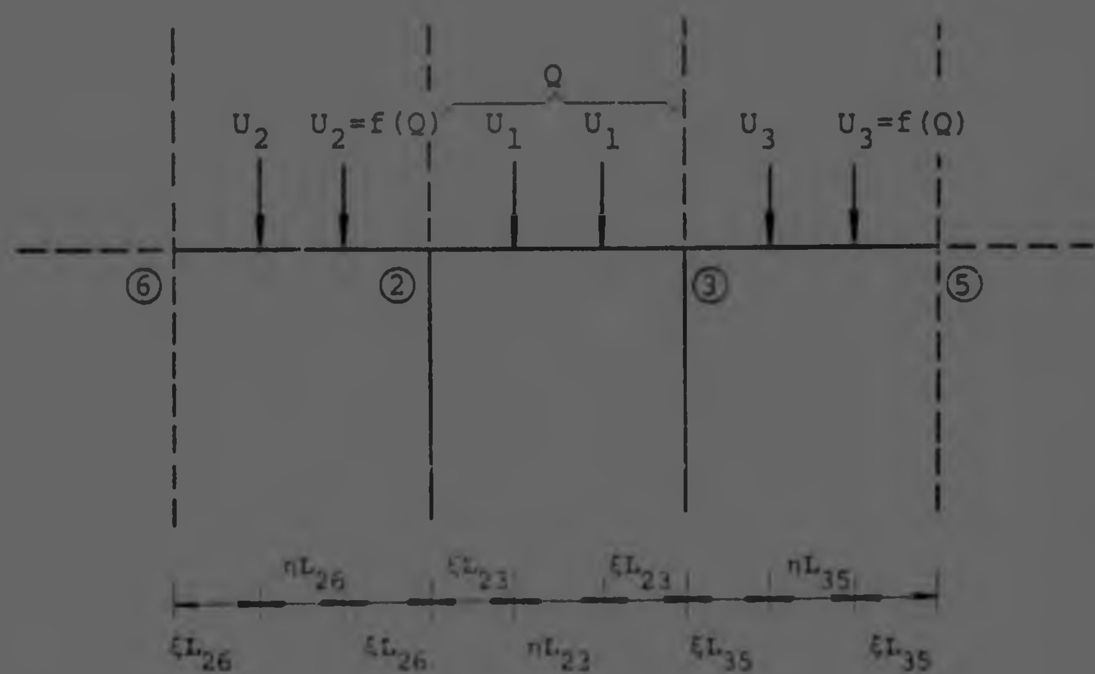

FIGURE 26: Alternative beam loading

3.4.4 Restraints

The restraints F_1 and F_1 of Figure 25 will be used to represent the conditions at the column base in bottom storeys, considering the soil-foundation interaction behaviour on a linear-elastic principle. The same function can be assumed by the stiffness expressions ΣK_{B1}, ΣK_{B4}, ΣK_{BL5} and ΣK_{BL6} when the respective nodes coincide with a column foundation. For other cases, such as in multi-storey buildings, the stiffnesses ΣK_B represent the restraining effect of beams at the remote ends of ancillary column members. Provision has also been made for the presence of a partial lateral bracing restraint. The stiffness of such a restraint will be represented by the parameter F_7.

3.5 Subassemblage for buckling

In determining the subassemblage to be analysed for buckling, consideration was given to the displaced framework in the sway-buckled state as shown in Figure 27. Based on the sway model as shown in Figure 27, the total subassemblage of Figure 25 will be analysed for buckling. Beams adjoining the core-module are assumed to be bent in double curvature and beam loads will be transferred to the joints. The effects of lateral load are ignored in the buckling analysis.

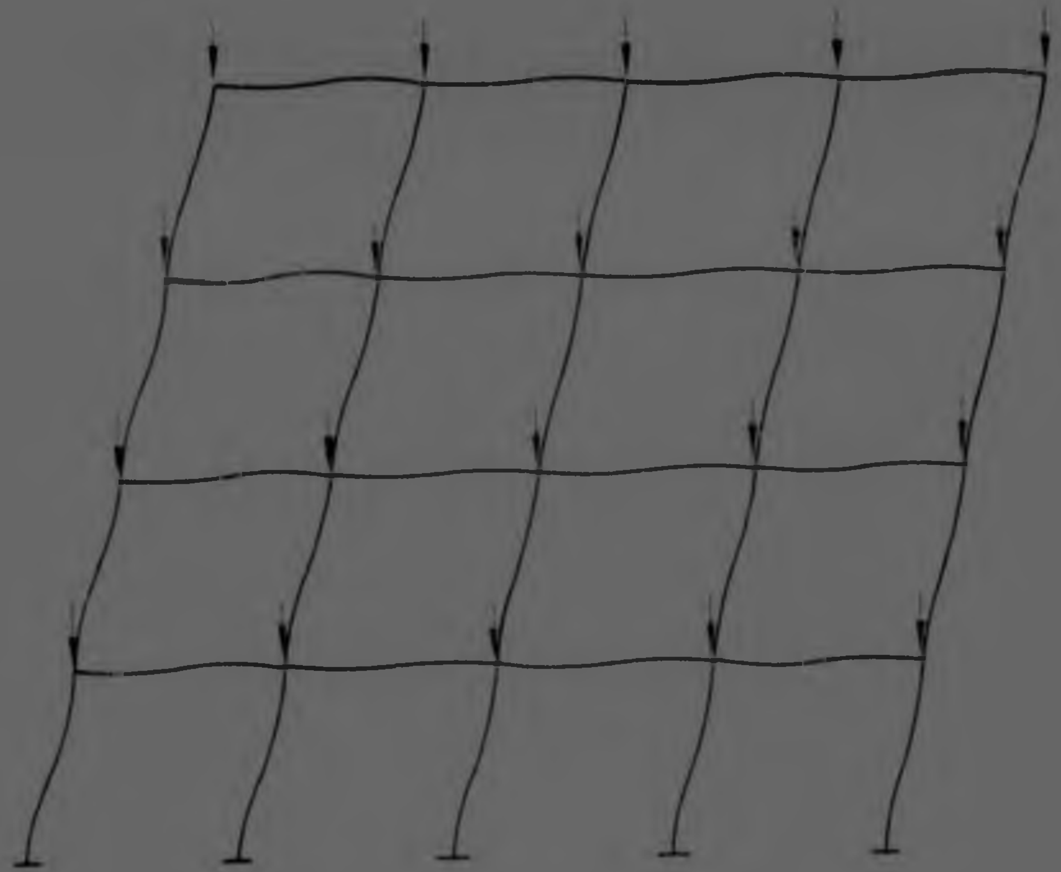

FIGURE 27: Displaced frame in the sway buckling state

When considering the special case of "Symmetry-Buckling", the influence of pre-buckling bending moments needs to be included. This means, that beam loadings must be retained in their original position for this special case.

3.6 Subassemblage for ...ical load

Once the elastic buckling load P_O has been established for the particular subassemblage, the related second-order state of stress must be evaluated. The general loading may include vertical and horizontal load components. For vertical loading, provision needs to be made for full-frame loading and for checkerboard loading. This is demonstrated in Figures 28 and 29, showing possible load arrangements and the resulting bending moments respectively. The dashed lines in Figure 29 refer to full loading and the solid lines to local checkerboard loading. The core-module section, for which stresses need to be calculated, is superimposed on both figures. The bending moment diagrams are non-linear since allowance has been made for the interaction of axial loads with the deformations of the members.

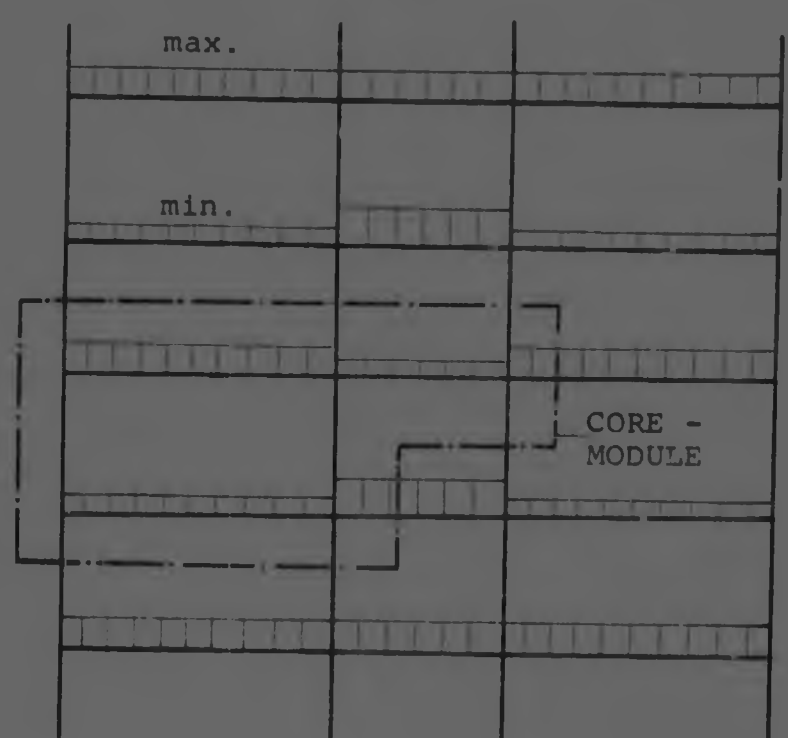

FIGURE 28: Frame subjected to vertical loading

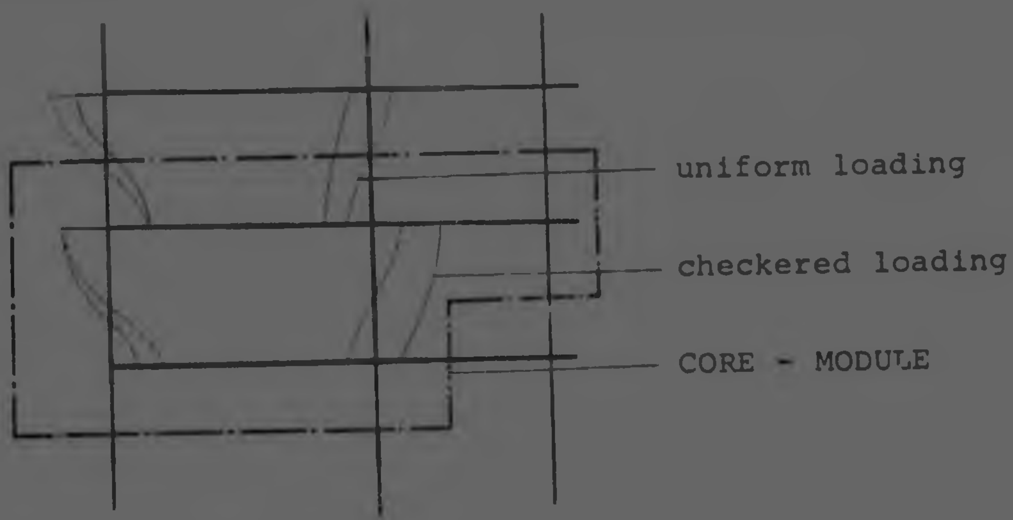

FIGURE 29: Column moments due to vertical loading

The checkered loading inside the confines of the core-module can easily be realised, since each beam loading of Figure 25 has been introduced as an independent variable. In addition, it is necessary to allow for the effects of the checkered beam loading just above the core-module. It has been assumed, that the influence this loading has on the core-module moments can be accounted for by suitably adjusting the stiffnesses of the upper columns.

The checkerboard case of Figures 28 and 29 will also have an effect on the buckling load. Hence, for the general case more than one investigation may be required for buckling and vertical loading. The analysis resulting in the lowest failure load will be significant.

For all cases the full subassemblage of Figure 25 is analysed provided the structure is sufficiently large. The stiffnesses of the beams adjoining nodes 5 and 6 will be determined giving due consideration to their deformed shape.

3.7 Subassemblage for horizontal load

For the load analysis of horizontal loading a simplified approach has been adopted. In this case the subassemblage of Figure 25 is reduced in size by cutting through the likely points of inflection of the columns and the beams. At these points hinges are inserted in the core-module. Furthermore, compensating loadings are applied to account for the upper-storey effect. A typical storey section will show the second-order moment response given in Figure 30 when subjected to horizontal loading at the nodes and in the presence of axial vertical loads. The interaction of the axial vertical loads with the sway will lead to the non-linear moment shapes.

The subassemblage for horizontal loading has been evolved from the typical moment pattern of Figure 30 and has the general shape as shown in Figure 31. Satisfactory overall-results have been obtained using the subassemblage of Figure 31.

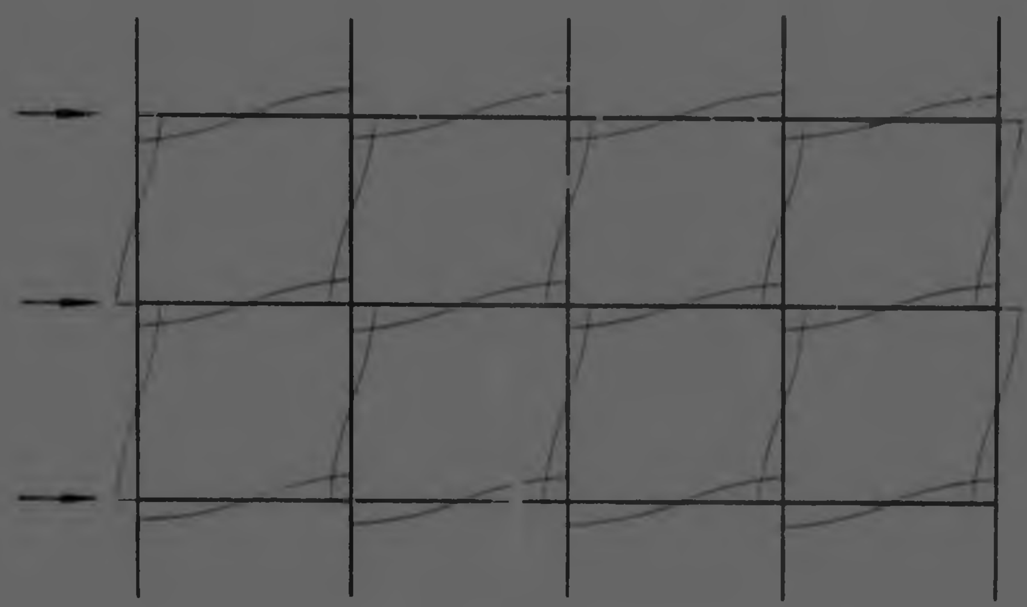

FIGURE 30: Frame moments due to horizontal loading

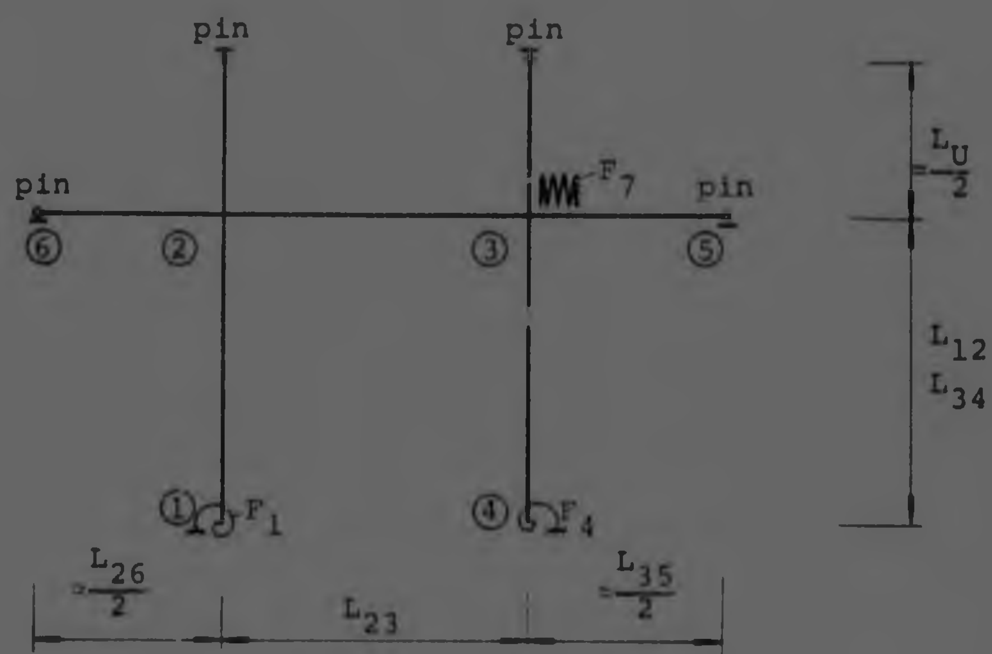

FIGURE 31: Subassemblage for horizontal loading

The subassemblage shown in Figure 31 applies to the bottom storey of a framework. When upper storeys are investigated for horizontal loading two modifications are required. Firstly, the stiffness at the bases, i.e. F_1 and F_4 need to be adjusted to represent a true hinge. Secondly, the column heights L_{12} and L_{34} will have to be modified to coincide with the estimated points of inflection in the relevant column members.

3.8 Curtailed subassemblages

For all cases of analysis, i.e. buckling, vertical and horizontal loading, the general subassemblages derived above must be suitable for inner storeys, bottom storeys, top-most storeys and for exterior storeys of multi-storey, multi-bay structures. For bottom storeys, the beams at level 1-4 of the general subassemblage of Figure 25 and the lower columns are omitted. The stiffnesses F_1, F_4, ΣK_{BL6} and ΣK_{BL5} will then represent the rotational behaviour at the column base using linear elastic priniciples. If the top-most storey of a multi-storey structure is investigated, all upper columns above the level of nodes 6-2-3-5 of the subassemblage of Figure 25 will be removed. For external subassemblages, the relevant horizontal and vertical members falling beyond the end of the building structure are similarly removed. Figure 32 serves to illustrate the cases described above by showing possible curtailed core-modules superimposed on a general multi-storey framework. The ancillary members of the subassemblages are indicated as dashed lines.

The mathematical analysis must contain procedures to deal with all possible subassemblages.

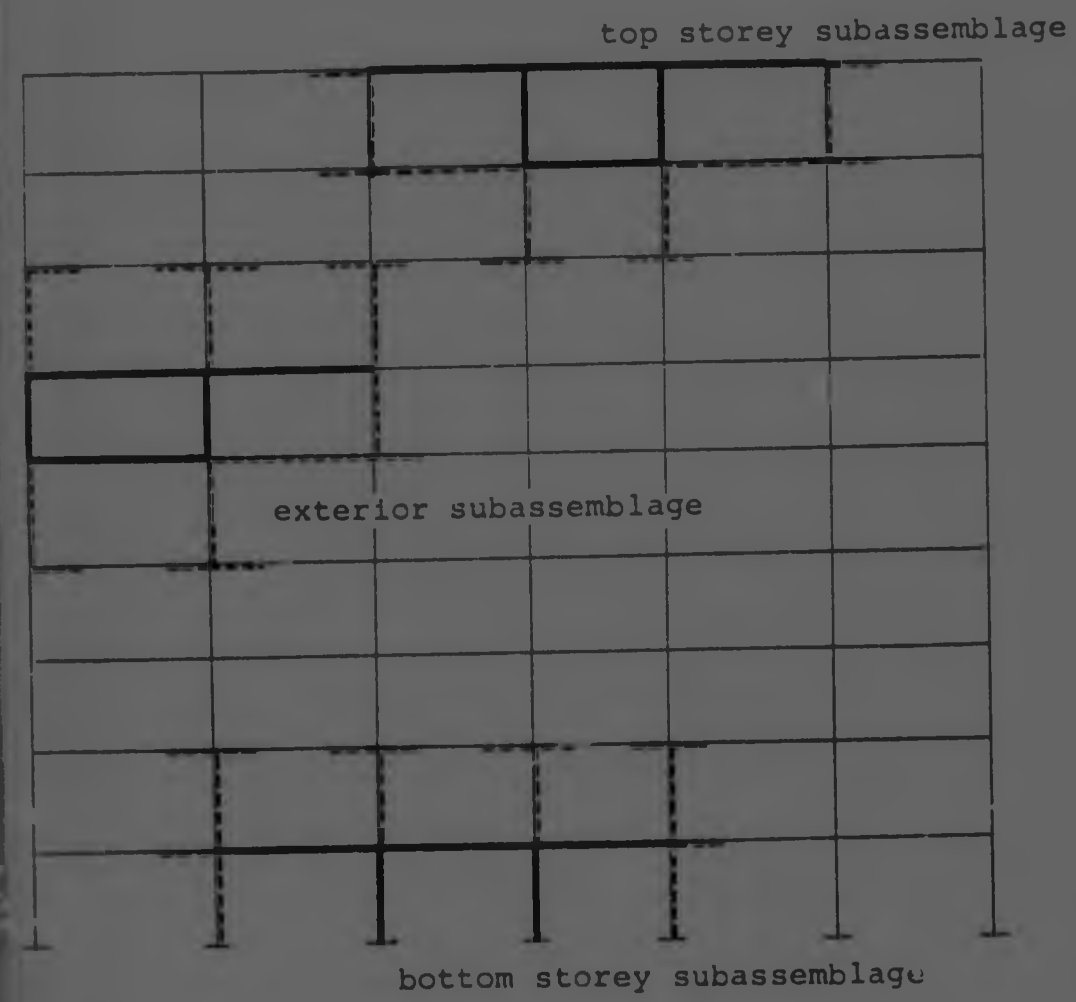

FIGURE 32: Curtailed subassemblages

3.9 Loads on core-module from upper storeys

3.9.1 Combined loading

When analysing a subassemblage such as shown in Figure 31, axial forces, shear forces and moments from upper storeys need to be included by considering the deformed shape of the members. Assigning the suffix (U) to forces from the upper storey, the procedure is illustrated in Figure 33 for a typical joint of the core-module. The factor ν defines the distribution of the total applied horizontal load H among the individual columns of the subassemblage.

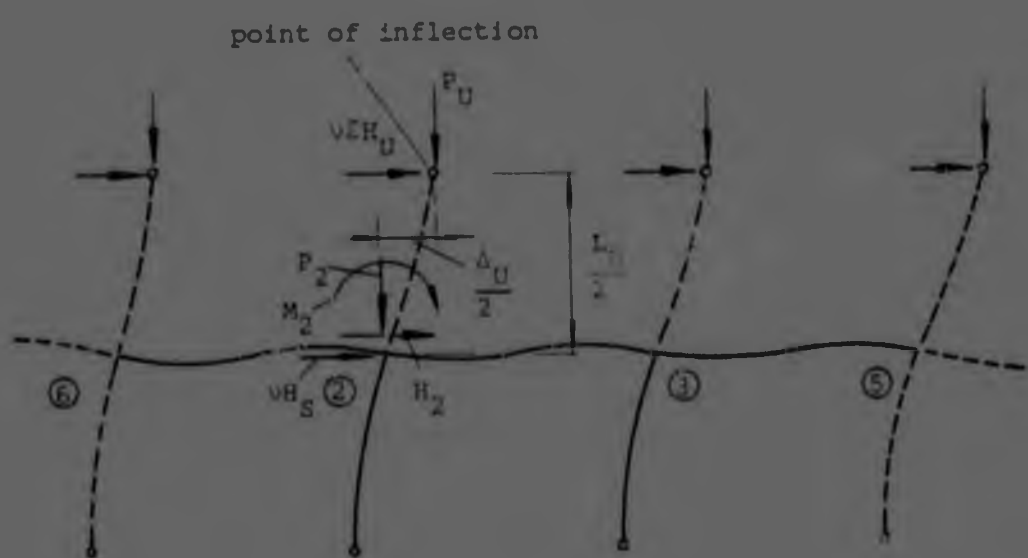

FIGURE 33: Loads from upper storeys

Approximate methods such as the Portal or Cantilever methods[9-10] may be used to establish this distribution factor when the member sections are not known. In order to obtain accurate results for the parameters α and λ_ℓ it is essential to make a good prediction of the distribution factor ν. In this thesis frames have been checked for which the member sizes were given (see Tables 6/1, 6/2 and 9). For these cases the shear was distributed in proportion to the stiffness of the columns and their restraining beams.

Assuming points of inflection in the upper columns at midheight and using Δ_U as the upper-storey sway, the relevant forces acting on the sway subassemblage can be approximated as given below. Joint 2 has been singled out for demonstration purposes. Forces at other joints can be obtained in a similar way.

Applied moment:

$$M_2 = \nu \Sigma H_U \frac{L_U}{2} + P_U \frac{\Delta_U}{2} = M_{AP2} + P_U \frac{\Delta_U}{2}$$

Shear:

$$H_2 = \nu \Sigma H_U + \nu H_S = \nu(\Sigma H_U + H_S)$$

Axial load:

$$P_2 = P_U$$

It is essential to retain the axial member forces such as generated by P_2 and Q in the analysis for horizontal loading. The stiffness of the members would otherwise be overestimated in a second-order, elastic analysis.

3.9.2 Vertical loading

A sway Δ_U such as identified for the case of horizontal loading can also occur in the presence of pure vertical loading. Non-symmetry of loadings or a non-symmetrical structure will then be responsible for the sway Δ_U, which in turn will give rise to the second term in the above moment expression. To enable the evaluation of the P-Δ moments for these cases, they will have to be included in the analysis of the subassemblage for vertical loading.

However, since the full subassemblage of Figure 25 is analysed in this instance, an error would occur due to the retention of the upper columns. Like other members at a joint, the upper columns would attract part of the P-Δ moment, whereas they should rather be removed for this analysis step. It is believed that satisfactory compensation can be made by applying a magnified joint moment instead. The magnified joint moment has been calculated by way of an iterative distribution procedure, details of which are set out in Appendix I. Using joint 2 as an example, the basic P-Δ moment can be expressed as before.

$$M_2 = P_U \frac{\Delta_U}{2}$$

The magnified moment may be written as follows:

$$\text{mag } M_2 = z_2 M_2$$

The magnification factor z_2 includes the stiffness of the upper column and the total stiffness oint 2 and takes the form of a binominal progression. .. P-Δ moment such as mag M_2 may become relevant for joints 1 to 6 of the subassemblage of Figure 25. For joints 1 and 4 the expression for the P-Δ moment would assume the following form:

$$M_1 = P_L \frac{\Delta_L}{2}$$

The suffix (L) refers to parameters relevant to the storey below the core-module. Details of the various factors z appear in Appendix I.

3.10 Concepts of analysis of subassemblages

The core-module in its general form as shown in Figure 25 comprises six nodes and is free to sway sideways. In order to analyse the devised subassemblages for ordinary sway buckling and "Symmetry-Buckling" as well as the corresponding stress states, it is necessary to follow two avenues of approach. The first one dealing with ordinary buckling and a second one covering the special case of "Symmetry-Buckling". In both instances extensive use will be made of the conventional slope-deflection method including stability functions. The case of ordinary sway buckling is analysed in section 4.1 (buckling) and section 4.2 (forces due to loading). "Symmetry-Buckling" is investigated in section 5.1 (buckling) and section 5.2 (load analysis).

CHAPTER 4

ANALYSIS OF CONVENTIONAL SWAY BUCKLING OF SUBASSEMBLAGES AND CORRESPONDING STRESSES

4.1 Conventional buckling analysis

4.1.1 General principles

The elastic buckling load for the case of conventional buckling is calculated using the slope-deflection method including stability functions. Since the elastic buckling load refers to a distribution of axial forces in the members, it is sufficient to assume that all vertical loading acts at the nodes of the structure and to ignore the effects of horizontal load. In rectangular frames, the horizontal load would primarily be responsible for the re-arrangement of axial forces due to vertical loads. It has been found that this has little effect on the final result for the elastic buckling load. When using the slope-deflection method a set of linear equations is obtained. The total number of independent equations will equal the number of independent joint rotations and sway displacements of the structure. This set of homogeneous linear equations can be expressed as in Equation 12.

$$\bar{B}\,D = 0 \qquad |\text{EQN. } 12|$$

where,

$\bar{B}$ = Stiffness matrix for conventional buckling

D = Displacement vector (rotation plus sway)

Excluding the trivial solution D = O, the lowest root of the determinantal Equation 13 will give the elastic buckling load P_O.

$$|\overline{F}' \quad 0 \qquad \text{|EQN. 13|}$$

In the following sections the various parameters required to solve Euqation 13 are derived.

4.1.2 Principal assumptions adopted in analysis

For the buckling analysis a number of simplifying assumptions have been made. These are given below:

a) Material properties are ideally elastic with constant modulus of elasticity.

b) Axial and shear force deformations are comparatively small and may be neglected.

c) Deflections within members are small enough for linear relationship to apply between bending moments and curvatures.

d) Members have uniform cross-sections between joints.

e) All joints are fully rigid.

f) Lateral torsional buckling and out-of-plane buckling is prevented.

4.1.3 Slope-deflection method including stability functions

As mentioned in section 4.1.1, the conventional slope-deflection technique has been adopted as the principal method of analysis to calculate the elastic buckling load of the subassemblage. Full details of the procedure as applied to the particular problem of this research can be found in Appendix II. In what follows, a brief summary is given of some salient features only. This will preserve the continuity of the derivation procedure and lead directly to the formulation of the stiffness matrix B.

A typical structural member connecting joints A and B is shown in Figure 34.

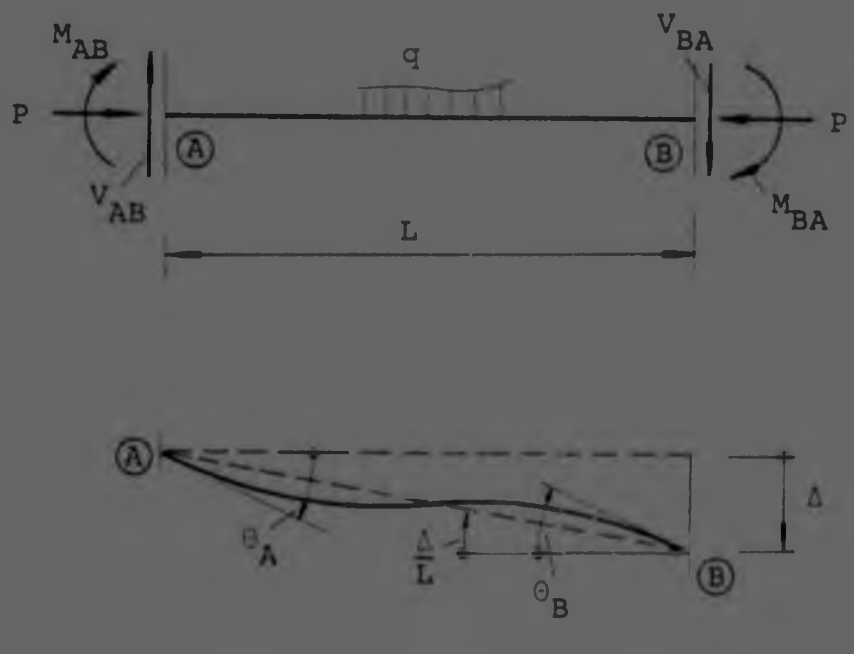

FIGURE 34: Typical member

According to elementary beam theory the member-end moment may be expressed as follows, if the member is subjected to a transverse load q and an axial compression force P.

$$M_{AB} = EKS\left[\Theta_A + C\Theta_B - (1+C)\frac{\Delta}{L}\right] + M_{FAB} \qquad |\text{EQN. } 14|$$

In Equation 14, Θ_A and Θ_B are the end rotations at joints A and B of the member respectively and Δ is the relative displacement of the ends with respect to the undeformed position of the member. The member stiffness K represents the ratio I/L. The forces and deformations are positive if acting in the directions as shown in Figure 34. The term M_{FAB} in Equation 14 is known as the fixed-end moment. The fixed-end moment is used to account for the effect of the transverse load q considering both ends, A and B, as fixed in position and direction. As mentioned in section 4.1.1, for the buckling analysis the beam load is divided between the nodes, so that effectively M_{FAB} is equal to zero in this case. The coefficients S and C in Equation 14 are known as stability functions and can be expanded as follows:

$$S = \frac{m(\sin m - m\cos m)}{2 - 2\cos m - m\sin m} \qquad |\text{EQN. } 15a|$$

$$C = \frac{m - \sin m}{\sin m - m\cos m} \qquad |\text{EQN. } 15b|$$

and

$$m = L\sqrt{\frac{P}{EI}} \qquad |\text{EQN. } 15c|$$

For the case of axial tension, that is, when P is negative by the adopted sign convention, the load parameter m may be retained as given in Equation 15c, but the trigonometric functions in Equations 15a and 15b are replaced by their hyperbolic equivalents. For zero axial load, the factors S and C approach 4 and 1/2 respectively.

The shear force V_{AB} can also be expressed in a similar way as the end moments. Conveniently, this is done as shown in Equation 16.

$$V_{AB} = \frac{EK}{L^2} S^2(1-C^2)\Delta - \frac{EK}{L} S(1+C)(\theta_A + \theta_B) - \frac{M_{FAB} + M_{FBA}}{L} + V_{ABO} \qquad |\text{EQN. } 16|$$

The last two terms in Equation 16 describe the fixed-end shear force. The fixed-end shear is the shear force of a member A-B (see Figure 34) fixed at both ends, allowing for the presence of axial forces. The fixed-end shear can be determined from the fixed-end moments M_F and the shear V_{ABO}. The parameter V_{ABO} is defined as the shear force due to applied load as obtained for a simply supported equivalent member A-B but ignoring the presence of axial forces. For the buckling analysis, in which all loads are considered to act at the nodes of the structure, the last two terms in Equation 16 are zero.

For the case of axial tension, that is, when P is negative by the adopted sign convention, the load parameter m may be retained as given in Equation 15c, but the trigonometric functions in Equations 15a and 15b are replaced by their hyperbolic equivalents. For zero axial load, the factors S and C approach 4 and 1/2 respectively.

The shear force V_{AB} can also be expressed in a similar way as the end moments. Conveniently, this is done as shown in Equation 16.

$$V_{AB} = \frac{EK}{L^2} S^2(1-C^2)\Delta - \frac{EK}{L} S(1+C)(\theta_A+\theta_B) - \frac{M_{FAB}+M_{FBA}}{L} + V_{ABO} \qquad |\text{EQN. } 16|$$

The last two terms in Equation 16 describe the fixed-end shear force. The fixed-end shear is the shear force of a member A-B (see Figure 34) fixed at both ends, allowing for the presence of axial forces. The fixed-end shear can be determined from the fixed-end moments M_F and the shear V_{ABO}. The parameter V_{ABO} is defined as the shear force due to applied load as obtained for a simply supported equivalent member A-B but ignoring the presence of axial forces. For the buckling analysis, in which all loads are considered to act at the nodes of the structure, the last two terms in Equation 16 are zero.

4.1.4 Axial member forces

4.1.4.1 Columns

The axial forces in the columns outside the core-module are determined in a simplified manner from the axial forces in the core-module member and the loading on the adjoining beams. This is demonstrated for the upper column running into joint 2 of the subassemblage of Figure 25. The buckling analysis is carried out for the load P_O, taken as the load acting between joints 2 and 3 of the subassemblage. All other loading is expressed as a function of P_O, i.e. n_iP_O as shown in Figure 35 for joint 2.

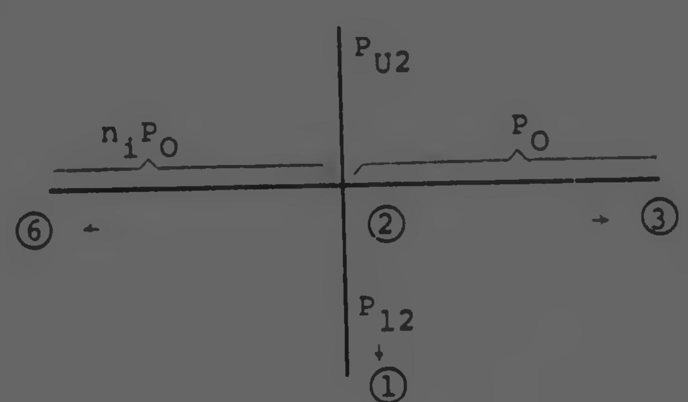

FIGURE 35: Axial force in upper-storey column

Assuming that the force P_{12} is given and that the beam loadings adjoining node 2 are n_iP_O and P_O respectively, the upper ancillary column will be subjected to an axial force as given in Equation 17.

$$P_{U2} = P_{12} - (1+n_1)\frac{P_D}{2} \qquad |EQN.\ 17|$$

Typically, the force P_{12} would be evaluated from the axial force equations of Table 4 in section 4.2.6.3 ignoring the effects of axial forces on the stiffness of the members. For this preliminary analysis step, the applied vertical loadings are considered in their original position.

Similarly, the forces in the ancillary columns adjoining node 1 and nodes 3-6 are obtained. The axial column forces are used to set up the relevant stability functions S and C for the member.

4.1.4.2 Beams

Conventional methods used to calculate the elastic buckling load and typical effective length charts usually neglect axial beam forces. This may lead to an overestimation of the elastic buckling loads, especially in the case of single-storey frames, for which axial beam forces can be significant when compared with the column forces. In the presented study, axial beam forces are considered where they can be significant, such as in the case of single-storey frames and in top storeys of multi-storey frames. For typical building str tures, it is assumed that axial beam forces can be neglected for all other cases.

For single-storey frames and top storeys o multi-storey frames the axi l beam forces are calculated in accordance with the slope-deflection approach outlined in section 4.2, solving the axial force equations of Table 4 and ignoring the effects of axial forces on the stiffness of the members. For this analysis step the vertical loadings are considered in their original position. It has been confirmed that results for P_O obtained in this way are satisfactory when compared with solutions based on the differential equation method of analysis.

4.1.5 The N and O-functions for buckling

Wood[1] has shown that a more accurate buckling result for a particular column can be obtained when the effective stiffness of beams running into the remote ends of the upper and lower columns are included. Based on Merchant's[2] original work, Wood[3] formulated additional stability functions N and O, which also make allowance for the presence of a partial lateral bracing restraint $\bar{F}_7$.

$$N = S - \frac{S^2(1+C)^2}{S^2(1-C^2)+\bar{F}_7} \qquad |\text{EQN. } 18a|$$

$$O = CS - \frac{S^2(1+C)^2}{S^2(1-C^2)+\bar{F}_7} \qquad |\text{EQN. } 18b|$$

The functions N and O are known as the no-shear stability functions. They refer to a displaced member A-B, such as shown in Figure 34, characterised by $\theta_B=0$ and $V_{AB}=0$. As a result, it is possible to represent an adjacent upper or lower column, including the beams at the remote ends, as a single rotational restraint at the relevant node. This is demonstrated for an arbitrary ancillary column A-B of the subassemblage shown in Figure 25. The member-end moment given in a general form in Equation 14 would assume the following expression in this case.

$$M_{AB} = EK\left(N - O^2\,\frac{K}{NK+6\Sigma K_B}\right)\Theta_A \qquad |\text{EQN. } 19|$$

The term ΣK_B in Equation 19 refers to the stiffness of beams at the remote ends of the columns. These beams are assumed to be bent in double curvature. The stability functions S and C in Equations 18a and 18b were defined earlier. The partial lateral bracing restraint $\bar{F}_{-}$ will be explained in section 4.1.7. The additional stability functions N and O are only relevant to the case of buckling.

4.1.6 Base stiffness for bottom storeys

Liapunov[68] demonstrated the importance of a correct assessment of the column base behaviour.

For practical cases the base rotation can be related to the soil properties by appropriate methods.[107-109] The rotation at the base due to the deformation of anchor bolts and the base plate was investigated by Sahmel[110] and another equivalent provision has been proposed by the SSRC Guide to Stability Design Criteria for Metal Structures[15] and by Schineis[111]. On this basis it is possible to represent the total base behaviour by an equivalent spring stiffness.

It has become popular, in the absence of exact information, to work with a simplifying approximation based on the research by Galambos[112]. Galambos proposed to use the following non-dimensional base stiffness values:

"Quasi-pinned" conditions : $\overline{K}_S = 0,1$

"Quasi-fixed" conditions : $\overline{K}_S = 1,0$

These values acknowledge that neither a true hinge nor a full fixity will exist for practical bases. The relative stiffness $\overline{K}_S$ represents the ratio of the base stiffness to the stiffness EI/L of the supported column.

A stiffness such as described in this section may become relevant for parameters ΣK_{BL6}, ΣK_{BL5}, F_1 and F_4 of the subassemblage shown in Figure 25.

If the rotational base restraints $\overline{K}_S$ are incorporated in the expressions for the member-end moment, the following modified version of Equation 14 is obtained:

$$M_{AB} = \overline{K}_S EK\Theta_A \qquad |\text{EQN. } 20|$$

where K is the stiffness of the supported column (K=I/L).

4.1.7 Partial lateral bracing restraint F_7

The stiffness of otherwise unbraced building frames will be increased by the presence of infill walls composed of brickwork, blockwork, masonry or similar materials and also due to steel cladding.

In the subassemblage analysis of this study provision has been made to consider the effects of composite action by introducing the dimensionless lateral stiffness ratio $\bar{F}_7$. A conservative computation of $\bar{F}_7$ was proposed by Wood[3], which in a generalised form has also been incorporated into the British Draft Code B20[7] and the ECCS Recommendations[5]. The lateral bracing stiffness F_7 of Figure 25 is here rendered dimensionless by making reference to the stiffness of the column between nodes 3 and 4 of the core module.

$$\bar{F}_7 = \frac{F_7 \, L_{34}^2}{E \, K_{34}}$$

and in an extended form for wall panels

$$\bar{F}_7 = \frac{\Sigma S_S L_{34}^2}{\gamma_m E \Sigma K_C} \times \frac{K_{12}+K_{34}}{K_{34}}$$

in which the first term should not exceed 2,0.

The meaning of the various parameters is as follows:

K_{12}, K_{34} = Stiffness of column members between nodes 1 and 2 and nodes 3 and 4.

L_{34} = Storey height

ΣS_S = Sum of the spring stiffnesses (horizontal force per unit horizontal deflection) of the cladding wall panels in that storey of the frame.

E = Modulus of elasticity

ΣK_c = Sum of the stiffnesses I/h of the columns in that storey of the frame.

γ_m = Partial safety factor of materials, proposed as 80 by the British Draft Code B 20[7].

The high value of γ_m=80 is based on the assumption that only 25 per cent of the wall panels are effective and represents a lower bound in the absence of more accurate information.

4.1.8 Joint stiffnesses of ancillary beam members

For the buckling analysis of the various subassemblages the rotations at the remote ends of the ancillary beams need to be known in order to determine the stiffening effects of such beams. For the purpose of this study, it is assumed that all ancillary beams are bent in double curvature. In this way, the beams can be expressed as approximate rotational restraints at the relevant nodes of the core-module. Ignoring axial forces, the basic Equation 14 is modified to

$$M_{AB} = 6EK\theta_A \qquad |\text{EQN. } 21|$$

4.1.9 Basic slope-deflection method applied to the general subassemblage

Using the principles outlined in the preceding sections, a stiffness matrix can be formulated for the problem of buckling in terms of six unknown joint rotations and one independent sway displacement. A set of seven homogeneous linear equations will be obtained for the general subassemblage of Figure 25 by:

a) Satisfying that ΣMoments = 0 for the six joints of the core-module

b) Formulating the sway-equilibrium equation corresponding to the sway Δ of the core-module.

This will lead to the matrix expression given in Equation 12, from which the elastic buckling load of the problem can be evaluated by satisfying the determinantal Equation 13.

The meaning of the displacement vector D is further illustrated in Figure 36, which shows the deformed core-module.

The combined end moments M_m of the ancillary members and the displacements are indicated. The end moments M_m can simply be expressed as the product of ancillary member stiffnesses and joint rotation.

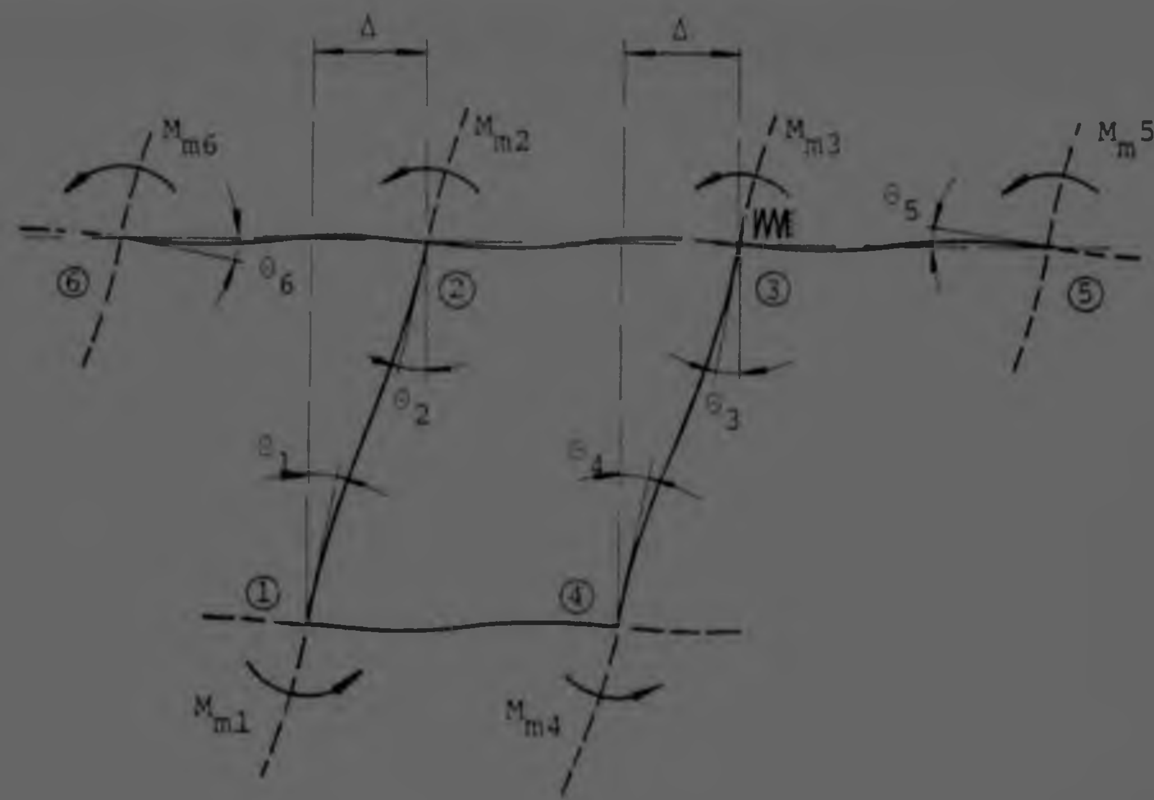

FIGURE 36: Deformed subassemblage

Executing the procedure outlined above will result in the equations summarised in Table 1. Matrix $\overline{B}$ of Table 1 refers to the general subassemblage shown in Figure 25. The equivalent matrices relevant to the curtailed subassemblages outlined in section 3.8 are obtained by setting the stiffnesses of the redundant members equal to zero. The detailed procedure leading to the stiffness matrix of Table 1 is set out in Appendix II/1. The same appendix explains the various abbreviations used in the stiffness parameters.

TABLE I: Equations $\bar{B}\,\theta = 0$

$NO_1 + K_{12}S_{12} + \frac{6I_{B1}}{L_{26}} + \frac{4I_{14}}{L_{23}}$	$K_{12}S_{12}C_{12}$	0	$\frac{2I_{14}}{L_{23}}$	0	0	$-SC_{12}L_{34}$		θ_1	
$K_{12}S_{12}C_{12}$	$NO_2 + K_{12}S_{12} + K_{23}S_{23} + K_{26}S_{23}$	$K_{23}S_{23}C_{23}$	0	0	$K_{26}S_{23}C_{23}$	$-SC_{12}L_{34}$		θ_2	
0	$K_{23}S_{23}C_{23}$	$NO_3 + K_{23}S_{23} + K_{34}S_{34} + K_{35}S_{23}$	$K_{34}S_{34}C_{34}$	$K_{35}S_{23}C_{23}$	0	$-SC_{34}L_{34}$		θ_3	
$\frac{2I_{14}}{L_{23}}$	0	$K_{34}S_{34}C_{34}$	$NO_4 + K_{34}S_{34} + \frac{6I_{B4}}{L_{35}} + \frac{4I_{14}}{L_{23}}$	0	0	$-SC_{34}L_{34}$	X	θ_4	$= 0$
0	0	$K_{35}S_{23}C_{23}$	0	$NO_{U5} + NO_{15} + K_{35}S_{23} + 6K_{B5}$	0	0		θ_5	
0	$K_{26}S_{23}C_{23}$	0	0	0	$NO_{U6} + NO_{16} + K_{26}S_{23} + 6K_{B6}$	0		θ_6	
SC_{12}	SC_{12}	SC_{34}	SC_{34}	0	0	$-SC_{122} - SC_{342} - \bar{F}_7 \frac{K_{34}}{L_{34}}$		$\frac{\Delta}{L_{34}}$	

4.2 Stresses corresponding to conventional buckling

4.2.1 General concept

It has been mentioned in previous chapters of this thesis that the determination of the "limiting slenderness ratio" requires the calculation of stresses corresponding to loading which includes the full set of applied loadings, but now in magnitude related to the buckling load P_0. Since it is generally impossible in a second-order elastic analysis such as the slope-deflection method to identify a unique stress and deformation state corresponding to the full elastic buckling load P_0, a somewhat lower load level αP_0 is examined instead. Based on the load parameter αP_0, a load vector L_V will be generated which comprises the complete set of applied loadings but now related to αP_0, e.g. the beam load Q of Figure 25 will be replaced by αP_0 and a horizontal load $H=n_i Q$ will become $n_i \alpha P_0$. The structure is analysed successively for two load vectors, one dealing with the vertical loading and one with all other loading. For a given load vector, displacements are obtained from the inverse of the relevant stiffness matrix $\bar{B}_1$.

$$D_1 = \bar{B}_1^{-1} L_V \qquad |\text{EQN. } 22|$$

where,

$\bar{B}_1$ = Stiffness matrix relevant to load analysis

D_1 = Displacement vector relevant to load analysis (rotation plus sway)

L_V = Load vector.

The final solution of Equation 22 gives the displacements, from which the bending moments, shear forces and axial forces can be calculated in accordance with the principles of the slope-deflection method.

The solution of Equation 22 is complicated by the fact that the axial member forces enter the stiffness matrix $\bar{B}_1$ as well as the load vector L_V. It must be remembered that the load vector contains second-order, fixed-end moments which are a function of the axial forces. Hence, besides the joint displacements all axial forces have to be retained as unknowns. A direct solution to Equation 22 for a given set of applied loadings is thus not possible. Therefore, an iterative procedure must be adopted by first setting up Equation 22 as if no axial forces were present. Solving this equation will then result in displacements corresponding to first-order, linear elastic theory. The displacement vector D_1 is used to calculate an improved system of axial member forces by solving Equation 23.

$$P = S_P D_1 + \bar{P}_F \qquad |EQN. 23|$$

where,

P = Axial member forces

S_P = Stiffness matrix for axial forces

$\bar{P}_F$ = Fixed-end axial forces

In the following step, the results of Equation 23 are used to formulate a revised stiffness matrix $\bar{B}_1$ and load vector L_V. This procedure is repeated until a satisfactory state of convergence is obtained.

In essence, the derivation of the stiffness matrix $\bar{B}_1$ follows the same principles as already outlined in section 4.1 of this chapter. The discrepancies in certain stiffness parameters and the consequent modifications to the stiffness matrix as well as the relevant load vectors will be examined in the following sections of this study. Items which remain unchanged will not be repeated.

4.2.2 Ancillary beams

Ancillary beams will be assumed to be bent in double curvature for the lateral load analysis, in which case Equation 21 remains valid. For the vertical load analysis no great error is made in the force and stress calculations for the core-module if the remote ends of the ancillary beams are taken as fully fixed. In this case, and ignoring axial forces in such beams, the basic expression given in Equation 14 is modified to

$$M_{AB} = 4EK\Theta_A \qquad |\text{EQN. } 24|$$

4.2.3 Sway correlation factors β and β_1

In section 3.9 of this thesis, the P-Δ moments of upper storeys were identified. These moments, which were defined as a function of the upper-storey sway Δ_U, will act as applied moments in terms of the slope-deflection approach. Since they have been related to a displacement parameter, the P-Δ moments will enter the load vector L_V in an iterative way, similar to the fixed-end moments. The structural analysis of the general subassemblage will focus on the core-module itself, which contains only one independent sway parameter, i.e. Δ. In order to restrict the analysis to the sway Δ, it becomes necessary to relate the upper-storey sway Δ_U to the sway Δ of the core-module. In fact, not only the upper-storey sway should be treated in this way, but also the lower-storey sway Δ_L. The lower storey sway will only feature for interior storeys, where P-Δ moments resulting from pure vertical loading may arise as described in section 3.9.2. In this case, the storey just below the core-module would transmit an approximate moment of magnitude $P_L\Delta_L/2$ to the core-modul .

The relative sways should be based on the results of a second-order analysis. This in itself could be a tedious task. However, since only the sway ratios are involved and since the secondary P-Δ moments are often small compared with the primary load moments, it was found that in most cases a first-order sway analysis would suffice. It must be stressed that the absolute sway Δ of the core-module is subsequently obtained on a second-order basis.

The sidesway charts of Wood & Roberts[55] are convenient for the assessment of the first-order sway relationships. This is demonstrated in principle for the limited frame of Figure 37.

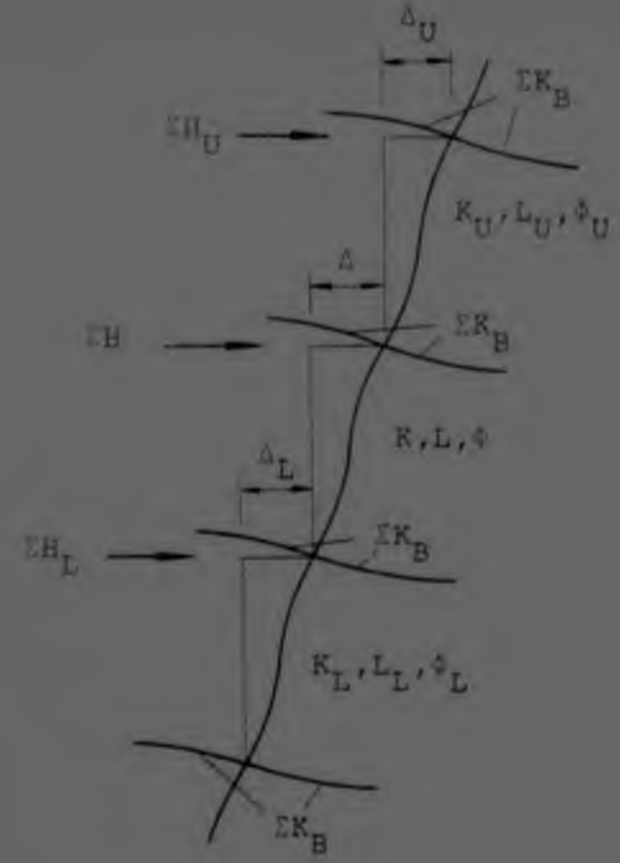

FIGURE 37: Relative sway of upper and lower storey

The suffixes (U) and (L) refer to the upper and lower storeys respectively. Using the relevant stiffness parameters, the sway index Φ can be obtained from typical charts such as reproduced from Reference 55 in Figure 38. The stiffness parameter K_t at the top and K_b at the bottom of the subassemblage sums the total stiffnesses of columns and beams of the entire storey.

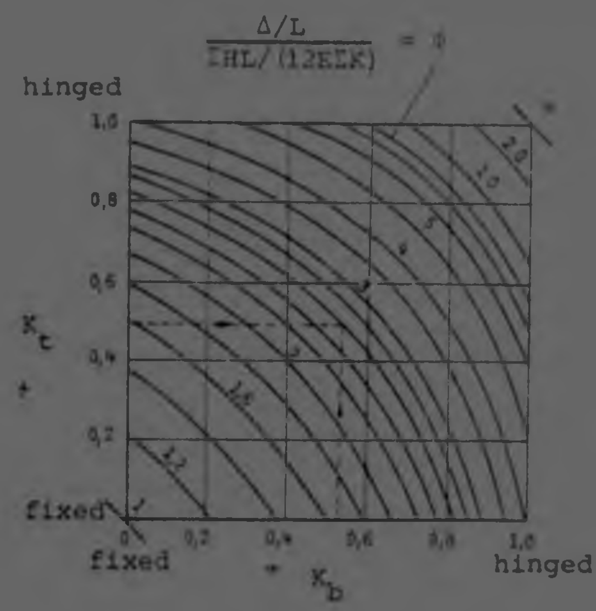

$$K_t = \frac{\Sigma(K_U+K)}{\Sigma(K_U+K) + 3\Sigma K_B}$$

$$K_b = \frac{\Sigma(K_L+K)}{\Sigma(K_L+K) + 3\Sigma K_B}$$

FIGURE 38: Size of sway in building frames[51]

For the applied horizontal loadings as shown in Figure 37, the sway ratios are as follows:

Upper storey:

$$\frac{\Delta_U}{L_U} = \frac{\Delta}{L}\,\frac{L_U}{L}\,\frac{\Sigma K}{\Sigma K_U}\,\frac{\Phi_U}{\Phi}\,\frac{\Sigma H_U}{\Sigma H}$$

and the sway correlation factor:

$$\beta = \frac{\Delta_U L^2}{L_U^2 \Delta} = \frac{\Phi_U}{\Phi}\,\frac{\Sigma K}{\Sigma K_U}\,\frac{\Sigma H_U}{\Sigma H} \qquad |\text{EQN. 25a}|$$

Lower storey:

$$\frac{\Delta_L}{L_L} = \frac{\Delta}{L}\,\frac{L_L}{L}\,\frac{\Sigma K}{\Sigma K_L}\,\frac{\Phi_L}{\Phi}\,\frac{\Sigma H_L}{\Sigma H}$$

and the sway correlation factor:

$$\beta_1 = \frac{\Delta_L}{L_L^2}\,\frac{L^2}{\Delta} = \frac{\Phi_L}{\Phi}\,\frac{\Sigma K}{\Sigma K_L}\,\frac{\Sigma H_L}{\Sigma H} \qquad |\text{EQN. 25b}|$$

If so desired, the first-order sway correlation factors β and β_1 could be adjusted to account for second-order effects by applying the well known concept of sway amplification. This is demonstrated for the value β. The second-order sway displacements of the storey under consideration (Δ_{II}) and the storey above (Δ_{UII}) may be expressed as follows:

$$\Delta_{II} = \frac{\Delta}{1 - \frac{\alpha \Sigma P_O}{\Sigma P_O}} = \frac{\Delta}{1 - \alpha}$$

$$\Delta_{UII} = \frac{\Delta_U}{1 - \frac{\Sigma P_U}{\Sigma P_{OU}}}$$

and then

$$\frac{\Delta_{UII}}{\Delta_{II}} = \frac{1 - \alpha}{1 - \frac{\Sigma P_U}{\Sigma P_{OU}}}\,\frac{\Delta_U}{\Delta}$$

This leads to the modified sway correlation factor of Equation 25c.

$$\beta' = \beta\,\frac{1 - \alpha}{1 - \frac{\Sigma P_U}{\Sigma P_{OU}}} \qquad |\text{EQN. 25c}|$$

in which,

α = Reduction factor defined in Equation 39

ΣP_O = Elastic buckling load of storey

ΣP_{OU} = Elastic buckling load of upper storey

ΣP_U = Total vertical load on upper storey, when storey below the upper storey is subjected to loading related to αP_O of that storey.

It is usually safe to use the approximation $\beta' = \beta$.

As already mentioned before (section 3.9.2.) pure vertical loading can also cause sidesway and thus P-Δ moments. In this case the resulting sway will be a function of the member stiffnesses and the size of the applied vertical loading. However, since the sway will be small or even zero, the P-Δ moments compared with the primary moments can be expected to be less significant than those for the case of combined horizontal and vertical loading. Where applicable, it is proposed to retain the expressions of Equations 25a and 25b for the sway correlation factors, replacing the horizontal load quotient by the appropriate ratio of the vertical forces. However, setting $\Delta_U = \Delta_L = \Delta$ will not result in a significant error for pure vertical loading.

4.2.4 Rotation correlation factors β_2 and β_3

The correlation factors β_2 and β_3 are exclusively concerned with the vertical load analysis, to which the general subassemblage of Figure 25 applies. They will be used to relate the far-end rotations of the ancillary columns to the rotations of the nodes of the core-module. Adjusting the basic slope-deflection expression of Equation 14 for such a case gives for a lower column

$$M_{AB} = EKS \left[(1+C)\beta_2\Theta_A - (1+C) \frac{\beta_1 \Delta L_L}{L^2} \right] \qquad |EQN. 26a|$$

and, similarly, for an upper column

$$M_{AB} = EKS \left[(1+C)\beta_3\Theta_A - (1+C) \frac{\beta \Delta L_U}{L^2} \right] \qquad |EQN. 26b|$$

where,

$$\beta_2 = \beta_3 = \frac{1}{1+C}\left(1 + \frac{C\Theta_B}{\Theta_A}\right) \qquad |EQN. 26c|$$

For zero axial load the expression for β_2 and β_3 simplifies to

$$\beta_2 = \beta_3 = \frac{1}{3}\left(2 + \frac{\Theta_B}{\Theta_A}\right) \qquad |EQN. 26d|$$

In Equations 26a to 26d, the suffix (A) refers to the near end of the column. The sway correlation factors β and β_1 have been derived in the preceding section.

The rotational behaviour of the ancillary columns, when the subassemblage is subjected to vertical loads, will vary between double and single-curvature bending, depending on the rotational restraints at the column ends and the loading on the adjoining beams. In many cases an estimation of the likely points of inflection will be sufficiently accurate. In this study, the case of a column bent in double curvature ($\Theta_A = \Theta_B$) has been taken as the reference stiffness with a value of β_2 or β_3 equal to 1,0. This condition would apply to the case of full and uniform frame loading and equal beam stiffnesses at both column ends. The case of single-curvature bending ($\Theta_B = -\Theta_A$) may be approximated for checkerboard loading as shown in Figures 28 and 29. The corresponding relative stiffness value is one third of that applicable to double-curvature behaviour, i.e. a figure of 0,33 would be relevant for Θ_2 or Θ_3. A blanket figure of 0,67 has been proposed elsewhere[113] . Two correlation values β_2 and β_3 have been suggested to allow for independent values to occur for the columns above and below the core-module.

A special situation may arise when a lower column is located in the bottom storey of a frame. In this case the far-end rotation of this lower column is governed by the base-soil interaction and the base plate particulars. For this case the correlation factor β_2, which refers to the lower column, should include for the degree of elastic base restraint $\bar{K}_S$ as defined in section 4.1.6. An expression suitable for this condition is given in Equation 27b. This equation has been derived from the basic slope-deflection Equation 14. ignoring the sway and the stiffness effects of axial column forces. Relating the stiffness to double-curvature conditions and assuming an elastic rotational base restraint at the remote end B, Equation 14 reduces to

$$M_{AB} = 6\beta_2 \, EK\theta_A \qquad |EQN.\ 27a|$$

with

$$\beta_2 = \frac{4 - \dfrac{4}{\overline{K}_S + 4}}{6} \qquad |EQN.\ 27b|$$

For a fully fixed base ($\overline{K}_S \to \infty$) a value $\beta_2 = 2/3$ would be approached, and a pin-ended column ($\overline{K}_S \to 0$) would correspond to a factor $\beta_2 = 1/2$.

On the basis of Equation 27b, the simplified practical cases discussed in section 4.1.6 result in the following correlation factors:

"Quasi-pinned" conditions : β_2 = 0,504

"Quasi-fixed" conditions : β_2 = 0,533

4.2.5 Load vector

The load vector relevant to the horizontal and vertical load analyses will comprise seven elements each, containing applied joint moments, applied joint loads, fixed-end moments and shear forces. The fixed-end moments are of the second-order type. Some typical results of fixed-end moments are given in Appendix II/2. The P-Δ moments derived in section 3.9 will also be included in the load vector. Since the load analysis is executed iteratively, the P-Δ moments will initially be introduced as zero and then adjusted in subsequent steps of the iteration cycle, as the sway Δ becomes more accurate.

4.2.6 Slope-deflection method applied to load analysis

4.2.6.1 Vertical load

Applying the procedure outlined in section 4.1.9 to the general subassemblage, and considering the vertical components of the load arrangement explained in section 4.2.1, results in a set of seven inhomogeneous linear equations given in matrix format by

$$\bar{B}_{1V}\, D_{1V} = L_{VV} \qquad |\text{EQN. } 28a|$$

where,

$\bar{B}_{1V}$ = Stiffness matrix related to vertical loading

D_{1V} = Displacement vector related to vertical loading (rotation plus sway)

L_{VV} = Load vector related to vertical loading.

The expanded form of Equation 28a appears in Table 2 for the subassemblage shown in Figure 25. The equations of Table 2 are relevant to the case of a completely interior subassemblage. The equations for curtailed subassemblages are derived by setting the stiffnesses of redundant members equal to zero. In addition, for bottom storeys, the correlation factors β_1 and β_2 are zero in conjunction with the base stiffnesses $\bar{F}_1$ and $\bar{F}_4$. In their place the new terms $\bar{F}_1K_{34}$ and $\bar{F}_4K_{34}$ become part of the matrix elements $\bar{B}_{1,11}$ and $\bar{B}_{1,44}$ respectively. The second suffix refers to the location of the element within the matrix $\bar{B}_1$ of Table 2. The detailed procedure leading to the system of linear

TABLE 2: Equations $\bar{B}_{1V}\, D_{1V} = L_{VV}$

$K_{12}S_{12}+\bar{F}_1 SC_{L1}B_2 + \frac{4I_{B1}}{L_{26}} + \frac{4I_{14}}{L_{23}}$	$K_{12}S_{12}C_{12}$	0	$\frac{2I_{14}}{L_{23}}$	0	0	$-SC_{12}L_{34}$ $-\bar{F}_1 SC_{L1}B_1 \frac{L_{L1}}{L_{34}}$	D_1	$-\frac{1}{E}\Big(B_0 M_{V23}+B_7 M_{V23}$ $-F_{L1}\frac{B_1}{2}\epsilon_1\frac{L_{L1}^2}{L_{12}^2}\delta\Big)$
$K_{12}S_{12}C_{12}$	$K_{12}S_{12}+K_{23}S_{23}$ $+K_{26}S_{23}+\bar{F}_2 SC_{U2}B_3$	$K_{23}S_{23}C_{23}$	0	0	$K_{26}S_{23}C_{23}$	$-SC_{12}L_{34}$ $-\bar{F}_2 SC_{U2}B \frac{L_{U2}}{L_{34}}$	D_2	$-\frac{1}{E}\Big(M_{V23}+M_{V26}-F_2$ $\frac{B}{2}\epsilon_2\frac{L_{U2}^2}{L_{12}^2}\delta\Big)$
0	$K_{23}S_{23}C_{23}$	$K_{23}S_{23}+K_{34}S_{34}$ $+K_{35}S_{23}+\bar{F}_3 SC_{U3}B_3$	$K_{34}S_{34}C_{34}$	$K_{35}S_{23}C_{23}$	0	$-SC_{34}L_{34}$ $-\bar{F}_3 SC_{U3}B \frac{L_{U3}}{L_{34}}$	D_3	$-\frac{1}{E}\Big(M_{V32}+M_{V35}-F_3$ $\frac{B}{2}\epsilon_3\frac{L_{U3}^2}{L_{34}^2}\delta\Big)$
$\frac{2I_{14}}{L_{23}}$	0	$K_{34}S_{34}C_{34}$	$K_{34}S_{34}+\bar{F}_4 SC_{L4}B_2$ $+\frac{4I_{B4}}{L_{35}}+\frac{4I_{14}}{L_{23}}$	0	0	$-\bar{F}_4 SC_{L4}B_1 \frac{L_{L4}}{L_{34}}$ $-SC_{34}L_{34}$	$\times$ D_4	$-\frac{1}{E}\Big(B_0 M_{V32}+B_9 M_{V35}$ $-F_{L4}\frac{B_1}{2}\epsilon_4\frac{L_{L4}^2}{L_{34}^2}\delta\Big)$
0	0	$K_{35}S_{23}C_{23}$	0	$K_{35}S_{23}+4K_{B5}$ $+\bar{F}_{U5}SC_{U5}B_3$ $+SC_{L5}B_2\bar{F}_{L5}$	0	$-\bar{F}_{U5}SC_{U5}B\frac{L_{U3}}{L_{34}}$ $-SC_{L5}\bar{F}_{L5}$	D_5	$-\frac{1}{E}\Big(M_{E53}+M_{E23}-P_5$ $\frac{B}{2}\epsilon_5\frac{L_{U3}^2}{L_{34}^2}\delta\Big)$
0	$K_{26}S_{23}C_{23}$	0	0	0	$K_{26}S_{23}+4K_{B6}$ $+\bar{F}_{U6}SC_{U6}B_3$ $+\bar{F}_{L6}SC_{L6}B_2$	$-\bar{F}_{U6}SC_{U6}B\frac{L_{U2}}{L_{34}}$ $-SC_{L6}\bar{F}_{L6}$	D_6	$-\frac{1}{E}\Big(M_{E62}+M_{E32}-F_6$ $\frac{B}{2}\epsilon_6\frac{L_{U2}^2}{L_{34}^2}\delta\Big)$
SC_{12}	SC_{12}	SC_{34}	SC_{34}	0	0	$-SC_{122}-SC_{342}$ $-\bar{F}_7\frac{K_{34}}{L_{34}}$	$\frac{\Delta}{L_{34}}$	0

equations of Table 2 is set out in Appendix II/2.

4.2.6.2 Horizontal load

Analysing the subassemblage of Figure 31 for the case of horizontal loading, a similar set of linear equations is obtained which is given in matrix format by

$$\bar{B}_{1H}D_{1H} = L_{VH} \qquad |\text{EQN. 28b}|$$

where,

$\bar{B}_{1H}$ = Stiffness matrix related to horizontal loading

D_{1H} = Displacement vector related to horizontal loading (rotation plus sway)

L_{VH} = Load vector related to horizontal loading

The extended form of Equation 28b is given in Table 3. Further details can be found in Appendix II/2.

4.2.6.3 Axial forces

It has been argued earlier in section 4.2.1, that the second-order load analysis is an iterative procedure because of the change in axial member forces. Hence, between successive iteration steps, in order to solve Equation 22, a new set of axial forces has to be calculated from Equation 23. The expanded form of Equation 23, which is derived by satisfying equilibrium at the joints, is given in Table 4 for the salient axial forces.

equations of Table 2 is set out in Appendix II/2.

4.2.6.2 Horizontal load

Analysing the subassemblage of Figure 31 for the case of horizontal loading, a similar set of linear equations is obtained which is given in matrix format by

$$\bar{B}_{1H} D_{1H} = L_{VH} \qquad |\text{EQN. } 28b|$$

where,

$\bar{B}_{1H}$ = Stiffness matrix related to horizontal loading

D_{1H} = Displacement vector related to horizontal loading (rotation plus sway)

L_{VH} = Load vector related to horizontal loading

The extended form of Equation 28b is given in Table 3. Further details can be found in Appendix II/2.

4.2.6.3 Axial forces

It has been argued earlier in section 4.2.1, that the second-order load analysis is an iterative procedure because of the change in axial member forces. Hence, between successive iteration steps, in order to solve Equation 22, a new set of axial forces has to be calculated from Equation 23. The expanded form of Equation 23, which is derived by satisfying equilibrium at the joints, is given in Table 4 for the salient axial forces.

TABLE 3: Equations $\bar{B}_{1H}\, D_{1H} = L_{VH}$

$K_{12}S_{12}$	$K_{12}S_{12}C_{12}$	0	0	0	0	$-SC_{12}L_{34}$		θ_1		$-\frac{M_{F12}}{E}$
$K_{12}S_{12}C_{12}$	$K_{12}S_{12}+K_{23}S_{23}$ $+K_{26}S_{23}$	$K_{23}S_{23}C_{23}$	0	0	$K_{26}S_{23}C_{23}$	$-SC_{12}L_{34}$		θ_2		$-\frac{1}{E}\Big(M_{F21}-M_{2AP}$ $-P_2\,\frac{\beta}{2}\,\frac{L_{U2}^2}{L_{34}^2}\,\Delta\Big)$
0	$K_{23}S_{23}C_{23}$	$K_{34}S_{34}+K_{23}S_{23}$ $+K_{35}S_{23}$	$K_{34}S_{34}C_{34}$	$K_{35}S_{23}C_{23}$	0	$-SC_{34}L_{34}$		θ_3		$-\frac{1}{E}\Big(M_{F34}-M_{3AP}$ $-P_3\,\frac{\beta}{2}\,\frac{L_{U3}^2}{L_{34}^2}\,\Delta\Big)$
0	0	$K_{34}S_{34}C_{34}$	$K_{34}S_{34}$	0	0	$-SC_{34}L_{34}$	x	θ_4	=	$-\frac{M_{F43}}{E}$
0	0	$K_{35}S_{23}C_{23}$	0	$K_{35}S_{23}$	0	0		θ_5		0
0	$K_{26}S_{23}C_{23}$	0	0	0	$K_{26}S_{23}$	0		θ_6		0
SC_{12}	SC_{12}	SC_{34}	SC_{34}	0	0	$-SC_{342}-SC_{122}$ $-\bar{F}_7\,\frac{K_{34}}{L_{34}}$		$\frac{\Delta}{L_{34}}$		$\frac{1}{E}\Big(V_{210}-\frac{M_{F12}+M_{F21}}{L_{34}}$ $+V_{340}-H-\frac{M_{F34}+M_{F43}}{L_{34}}\Big)$

TABLE 1: Axial force equations $P = S_P D_P + F_P$

P_{12}	0	$ESC_{23}\left(-1 + \frac{L_{23}}{K_{23}} \frac{K_{26}}{L_{26}}\right)$	$-ESC_{23}$	0	$ESC_{23} \frac{L_{23}}{K_{23}} \times \frac{K_{26}}{L_{26}}$	0	$P_2 - \frac{M_{F23}+M_{F32}}{L_{23}}$ + [illegible] O $+ \frac{M_{F26}+M_{F62}}{L_{26}} - V_{260}$
P_{23}	ESC_{12}	ESC_{12}	0	0	0	$-\frac{ESC_{122}}{L_{34}}$	$\frac{M_{F12}+M_{F21}}{L_{12}} - V_{210} + H$
P_{34}	0	ESC_{23}	$ESC_{23}\left(1 - \frac{L_{23}}{K_{23}} \frac{K_{35}}{L_{35}}\right)$	$-ESC_{23} \frac{L_{23}}{K_{23}} \times \frac{K_{35}}{L_{35}}$	0	0	$\frac{M_{F32}+M_{F23}}{L_{23}} - V_{320} + P_3 + V_{350} - \frac{M_{F35}+M_{F53}}{L_{35}}$
R_5	0	0	$ESC_{23} \frac{K_{35}}{L_{35}} \times \frac{L_{23}}{K_{23}}$	$ESC_{23} \frac{K_{35}}{L_{35}} \times \frac{L_{23}}{K_{23}}$	0	0	$\frac{M_{F35}+M_{F53}}{L_{35}} - V_{530} + P_5$
R_6	0	$-ESC_{23} \frac{K_{26}}{L_{26}} \times \frac{L_{23}}{K_{23}}$	0	0	$-ESC_{23} \frac{K_{26}}{L_{26}} \times \frac{L_{23}}{K_{23}}$	0	$P_6 - \frac{M_{F26}+M_{F62}}{L_{26}} + V_{260}$

$$\times \begin{bmatrix} \theta_1 \\ \theta_2 \\ \theta_3 \\ \theta_5 \\ \theta_6 \\ \Delta \\ + \end{bmatrix}$$

The expressions in column 7 of the matrix $\bar{S}_p$ contain values relevant to the vertical and horizontal load analyses. They need to be separated for the individual analysis steps.

The detailed procedure leading to the development of the system of linear equations of Table 4 is set out in Appendix II/2.

CHAPTER 5

ANALYSIS OF "SYMMETRY-BUCKLING" OF SUBASSEMBLAGES AND CORRESPONDING STRESSES

5.1 Analysis of "Symmetry-Buckling"

5.1.1 General concept

In contrast to the case of conventional buckling, where all loads are considered to be applied at the joints of the structure causing axial forces only, a special approach can be adopted for a symmetrical structure subjected to symmetrical loading acting between the joints. In this case, which is defined as "Symmetry-Buckling", symmetrical pre-buckling bending moments, axial forces and deflections will arise which may affect the stiffnesses of members and the size of the elastic buckling load. At the instance of sway buckling, an antisymmetrical displacement mode is superimposed upon the symmetrical pre-buckling deformations.

In essence, two methods have been used to analyse the special condition of "Symmetry-Buckling". Chwalla[104] and Scholz[97] adopted a purely equilibrium-based approach, Masur et al[105] and Lu[106] chose the extended slope-deflection method, taking the differentials of the stability functions into account. Lu[106] concluded that the difference in the elastic buckling load, comparing "Symmetry-Buckling" with an approach neglecting pre-buckling bending effects, would not exceed 10 per cent. Most of this discrepancy is attributable to the reduction in beam stiffness due to the axial thrust generated in portal frames.

The reason for including the case of "Symmetry-Buckling" in this study as a separate entity is twofold. Firstly, because the conventional slope-deflection concept cannot solve this problem in the usual way. Secondly, although the condition of "Symmetry-Buckling" may have a small effect on the elastic buckling load, it was found to be of significance for the computation of the "limiting slenderness ratio" λ_ℓ. It has been pointed out that this parameter is of particular importance in the method proposed in this research. For these reasons, the problem of "Symmetry-Buckling" has been fully analysed.

Chwalla[134] has proven for a simple portal frame that "Symmetry-Buckling" is characterised by a bifurcation point in the load-rotation relationship if analysed by linear elastic, second-order theory. This indicates that a finite state of deformations and thus stresses exists for the elastic buckling load P_O.

In Figure 39 a frame qualifying for the case of "Symmetry-Buckling" and an axially loaded, perfect column are compared.

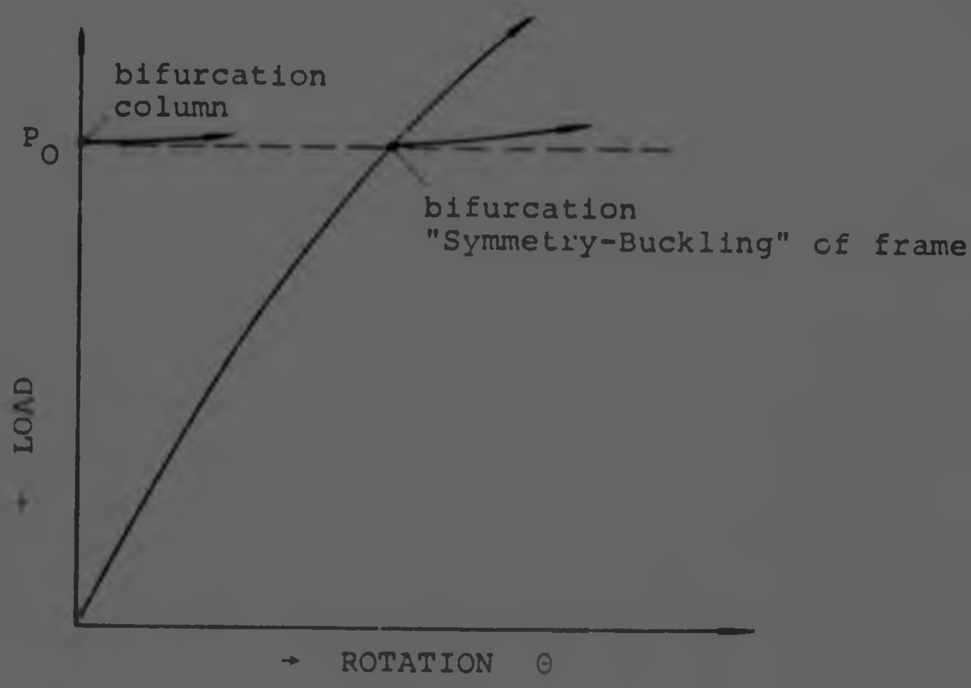

FIGURE 39: Load bifurcation - "Symmetry-Buckling"

In order to establish the condition under which the structure becomes laterally unstable, it is necessary to consider the equilibrium of a frame qualifying for the case of "Symmetry-Buckling" in its infinitesimally displaced shape, observing the presence of pre-buckling deformations. In this study the method adopted for this purpose is based on the extended slope-deflection concept including the differentiated stability functions. If applied to the investigated structure a homogeneous system of linear equations is obtained, which is expressed in matrix form in Equation 29. For the infinitesimally displaced structure no new externally applied loading is generated, so that the load vector term is equal to zero.

$$\bar{C}\ \delta D_1 = 0 \qquad |\text{EQN. } 29|$$

where,

$\bar{C}$ = Stiffness matrix for "Symmetry-Buckling"

δD_1 = Displacement vector of infinitesimally displaced frame (rotation plus sway)

To arrive at a set of equations as implied by Equation 29, which contains as variables only the infinitesimal displacements δD_1, the unknown changes in axial force δP need to be expressed as functions of the primary displacements D_1. This is achieved by satisfying horizontal and vertical equilibrium at the joints of the structure. The resulting equations are used to solve for δP and, subsequently, these expressions are substituted into Equation 29. Only in this way, which is not a programmable process, because it involves solutions and back-substitutions of general algebraical equations, can the homogeneous Equation 29 be found.

As for the non-symmetrical cases, the elastic buckling load P_O is calculated from the determinant of the stiffness matrix by searching for the lowest possible root of Equation 30, excluding the trivial solution $D_1 = 0$.

$$|\bar{C}| = 0 \qquad |\text{EQN. } 30|$$

The load arrangement related to P_0 must not only satisfy Equation 30, but the corresponding load vector must also simultaneously fulfil the requirements of Equations 22 and 28a. The displacement vector D_1 obtained from Equation 22 will be used in determining the stiffness matrix $\bar{C}$ and thus the determinantal Equation 30. The displacement vector D_1 is not suitable for calculating discrete bending moments corresponding to loading equal to P_0, since the determinants of Equations 22 and 29 almost simultaneously attain a zero value. This makes a unique solution impossible. In fact, any number of solutions satisfying both equations may exist. However, since the overall equilibrium state as such is not disturbed in the vicinity of the zero determinant, the resulting solution for the displacements as a whole can still be used to determine the elastic buckling load P_0. This has been confirmed when calculated results were compared with purely equilibrium-based solutions.

5.1.2 Slope-deflection method including the differentials of the stability functions

It has been mentioned before that for the case of "Symmetry-Buckling" it is necessary to consider the equilibrium of a structure and its members in its infinitesimally displaced shape, observing the effects of loading applied directly to the member between the joints. For this purpose a member A-B, which is already deformed due to applied loading, is assumed to be further displaced by an infinitesimal amount as shown in Figure 40.

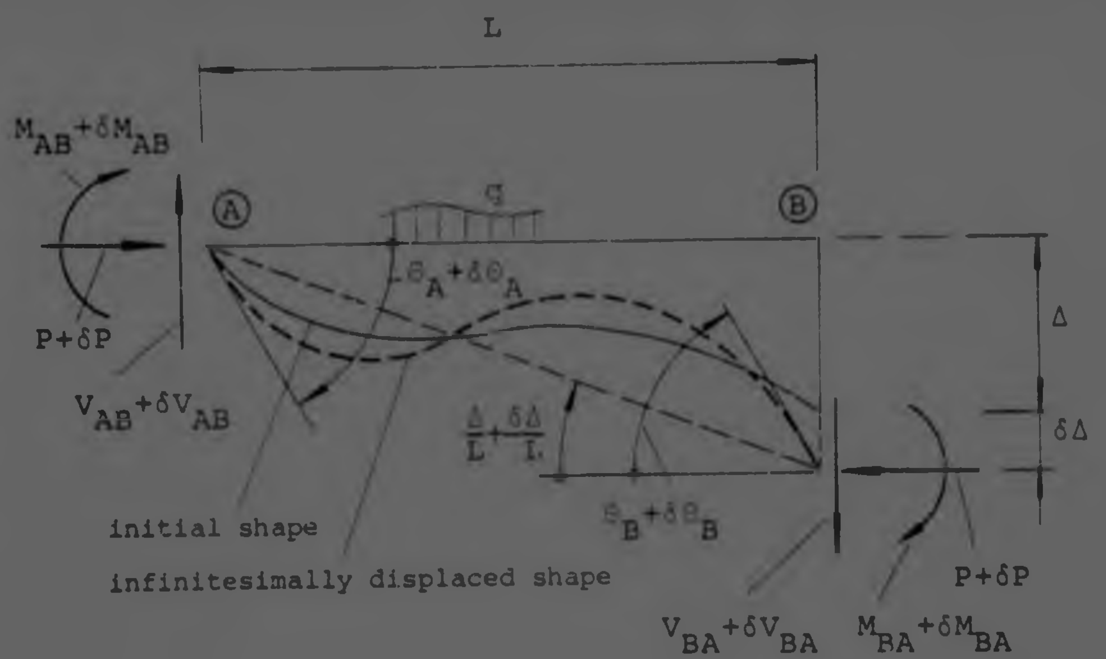

FIGURE 40: Infinitesimally displaced member

The terms δM, δP and δV are the force changes corresponding to the imposed infinitesimal displacements $\delta\Theta$ and $\delta\Delta$. The incremental moment and shear changes, which can be found by differentiation of the basic expressions of Equation 14 and Equation 16 respectively, are obtained as follows, ignoring products of second-order magnitude.

$$\delta M_{AB} = EK\left\{S\left[\delta\Theta_A + C\delta\Theta_B + \delta C\Theta_B - (1+C)\frac{\delta\Delta}{L} - \delta C\frac{\Delta}{L}\right] + \delta S\left[\Theta_A + C\Theta_B - (1+C)\frac{\Delta}{L}\right]\right\} + \delta M_{FAB} \qquad |\text{EQN. } 31|$$

and

$$\delta V_{AB} = \frac{EK}{L^2}\left[S^2\ (1-C^2)\delta\Delta+2S\delta S(1-C^2)\Delta\ -2S^2C\delta C\Delta\right]$$

$$-\ \frac{EK}{L}\left[S(\delta\Theta_A+\delta\Theta_B)(1+C)+(S\delta C+\delta S+C\delta S)(\Theta_A+\Theta_B)\right]$$

$$-\ \frac{\delta M_{FAB}+\delta M_{FBA}}{L} \qquad |\text{EQN. } 32|$$

The expressions in Equations 31 and 32 contain primary terms such as S, C, Δ, Θ_A, Θ_B, and the equivalent differentiated values including the incremental changes to the fixed-end moment, i.e. δM_F. The changes in the stability functions, δC and δS, and in the fixed-end moments, δM_F, are caused by the change in P due to $\delta\Theta$ and $\delta\Delta$. The differentials of the stability functions were originally derived by Masur[114] and were subsequently applied to simple portals by Lu[106]. Conveniently, they can be expressed as follows, utilising the basic stability functions S and C.

$$S' = \frac{\delta S}{\delta P} = \frac{S}{2P}\ (1-C^2S) \qquad |\text{EQN. } 33a|$$

$$C' = \frac{\delta C}{\delta P} = \frac{C+1}{2P}\left[1-CS(1-C)\right] \qquad |\text{EQN. } 33b|$$

Further details in connection with the incremental force changes are given in Appendix III. The case of zero axial forces for the members and the fixed-end moments for a number of beam loadings are covered in the same appendix.

5.1.3 Extended slope-deflection method applied to the general subassemblage

The stiffness matrix $\bar{\bar{C}}$ for "Symmetry-Buckling" is obtained in a similar way as matrix $\bar{\bar{B}}$ for ordinary buckling. Seven homogeneous linear equations result from the following procedure:

a) Satisfying that $\Sigma\delta M = 0$ for the six joints of the core-module.

b) Formulating the sway-equilibrium equation for the incremental sway change $\delta\Delta$ of the core-module.

c) Substituting the incremental axial force changes δP into equations derived from steps a) and b) above.

Expressing the resulting equations in matrix form leads to the 49 elements of the stiffness matrix $\bar{\bar{C}}$ given in Table 5.

Table 5 has been prepared for the general case. It must be remembered that "Symmetry-Buckling" is characterised by truly symmetrical pre-buckling deformations upon which an antisymmetrical displacement mode is superimposed at the instance of buckling. Because of this condition, the incremental axial froce changes δP in the beams are zero and certain terms $\alpha_i \delta P_{23}$ will thus disappear. These are listed below:

$$\alpha_3 \delta P_{23} = 0$$

$$\alpha_4 \delta P_{23} = 0$$

$\alpha_8\ \delta P_{23} = 0$

$\alpha_{10}\delta P_{23} = 0$

$\alpha_{11}\delta P_{23} = 0$

$\alpha_{12}\delta P_{23} = 0$

This will also reduce the terms $\alpha_7\alpha_8\delta P_{23}$ to zero and $1-\alpha_7\alpha_8\delta P_{23}$ to 1,0. The latter expression has been abbreviated to α_{78} in the stiffnes matrix of Table 5. The parameters α_i contain the symmetrical pre-buckling deformations of the structure, the ordinary stability functions and their differentials and appear as the coefficients of the axial force changes δP. The derivation of these coefficients is given in Appendix III.

The representation of the infinitesimal force changes in the ancillary members has also been simplified by ignoring axial force variations. It was felt, that this is justifiable on the grounds that other approximations have already been introduced with respect to the member behaviour at the remote ends.

The lowest root of the determinantal equation of matrix C of Table 5 corresponds to the elastic buckling load applicable to the case of "Symmetry-Buckling", analysing a completely interior storey. Curtailed subassemblages are investigated by introducing zero stiffnesses for the redundant members. In addition, for bottom storeys, the terms in brackets for elements $\bar{C}_{11}$ and $\bar{C}_{14}$ must be set equal to 1,0.

The procedure applicable to the case of "Symmetry-Buckling" can also be followed for non-symmetrical structural or load arrangements such as occur in the external subassemblages of otherwise completely symmetrical frames, provided the pre-buckling sway effects are eliminated by setting $\Delta = 0$ at all times.

5.2 Stresses corresponding to "Symmetry-Buckling"

5.2.1 General

The elastic buckling load obtained from matrix $\bar{C}$ of Table 5 together with the associated axial column forces will be used to find the second-order bending moments within the structure, with the ultimate objective of calculating the "limiting slenderness ratio". The differential equation method is employed for this purpose. It could be argued, once the elastic buckling load is known from matrix $\bar{C}$, that Equation 22 could be solved for the displacements D_1, from which the second-order moments would follow, using the slope-deflection approach. However, such a solution is unreliable by virtue of the close proximity of the zero determinants for both matrices $\bar{B}_1$ and $\bar{C}$. It is because of this shortcoming, that recourse has been made to the differential equation method.

5.2.2 Differential equation method applied to general subassemblage

The differential equation method is now applied to the relevant subassemblages. The complexity of the problem remains substantial despite various simplifications. For the case of "Symmetry-Buckling", the storey sway is irrelevant since no sway exists prior to buckling. In addition, the influence of loading on the beams next to nodes 1 and 4 and the ancillary beams adjoining nodes 5 and 6 will be accounted for by an approximate procedure. In this context, it must be remembered that other simplifications have been made for interior storeys in regard to member forces and rotations at the remote ends of ancillary columns. Furthermore, most importantly, the section attaining yield first, is typically found in the region between joints 2 and 3 of the subassemblage. Here the effect of loading on the ancillary beams is greatly reduced.

For "Symmetry-Buckling" the same load cases are investigated as before, namely uniformly distributed and point loading on the beams. The deformed subassemblage shown in Figure 41 may either be applicable to the bottom storey or to an inner storey of a framework. As applicable, the ancillary members and the beam between joints 1 and 4 are represented as elastic rotational restraints. In bottom storeys, the column base behaviour is considered in a similar manner.

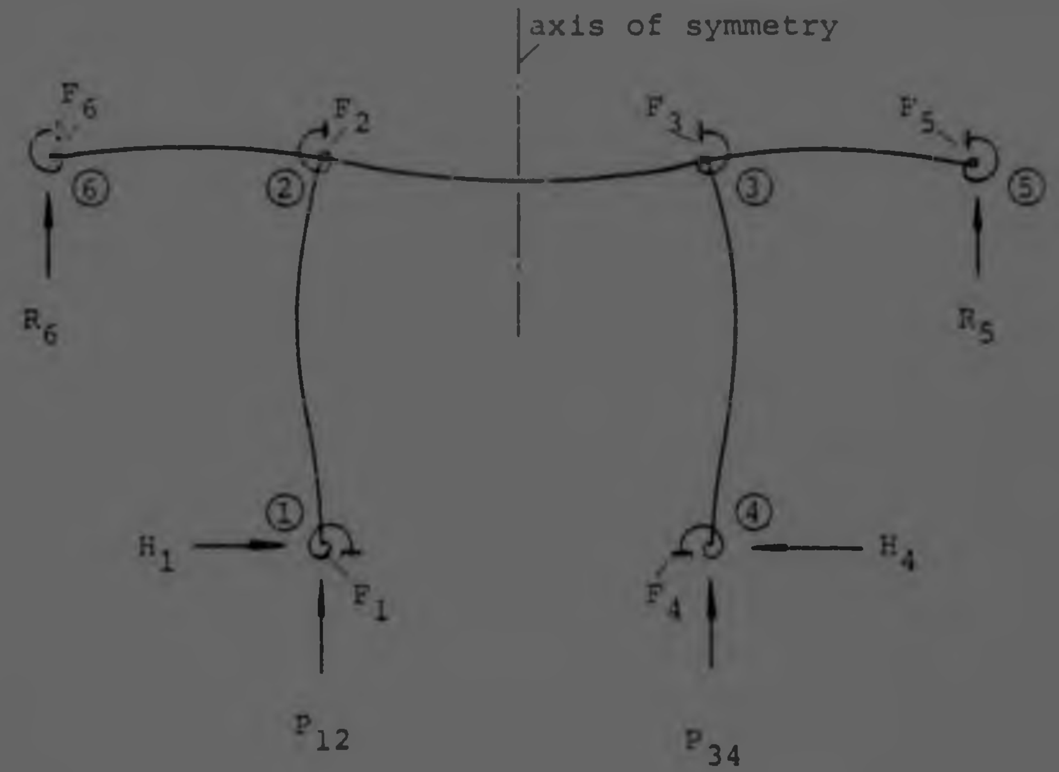

FIGURE 41: Subassemblage for "Symmetry-Buckling

For the differential equation procedure, the deformed elastic shape of each member is found from the following basic member equations:

$$EI\frac{d^2y_i}{dx_i^2} + M + P\,y_i = 0 \qquad \text{EQN. 34}$$

where M is defined as the bending moment at a position x_i comprising the member-end moment at the origin (x_i=0) plus the effect of any applied transverse loads. The solution of equations such as Equation 34 attain the following transcendental configuration:

$$y_i = C_1 \sin \frac{mx_i}{L} + C_2 \cos \frac{mx_i}{L} + a_1 x_i^2 + a_2 x_i + a_3 \quad |\text{EQN. } 35|$$

Herein, m is the axial member force parameter, C_1 and C_2 are constants of integration, coefficients a_1, a_2 and a_3 are functions of the moments M, shears V and axial forces P, and y_i and x_i are the co-ordinates of deflection and distance respectively. Because of symmetry, it is sufficient to investigate one half of the subassemblage as shown in Figure 42.

The bending moments M required for substitution into Equation 34 have to be formulated separately for each deformed member of the subassemblage. This is illustrated in Figure 42 for the case of point loadings on the beams.

The bending moment M for member 4-3 would, for example, take the following form:

$$M = P_{34}y_2 + H_4x_2 - \frac{q_{34}x_2^2}{2} - M_{m4} - \text{ad } M_{43}$$

The term ad M_{43} will be explained in section 5.2.3

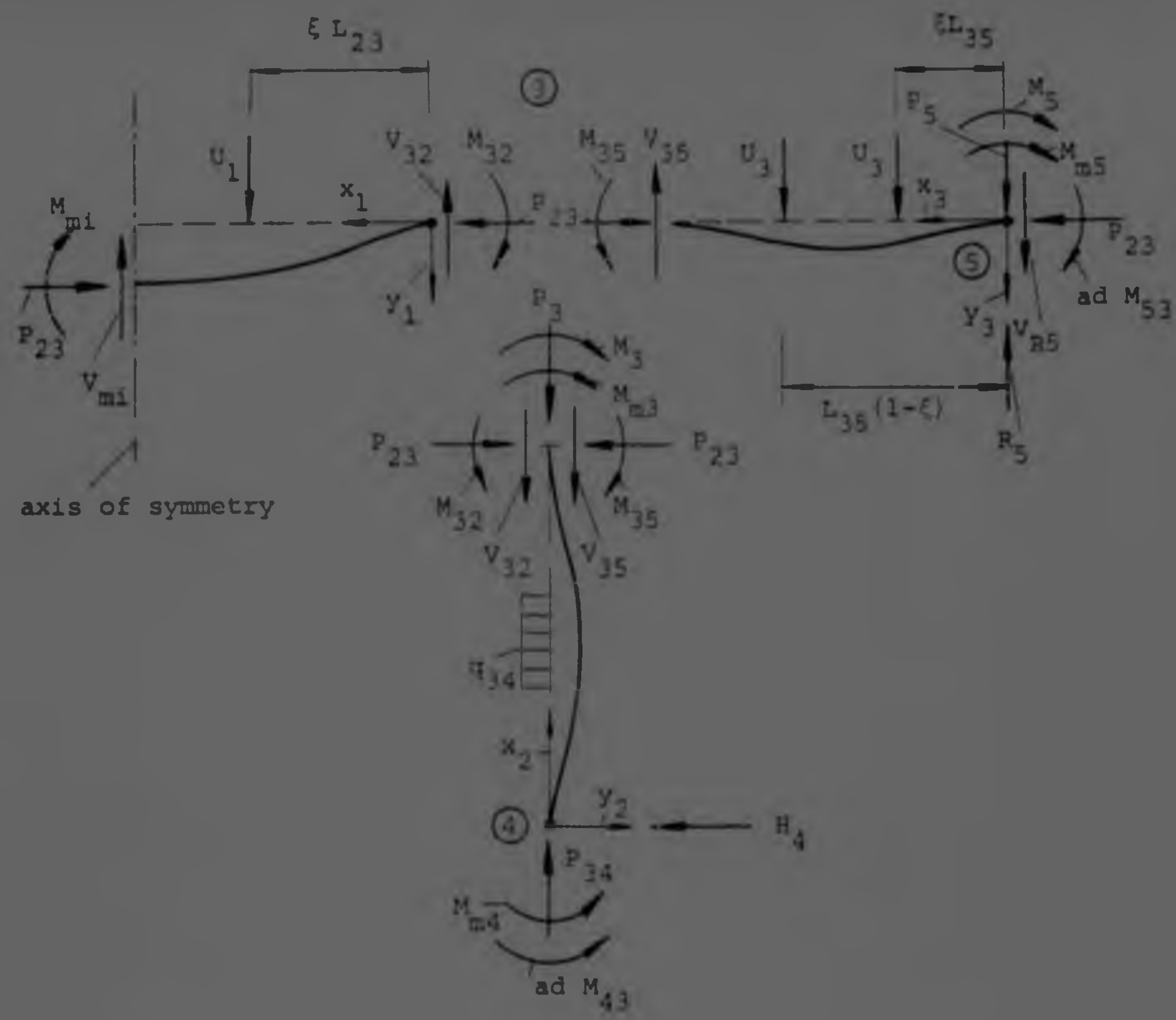

FIGURE 42: Deformed members

Applying the preceding principles to the subassemblage of Figure 41, it has been found that the structure is left with one redundancy. This unknown has first to be determined before the member moments can be calculated on an equilibrium basis. Conveniently, the horizontal shear force H_4 at joint 4 has been chosen as the unknown force. Since H_4 will appear in the arguments of a trigonometric equation, the solution must be attempted on a trial and error basis. The relevant equation for H_4 is derived after a lengthy procedure which is demonstrated in detail in Appendix IV/1 for various load arrangements. The method commences with the development of expressions such as given in Equations 34 and 35.

The final results for the cases which have been investigated are given below. Two formulae have been obtained for each load case. The first equation refers to conditions applicable to bottom storeys and top-most storeys and the second equation to intermediate storeys of multistorey frames. For the latter, it has been assumed that no axial beam forces exist. This will generally simplify the formulations.

<u>Case 1</u>: Dual-point loading on beams

$$C_9 \frac{m_{23}}{L_{23}} \cos m_{23}\xi + a_4 \frac{m_{23}}{L_{23}} \sin m_{23}\xi - b_4$$

$$- C_{12} \frac{m_{23}}{L_{23}} \left(\tan \frac{m_{23}}{2} \cos m_{23}\xi - \sin m_{23}\xi\right) = 0 \quad |\text{EQN. 36a}|$$

$$C_9 - \left[C_{11} - \frac{U_1}{2} (\xi L_{23})^2\right] \frac{1}{EI_{23}} = 0 \quad |\text{EQN. 36b}|$$

<u>Case 2</u>: Uniformly distributed beam loading

$$C_5 \frac{m_{23}}{L_{23}} \cos \frac{m_{23}}{2} - C_6 \frac{m_{23}}{L_{23}} \sin \frac{m_{23}}{2} - b_4 + c_4 L_{23} = 0 \quad |\text{EQN. 37a}|$$

$$C_5 + \left(c_4 \frac{L_{23}^3}{24} + a_4 \frac{L_{23}}{2} - b_4 \frac{L_{23}^2}{8} \right) \frac{1}{EI_{23}} = 0 \quad |\text{EQN. 37b}|$$

The constants of integration C_4, C_5, C_6, C_9, C_{11} and C_{12} as well as the force parameters contained in coefficients a_4, b_4 and c_4 are also explained in Appendix IV/1.

Cases for which the horizontal shear H_4 is zero are not covered by Equations 36a to 37b. However, for zero shear the columns are effectively not subjected to moments and the beam moment computations are trivial. A typical case is a completely interior regular subassemblage of a multi-storey, multi-bay structure for which moments can be established on a first-order, fixed-end basis.

For the general case, after calculating the shear force H_4 by satisfying the relevant Equations 36a, 36b or 37a, 37b, the bending moment at any section of the subassemblage can be computed, starting with the member-end moments.

5.2.3 <u>Additional bending moments</u>

So far, in the analysis for loading, beam members adjoining nodes 1 and 4 or 5 and 6 in Figure 41 have only been introduced with their rotational stiffnesses F_1,F_4,F_5 and F_6.

For upper subassemblages of multi-storey frames and for multi-bay structures, additional moments may be generated at joints 1, 4, 5 and 6 when the adjoining beams are subjected to loadings. This would give rise to bending moments throughout the subassemblage as demonstrated for joint 4 in Figure 43.

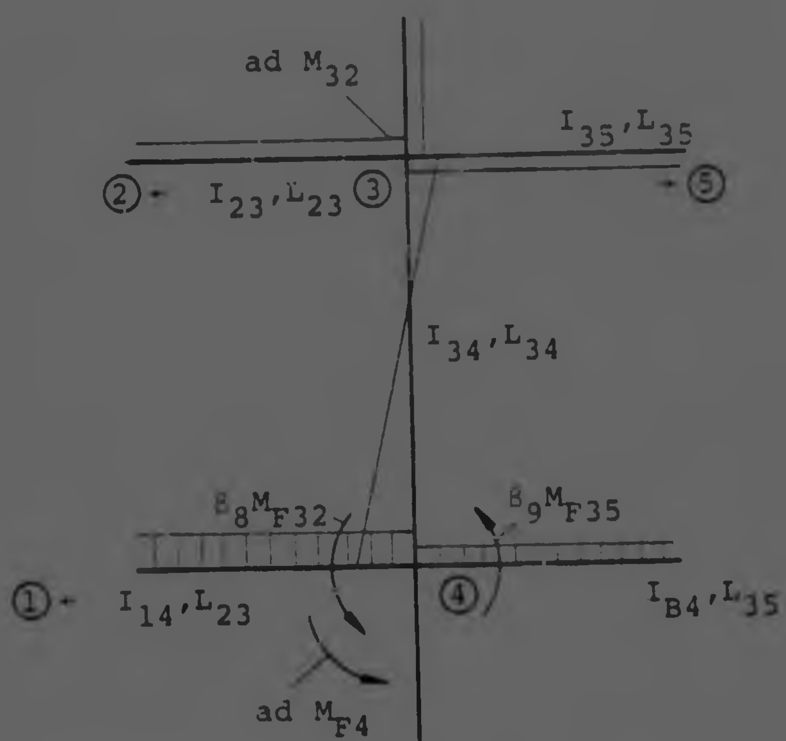

FIGURE 43: Additional beam loading

This moment effect is accounted for in an approximate way by distributing the difference of the fixed-end moments ad M_F, if any, at the joint in proportion to the stiffness of the members. The technique is based on the equations of the slope-deflection method and effectively comprises the first iteration step of the moment distribution approach presented by Kani[112]. With reference to the case of Figure 43, the additional bending moment at joint 3 would be defined by

$$\text{ad } M_{32} = \left(\beta_8 M_{F32} + \beta_9 M_{F35}\right) 2\mu_{32}\mu_{43} \qquad |\text{EQN. } 38|$$

The coefficients μ_{ij} represent stiffness ratios and are used in the same way as a carry-over factor. Similarly, additional moments can arise from beam loading on the ancillary member next to joint 5. Full details of the results of the distribution process are given in Appendix IV/2.

CHAPTER 6

THE LIMITING SLENDERNESS RATIO

6.1 General

In chapter 2 of this study the "limiting slenderness ratio", λ_ℓ, has been identified as the principal parameter of the so-called "limiting frame" of a specific group of frames. When subjected to loading equal to its elastic buckling load P_G ("Symmetry-Buckling") or to loading related to a fictitious "elastic buckling load" αP_G (non-symmetrical conditions), the "limiting frame" would just reach yield at a critical section.

In section 2.2 the "limiting slenderness ratio" λ_ℓ was shown to be of major importance in selecting the appropriate design curve from the array of possible curves given in the design graph of Figure 23. The calculation of the "limiting slenderness ratio" λ_ℓ was further demonstrated in section 2.2.2, where an example was presented.

In this chapter, the relationship between the elastic buckling load of a frame and the "limiting slenderness ratio" λ_ℓ will be examined and the concept of the "limiting slenderness ratio" will be applied to the general subassemblage.

The "limiting slenderness ratio" can be interpreted as a measure of the elastic response of the structure to loading related to its elastic buckling load. In fact, a direct relationship exists between the magnitude of the "limiting slenderness ratio", the elastic buckling load of a frame and the actually applied loadings (Figures 9a, 9b, 12a and 12b). It has previously been mentioned that the loading which is instrumental in determining the "limiting slenderness ratio" has a slightly different meaning and definition when considering non-symmetrical conditions in contrast to the special case of "Symmetry-Buckling". This will be further illustrated.

<u>Case 1</u>: "Symmetry-Buckling"

The significant loading for this case is equal to the elastic buckling load P_o. A true bifurcation point exists in the load-rotation relationship as shown in Figure 44. This behaviour is based on an elastic analysis and on perfect conditions in regard to symmetry of loading and geometry. A frame qualifying for the case of "Symmetry-Buckling" may theoretically fail in two ways when analysed on a linear elastic, second-order basis - in a symmetrical buckling mode or by sway buckling. Sway buckling will usually occur at a load level lower than the critical load computed for the symmetrical case. The initiation of sway buckling, therefore, represents a bifurcation of the equilibrium configuration.

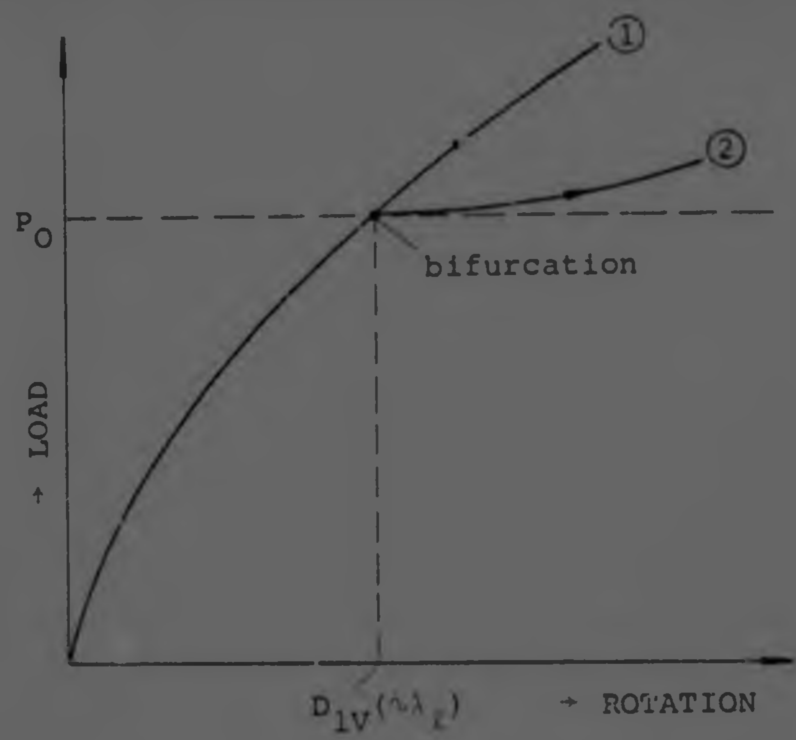

FIGURE 44: "Symmetry - Buckling"

The load P_O and branch 2 of the curve shown in Figure 44 refer to the sway buckling mode, whereas branch 1 corresponds to the no-sway mode of buckling. The post-buckling rotation for branch 2 of Figure 44 can only be calculated, on an elastic basis, if the approximation d^2y_i/dx_i^2 in Equation 34 is replaced by the correct expression for the curvature $(d^2y_i/dx_i^2)/\left[1 + (dy_i/dx_i)^2\right]^{3/2}$.

The parameter D_{1V} refers to the vector of deformations associated with a frame qualifying for "Symmetry-Buckling" and loaded with its elastic buckling load P_O. At the load level of P_O a finite state of deformations, bending moments and stresses exists which can directly be related to the relevant "limiting slenderness ratio" λ_ℓ. This will be confirmed in section 6.2.

The curve shape and the location of the bifurcation point in Figure 44 depends on the sectional properties of the members, the frame dimensions and the nature of the loading.

Case 2: Non-symmetrical conditions

For this case, which would apply to non-symmetrical structures, non-symmetrical loading or imperfect symmetrical structures, elastic analysis would reveal a progressive lateral collapse and no bifurcation of equilibrium would exist. The collapse curves, when shown in a load-displacement diagram, would approach the elastic buckling load of the structure in an asymptotic way. The curve shapes would again vary with the stiffness of the structure and the disposition and composition of the applied loading. Three arbitrary curves are shown in Figure 45. A flatter curve would be obtained for a more flexible structure or larger bending effects. A variation in stiffness could also have an effect on the absolute magnitude of the elastic buckling load P_O.

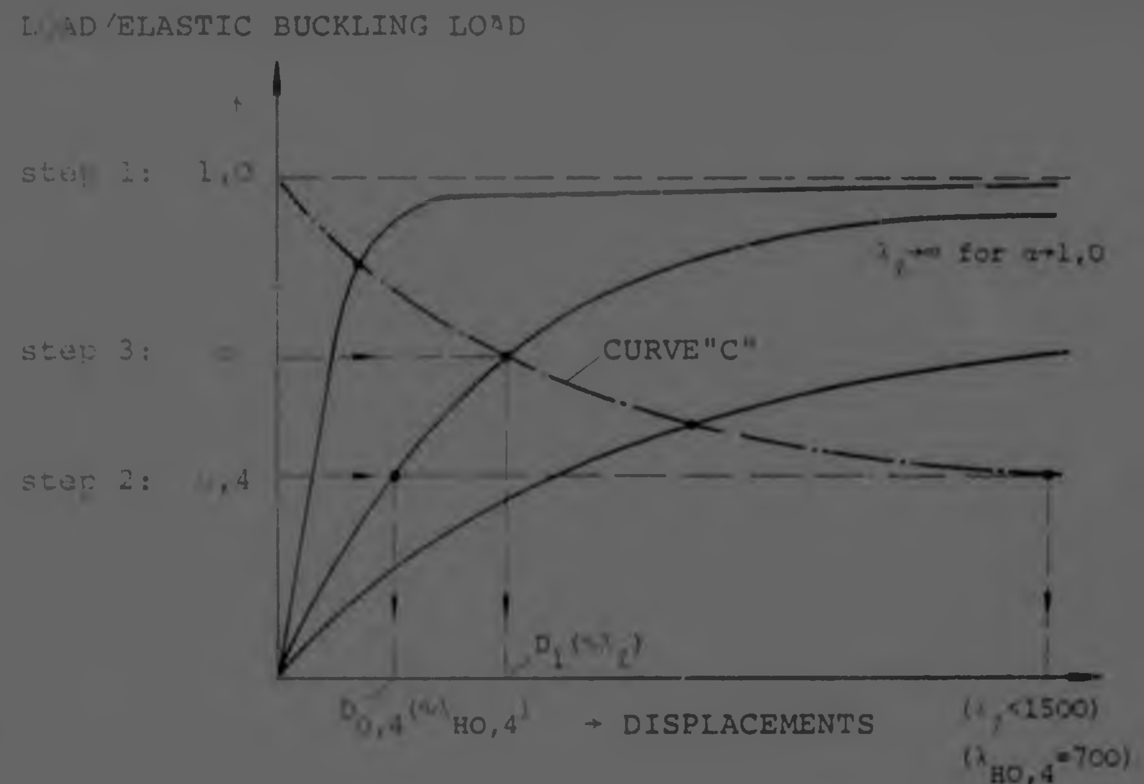

FIGURE 45: Non - symmetry failure

All curves such as shown in solid lines in Figure 45 would reach infinite displacements D_1 at the level of the elastic buckling load P_0. Thus, if the "limiting slenderness ratio" were directly related to the elastic buckling load P_0, in this case λ_ℓ would theoretically approach infinity for all non-symmetrical cases. It will be shown in section 6.2 that the "limiting slenderness ratio" is directly related to the second-order forces which in turn are a function of the displacement vector D_1.

The original interaction curve suggested by Merchant-Rankine and the modification by Wood are in line with this condition, i.e. $\lambda_{\ell} \rightarrow \infty$ for P_O. These methods are thus not suitable for distinguishing adequately between structures of various stiffness and loading conditions. At the same time, it can be seen that these interaction rules constitute a lower-boundary approach with respect to the curve termination point on the vertical axis through $P_F/P_O=1$ of the design curves of Figure 23. By implication, the value $\lambda_{\ell} \rightarrow \infty$ corresponds to a slope $(P_O/P_P)_{\ell}=0$ at all times by virtue of Equations 5 and 8.

In order to overcome this problem in this research, a somewhat lower load than P_O is designated as the fictitious "elastic buckling load" of the structure. For this load, which is called αP_O $(0<\alpha<1)$, a finite displacement state and thus "limiting slenderness ratio" can be identified as shown in Figure 45. It is significant to realise that, generally, for a structure of limiting conditions the ratio of $(\alpha P_O/P_P)_{\ell}$ is now not equal to zero, since $\lambda_{\ell} \neq \infty$.

To determine a suitable reduction value α, the following points were considered:

a) The formulation of α would have to contain a parameter taking stiffness and loading into account.

b) The load level αP_O should lead to rational values for the "limiting slenderness ratio".

c) A generalised approach covering all possible cases would be desirable.

After a thorough investigation it was felt that curve "C" of Figure 45 fulfills the requirements stipulated above. This curve, passing through αP_O, has been carefully chosen to link points on the load-displacement curves just before the deformations start to increase rapidly, thereby rendering the structure undesirable. Numerous variations to curve "C" of Figure 45 were also tested by computer but found to be less efficient than the curve obtained from Equation 39. The formula for α given in Equation 39 has yielded satisfactory results in terms of the "limiting slenderness ratio" for a large number of frames analysed by computer.

$$\alpha = \frac{0{,}4}{1-0{,}6\left(\frac{700-\lambda_{HO,4}}{700}\right)^2} \qquad |\text{EQN. } 39|$$

$$\alpha \le 1; \quad \lambda_{HO,4} \le 700; \quad \lambda_\ell \le 1500$$

The value $\lambda_{HO,4}$ is defined as the largest slenderness ratio associated with all conditions producing a deviation from the special case of "Symmetry-Buckling". This will include non-symmetrical loading and non-symmetrical structural arrangements. The slenderness ratio $\lambda_{HO,4}$ will be computed in the same way as the "limiting slenderness ratio" λ_ℓ with an applied loading related to 0,4 P_O. For instance, for a symmetrical frame subjected to a symmetrical vertical loading of $0{,}4\ P_0$ and a horizontal load of $0{,}4n_iP_0$, $\lambda_{HO,4}$ would be based on results derived from the application of the horizontal load $0{,}4n_iP_0$. In this way, Equation 39 would lead to a value of $\alpha=1{,}0$ for the case of "Symmetry-Buckling", thus providing a gradual transition between non-symmetrical conditions ($\lambda_{HO,4}>0$) and "Symmetry-Buckling" ($\lambda_{HO,4}=0$).

It is also evident that for a particular group of frames as defined in section 2.2.3 of this thesis, the value α would remain unchanged. The elastic response to lateral load of such frames in terms of the value $\lambda_{HO,4}$ would be identical.

If for certain cases Equation 39 fails to produce a realistic result for λ_ℓ, i.e. $\lambda_\ell>1500$, or if $\lambda_{HO,4}>700$ and $\alpha<0{,}4$, satisfactory solutions may still be obtained by reducing α until λ_ℓ falls below 1500. The change in α can be justified because of the fairly insensitive nature of the relationship between αP_0, λ_ℓ and the failure load P_F. This has already been demonstrated in section 3.2 of this study.

The value α in Equation 39 is based on a slenderness ratio $\lambda_{HO,4}$ expressed in terms of column properties and refers to a ratio $d_C/2r_C$ equal to unity. The reason for setting $d_C/2r_C$ equal to unity becomes apparent when examining the formulae for the "limiting slenderness ratio" (Equations 40 and 41), which will be derived in the following section.

The load-displacement behaviour of structures (Figure 45), and thus the value of α, which reflects this behaviour, should not be a function of the parameter y/r=d/2r which appears in Equations 40 and 41. Since the computation of $\lambda_{HO,4}$ will be based on these equations, the ratio d/2r is eliminated by equating d/2r to 1,0.

The evaluation of the cubic equation for α comprises the following three steps within the frame analysis procedure as a whole:

Step 1

Establishment of elastic buckling load P_O.

Step 2

Second-order load analysis for a load arrangement related to $0{,}4P_O$, and subsequent calculation of the corresponding slenderness ratio, $\lambda_{HO,4}$, using column properties and a ratio $d_C/2r_C$ equal to 1,0.

Step 3

Based on the results of step 2, the final reduction factor α is predicted evaluating Equation 39.

Using the result obtained from step 3, the required "limiting slenderness ratio" λ_ℓ corresponding to the load level αP_O is determined.

The calculation procedure set out above is necessary for the following two reasons:

i) A direct prediction of the reduction factor α is not possible.

ii) It picks up the general elastic response behaviour of the problem, thereby fulfilling the abovementioned requirement a).

6.2 "Limiting slenderness ratio" applied to subassemblage

The relevant subassemblage is thus subjected to the elastic buckling load P_O in the case of "Symmetry-Buckling" and to the fictitious "elastic buckling load", αP_O, for non-symmetrical conditions. All other relevant loads f(Q), now presented as $f(\alpha P_O)$, are also applied to the structure at the same time, for example, if $q_{35}L_{35} = Q/2$, it now becomes $\alpha P_O/2$.

Using the analysis principles set out in chapters 4 and 5, second-order displacements and forces are obtained. These in turn are utilised to calculate the "limiting slenderness ratio" for discrete critical sections of the structure.

Before developing the necessary formulations for the "limiting slenderness ratio" it is opportune to illustrate the prevailing moment and axial force state. A possible distribution for the members of interest is shown in Figures 46a and 46b.

The dots shown in Figure 46a indicate possible critical sections for which the "limiting slenderness ratio" will be calculated. It would also be feasible to include column sections between the nodes.

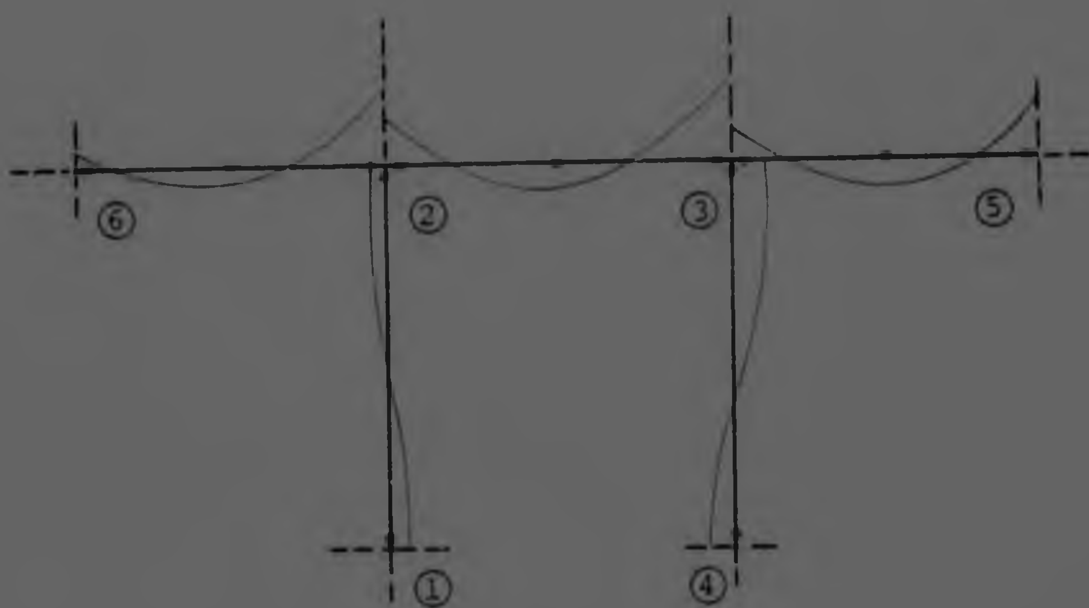

FIGURE 46a: Bending moments

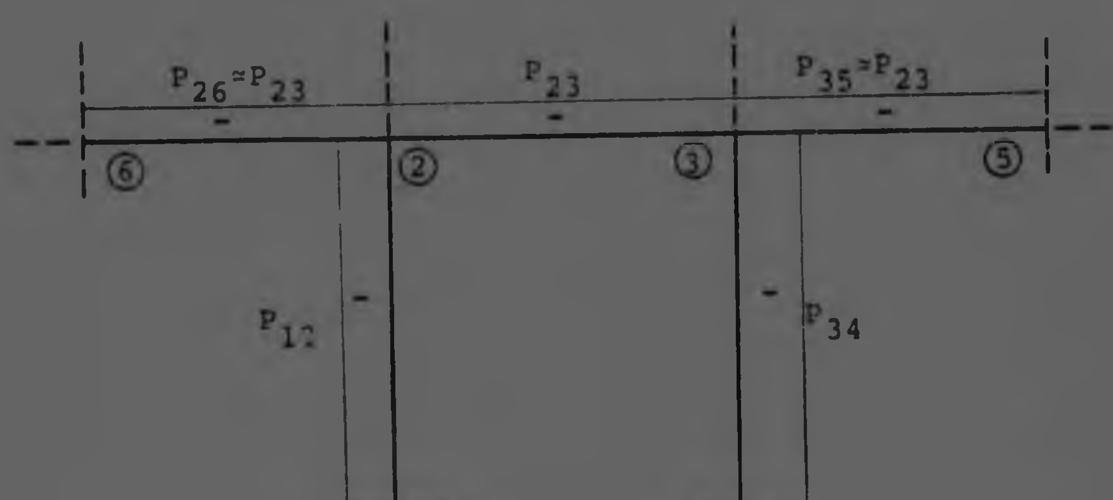

FIGURE 46b: Axial forces

For a typical symmetrical cross-section, the stresses may be composed of the two contributions shown in Figure 47.

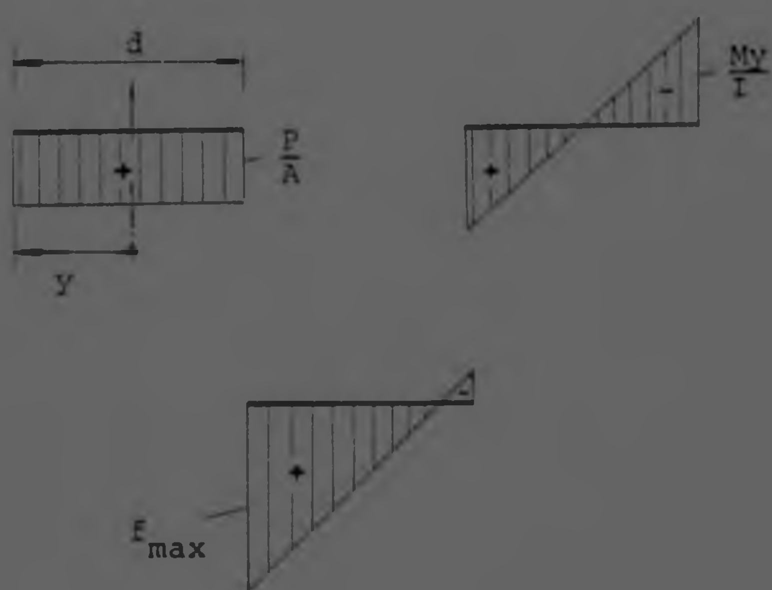

FIGURE 47: Sectional stresses

The maximum fibre stress can be expressed as follows, using compression stresses as positive:

$$f_{max} = \frac{P}{A} + \frac{My}{I}$$

Substituting for f_{max} the stress f_p on the stress-strain curve at which yielding effectively occurs, the following quadratic equation in λ_i is obtained from the above stress expression:

$$\lambda_\ell^2 - \lambda_\ell \left(\frac{y}{r}\frac{M}{I}\frac{L}{f_p}\right) - \frac{PL^2}{If_p} = 0$$

This expression has the solution given in Equation 40. The detailed derivation of the final solution is presented in Appendix V.

$$\lambda_\ell = \frac{y}{r}\frac{M}{I}\frac{L}{f_p}\left[\frac{1}{2} + \frac{1}{2}\sqrt{1 + \frac{4f_pPI}{\left(\frac{y}{r}M\right)^2}}\right] \qquad |\text{EQN. } 40|$$

Equation 40 relates the "limiting slenderness ratio" λ_ℓ to the sectional forces M and P and to the sectional properties I, L, y, r, f_p of the actual structure.

Sections for which the axial member force is small compared to the bending moment can be assessed by Equation 41. In this case, the second term under the square root of Equation 40 is negligible, so that the following expression is an adequate approximation:

$$\lambda_\ell = \frac{y}{r}\frac{M}{I}\frac{L}{f_p} \qquad |\text{EQN. } 41|$$

Equation 41 will be used when evaluating beam sections and Equation 40 will serve to analyse columns.

It has been found useful to relate all critical sections to a particular reference section and to include for the possibility of different beam to column strengths. This will slightly modify Equations 40 and 41. Details of these modifications and the application of the procedure to the investigated subassemblages are presented in Appendix V.

It must also be borne in mind that provision has to be made for separate analysis steps for vertical and horizontal loading respectively. The results of both these steps need to be combined. The largest "limiting slenderness ratio" obtained in this manner is the most significant and will be retained for further processing with the ultimate objective of selecting the appropriate curve in the design graph of Figure 23.

For the evaluation of α in Equation 39, the slenderness ratio $\lambda_{HO,4}$ will be calculated in accordance with Equations 40 and 41, using a ratio $d_C/2r_C = 1{,}0$ and properties relating to the column member between joints 3 and 4.

CHAPTER 7

THE COMPUTER PROGRAM

7.1 Objectives

The principal purpose of the computer program is to obtain the results of the elastic analyses required for the evaluation of the interaction curves of Figure 23. This involves the evaluation of the elastic buckling load, the stresses pertaining to loading related to the elastic buckling load and the "limiting slenderness ratio" for both, conventional buckling and "Symmetry-Buckling". It is also possible to use the information obtained from the elastic analyses, together with the plastic collapse load, to calculate the failure load, P_F, of the structure by computer. For this purpose, the straight-line Equation 11 has been incorporated in the computer procedure.

7.2 Procedure

The complex procedure involved in obtaining numerical results and the fact that certain solutions are only found after a number of iterative cycles makes it necessary to employ a suitable computer program. The computation of the elastic buckling load and the establishment of the corresponding second-order state of stress is essentially based on the solutions of a set of linear equations. The various sequences of this analysis are executed using the well known principles of matrix algebra which will not be discussed in detail in this thesis.

The program developed for the purpose of this research is best illustrated by way of a flow chart which outlines in block form the main steps in the computation process (see Figure 48). A concise summary of the major operations is given below:

Step 1

For a given frame investigate a possible elastic buckling load P_O within a predetermined interval.

Step 2

Evaluate numerically all functions f (P_O).

Step 3

Calculate corresponding second-order axial forces for vertical loads by solving the matrices $D_1=\bar{B}^{-1}L_V$ and $P=S_P D_1+\bar{P}_F$ until satisfactory convergence is achieved. In this form step 3 is only executed for cases of "Symmetry-Buckling". For conventional buckling a first-order evaluation of these matrices is sufficient.

Step 4

Satisfy determinants of stiffness matrices to zero:

DET $|\bar{B}| = 0$ for conventional buckling

DET $|\bar{C}| = 0$ for "Symmetry-Buckling".

This step will determine the elastic buckling load of the system.

Step 5

Establish the second-order displacements and forces for loading related to the elastic buckling load of the structure. In the case of "Symmetry-Buckling", solve the equations obtained from the differential equation method. For non-symmetrical cases, determine the reduction factor α first and then solve [illegible] L_V and $P=S_P D_1+\bar{P}_F$ as in step 3 above.

Step 5 will be executed separately for vertical loading and then for other loading, by analysing the appropriate subassemblages. After completing step 5 for the vertical load analysis, the resulting state of axial forces is retained. This will maintain the stiffness level of the structure and will allow for the interaction of axial forces and the sway displacement. The results of both analysis steps, i.e. first for vertical load and then for the remaining load, will be combined to give the final result.

Step 6

Compute the "limiting slenderness ratios" λ_ℓ, and identify the numerically largest value.

Step 7

Once a plastic collapse load P_p has been evaluated for the structure, the frame failure load P_F can also be predicted by computer by using the straight-line approximation of Equation 11.

A flow chart of the program steps is given in Figure 48. In the computer program provision has been made for the numerical evaluation of single problems as well as the repetitive evaluation of cases within a range of geometric parameters.

7.3. Some program details

7.3.1 Language, notation, units

The computer program has been written in Fortran IV and comprises about 1 450 statements. Input of data relevant to the problem is effected by means of eight data cards containing about one hundred data elements. Although no external functions or subroutines are called, reference is made to a number of standard library functions.

The notation for the constants and variables follows closely the designations used in the text of this study. The printout elements are well explained in the output itself. The numerical results of the analysis process are preceded by a complete printout of the data on which the results were based, thus, facilitating cross-reference and checking. Any set of compatible units may be chosen for the data field. A switch of units will usually be resorted to, when the programmed dimensions of the input or output fields would not suffice.

7.3.2 Special instructions, error messages

A number of error messages have been incorporated into the program. These are mainly concerned with the adequacy of the overall load interval within which the final result is sought by iteration. It may occur, through errors in the data compilation, that no result is obtained within the stipulated load boundaries. In this instance, a message to this effect is printed out and the problem evaluation is terminated.

7.3.3 Computer model, computer time and cost

The IBM Processor 370/158, running under the operating system VS1, and the associated peripherals were used for the program execution. Program compilation takes about 40s and the processing time per problem varies between 0,7s for 10 steps within the interval and 3,75s for 100 steps within the load interval. To save cost, it is recommended to prepare and read data cards covering the complete frame.

With the variation of the interval steps as above the cost per subassemblage analysis will fluctuate between R 0,30 and R 1,30 if a total of fifty subassemblages are analysed at a time. These costs are based on the following rates charged by the Computer Centre of the University of the Witwatersrand, Johannesburg:

Processor (CPU)	:	R 1 100/hr
Memory occupancy		
(based on CPU time + 30 per cent)	:	R 26/hr/100 K
Printing on computer centre		
supplied stationery	:	R 0,07/100 LINES
Step execution	:	R 1,0/EXEC. STEP
Use of peripherals		
Printers	:	R 1,15/1000 CARDS
Reader	:	R 1,15/1000 CARDS

7.3.4 Iteration procedure

The buckling load is the lowest load satisfying the condition that the determinants of matrix $\bar{B}$ or $\bar{C}$ (see Equations 13 and 30) reach a value of zero. This can only be accomplished by using an iterative approach within the load interval in which the buckling load is expected. A possible result is indicated where from one interval step to the next the sign of the determinant changes. The values of the determinant, DET_1 and DET_2, corresponding to the loads P_{01} and P_{02} before and after the zero intersection, are used to predict a preliminary solution for the actual buckling load P_0. The technique of prediction adopted in this program is known as the 'Regula Falsi' given in Equation 42.

$$P_0 = \frac{DET_1\ P_{02} - DET_2\ P_{01}}{DET_1 - DET_2} \qquad |EQN.\ 42|$$

Successive predictions for P_O are made in this way, each time reducing the interval sizes and narrowing the boundary values. Subsequent solutions are compared and if the desired degree of convergence is obtained the procedure is terminated.

For the most general case, where the axial beam forces are not zero, the system of linear equations given by $\bar{B}_1D_1-L_V=0$ of Equation 22 must also be satisfied as the determinants DET $|\bar{B}|$ or DET $|\bar{C}|$ attain a zero value. This procedure is illustrated in Figure 49 which shows the results of two consecutive iteration steps. P_{O1} and P_{O2} refer to step 1 and P_{O3} and P_{O4} refer to the subsequent step. The corresponding determinantal values are DET_1, DET_2, DET_3 and DET_4. The exact values for the determinant appear as a solid line in the bottom section of the diagram.

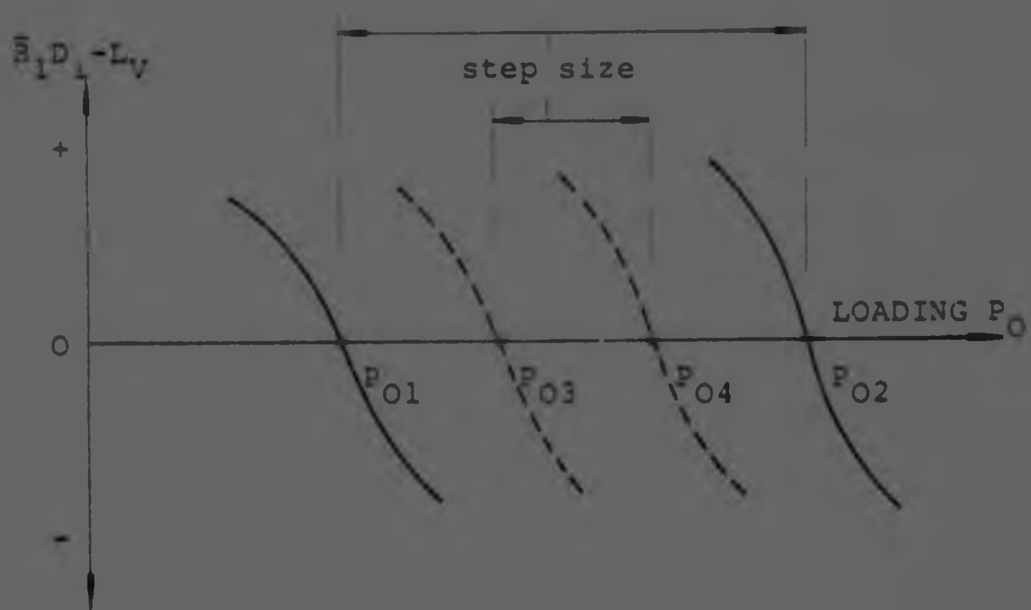

FIGURE 49: Iteration procedure (top section of diagram)

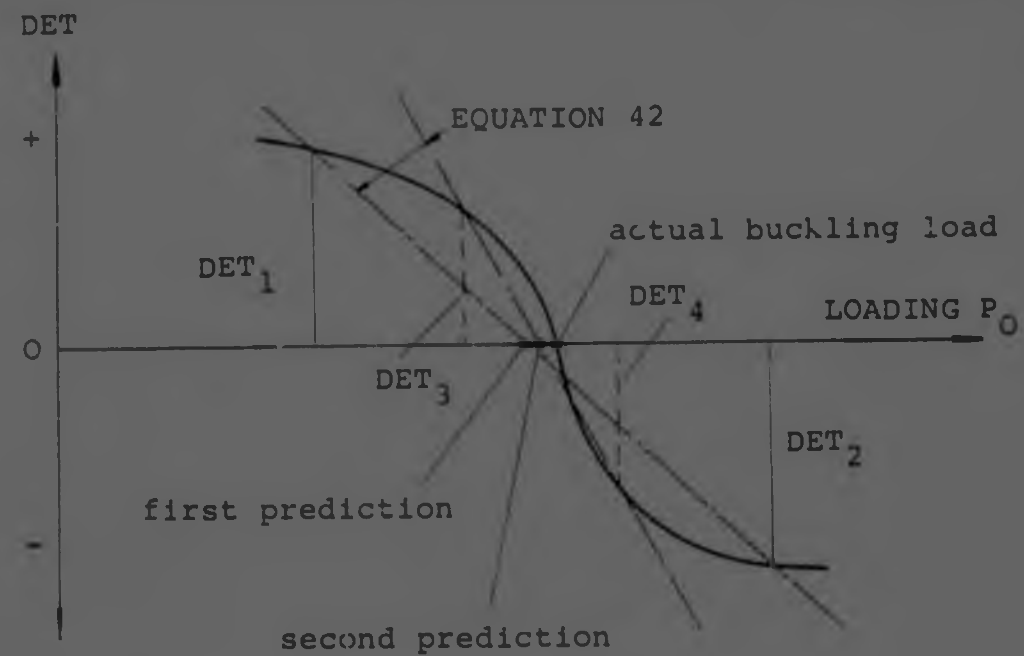

FIGURE 49: Iteration procedure (bottom section of diagram)

7.3.5 Lowest buckling mode

Precautions must be taken not to miss the lowest root of the buckling matrices $\bar{B}$ and $\bar{C}$, and pick up instead a higher value belonging to a subsequent buckling mode. This can happen when the determinant of the stiffness matrix suddenly "dives" down, using the description coined by Wood'. In this research a similar phenomenon was observed when analysing upper storeys of multi-storey structures. The problem can be avoided by increasing the step numbers within the load interval for the first iteration cycle. A step size of $\delta P_O=1,6\times10^{-3}$ EI/L^2 will usually suffice in this instance, whilst a step size of $\delta P_O=2,5\times10^{-2}$ EI/L^2 is recommended for all other cases.

CHAPTER 8

THE DESIGN PROCESS

8.1 General principles

If the method developed in this research is applied to a particular problem, the designer has to combine the plastic collapse load P_p of the structure with certain elastic parameters, i.e. αP_O and λ_ℓ. The purpose of this investigation has been to provide information about the elastic parameters and propose a suitable interaction procedure.

The computer analysis described in the previous chapter can be used to obtain the elastic buckling load P_O, the reduction factor α and the "limiting slenderness ratio" λ_ℓ for various subassemblages. For the general multi-storey, multi-bay framework the designer has to investigate all subassemblages contained in the structure.

In many practical frames critical subassemblages can be identified by inspection and the analysis will then concentrate on a lesser number of cases. In regular building frames, beams are often kept constant throughout a particular storey and columns extend two storeys in height before a splice occurs. In this case it is generally sufficient to analyse the lower of the storeys in which the columns remain unchanged. For a multi-bay regular frame, at most three subassemblages need to be investigated per storey, one completely internal and, in addition, the left and right exterior bays.

Each set of elastic parameters established in this way is combined with the plastic collapse load of the total framework by forming the ratio of elastic buckling load or fictitious "elastic failure load" to plastic collapse load for the actual frame and for the "limiting frame". These slopes, when entered in the design graph of Figure 23, will define the failure load P_F of the structure. The lowest load so predicted is taken as the second-order, elasto-plastic failure load of the entire framework.

8.2 Detailed design procedure

If the design load at the ultimate limit state is taken as the factored working load, namely as $Q=\gamma_f W$, the following condition should be satisfied for a satisfactory solution:

$$P_F \geq Q = \gamma_f W \qquad |\text{EQN. } 43|$$

On the basis of Equation 43 the design steps can be stipulated as follows:

Step 1

Calculate $Q=\gamma_f W$

Step 2

Choose members and establish M_P or M_{PC}.

A plastic collapse analysis is recommended for this purpose. In this case $P_P = Q$.

Step 3

Calculate the exact P_P for the chosen members and obtain the elastic buckling load P_O, the reduction factor α and the "limiting slenderness ratio" λ_ℓ.

Step 4

Find the ratio $\alpha P_O/P_P$ for the actual frame and the "limiting frame".

Step 5

With the results of step 4 enter the design curves of Figure 23 and find P_F/P_P and then P_F.

Step 6

Show that $P_F \geq Q = \gamma_f W$, or that $P_F/W \geq \gamma_f$

If necessary change section sizes and values of M_P, and then repeat steps 3 to 5 until $P_F \geq Q = \gamma_f W$.

For the establishment of the plastic collapse load P_P cognisance must be taken of the presence of axial column loads. These may be sufficiently large to warrant a reduction in the plastic moment capacity of the section. This would change the plastic moment M_P to M_{PC}. As an approximation for regular flanged sections the previously given Equations 1 and 2 are recommended by design codes [8,10].

8.3 Design example

The framework analysed by Cheong Siat Moy in Reference 63 is re-analysed here to demonstrate the procedure outlined in the preceding section. This frame is of particular interest, since Cheong Siat Moy showed that an ordinary "stress-controlled" approach does not necessarily lead to a safe solution. The frame had to be strengthened to resist the real second-order forces. Instead of considering the entire frame, only the two lowest storeys of the ten-storey structure were analysed by Cheong Siat Moy. Further details related to the problem are given in Figure 50.

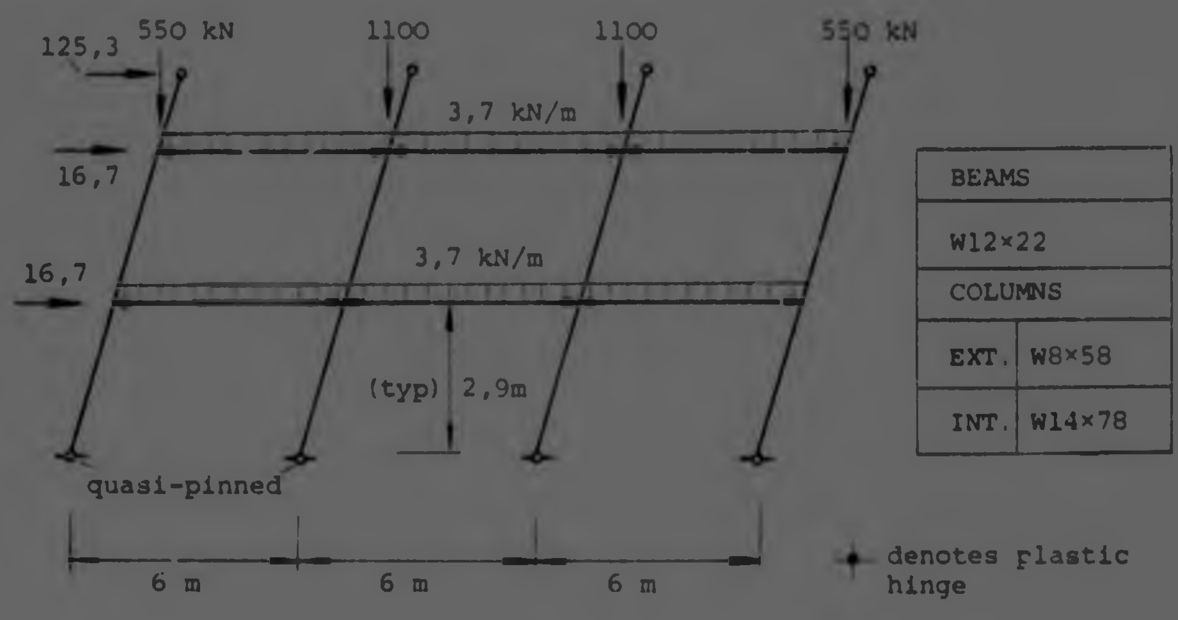

FIGURE 50: Frame example - First trial

The sections given in Figure 50 are taken from the section tables issued by the American Institute of Steel Construction (AISC)[60]. The loadings refer to the working load level and the plastic collapse load is derived from a combined sway mechanism with hinges in the beams. The plastic moment capacity of the beams is M_p=120 kNm. In accordance with the solution by Cheong Siat Moy, the columns are considered to be bent about their minor axis and the yield strengths of both, beams and columns are taken as 250 MPa. The load factor γ_f applied to the working load W is equal to 1,30 as suggested by the AISC Code[8] for the case of combined horizontal and vertical loading. For the given conditions described above, the load factor pertaining to the plastic collapse mode has been calculated as $P_p/W = 1{,}37$.

In line with step 3 of the design procedure, a number of subassemblages must be analysed for the elastic parameters αP_o and λ_ℓ. At most six cases need to be considered, however, it was estimated and confirmed that the lower storey would give the worst results. The computer results applicable to the relevant subassemblage are given below. Subsequently, they are further processed, following the design steps given in section 8.2

Step 3

$$\frac{P_p}{W} = 1{,}37$$

Ratio of elastic buckling load to working load:

$$\frac{P_O}{W} = 3,02$$

Reduction factor defined in Equation 39:

$$\alpha = 0,778$$

"Limiting slenderness ratio" (Equation 40) from a second-order elastic analysis to determine axial forces and moments under αP_O:

$$\lambda_\ell = 551$$

<u>Step 4</u>

actual frame : $\dfrac{\alpha P_O}{P_P} = \dfrac{0,778 \times 3,02}{1,37} = 1,72$

"limiting frame" : $\left(\dfrac{\alpha P_O}{P_P}\right)_\ell = \dfrac{\alpha P_O}{P_P} \dfrac{\lambda}{\lambda_\ell} = 1,72 \times \dfrac{48}{551} = 0,15$

(Equation 9)

<u>Step 5</u>

$\dfrac{P_F}{P_p} = 0,75$ from Figure 23, using the results of step 4

<u>Step 6</u>

$$\frac{P_F}{W} = \frac{P_F}{P_p} \frac{P_p}{W} = 0,75 \times 1,37 = 1,03 < \gamma_f = 1,30$$

From this inequality follows, that the trial frame given in Figure 50 is inadequate and needs strengthening. This confirms the findings of Cheong Siat Moy.

The revised frame suggested by Cheong Siat Moy shows the following member sections:

2nd Trial

Beams : W14×26

External Columns : W14×74

Internal Columns : W14×84

The structural analysis, which follows the same procedure as above, results in the values given below for steps 3 to 6.

Step 3

$\frac{P_P}{W} = 1{,}87$

$\frac{P_O}{W} = 3{,}82$

$\alpha = 0{,}782$

$\lambda_\ell = 461$

Step 4

actual frame : $\frac{P_O}{P_P} = 1{,}6$

"limiting frame" : $1{,}6 \cdot \frac{33}{461} = 0{,}11$

Step 5

$\frac{P_F}{P_P} = 0{,}72$ from Figure 23

Step 6

$\frac{P_F}{W} = 0{,}72 \times 1{,}87 = 1{,}35 > 1{,}30$

The final step confirms that the revised frame is now adequate. In fact, the frame is overdesigned by about 4 per cent in terms of the load factor. This is not surprising since the sections chosen in trial 2 are just adequate by the "stress-controlled" design approach. It is typical that a second-order, elasto-plastic analysis of such a frame reveals a small reserve strength.

The result obtained above refers to a bare frame analysis and is, therefore, directly comparable to the Merchant-Rankine formula. Step 6 for the Merchant-Rankine rule takes the following form:

$$\frac{P_F}{W} = \frac{\frac{P_P}{W}}{1 + \frac{P_P}{P_O}} = 1{,}26 < 1{,}30$$

This inequality suggests that trial frame 2 is still not adequate and further strengthening is necessary when analysed by the Merchant-Rankine rule. Compared to the "stress-controlled" approach and the technique developed in this study an uneconomical solution would eventually be adopted.

CHAPTER 9

COMPARISONS WITH PREVIOUS RESEARCH

9.1 General

In chapter 2 of this study the general shape of the proposed interaction curve was developed for a particular group of frames. The same procedure can be repeated for a number of other frames specifically selected for this purpose. As a result the array of curves presented in the design graph of Figure 23 has been obtained.

In the derivation process for each curve use was made of two exact points, the starting point and the termination point, however, the failure locus between these boundaries was hypothesised. Considering the entire curve development procedure, it is believed that, on the whole, no great error could have been introduced despite the fact that no exact theoretical solutions in the inelastic range were incorporated. In this context it must also be appreciated that an explicit mathematical description, based on a rigorous elasto-plastic analysis, for any of the curves of Figure 23, has not been published so far. By implication, each curve represents an infinite number of different frames which only in the elastic range have a common response parameter.

In order to assess and possibly improve the accuracy of the initially hypothesised inelastic curve sections, solutions obtained by the proposed technique were compared with a number of discrete theoretical results as well as results of laboratory tests. The final comparisons are given in tabulated form in the next section of this study.

9.2 Comparisons

In the comparisons of Table 6/1 and 6/2 care was taken to cover a wide range of frames. Only the pertinent results of the analysis are given. Hence for multi-storey, multi-bay structures, the parameters shown in columns 2, 4, 5, 6 and 7 of Tables 6/1 and 6/2 refer to that subassemblage which, in combination with the plastic collapse load of the entire frame, resulted in the lowest overall failure load. The failure load is expressed as the ratio P_F/P_P. The elastic buckling load P_O and the plastic collapse load P_P are given in various units, as they appear in the literature, either as absolute values or in terms of load factors. The ratio $(\alpha P_O/P_P)_L$ is evaluated from Equation 6, 9 or 10, as applicable. For comparative purposes, the correct elasto-plastic results from a computer analysis or laboratory tests are also shown. These were taken from the references given in column 1. Furthermore, the solution of the generalised Merchant-Rankine formula has been added in each case in column 10 of both tables.

TABLE 6/1: Comparisons with analyses

	1	2	3	4	5	6	7	8	9	10
								P_F/P_P		
	FRAME	P_O or γ_O	P_P or γ_P	α	λ_ℓ	$\frac{\alpha P_O}{P_P}$	$\left(\frac{\alpha P_O}{P_P}\right)_\ell$	EXACT ANALYSIS	THIS RESEARCH	MERCHANT-RANKINE
1	Two-storey frame by Horne[116] and Jennings & Majid[35]	10 561 kg	3 610 kg	0,508	414	1,49	0,36	0,7778	0,78	0,77
2	Four-storey frame by Jennings&Majid[35] and Wood[32]	12,9	2,15	0,729	626	4,37	0,30	0,90	0,90	0,86
3	Two-storey frame by Davies[27]	187,5t	10,23t	0,437	708	8,0	0,50	0,97	0,97	0,95
4	Portal frame by Ojalvo & Lu[40]	4,99 kips/ft	4,94×0,86 kips/ft	1,0	75	1,17	0,94	0,97	0,97	0,54
5	Ten-storey frame by Cheong Siat Moy[63] (2-bottom storeys)	3,82	1,87	0,782	461	1,6	0,11	>0,7	0,72	0,67

TABLE 6/1: Comparisons with analyses - cont.

	1	2	3	4	5	6	7	8	9	10
								P_F/P_P		
	FRAME	γ_O	γ_P	α	λ_ℓ	$\frac{\alpha P_O}{P_P}$	$\left(\frac{\alpha P_O}{P_P}\right)_\ell$	EXACT ANALYSIS	THIS RESEARCH	MERCHANT-RANKINE
6	Fifteen-storey frame by Korn&Galambos[30]	12,02	1,632	0,50	501	3,68	0,22	0,86	0,87	0,88
7	Four-storey frame by Korn&Galambos[30]	3,61	2,067	0,56	459	0,98	0,18	0,62	0,62	0,64
8	Eight-storey frame by Korn&Galambos[30]	30,7	1,511	0,41	603	8,33	0,44	0,94	0,95	0,95
9	Two six-storey frames by Korn&Galambos[30]	8,66	1,571	0,59	399	3,25	0,27	0,87	0,87	0,85
10		11,5	1,719	0,53	400	3,55	0,30	0,89	0,89	0,87

TABLE 6/2: Comparisons with tests

	1	2	3	4	5	6	7	8	9	10
	FRAME	P_O	P_P	α	λ_ℓ	$\frac{\alpha P_O}{P_P}$	$\left(\frac{\alpha P_O}{P_P}\right)_\ell$	P_F/P_P TEST RESULT	THIS RESEARCH	MERCHANT-RANKINE
1		27,52 kips	12,43×0,96 kips	1,0	129	2,31	0,69	0,94	0,93	0,70
2	Three portal frames by Lu[4]	14,36 kips	12,43×0,96 kips	1,0	115	1,20	0,61	0,85	0,83	0,55
3		8,82 kips	11,43×0,97 kips	1,0	110	0,80	0,60	0,83	0,74	0,44
4	Three-storey frame by McNamee & Lu[31]	207,9 kN	121 kN	1,0	101	1,72	0,68	0,91	0,91	0,63
5	Seven-storey frame by Low[58]	382 N	359 N	1,0	269	1,06	0,41	0,71	0,72	0,52

TABLE 6/2: Comparisons with tests - cont.

	1	2	3	4	5	6	7	8	9	10
	FRAME	P_O	P_P	α	λ_ℓ	$\frac{\alpha P_O}{P_P}$	$\left(\frac{\alpha P_O}{P_P}\right)_\ell$	P_F/P_P		
								TEST RESULT	THIS RESEARCH	MERCHANT-RANKINE
6	Four portal frames by Scholz[97]	$\frac{1}{5,57}\frac{EI\pi^2}{h^2}$	$\frac{1}{7,35}\frac{EI\pi^2}{h^2}$	1,0	554	1,32	0,51	0,82	0,81	0,57
7		$\frac{1}{7,13}\frac{EI\pi^2}{h^2}$	$\frac{1}{29,4}\frac{EI\pi^2}{h^2}$	1,0	735	4,12	0,60	0,94	0,94	0,80
8		$\frac{1}{9}\frac{EI\pi^2}{h^2}$	$\frac{1}{66}\frac{EI\pi^2}{h^2}$	1,0	1 139	7,33	0,46	0,96	0,95	0,88
9		$\frac{1}{12,25}\frac{EI\pi^2}{h^2}$	$\frac{1}{115,5}\frac{EI\pi^2}{h^2}$	1,0	2 250	9,43	0,23	1,0	0,95	0,90

9.3 Comment on comparisons

From the comparisons of Table 6/1 and Table 6/2, it can be concluded that results based on the proposed method, which appear in column 9, are in good agreement with exact solutions (column 8) for the investigated structures. This is equally applicable for frames with low reductions in load carrying capacity due to instability (i.e. frames 3, 4 and 8 of Table 6/1 and frames 1, 7, 8 and 9 of Table 6/2) as well as for frames with large reductions due to instability (i.e. frames 1, 5 and 7 of Table 6/1 and frame 5 of Table 6/2).

It has also been confirmed that the Merchant-Rankine approach, in most cases, is a conservative approximation. However, in general, this method becomes extremely inaccurate for frames which are characterised by a low "limiting slenderness ratio" or a high value of α. This includes, in particular, symmetrical frames subjected to pure vertical loading for which α equals 1,0. Differences ranging from 9 per cent (frame 8 of Table 6/2) to 89 per cent (frame 3 of Table 6/2) have been identified for these symmetrical cases. For the same frames, the method developed in this research, is accurate within 2,4 per cent for eight cases and differs by 5 per cent and 12 per cent respectively for two further frames (frames 9 and 3 of Table 6/2) which were tested in the laboratory.

A consistenly good correlation has been obtained between results of the proposed method and the theoretical solutions given in Table 6/1.

Ten model frames which have been analysed and were subsequently tested in the laboratory are compared in Table 9 of chapter 10.

CHAPTER 10

LABORATORY TESTS

10.1 Objective of tests

It has been shown in the preceding chapter of this study that discrete experimental and theoretical results are in good agreement with the proposed design curves of Figure 23. The observed correlation should suffice to confirm the validity of the presented method as a whole.

However, it can be argued that the unrelated and arbitrary examples taken from previous research do not necessarily confirm the fundamental curve shapes developed in chapter 2, and in particular the two principal hypotheses formulated in section 2.3.1. In chapter 2 it has been found that a single curve in the inelastic instability range corresponds to a specific group of frames with a common load arrangement and a certain global parameter in regard to geometric properties. This parameter reduces to the dimensional ratio of beam to column length if the sectional properties and the arrangement of the subassemblage remain constant. By keeping the length ratios unchanged but varying the absolute member lengths, and thus the slenderness ios, the entire range of a particular interaction curve can be covered. This is illustrated in Figure 51.

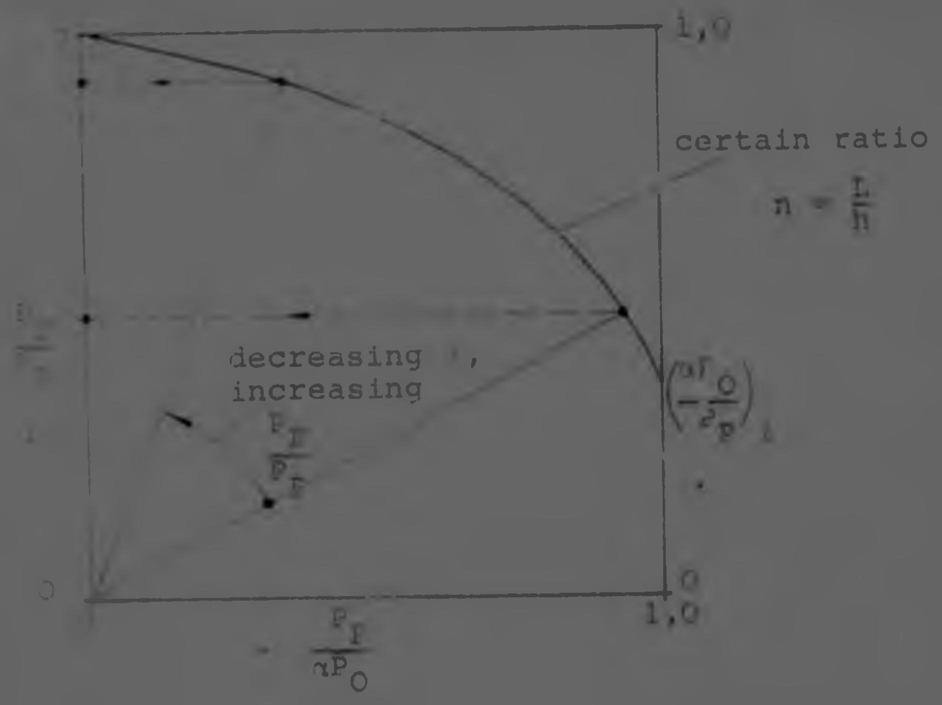

FIGURE 51: Interaction curves for constant geometry

In order to test the individual curve shape, a number of frames were selected so that they belong to one particular curve and that they correspond to curve points progressively approaching $P_F/P_P=1,0$. Because of the inevitable scatter of test results, it was decided to monitor curves with a pronounced deflection. In order to meet these objectives adequately, structures with a large slenderness ratio had to be included in the test series to obtain curve points in the regions of larger losses due to instability.

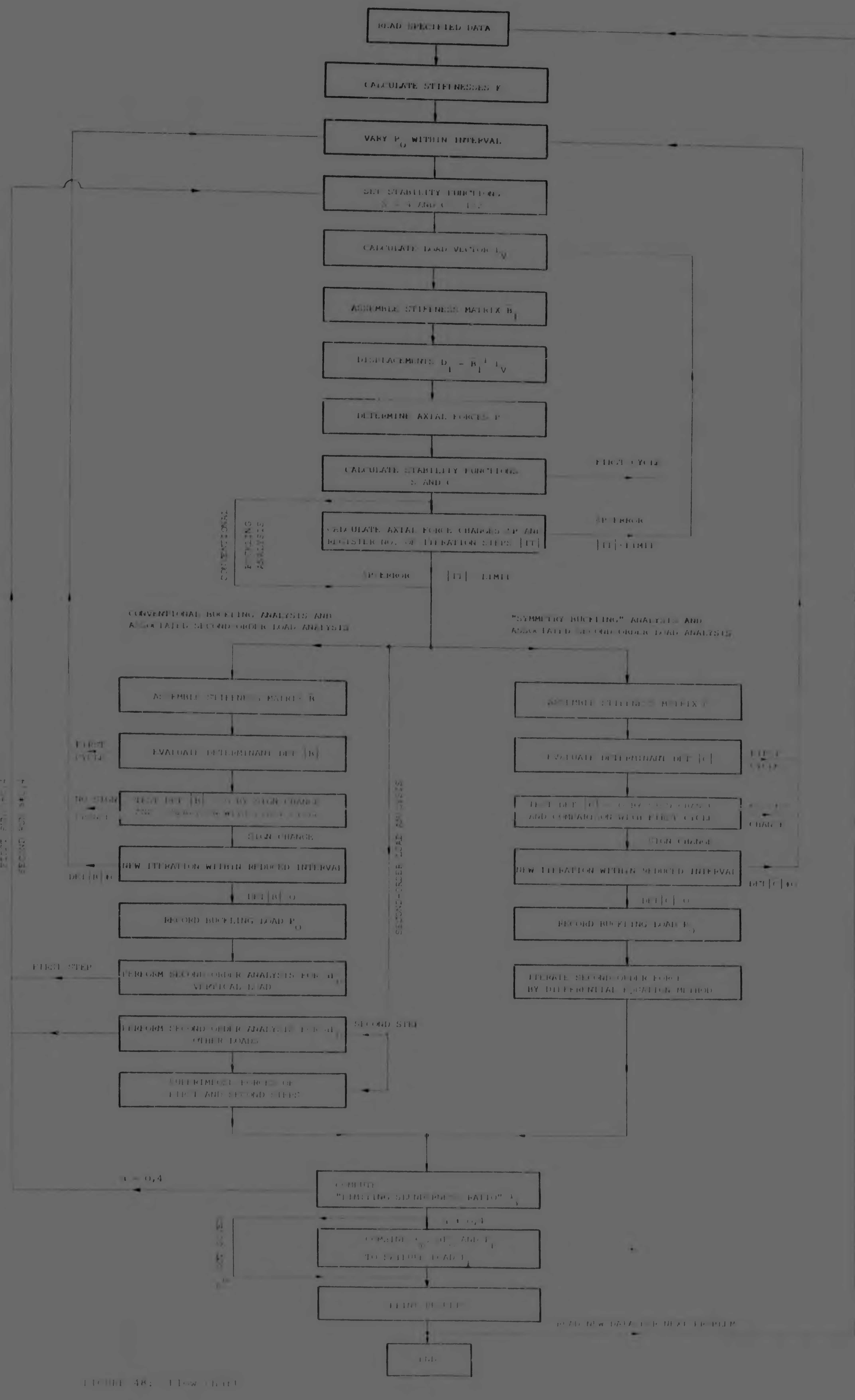

FIGURE 48. Flow chart

TABLE 5: Stiffness matrix of infinitesimally displaced subassemblage

$NO_1 - \frac{K_{12}S_{12}}{L_{12}}\frac{a_7a_9}{a_{78}} + \frac{6I_{91}}{L_{26}} + \frac{4I_{14}}{L_{23}} + K_{12}S_{12}$	$K_{12}S_{12}C_{12} + a_7 SC_{12}(1 + \frac{a_7a_9}{a_{78}})$ [illegible] $(1 + \frac{K_{26}}{K_{23}}\frac{L_{23}}{L_{26}}) - \frac{a_7a_9}{a_{78}} SC_{12}$	$-a_7 SC_{23}(1 + \frac{a_7a_9}{a_{78}})$	$\frac{2I_{14}}{L_{23}}$	0	$a_7\frac{K_{26}}{K_{23}}\frac{L_{23}}{L_{26}}SC_{23}(1 + \frac{a_7a_9}{a_{78}})$	[illegible]
$K_{12}S_{12}C_{12} - SC_{12}\frac{a_2a_8 - a_3}{a_{78}}$	$NO_2 + SC_{23}[a_2 + \frac{a_7}{a_{78}}(a_2a_8 - a_3)](1 - \frac{K_{26}}{K_{23}}\frac{L_{23}}{L_{26}}) + SC_{12}\frac{a_2a_8 - a_3}{a_{78}} + K_{12}S_{12} + K_{23}S_{23} + K_{26}S_{26}$	$K_{23}S_{23}C_{23} - SC_{23}[a_2 + \frac{a_7}{a_{78}}(a_2a_8 - a_3)]$	0	0	$K_{26}S_{26}C_{26} + \frac{K_{26}}{K_{23}}\frac{L_{23}}{L_{26}} SC_{23}[a_2 + \frac{a_7}{a_{78}}(a_2a_8 - a_3)]$	$-SC_{[illegible]}$ [illegible]
$SC_{12}\frac{a_4 + a_5a_{12}}{a_{78}}$	$K_{23}S_{23}C_{23} + SC_{23}[a_5 + \frac{a_7}{a_{78}}(a_4 + a_5a_{12})] + a_7 SC_{23}\frac{K_{26}}{K_{23}}\frac{L_{23}}{L_{26}}\frac{a_4 + a_5a_{12}}{a_{78}} + SC_{12}\frac{a_4 + a_5a_{12}}{a_{78}}$	$NO_3 + SC_{23}[a_5 + \frac{a_7}{a_{78}}(a_4 + a_5a_{12})] - a_5\frac{K_{35}}{L_{35}}\frac{L_{23}}{K_{23}}SC_{23} + K_{23}S_{23} + K_{34}S_{34} + K_{35}S_{35}$	$K_{34}S_{34}C_{34}$	$K_{35}S_{35}C_{35} - a_5\frac{K_{35}}{K_{23}}\frac{L_{23}}{L_{35}}SC_{23}$	$-a_7 SC_{23}\frac{K_{26}}{K_{23}}\frac{L_{23}}{L_{26}}\frac{a_4 + a_5a_{12}}{a_{78}}$	$-SC_{34}$ [illegible] $\frac{a_4 + a_5a_{12}}{a_{78}}$
$\frac{a_6a_{12}}{a_{78}}SC_{12} + \frac{2I_{14}}{L_{23}}$	$a_6 SC_{23}(1 + \frac{a_7a_{12}}{a_{78}}) - \frac{a_6a_{12}}{a_{78}}(SC_{12} + a_7\frac{K_{26}}{K_{23}}\frac{L_{23}}{L_{26}}SC_{23})$	$K_{34}S_{34}C_{34} + a_6 SC_{23}(1 + \frac{a_7a_{12}}{a_{78}}) - a_6\frac{K_{35}}{K_{23}}\frac{L_{23}}{L_{35}}SC_{23}$	$NO_4 + K_{34}S_{34} + \frac{6I_{84}}{L_{35}} + \frac{4I_{14}}{L_{23}}$	$-a_6\frac{K_{35}}{K_{23}}\frac{L_{23}}{L_{35}}SC_{23}$	$-\frac{K_{26}}{L_{26}}\frac{L_{23}}{K_{23}}\frac{a_6a_7a_{12}}{a_{78}}$	$-SC_{34}$ [illegible] $- \frac{a_6a_{12}}{a_{78}}SC_{[illegible]}$
$\frac{a_{10}}{a_{78}}SC_{12}$	$\frac{a_{10}}{a_{78}}SC_{12} + \frac{a_{10}a_7}{a_{78}}SC_{23}(1 - \frac{K_{26}}{K_{23}}\frac{L_{23}}{L_{26}})$	$K_{35}S_{35}C_{35}$	0	$NO_{U5} + NO_{L5} + 6K_{B5} + K_{35}S_{35}$	$-\frac{a_{10}a_7}{a_{78}}SC_{23}\frac{K_{26}}{K_{23}}\frac{L_{23}}{L_{26}}$	$-SC_{[illegible]}\frac{a_{10}}{a_{78}}$
$\frac{a_{11}}{a_{78}}SC_{12}$	$\frac{a_{11}}{a_{78}}SC_{12} + K_{26}S_{26}C_{26} + \frac{a_{11}a_7}{a_{78}}(1 - \frac{K_{26}}{K_{23}}\frac{L_{23}}{L_{26}}SC_{23})$	$\frac{a_{11}a_7}{a_{78}}SC_{23}$	0	0	$NO_{U6} + NO_{L6} + 6K_{B6} + K_{26}S_{26} + \frac{K_{26}}{K_{23}}\frac{L_{23}}{L_{26}}SC_{23}\frac{a_7a_{11}}{a_{78}}$	$-SC_{[illegible]}\frac{a_{11}}{a_{78}}$
$SC_{12}[1 + \frac{1}{a_{78}}(a_7a_8 - a_9a_{12})]$	$SC_{12}[1 + \frac{1}{a_{78}}(a_7a_8 - a_9a_{12})] + SC_{23}[a_7 - a_9 + \frac{a_7}{a_{78}}(a_7a_8 - a_9a_{12})] - SC_{23}\frac{K_{26}}{K_{23}}\frac{L_{23}}{L_{26}}a_7[1 + \frac{1}{a_{78}}(a_7a_8 - a_9a_{12})]$	$SC_{34} + SC_{23}[a_7 - a_9 + \frac{a_7}{a_{78}}(a_7a_8 - a_9a_{12})] + \frac{K_{35}}{K_{23}}\frac{L_{23}}{L_{35}}a_9 SC_{23}$	SC_{34}	$\frac{K_{35}}{L_{35}}\frac{L_{23}}{K_{23}}a_9 SC_{23}$	$-SC_{23}\frac{K_{26}}{K_{23}}\frac{L_{23}}{L_{26}}a_7[1 + \frac{1}{a_{78}}(a_7a_8 - a_9a_{12})]$	$-SC_{[illegible]}[1 + \frac{1}{a_{78}}(a_7a_8 - a_9a_{12})] - SC_{34}$ [illegible]

The foregoing considerations led to the choice of the two test series, P and M, each comprising five frames. Portal frames P1 to P5, subjected to proportional vertical and horizontal loading were tested in order to verify one curve and the double-storey frames M1 to M5 with similar loading were used to monitor a second design curve of Figure 23.

10.2 Details of test frames

Details of the test frames are given in Figure 52 and Table 7 respectively.

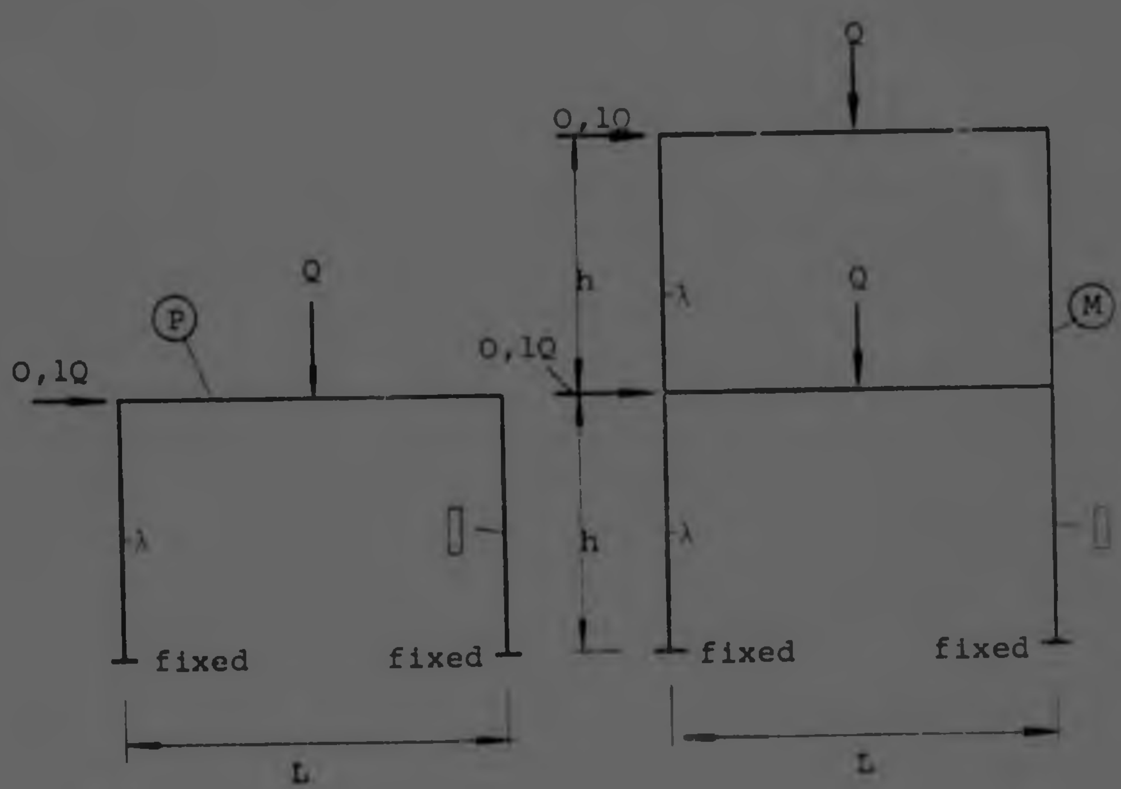

FIGURE 52: Test frames

TABLE 7: Geometry of test frames

FRAME	L (m)	h (m)	$\lambda = \frac{h}{r}$
P1	1,125	0,750	431
P2	0,937	0,625	359
P3	0,750	0,500	287
P4	0,656	0,437	251
P5	0,500	0,333	190
M1	1,125	0,750	431
M2	0,937	0,625	359
M3	0,750	0,500	287
M4	0,656	0,437	251
M5	0,500	0,333	190

The cross-sections of all members were rectangular (29mm × 6mm) and loading was applied in a way to cause bending about the minor axis. Also shown in Figure 52 is the load disposition, consisting of a central point load on the beams and a horizontal load acting at the beam levels. The load ratio of vertical to horizontal load was kept constant at 10:1.

The calculation of the failure load P_F requires the knowledge of certain material strength parameters. These were determined from specimens subjected to a bending test as shown in Figure 53. A bending test was given preference for two reasons. Firstly, failure of the actual frame occurs in a similar mode and, secondly, all the required parameters follow directly from such a test procedure.

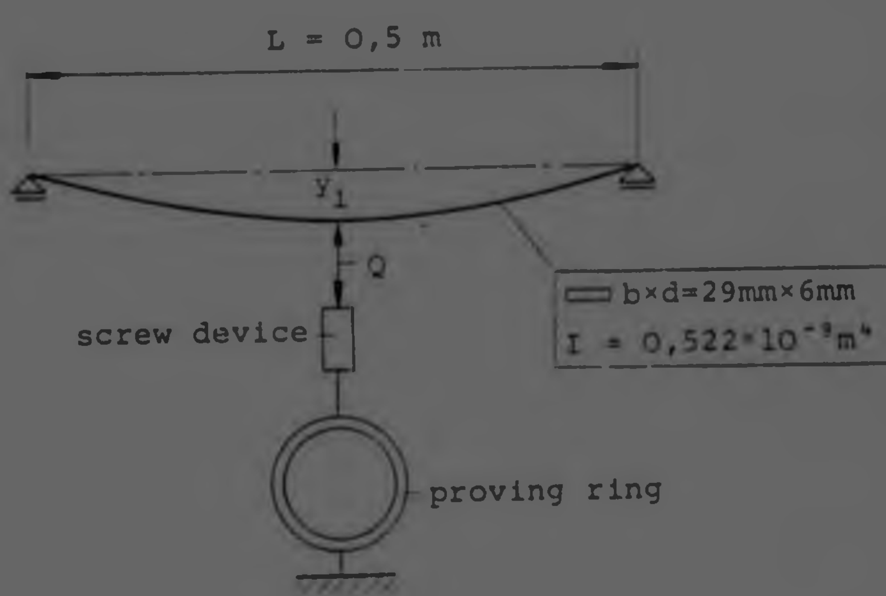

FIGURE 53: Bending test

The load-deflection curves and the measured plastic collapse load P_p obtained from the bending tests were used to calculate the modulus of elasticity E, the plastic moment capacity M_p and the yield stress f_Y of the material. The plastic collapse load follows from the load-deflection curve by extrapolating the plastic slope backwards until it meets the elastic slope. The three salient parameters were evaluated from the expressions given in Equations 44a, 44b and 44c.

$$E = \frac{QL^3}{48Iy_1} \qquad Q < Q_{yield} \qquad |\text{EQN. 44a}|$$

$$M_p = \frac{P_p L}{4} \qquad |\text{EQN. 44b}|$$

$$f_Y = \frac{P_p L}{bd^2} = \frac{4M_p}{bd^2} \qquad |\text{EQN. 44c}|$$

Six beams, denoted BM1 to BM6, were tested and assessed in this way.

The pertinent results of the test beams are given in Table 8 together with the values adopted for the analysis of the frames. No significant residual stresses could be identified.

TABLE 8: Results of bending tests

BEAM	P_p (kN)	E (MPa)	M_p (kNm)	f_y (MPa)
BM 1	0,530	$1,92 \times 10^5$	0,06621	253,7
BM 2	0,530	$1,896 \times 10^5$	0,06621	253,7
BM 3	0,530	$1,912 \times 10^5$	0,06621	253,7
BM 4	0,530	$1,935 \times 10^5$	0,06621	253,7
BM 5	0,530	$1,914 \times 10^5$	0,06621	253,7
BM 6	0,518	$1,908 \times 10^5$	0,0648	248
USED IN ANALYSIS	0,530	$1,91 \times 10^5$	0,0662	253,7

10.3 Test arrangement

The arrangement chosen for the frame tests is shown in Figure 54. Provision was made to test single and double-storey frame models.

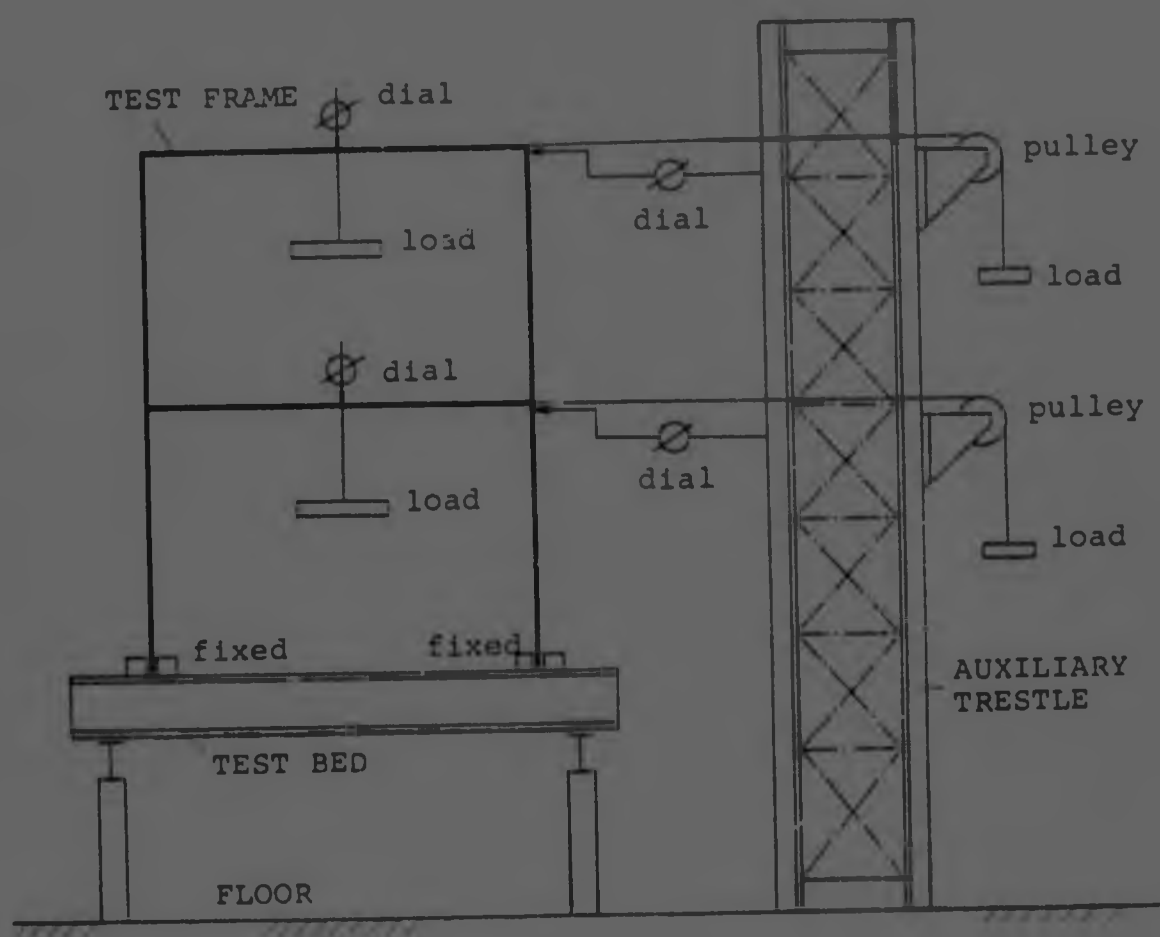

FIGURE 54: Test arrangement

Since the applied loadings induced bending about the minor axis only and because of the flat cross-sectional shape, no out-of-plane buckling was expected. This allowed the testing of single frames and thus eliminated the influence of transverse bracing which has been known to disturb the accuracy of certain measurements in twin-test arrangements.

The test loading for the experiments was effected by gravity loading applied at the beam centres and via pulleys at the beam levels in a horizontal direction. Care was taken to keep vertical and horizontal loading proportional at all times. The loading system as a whole could freely move with the frame at all stages of the experiment. Lateral displacements at the beam levels were recorded for all frames. In addition, for frame M2, measurements were taken of the deflections at midspan of the beam members. Horizontal and vertical loads were applied in successive increments and the frame displacements were measured after each load application. The increment of load was gradually reduced as the applied load approached the predicted failure load.

Three photographs are reproduced in Figures 55, 56 and 57, depicting frame M2 at various stages of testing. In Figure 55, frame M2 is shown on the testing rig just prior to the load application. Figure 56 depicts the same frame during loading and in Figure 57 the deformed frame, after testing, is shown with all loads removed.

In another experiment, an identical frame M2 was tested with the horizontal loads omitted. The deformed shape of this frame, after load removal, is shown in Figure 58.

FIGURE 55: Frame M2 before testing

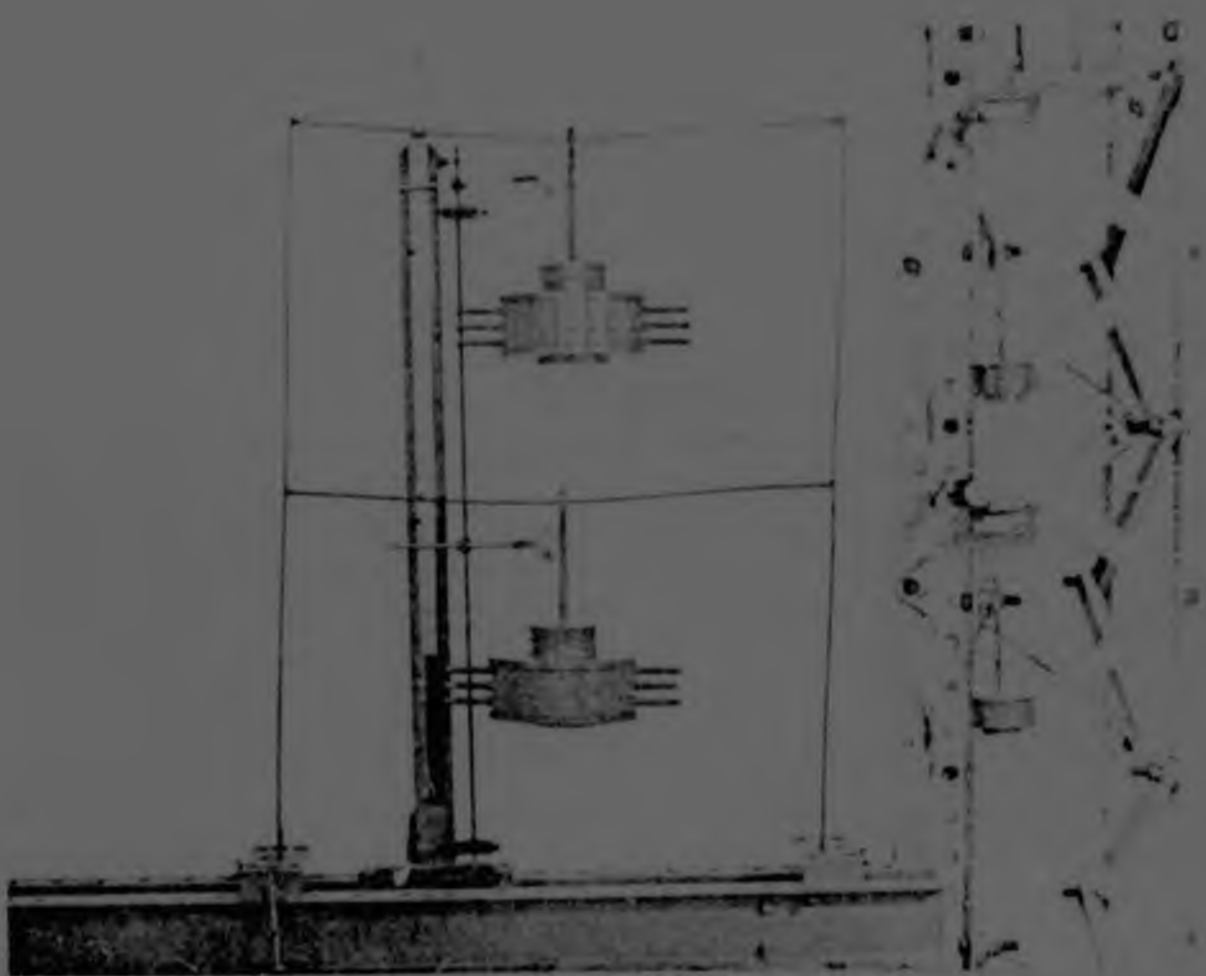

FIGURE 56: Frame M2 during testing

FIGURE 57: Frame M2 after testing

FIGURE 58: Frame M2 after testing for vertical loading

10.4 Results of tests

The main objective of the experiments was to determine the maximum load the frames could carry at failure. For the purpose of this research, failure was defined as that condition of loading for which the displacements continued to increase under constant load without coming to a standstill within reasonable limits. This condition would thus coincide with a peak in the load displacement curves as shown for frame M2 in Figures 59a and 59b.

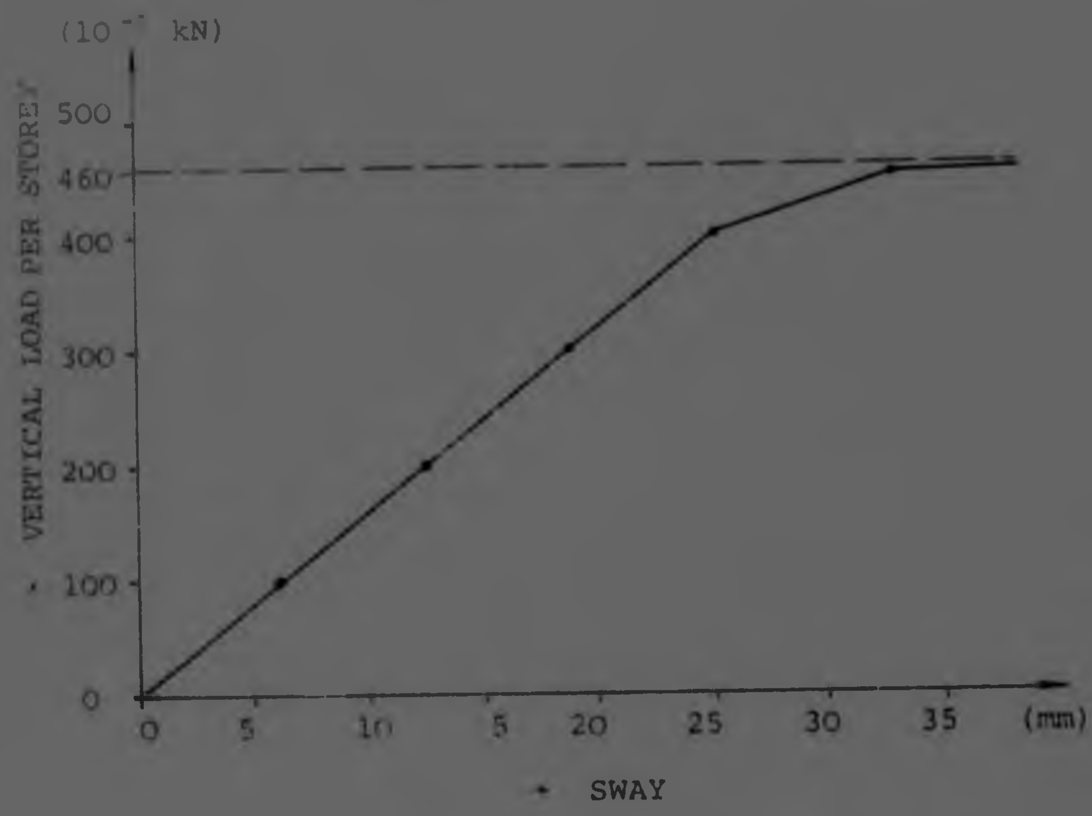

FIGURE 59a: First storey sway - Frame M2

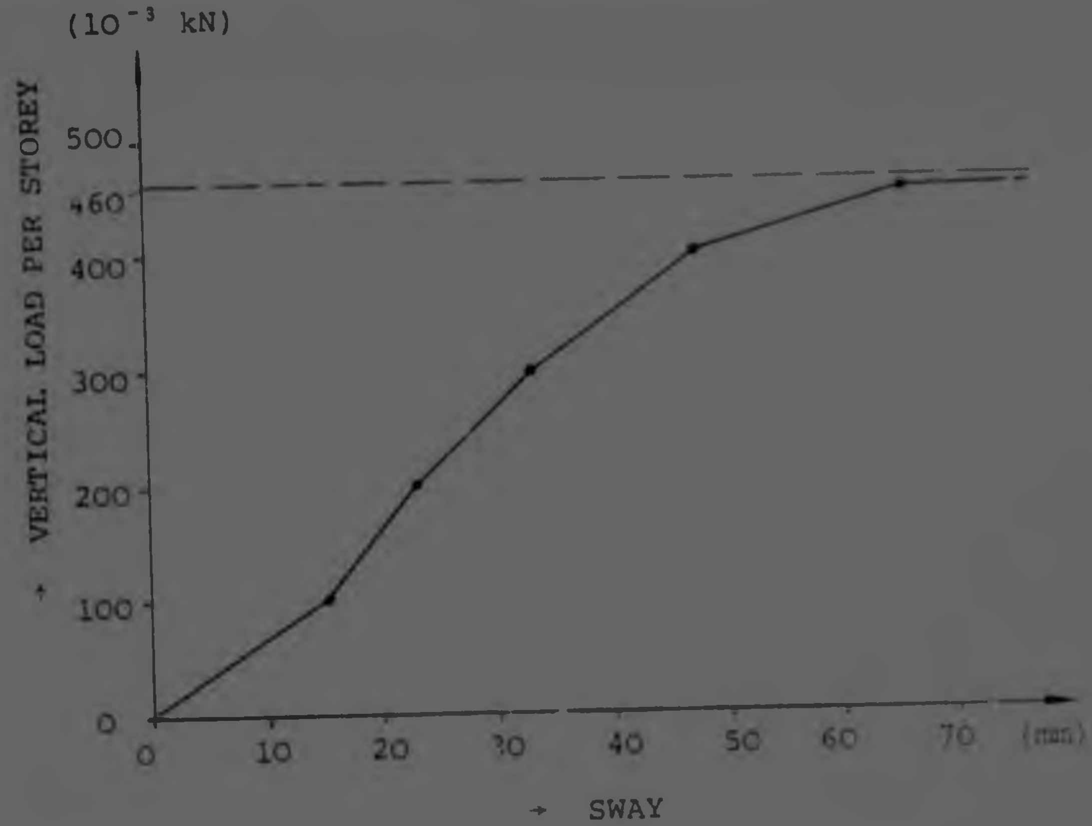

FIGURE 59b: Second storey sway - Frame M2

The complete set of failure loads for the ten frames tested in the laboratory is given in column 8 of Table 9. The recorded failure loads P_F have been expressed as a function of the plastic collapse load P_P applicable to the particular frame.

The values in columns 2 to 7 of Table 9 are those required to establish the failure load, using the interaction method developed in this research. The values P_O, α and α_ℓ were obtained using the computer analysis described in chapter 7 of this thesis. The ratio P_F/P_P in column 9 of Table 9 has been evaluated from the design curves of Figure 23, using the two slopes $\alpha P_O/P_P$ and $(\alpha P_O/P_P)_\ell$ for

TABLE 9: Test results of model frames

1	2	3	4	5	6	7	8	9	10	11
							FAILURE LOAD P_F/P_P			
FRAME	P_O (kN)	$P_P = 5,33 \frac{M_P}{h}$ (kN)	α	λ_ℓ	$\frac{\alpha P_O}{P_P}$	$\left(\frac{\alpha P_O}{P_P}\right)_\ell$	TEST RESULT	THIS RESEARCH	MERCHANT-RANKINE	8 - 9 (%)
P1	2,077	0,471	0,55	1 923	2,42	0,54	0,91	0,90	0,82	+1,1
P2	2,991	0,565	0,55	1 92[illegible]	2,91	0,54	0,92	0,92	0,84	0
P3	4,673	0,706	0,55	1 923	3,64	0,54	0,94	0,93	0,87	+1,1
P4	6,117	0,807	0,55	1 923	4,17	0,54	0,96	0,94	0,88	+2,1
P5	10,535	1,060	0,55	1 923	5,47	0,54	0,96	0,95	0,91	+1,0

TABLE 9: Test results of model frames - cont.

1	2	3	4	5	6	7	8	9	10	11
FRAME	P_O (kN)	$P_p = 5{,}33 \frac{M_p}{h}$ (kN)	α	λ_ℓ	$\frac{\alpha P_O}{P_p}$	$\left(\frac{\alpha P_O}{P_p}\right)_\ell$	FAILURE LOAD P_F/P_p			
							TEST RESULT	THIS RESEARCH	MERCHANT-RANKINE	8 - 9 (%)
M1	0,995	0,471	0,54	1 111	1,14	0,44	0,77	0,75	0,68	+2,6
M2	1,433 (1,433)	0,565 (0,565)	0,54 (1,0)	1 111 (1 600)	1,37 (2,54)	0,44 (0,57)	0,81 (0,93)	0,79 (0,91)	0,72 (0,72)	+2,5
M3	2,239	0,706	0,54	1 111	1,71	0,44	0,84	0,83	0,76	+1,2
M4	2,931	0,807	0,54	1 111	1,96	0,44	0,87	0,85	0,78	+2,3
M5	5,047	1,060	0,54	1 111	2,57	0,44	0,89	0,88	0,83	+1,1

the actual and the "limiting" frames respectively. For comparison purposes the solutions based on the Merchant-Rankine formula are given in column 10 of Table 9.

It has been mentioned that frame M2 was also tested for vertical loading. The results relevant to this experiment are shown in brackets in Table 9.

The last column of Table 9 gives the percentage difference between the test results and the solutions predicted by the analysis approach developed in this thesis. The test results are taken as 100 per cent.

As indicated before, the tests were designed to monitor certain failure curves of the interaction graphs given in Figure 23. The curve checked by the portal frames P has the selection parameter $(\alpha P_O/P_P)_\ell$=0,54 and the relevant curve applicable to the double-storey frames M has the reference parameter $(\alpha P_O/P_P)_\ell$=0,44. Both these parameters appear in column 7 of Table 9 for all frames of a particular group of frames.

The fact that all λ_ℓ, α and $(\alpha P_O/P_P)_\ell$ at λ_ℓ are equal for the respective test groups P and M comes as no surprise. It may be recalled that these conditions were presumed when hypothesising the interaction curve shapes of Figure 23. The consistency of these computer results thus confirms the va[illegible] of the tendered design proposition for the general frame and substantiates the two principal hypotheses formulated [illegible] section 2.3.1 of this study.

In Figures 60 and 61 the test results of Table 9 are plotted against the interaction diagram of Figure 23, showing only the two relevant design curves. The curve points are shown thus □ and the test results are marked thus +.

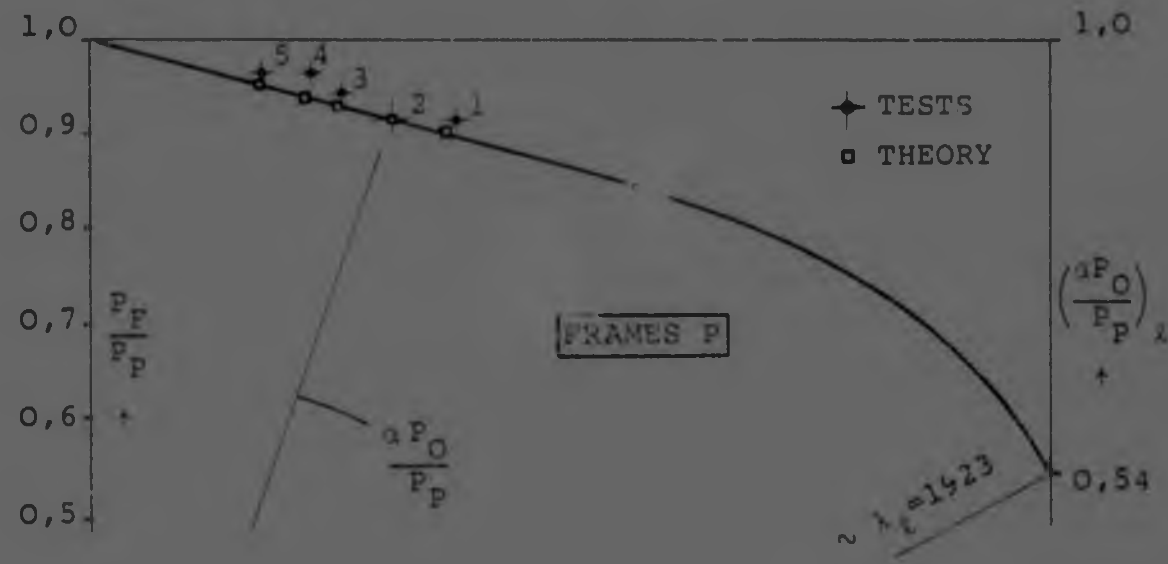

FIGURE 60: Test results for frames P plotted on interaction graph

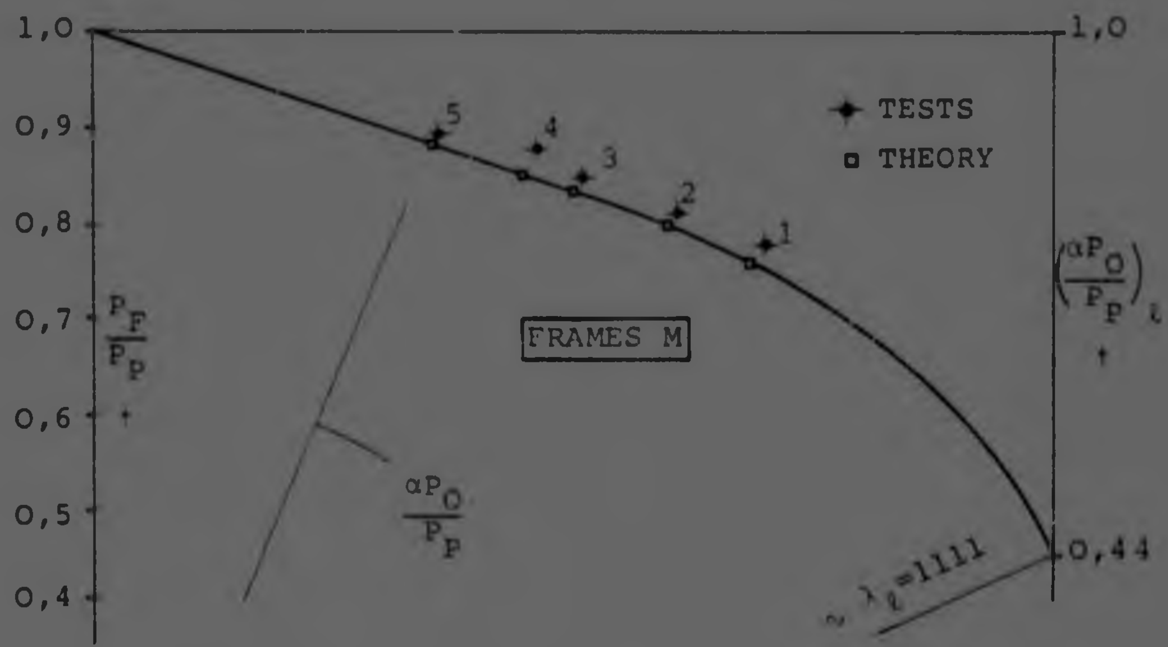

FIGURE 61: Test results for frames M plotted on interaction graph

10.5 Summary of test results

From the comparisons given in Table 9 and Figures 60 and 61, it can be seen that satisfactory correlation has been obtained between the test results and the frame analysis method proposed in this thesis.

In nine cases the predicted failure loads were slightly below the experimental values and in one case the test result was identical with the theoretical solution. The range by which tests exceeded the results of the analysis was found to extend from 0 per cent to +2,6 per cent, with a mean variation of +1,5 per cent. By comparison, the mean deviation of results evaluated according to the Merchant-Rankine rule has been calculated as +8,9 per cent for the ten frames tested for this study. For the Merchant-Rankine rule, the range of the results was found to extend from +5,2 per cent to +11,7 per cent. Hence, the proposed method represents a distinct improvement in the prediction of the failure load P_F.

The results given in Figures 60 and 61 show that frames of lower slenderness ratios, within a specific group of frames, approach progressively the maximum ratio P_F/P_P=1,0 as the slenderness decreases. This confirms the second hypothesis formulated earlier in section 2.3.1 of this study.

The reason for the slight underestimation of the failure load by the proposed analysis approach can be attributed to strain-hardening, the stiffening effect of welds at the member intersections and the nature of the base restraint. The latter two aspects are equivalent to a reduction in member length. In the analysis, the distance between the centre lines of the members and at the base the distance to the centre of the embedded column length were used. The assumption of an ideal point load is also an approximation. If these disturbances would be allowed for, an even better correlation between theoretical solution and test result were possible.

A further point of interest is the test performance of frame M2, when subjected to pure vertical loading. The proposed method of analysis predicts the failure load quite adequately as shown in brackets in Table 9. For the same frame the result obtained by the Merchant-Rankine method is out by +22,6 per cent. In fact, for this particular frame and loading, this method does not distinguish between a frame subjected either to combined or pure vertical loading. For both cases a beam mechanism is suggested as the failure mode. This results in the same value for the plastic collapse load P_P and thus P_F. A case such as this was discussed before in section 2.4, paragraph b).

to strain-hardening, the stiffening effect of welds at the member intersections and the nature of the base restraint. The latter two aspects are equivalent to a reduction in member length. In the analysis, the distance between the centre lines of the members and at the base the distance to the centre of the embedded column length were used. The assumption of an ideal point load is also an approximation. If these disturbances would be allowed for, an even better correlation between theoretical solution and test result were possible.

A further point of interest is the test performance of frame M2, when subjected to pure vertical loading. The proposed method of analysis predicts the failure load quite adequately as shown in brackets in Table 9. For the same frame the result obtained by the Merchant-Rankine method is out by +22,6 per cent. In fact, for this particular frame and loading, this method does not distinguish between a frame subjected either to combined or pure vertical loading. For both cases a beam mechanism is suggested as the failure mode. This results in the same value for the plastic collapse load P_p and thus P_F. A case such as this was discussed before in section 2.4, paragraph b).

CHAPTER 11

DEVELOPMENT OF DESIGN GRAPHS

11.1 Principles

One of the important features of the method developed in this research is the fact that the results can be presented in graphical form. This enables the "manual" evaluation of common cases, i.e. an analysis without computer is possible, once the plastic collapse load is known.

A rational presentation of results in graphical form has been achieved for two reasons. Firstly, because an infinite number of similar frames can be represented by a common identification parameter, namely the "limiting slenderness ratio". This was demonstrated in chapter 2 of this study. Secondly, if the "limiting slenderness ratio" is determined for a basic case, i.e. a case of equal strength, member depth and moment of inertia for beams and columns, other "limiting slenderness ratios" pertaining to conditions different from this basic case can be obtained by simple linear modification. This will be confirmed in a later section of this chapter.

These two fundamental findings greatly reduce the number of variables usually associated with the problem of inelastic failure. The remaining variables would mainly be concerned with the loading and the nature of the subassemblage.

11.2 Scope

11.2.1 Geometry

It is envisaged that a graphical method should cater for the typical building structure with respect to loading, frame geometry and column base conditions. For the general multi-bay, multi-storey structure the significant sub-assemblages to be covered by a graphical method are shown superimposed on a general framework in Figure 62. Only the core-module members are indicated in prominent lines.

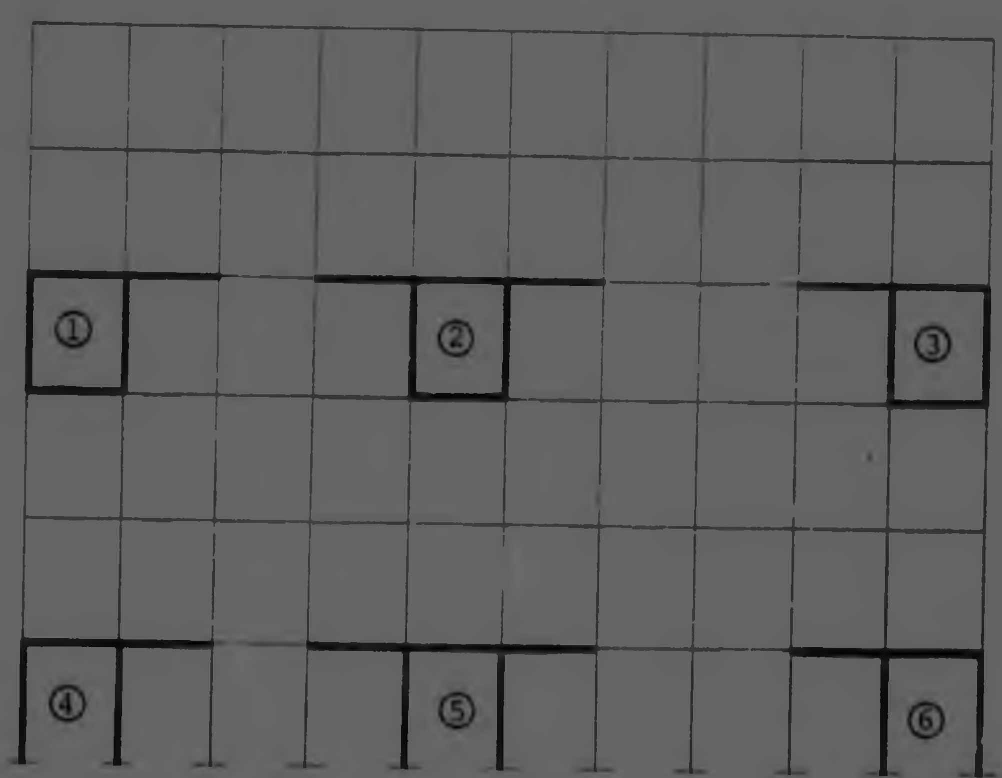

FIGURE 62: Subassemblages for design graphs

Each of the subassemblages of Figure 62 corresponds to one set of design graphs comprising a graph A for the buckling load P_O and a graph B for the "limiting slenderness ratio" λ_ℓ and reduction value α.

In addition, for single-bay frames, two further subassemblages need to be investigated - one applicable to the bottom storey and another for intermediate and topmost storeys. With respect to the column base conditions, at least two types of elastic base restraint, that of a "quasi-pinned" and a "quasi-fixed" base, should be included for the bottom storey subassemblages. This will result in a minimum of twelve graphs A and twelve graphs B for the case of bare frames, provided a specific type of subassemblage with all its related load combinations and different storey numbers is presented in a single graph B. By restricting the number of graphs in this way certain simplifications and omissions are inevitable. The major assumptions are given below:

a) A two-bay structure can be adequately assessed by analysing two core-modules, i.e. 1 and 3 or 4 and 6 of Figure 62.

b) Where applicable, the columns above and below the core-module are identical to the core-module columns. The core-module columns are of constant size.

c) All beams belonging to one subassemblage are of equal size.

On first sight these limitations seem to be more severe than they really are. Firstly, many practical frames have constant beam sizes throughout the entire storey and column sections are often kept unchanged over two storeys in height. Secondly, the failure load, P_F, is not very sensitive to the elastic parameters used in the presented method, e.g. a higher than actual buckling load P_O will be partially compensated by a lower reduction value α and an adjusted "limiting slenderness ratio" λ_ℓ. This was demonstrated in section 3.2. Hence, for most practical frames, the twelve graphs as suggested, will be adequate in predicting the failure load. However, if so desired, the range of graphs could easily be extended to cover further parametric variations and also the case of a partial lateral bracing restraint.

11.2.2 Loading

Typical loading in buildings consists of uniformly distributed vertical beam loading and horizontal wind loading. The wind shear is usually represented by shear forces applied at the levels of the beams. The design graphs for "manual" use should be based on these loading conditions. Furthermore, allowance should be made for patterned beam loadings when covering the case of vertical loading. Since all parameters required for the graphical presentations are obtained by computer, it is not difficult to analyse the case of checkerboard loading as well. However, this could introduce a new variable in that a distinction has to be made between dead and live loadings.

Apart from the load configuration, the load size needs to be considered. The size of the vertical column load is linked to the number of storeys above the considered subassemblage. Each additional storey will progressively increase the axial force in the columns, which implies that a separate curve will appear in graphs A and B for different numbers of storeys. Alternatively, a separate graph could be drawn for each additional storey.

The same considerations as for vertical load also apply to the storey shear. In this case, the shear not only varies with the number of storeys, but the load intensity for each individual storey may assume different values. A different curve will thus result for various wind load intensities.

11.3 Graphical presentations

After careful evaluation of all points examined in the preceding section of this chapter, it was found convenient to use the general layout shown in Figures 63a and 63b for the design graphs

The graph for the elastic buckling load P_O, shown in Figure 63a, uses the variable $(I_C/I_B)(L/h)$ on the horizontal axis and the ratio of the elastic buckling load P_O to Euler load P_E on the vertical axis. The Euler load P_E

applies to the elastic buckling load of a strut pinned at both ends.

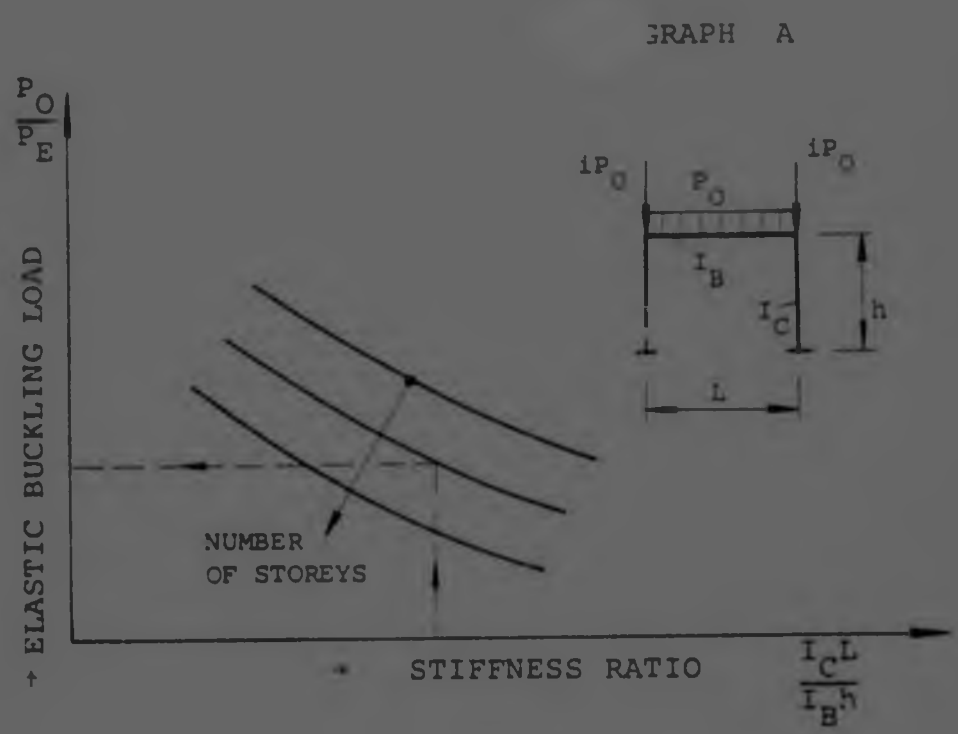

FIGURE 63a: Design graph for buckling parameter

The elastic buckling load P_O refers to the beam loading shown in Figure 63a. The presence of storeys above the investigated storey is accounted for by additional axial loadings iP_O.

A typical graph giving the "limiting slenderness ratio", λ_ℓ, and the reduction factor α is shown in Figure 63b. One such graph is applicable to a specific subassemblage and will refer to a definite number of storeys.

Loadings from storeys above the investigated storey are represented by the term iQ.

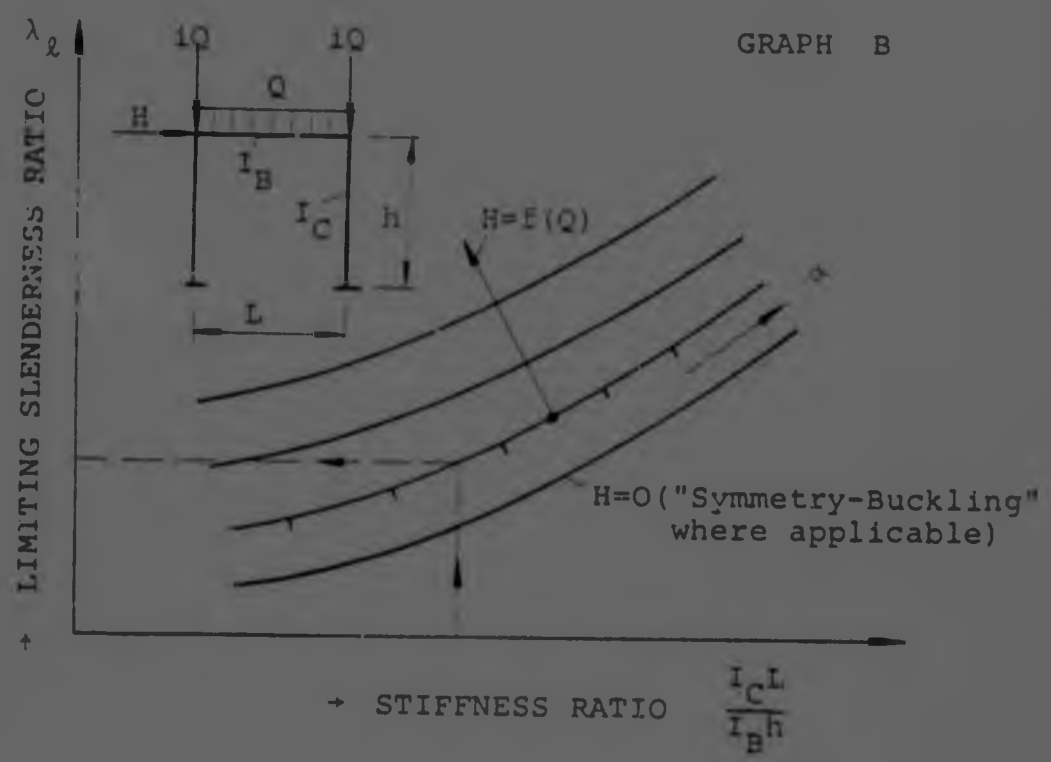

FIGURE 63b: Design graph for "limiting slenderness ratio"

A number of different horizontal load parameters H will have to be analysed for each graph B such as shown in Figure 63b. The case H=O for "Symmetry-Buckling" is more conveniently presented in a separate graph. For both, graphs A and B, interpolations may be required when dealing with the analyses of the real structure.

11.4 Graph parameters

11.4.1 Wind shear

In Figure 63b the wind shear H appears as the sole effect from lateral wind loading. However, it is obvious that for a subassemblage analysis a compensating joint moment will also be generated and needs to be considered.

A simple relationship between shear and joint moment can be established once the storey shear H is known. In this way implicit allowance can be made for the moment as well as the shear. The moment-shear function incorporated in the design graphs is based on the principle illustrated in Figure 64. The column shear, H_C, is related to the subassemblage shear, H, by $H=\Sigma H_C$.

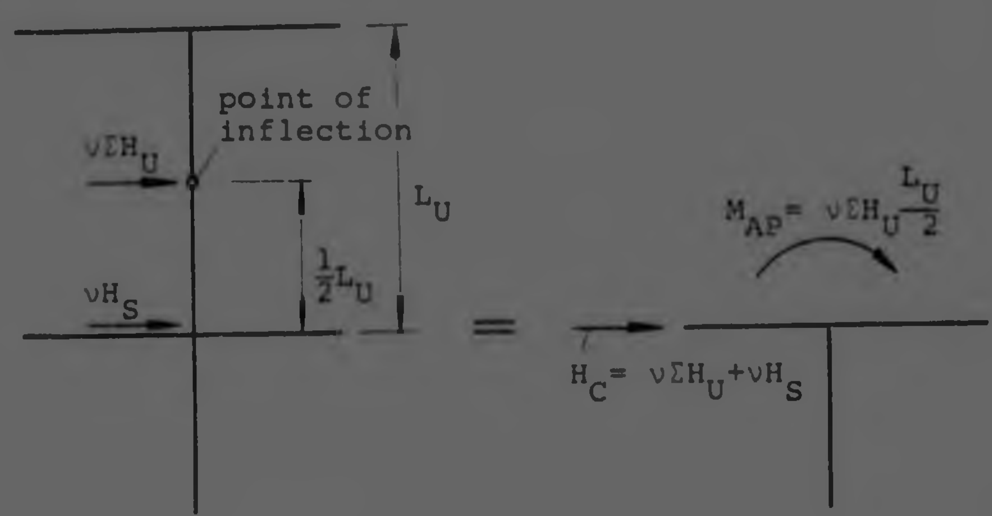

FIGURE 64: Shear and moments from upper storeys

If the point of inflection occurs at $L_U/2$, the applied moment can be expressed as follows:

$$M_{AP} = \nu \Sigma H_U \frac{L_U}{2}$$

After some manipulation the joint moment M_{AP} can finally be related to the wind shear H_C as given in Equation 45.

$$\frac{M_{AP}}{L_U} = \frac{n_S - \frac{1}{2}}{2\left(n_S + \frac{1}{2}\right)} H_C \qquad |\text{EQN. } 45|$$

This formula applies to two columns in the subassemblage and the term n_S is the number of storeys above the storey under consideration. It is also assumed that the shear distribution factor ν remains unchanged throughout the height of the building. The factor ν has been discussed in section 3.9.1. Using Equation 45, it is then possible to represent both load variables, namely H and M_{AP}, by the single variable H which appears in the design graphs.

11.4.2 Stress f_p at the onset of yield

The stress f_p incorporated in the design graphs is taken as 240 MPa. This value is suggested by the British Draft Code B20[7] as the design strength for mild steel sections of grade 43A, 43B, 43C, 43D and 43E with a thickness up to and including 40 mm. Any deviation from this stress value can be accounted for by proportional modification of the "limiting slenderness ratio".

11.4.3 Modification of graph results

The "limiting slenderness ratio", λ_ℓ, obtained from the computer analysis and displayed in graphs of the type as shown in Figure 63b will be based on the results of Equations 40 and 41 developed in chapter 6 of this thesis. Using Equation 41 for demonstration purposes, the following two cases can be observed. The suffix (B) refers to beams and a suffix (C) to columns, the beam length is L and the column height is h.

a) First-yield occurs in beam (Equation 41):

$$\lambda_{\ell B} = \frac{M_B}{f_{PB}} \frac{L}{I_B} \frac{d_B}{2r_B}$$

This can be expressed in terms of column and beam parameters by using the conversion

$$\lambda_{\ell B} = \frac{L}{h} \frac{r_C \lambda_{\ell C}}{r_B}$$

Hence, the following expression is obtained:

$$\lambda_{\ell C} = \frac{M_B}{f_{PC}} \frac{f_{PC}}{f_{PB}} \frac{I_C}{I_B} \frac{d_B}{d_C} \frac{h}{I_C} \frac{d_C}{2r_C}$$

It is now demonstrated that a basic "limiting slenderness ratio" can be presented as a function of the ratio $(I_C/I_B)(L/h)$ and that other "limiting slenderness ratios" can be derived from this basic value. For this purpose, the beam moment M_B is expressed as a function of the buckling load parameter $m_O = h\sqrt{P_O/EI_C}$ and the beam length L is introduced as nh. The terms m_O and n have been explained previously (section 2.2.2). It then follows, that the bending moment M_B is proportional to

$$M_B \sim P_O h = \frac{m_O^2}{h} EI_C$$

and substituting this into the slenderness formula for $\lambda_{\ell C}$, yields the following final relationship:

$$\lambda_{\ell C} \sim \frac{M_B (m_O^2) E}{f_{PC}} \frac{f_{PC}}{f_{PB}} \frac{I_C}{I_B} \frac{d_B}{d_C} \frac{d_C}{2r_C} \qquad |\text{EQN. 46a}|$$

b) First-yield occurs in column:

Using the same considerations as for the previous case, a similar equation can be derived when first-yield occurs in the column. From Equation 41 follows that

$$\lambda_{\ell C} \sim \frac{M_C (m_O^2) E}{f_{PC}} \frac{d_C}{2r_C} \qquad |\text{EQN. 46b}|$$

The design graphs such as shown in Figure 63b will conveniently be based on the results obtained from the evaluation of the first terms in Equations 46a and 46b respectively. This implies a value of 1,0 for all other ratios appearing in the two equations.

It is important to recognise that the first terms in Equations 46a and 46b are primarily a function of the column and beam stiffnesses since the relevant bending moment can also be expressed as a function of $(I_C/I_B)(L/h)$. Hence, Equation 46b can be presented as

$$\lambda_{\ell C} \sim f\left(M_C;\frac{I_C}{I_B}\frac{L}{h}\right)\ \frac{E}{f_{PC}}\ \frac{d_C}{2r_C}$$

This fundamental expression indicates that the "limiting slenderness ratio" λ_ℓ can be plotted as a function of the member stiffnesses for a given subassemblage and specific ratios E/f_{PC}, I_C/I_B, d_B/d_C, f_{PC}/f_{PB} and $d_C/2r_C$. At the same time it is also apparent that for the first terms of Equations 46a and 46b, I_C/I_B and L/h are interchangeable, so that a variation in L/h can cover the whole stiffness range of practical frames.

The design graphs for the "limiting slenderness ratio" would therefore be compiled from the evaluation of Equations 46a and 46b, varying the parameter L/h, but keeping I_C/I_B=1,0. The largest value λ_ℓ obtained in this way will be presented in graphical form. In order to adapt this value to the actual frame, modification factors f_{PC}/f_{PB}, I_C/I_B, d_B/d_C and $d_C/2r_C$ need to be applied. This procedure may be adopted by allowing for the following additional aspects:

i) One needs to know whether the "limiting slenderness ratio", which appears in the design graphs, refers to a column or a beam section. A "limiting slenderness ratio" based on first-yield in a column section must be modified by $d_C/2r_C$, whereas a case of first-yield in a beam section requires adjustment by f_{PC}/f_{PB}, I_C/I_B, d_B/d_C and $d_C/2r_C$. In order to deal with this situation, the results appearing in the design graphs will be clearly identified as belonging either to a column or a beam member.

ii) In rare instances it may occur that the largest "limiting slenderness ratio" prior to multiplication with any of the modification factors (graph value) would be exceeded in size by a "limiting slenderness ratio" of another critical section, once the relevant adjustment factors have been applied. This is demonstrated in an example.

First terms of Equation 46a and 46b:

Equation 46a : $\lambda_{\ell C} = 400$ (graph value)
Equation 46b : $\lambda_{\ell C} = 300$ (not appearing in graph)

After application of the modification factors:

Equation 46a : $\lambda_{\ell C} = 400\,\frac{1}{1}\times\frac{1}{1{,}75}\cdot\frac{1{,}2}{1}\times\frac{1}{0{,}8} = 343$

Equation 46b : $\lambda_{\ell C} = 300\times\frac{1}{0{,}8} = 375$

Hence, using the graphs as outlined in i) above would result in the design value of $\lambda_{\ell C} = 343$, whereas the more critical value of 375 remains undetected.

A similar reversal of the critical sections may arise if first-yield is initially predicted to occur in the column.

Three comments are of importance in this context. Firstly, the occurrence of this problem is associated with the condition of first-yield in a column section, which was only observed for extreme cases of high lateral loads or weak column sections. It has been experienced that for most practical frames first-yield appears in a beam member. Secondly, it has been observed that the error described above only leads to marginal differences in the "limiting slenderness ratio" λ_{ℓ} and the failure load P_F. Thirdly, a conservative approach could easily be reached by applying both modification factors, i.e. those relevant to Equation 46a or 46b, and proceeding with the larger of the two results.

For the design graphs of Appendix VI/2 it is adequate to follow the procedure outlined in subsection i) and ignore the recommendations of subsection ii).

11.4.4 Reduction factor α

The reduction factor α, as it appears in the design graphs such as given in Figure 63b, is related to the stress f_p at the onset of yield. The stress f_p has been defined in section 11.4.2 and the factor α in Equation 39. In Equation 39, α has been expressed as a function of the term $\lambda_{HO,4}$ which in turn is directly proportional to f_p. The parameter $\lambda_{HO,4}$ would be evaluated from Equation 40 or 41. Small deviations from the stress f_p incorporated in the design graphs can be ignored. However, for larger discrepancies the factor α needs to be adjusted. If α, $\lambda_{HO,4}$, and f_p refer to the conditions of the design graphs, the revised value α' for a different stress at the onset of yield, e.g. f_p', may be obtained as follows:

Step 1 (Equation 39 solved for $\lambda_{HO,4}$)

$$\lambda_{HO,4} = 700 \left(1 - \sqrt[3]{\frac{1 - \frac{0,4}{\alpha}}{0,6}} \right)$$

Step 2

$$\lambda'_{HO,4} = \frac{f_p}{f_p'} \lambda_{HO,4}$$

Step 3 (Equation 39)

$$\alpha' = \frac{0,4}{1-0,6\left(\frac{700-\lambda'_{HO,4}}{700}\right)^3}$$

in which,

f_p' = stress at onset of yield ≠ 240 MPa

$\lambda'_{HO,4}$ = slenderness ratio based on loading related to 0,4 P_O and a stress at onset of yield of f_p'.

11.5 Sample charts

Based on the foregoing discussion, a set of charts were prepared and have been enclosed in Appendix VI. These charts cover the case of a single-bay frame subjected to vertical or combined loading with a maximum of six storeys, assuming equal vertical loading in all storeys. The graphs referring to the bottom storeys have been derived for a rotational restraint at the column bases equal to $\bar{K}_S = 10$.

The graph values were obtained by computer, solving the basic expressions for the "limiting slenderness ratio" in Equations 40 and 41, keeping the ratios f_{PC}/f_{PB}, I_C/I_B, d_B/d_C and $d_C/2r_C$ at unity. By varying the dimensional ratio $n=L/h$, the stiffness range $(I_C/I_B)(L/h)$ from 0,5 to 4,0 has been evaluated. This will include for most practical frame structures.

The influence of various modification factors on the "limiting slenderness ratio" is accounted for by factoring the graph values by the relevant ratios. The modifying ratios, which appear in Equations 46a and 46b, will not directly affect the reduction factor α, provided $f_{PC} = f_{PB} = 240$ MPa. By definition, the factor α is related to the elastic second-order moment response, and thus primarily a function of the first terms in Equations 46a and 46b respectively.

For the graphs, it has been indicated whether first-yield occurs in the column or in the beam. For graphs B a separate diagram has been presented for each storey except for the case of "Symmetry-Buckling". The latter case is covered in graphs B1 and B2 of Appendix VI/2.

11.6 Example by design charts

The four-storey frame analysed by Jennings & Majid[11] is considered. The salient results for the failure load of this frame, when analysed by computer, appear in Table 6/1 of chapter 9. The load factor for plastic collapse has been established as 2,15.

The graphical method is applied to the bottom storey of this four-storey frame. The three upper storeys could be treated on a similar basis. The values read from the graphs of Appendix VI refer to the case of a bottom storey with fixed bases ($\overline{K}_S$ = 10) and represent a 3½-storey frame, which allows for the fact that the roof of the frame is only subjected to half the normal floor loading. The salient results with explanations have been entered in Table 10.

The other three storeys of this frame were analysed in the same way. The lowest failure load predicted for any of the four storeys is that applicable to the bottom storey, for which the solution is given in Table 10.

TABLE 10: Analysis by charts

	DETAILS	REMARK
PROBLEM	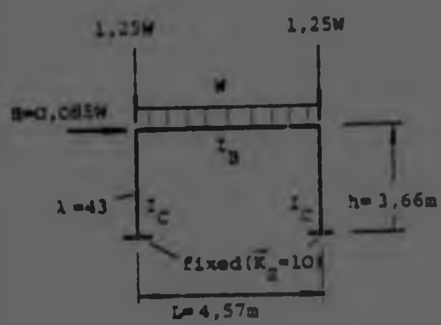	I_B = 5 092× 10^{-8} m^4 I_C = 4 789× 10^{-8} m^4 E = 2,06× 10^5 MPa f_{PC} = f_{PB} = 253 MPa W = 16,5 kN r_C = 84,4 mm d_B = 254 mm d_C = 203,2 mm
BUCKLING LOAD PARAMETER	$\frac{P_O}{P_E}$ = 0,31	GRAPH A1 : $\frac{L}{h}\cdot\frac{I_C}{I_B}$ = 1,17 i = 1,25
BASIC "LIMITING SLENDERNESS RATIO"	λ_ℓ = 430	extrapolate from GRAPHS B4 and B5
MODIFIED "LIMITING SLENDERNESS RATIO"	$\lambda_\ell = 430 \times \frac{240}{253}\cdot\frac{4\ 789}{5\ 092}$ $\cdot \frac{25,4}{20,32}\cdot\frac{20,32}{2\times 8,48}$ λ_ℓ = 575	EQUATION 46a and section 11.4.2
REDUCTION FACTOR	α = 0,65	extrapolate from GRAPHS B4 and B5 ignore section 11.4.4
LOCATION PARAMETER	$\frac{\alpha P_O}{P_P}$ = 4,13	actual frame
CURVE SELECTION PARAMETER	$\left(\frac{\alpha P_O}{P_P}\right)_\ell = \frac{\alpha P_O}{P_P} \times \frac{43}{575}$ = 0,31	" limiting frame " EQUATION 9
FAILURE LOAD	$\frac{P_F}{P_P}$ = 0,90	Figure 23

It is interesting to note that the failure load obtained by using the charts of Appendix VI is identical to the accurate computer solution given in Table 6/1. It must be remembered, that the derivations of the graphs are based on a number of simplifying assumptions, such as equal column stiffnesses in storeys above and below the investigated storey and equal conditions at the remote ends of such columns. In addition, interpolation was required with respect to the storey number as well as the size of the lateral load. This seemingly confirms the insensitive nature of the relationship which exists between the elastic buckling load P_O, the reduction factor α, the "limiting slenderness ratio" λ_ℓ and the failure load P_F.

CHAPTER 12

OUTLINE OF AN ANALYTICAL APPROXIMATION

12.1 Formulation of principles

The major numerical work of this research project is associated with the calculation of the elastic buckling load and the assessment of stresses for loading related to the elastic buckling load. In this study, the elastic buckling load is obtained by satisfying the determinantal equation of the stiffness matrix relevant to a particular subassemblage to zero, and the load effects are assessed on the basis of a second-order, elastic analysis. The results of both analysis steps are used to determine a reduction factor α (Equation 39) and a "limiting slenderness ratio", λ_{ℓ} (Equations 40 or 41).

In section 1.7 of this thesis it has been pointed out that satisfactory approximate methods exist to establish the elastic buckling load without the need to evaluate the determinant of the stiffness matrix.[44, 85-88] These methods are based on the first-order storey sway or directly on the storey stiffness. In addition, a second-order, elastic analysis for loading may be approximated by exploiting the results of a first-order analysis and applying the principle of moment magnification.[69, 117-119] On this basis an approximate analytical procedure to obtain the elastic parameters can be formulated as follows:

a) Establish the elastic buckling load P_O by using the concept of storey-stiffness developed by Cheong Siat Moy[37,66].

b) Execute a first-order, elastic analysis for vertical load related to P_O and a first-order, elastic analysis for a magnified horizontal loading related to P_O. This procedure has to be performed twice. First for α=0,4 and then for the final value of α.

c) From the results of b) find the "limiting slenderness ratio" λ_ℓ from Equation 40 or 41. Firstly, for a value α=0,4 to predict the final α from Equation 39, and again for the final value of α.

The procedure is further explained in the following sections of this chapter.

12.2 Elastic buckling load by the storey-stiffness concept

Cheong Siat Moy[37,43,66] obtained the elastic buckling load from the condition of zero storey stiffness as follows:

$$\Sigma P_i = \frac{12E}{h^2} \sum \left(\frac{I_C}{1 + \frac{P_U + P_S}{P_S} \; \frac{I_C/h}{\Sigma I_B/L}} \right)$$

where,

ΣP_i = Total vertical load on a storey at the instance of sway buckling

P_U, P_S = Axial column load in the upper storey and the storey itself respectively

The summation of the expression in brackets has to extend over the entire storey proceeding from column to column. Several examples solved by Cheong Siat Moy[37] demonstrated that it is sufficiently accurate to consider the elastic buckling load of the entire frame as being that of the weakest storey.

12.3 Approximate second-order, elastic analysis

Several researchers[59, 113-119] have developed a direct P-Δ procedure utilising the results of a first-order analysis. Applied to the problem of this research it will take the following general form for the case of combined loading:

a) Calculation of the first-order storey sways Δ_{Ii} for loading related to αP_O. The "manual" approach based on the charts by Wood & Roberts[55] is suitable for this purpose.

b) The second-order storey sway Δ_{IIi} for the i-th storey is then estimated as follows:

$$\Delta_{IIi} = \frac{\Delta_{Ii}}{1 - \dfrac{\Delta_{Ii}}{\dfrac{\Sigma H_i}{\Sigma P_i} h}}$$

where ΣH_i is the total storey shear and ΣP_i is the sum of the vertical load on the storey, both at the load level αP_0. The storey height is h.

c) Equivalent additional horizontal sway loads δH_i are calculated from the sways Δ_{IIi} as follows:

$$\delta H_i = \Sigma P_i \frac{\Delta_{IIi}}{h}$$

d) A first-order analysis is then carried out for the entire structure subjected to all applied loading related to αP_0 and the additional sway loads δH_i. It is assumed that in this way allowance has been made for the sway-displaced shape of the structure. The resulting moments and axial forces are taken as the second-order forces required to calculate the "limiting slenderness ratio" λ_ℓ and the reduction factor α. For λ_ℓ and α it will be sufficient to concentrate on the critical sections of the structure.

In the method described above, moment magnification is restricted to the portions of moments resulting from lateral loads. If a frame is subjected to vertical loading only, it is usually satisfactory to obtain α and λ_ℓ directly from a first-order, elastic analysis without moment magnification. The error introduced by this approach will generally be marginal with the exception of certain portal frames with a low lateral stiffness. The method is demonstrated on the double-storey frame M2, which was previously analysed in chapter 10 of this study (Table 9).

12.4 Example

12.4.1 Elastic buckling load of frame M2

Each storey needs to be investigated on a separate basis:

Top-storey

$$\Sigma P_t = \frac{12\ E}{h^2} \sum \left(\frac{I_C}{1 + \frac{P_U + P_S}{P_S} \; \frac{I_C/h}{\Sigma I_B/L}} \right)$$

$$\Sigma P_t = \frac{12 \times 1{,}91 \times 10^{8}}{0{,}625^2} \quad \frac{2 \times 0{,}522 \times 10^{-9}}{1 + 1 \times 1{,}5} = 2{,}45 \text{ kN}$$

$$P_O = \Sigma P_t = 2{,}45 \text{ kN}$$

Bottom-storey

According to Cheong Siat Moy[64], the storey stiffness expression takes a slightly different form for bottom storeys, i.e. for fixed bases:

$$\Sigma P_b = \frac{12\ E}{h^2} \sum \left[\frac{I_C \left(3 + \frac{I_C/h}{\Sigma I_B/L} \right)}{3 + 4 \; \frac{I_C/h}{\Sigma I_B/L}} \right]$$

$$\Sigma P_b = \frac{12 \times 1{,}91 \times 10^{8}}{0{,}625^2} \quad \frac{2 \times 0{,}522 \times 10^{-9} (3 + 1{,}5)}{3 + 4 \times 1{,}5} = 3{,}062 \text{ kN}$$

$$P_O = \tfrac{1}{2} \Sigma P_b = 1{,}531 \text{ kN}$$

The lowest value is significant, i.e. $P_O = 1{,}531$ kN.

12.4.2 First-order storey sways

These are calculated for $H = 0,1 \times 0,4 \times P_O$, the applied horizontal load related to αP_O.

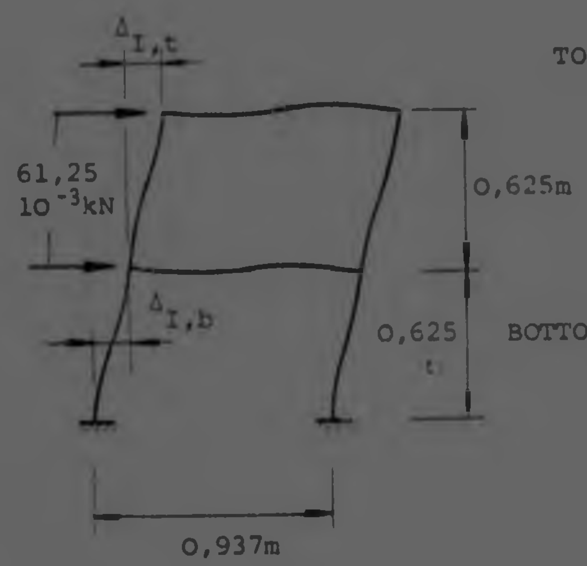

TOP STOREY: $K_b = \frac{2(1,5+1,5)}{2\times3+3\times1} = 0,67$

$K_t = \frac{1,5\times2}{2\times1,5+3\times1} = 0,5$

$\Phi = 3,2$

BOTTOM STOREY: $K_b \approx 0$

$K_t = 0,67$

$\Phi = 2,0$

The procedure developed by Wood & Roberts[85] is used to obtain the first-order storey sways. The method is based on sway charts such as shown in Figure 38.

$$\Delta_{I,t} = \frac{\Phi \; \Sigma H_t h^3}{12E\Sigma I_c} = \frac{3,2\times61,25\times10^{-3}\times0,625^3}{12\times1,91\times10^8\times2\times0,522\times10^{-9}} \times 10^3$$

$$\Delta_{I,t} = 20 \text{ mm}$$

$$\Delta_{I,b} = \frac{\Phi \; \Sigma H_b h^3}{12E\Sigma I_c} = \frac{2,0\times2\times61,25\times10^{-3}\times0,625^3}{12\times1,91\times10^8\times2\times0,522\times10^{-9}} \times 10^3$$

$$\Delta_{I,b} = 25 \text{ mm}$$

12.4.3 Approximate second-order sway, and sway loads δH_i

$$\Delta_{II,t} = \frac{\Delta_{I,t}}{1 - \dfrac{\Delta_{I,t}}{\dfrac{\Sigma H_t}{\Sigma P_t}\, h}} = \frac{20}{1 - \dfrac{20}{0{,}1 \times 625}}$$

$$\Delta_{II,t} = 29{,}4 \text{ mm}$$

$$\Delta_{II,b} = \frac{\Delta_{I,b}}{1 - \dfrac{\Delta_{I,b}}{\dfrac{\Sigma H_b}{\Sigma P_b}\, h}} \quad \frac{25}{1 - \dfrac{25}{0{,}1 \times 625}}$$

$$\Delta_{II,b} = 41{,}7 \text{ mm}$$

Hence, the corresponding additional sway loadings are:

$$\delta H_t = \Sigma P_t \frac{\Delta_{II,t}}{h} = 612{,}5 \times \frac{29{,}4}{625} \times 10^{-3} = 28{,}8 \times 10^{-3} \text{ kN}$$

$$\delta H_b = \Sigma P_b \frac{\Delta_{II,b}}{h} = 2 \times 612{,}5 \times \frac{41{,}7}{625} \times 10^{-3} = 81{,}7 \times 10^{-3} \text{ kN}$$

12.4.4 First-order analysis for vertical load and magnified horizontal load

The loading moments given in Figure 65 are applicable to loading related to a reduction factor α=0,4. Established conventional computer programs can be used to obtain the first-order forces for the given loading. The values in brackets for the bending moments due to horizontal load are explained in section 12.4.5.

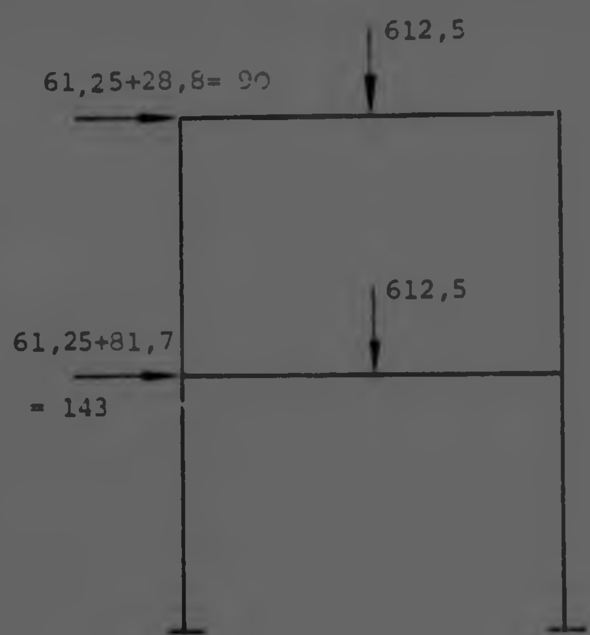

LOADING (10^{-3} kN)

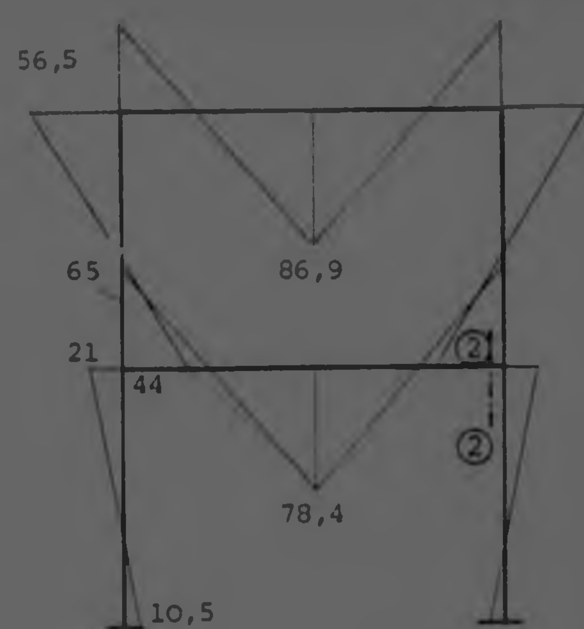

BENDING MOMENTS (10^{-3} kNm)
VERTICAL LOAD

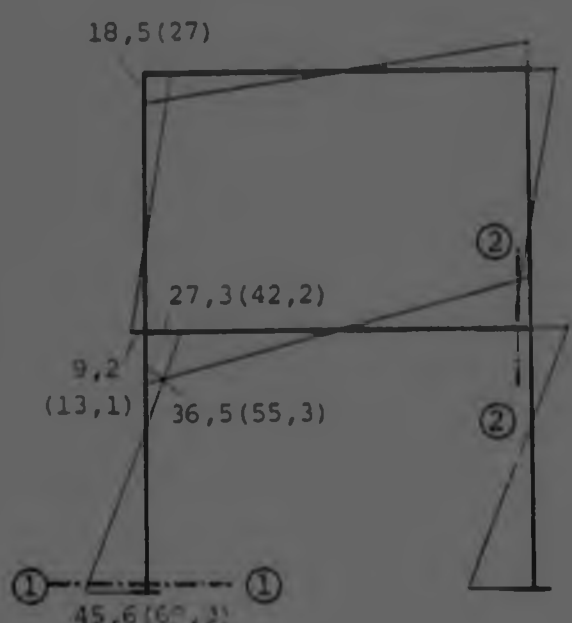

BENDING MOMENTS (10^{-3} kNm)
HORIZONTAL LOAD

FIGURE 65: Approximate analytical solution - example

12.4.5 Value α and "limiting slenderness ratio" λ_ℓ

The value $\lambda_{HO,4}$, required for Equation 39, is now calculated from Equation 41. For Equation 39 the slenderness ratio $\lambda_{HO,4}$ should be found in terms of column properties having a ratio $d_C/2r_C$ equal to unity. The largest $\lambda_{HO,4}$ for the example occurs at section 1 - 1 shown in Figure 65.

$$\lambda_{HO,4} = \frac{M_C}{I_C}\,\frac{h}{f_{PC}} = \frac{45,6 \times 10^{-3} \times 0,625}{0,522 \times 10^{-9} \times 253,7 \cdot 10^{3}} = 215$$

The final value of α is then calculated from Equation 39 as

$$\alpha = \frac{0,4}{1-0,6\left(\frac{700-215}{700}\right)^2} = 0,50$$

It is now necessary to obtain the bending moments for a loading related to $\alpha F_O = 0,50 \times 1,531$ kN = 0,766 kN. The bending moments due to vertical load are found by proportional magnification, i.e. by factoring the relevant values of Figure 65 by 0,50/0,4=1,25. For horizontal loading, the procedure applied in section 12.4.2 and 12.4.3 needs to be repeated for an applied load of $H=0,1 \cdot 0,50 \cdot 1,531 = 76,6 \times 10^{-3}$ kN.

The salient results are given below:

$$\Delta_{I,t} = 1,25 \cdot 20 = 25 \text{ mm}$$

$$\Delta_{I,b} = 1,25 \cdot 25 = 31,3 \text{ mm}$$

$\Delta_{II,t} = 41,7$ mm

$\Delta_{II,b} = 62,7$ mm

$\delta H_t \quad = 51,1 \times 10^{-3}$ kN

$\delta H_b \quad = 153,7 \times 10^{-3}$ kN

The total horizontal loads applied at the level of the top and bottom beam are $(76,6+51,1) \times 10^{-3} = 127,7 \times 10^{-3}$ kN and $(76,6+153,7) \times 10^{-3} = 230,3 \times 10^{-3}$ kN respectively.
A first-order analysis for this loading leads to the bending moments given in brackets in Figure 65 for the case of horizontal loading. Thus, the largest "limiting slenderness ratio" λ_ℓ expressed in terms of the column properties is found for section 2 - 2 :

$$\lambda_\ell = \frac{(1,25 \times 65 + 55,3) \times 10^{-3} \times 0,937 \times \sqrt{3}}{0,522 \times 10^{-[illegible]} \times 253,7 \times 10^{[illegible]} \times 1,5} = 1\ 116$$

The ratio $d_C/2r_C = \sqrt{3}$ applies to the case of a rectangular cross-section.

12.4.6 Estimated failure load

The parameters required to evaluate the interaction graph of Figure 23 can now be calculated. The plastic collapse load for frame M2 amounts to $P_p = 0,565$ kN .

$$\frac{\alpha P_0}{P_p} = \frac{0,50 \times 1,531}{0,565} = 1,36$$

$$\left(\frac{\alpha P_O}{P_P}\right)_\ell = 1,36 \times \frac{\lambda}{\lambda_\ell} = 1,36 \times \frac{359}{1116} = 0,44$$

The failure load associated with the two parameters is equal to P_F=0,79 P_P, which is identical to the computer result and slightly less than the test result of 0,81, both given in Table 9.

12.4.7 Frame M2 analysed for vertical loading

For the case of vertical loading, the first-order moments are directly used without magnification. The corresponding value α is taken as 1,0. Hence, there is no need to evaluate Equation 39. The worst bending moment occurs at the centre of the top-storey beam (Figure 65). For α = 1,0 follows

$$M = \frac{1}{0,4} \times 86,9\times10^{-3} = 217,25\times10^{-3} \text{ kNm}$$

The "limiting slenderness ratio" with respect to column properties is found from Equation 41 as

$$\lambda_\ell = \frac{217,25\times10^{-3}\times0,937}{0,522\times10^{-3}\times253,7\times10^{3}\times1,5}\sqrt{3}$$

$$\lambda_\ell = 1\ 773$$

The relevant ratios required for the evaluation of the interaction curves of Figure 23 are:

$$\frac{\alpha P_O}{P_P} = \frac{1,0 \times 1,531}{0,565} = 2,71$$

$$\left(\frac{\alpha P_O}{P_P}\right)_\ell = 2,71 \times \frac{359}{1773} = 0,55$$

The failure load for these two ratios amounts to $P_F = 0,91\ P_P$, which is identical to the computer result and less than the tɘst result of $0,93\ P_P$ (Table 9).

CHAPTER 13

CONCLUSION

In this thesis an alternative, approximate second-order, elasto-plastic method of analysis has been developed for unbraced and partially-braced building frames.

The method is based on an interaction approach and incorporates the plastic collapse load and certain elastic parameters. The principal elastic parameters are the elastic buckling load and the "limiting slenderness ratio". The "limiting slenderness ratio" defines a "limiting frame" similar to the actual frame. When subjected to loading related to its elastic buckling load, this "limiting frame" is assumed to fail by reaching first-yield at a critical section. The failure load of the "limiting frame" constitutes one boundary in the interaction procedure, the second boundary being the plastic collapse load of the actual frame. Both values are taken as the two extreme points of a specific failure curve applicable to a particular group of frames. The failure load of the actual frame can be identified on the failure curve by a location parameter which incorporates properties of the actual frame. For the general multi-storey, multi-bay structure the properties of the "limiting frame" are determined from appropriate subassemblages. That combination of elastic parameters obtained for a particular subassemblage with

CHAPTER 13

CONCLUSION

In this thesis an alternative, approximate second-order, elasto-plastic method of analysis has been developed for unbraced and partially-braced building frames.

The method is based on an interaction approach and incorporates the plastic collapse load and certain elastic parameters. The principal elastic parameters are the elastic buckling load and the "limiting slenderness ratio". The "limiting slenderness ratio" defines a "limiting frame" similar to the actual frame. When subjected to loading related to its elastic buckling load, this "limiting frame" is assumed to fail by reaching first-yield at a critical section. The failure load of the "limiting frame" constitutes one boundary in the interaction procedure, the second boundary being the plastic collapse load of the actual frame. Both values are taken as the two extreme points of a specific failure curve applicable to a particular group of frames. The failure load of the actual frame can be identified on the failure curve by a location parameter which incorporates properties of the actual frame. For the general multi-storey, multi-bay structure the properties of the "limiting frame" are determined from appropriate subassemblages. That combination of elastic parameters obtained for a particular subassemblage with the plastic collapse load of the entire frame which yields the lowest failure load is significant.

A suitable computer program has been developed to deal with the aspects related to the elastic analyses. The failure load is eventually evaluated from a multi-curve interaction graph.

The hypothesised inelastic portions of these failure curves have been tested against a number of discrete theoretical solutions and were compared with laboratory results from previous research as well as model frames especially designed for the purpose of this investigation. In all cases a satisfactory correlation between tests, theory and the proposed design approach was obtained.

The principal objective of this research was, to formulate a simple analysis method which would improve on the results calculated by the Merchant-Rankine rule, which is known to be conservative in many cases. It is believed that the proposed method has achieved this objective without adding unduly to the complexity of the procedure as a whole. Comparing both methods with exact results has shown that the new approach predicts the actual failure load of a frame more accurately than the Merchant-Rankine formula.

An added advantage of the method developed in this research is the possibility to present the salient elastic parameters in graphical form. This has been demonstrated for a single-bay, multi-storey framework. Other cases could be treated in a similar way, so that many common frame problems may be analysed without a computer, once the plastic collapse load is given.

An approximate analytical approach incorporating established methods of analysis has also been formulated.

In summary, it has been concluded that the method developed in this research appears to be a satisfactory substitute for a strict theoretical full-scale, elasto-plastic computer analysis. In this study the new method has been applied to steel structures, although the same principles could also be used for other materials.

In pursuance of the research objectives formulated at the start, it became apparent that certain related aspects could further enhance the potential of the presented method. In addition to investigating the method in conjunction with other materials, the following areas are recommended for future research:

a) Working load deflections

It seems possible that the design curves of Figure 23 may be useful in determining the load level corresponding to the elastic-plastic transition state of the structure. Considering that the establishment of the "limiting slenderness ratio", λ_{ℓ}, was based on the supposition that the structure, if subjected to for a single-bay, multi-storey framework. Other cases could be treated in a similar way, so that many common frame problems may be analysed without a computer, once the plastic collapse load is given.

An approximate analytical approach incorporating established methods of analysis has also been formulated.

In summary, it has been concluded that the method developed in this research appears to be a satisfactory substitute for a strict theoretical full-scale, elasto-plastic computer analysis. In this study the new method has been applied to steel structures, although the same principles could also be used for other materials.

In pursuance of the research objectives formulated at the start, it became apparent that certain related aspects could further enhance the potential of the presented method. In addition to investigating the method in conjunction with other materials, the following areas are recommended for future research:

a) Working load deflections

It seems possible that the design curves of Figure 23 may be useful in determining the load level corresponding to the elastic-plastic transition state of the structure. Considering that the establishment of the "limiting slenderness ratio", λ_{ℓ}, was based on the supposition that the structure, if subjected to a load level equivalent to αP_O, should nowhere attain a stress in excess of a predetermined elastic limit, the working load W could be examined in just the same way. If elastic structural behaviour is confirmed for W, a conventional elastic displacement analysis may follow. Alternatively, if a structure based on a strength analysis cannot produce the desired elastic behaviour at working loads, a strengthening of members may be required.

b) In-plane member instability (yielding between nodes)

It should be examined whether some provision in this regard could be incorporated in the method presented in this study, by introducing a further critical section between the ends of column members. This aspect could be included in the search for the maximum "limiting slenderness ratio", λ_ℓ, in the same way as demonstrated for other sections shown in Figure 46a.

c) Lateral torsional buckling

The basic method proposed in this research ignores lateral buckling. However, it appears that the effect of lateral torsional buckling may be included on an approximate basis by following the procedure adopted by the American Institute of Steel Construction, AISC-1978[8]. In this approach, the plastic moment capacity M_P is reduced to a moment capacity which could be accepted by a member before lateral torsional buckling occurs. On the basis of this reduced moment capacity, the plastic collapse load could be calculated and then used in the proposed interaction method. Alternatively, adequate lateral bracing should be provided.

d) Further P-Δ effects

Cheong Siat Moy[79] has pointed out that an initial storey eccentricity, axial member shortening, unequal temperature influences, foundation settlement and semi-rigid connections can generate additional P-Δ contributions, thereby reducing the load carrying capacity of the structure. It is of interest to investigate whether provisions for these aspects could be incorporated in the method proposed in this research.

An initial storey sway Δ_i could be accounted for if the analysis were formulated in terms of a generalised member orientation in contrast to the orthogonal system of members assumed for the basic slope-deflection method. Alternatively, this effect may be approximated by applying an additional horizontal storey load equal to $\Sigma P_S\ \Delta_i/h$, where ΣP_S is the total vertical load on the storey.

Korn[120] has demonstrated how to extend the slope-deflection method to include for the effects of axial member shortening. Furthermore, temperature influences and foundation settlements can be evaluated by including these as "load"elements in the relevant load vector. Cheong Siat Moy[78] proposed to allow for semi-rigid connections by reducing the stiffnesses of restraining beams.

In terms of the method developed in this research, the inclusion of the abovementioned aspects will result in a smaller reduction factor, α, and an adjusted "limiting slenderness ratio", λ_ℓ, indicating a further loss in load carrying capacity.

e) Pitched-roof portals

In recent design specifications[5,7], the stability of pitched-roof portals is controlled by stiffness and sway limitations. It would be of interest to extend the presented method to this type of structure and compare the results with the provisions of the design specifications.

f) Residual stresses

Liapunov[65] investigated a 32-storey, three-bay frame allowing for the presence of residual cooling stresses for flanged sections in accordance with Reference 121. He concluded that the effect of such residual cooling [illegible]es on the failure load of this frame was negligible. The examination of residual stresses in conjunction with the method developed in this study would be a further aspect for future research.

APPENDICES

APPENDIX I

P-Δ MOMENTS FOR VERTICAL LOAD

In certain instances a P-Δ moment is generated by pure vertical loading. One such case is shown in Figure 66. Although of minor importance compared with the case of combined loading, provision has been made to invoke such P-Δ moment by means of a factor z when analysing the various subassemblages.

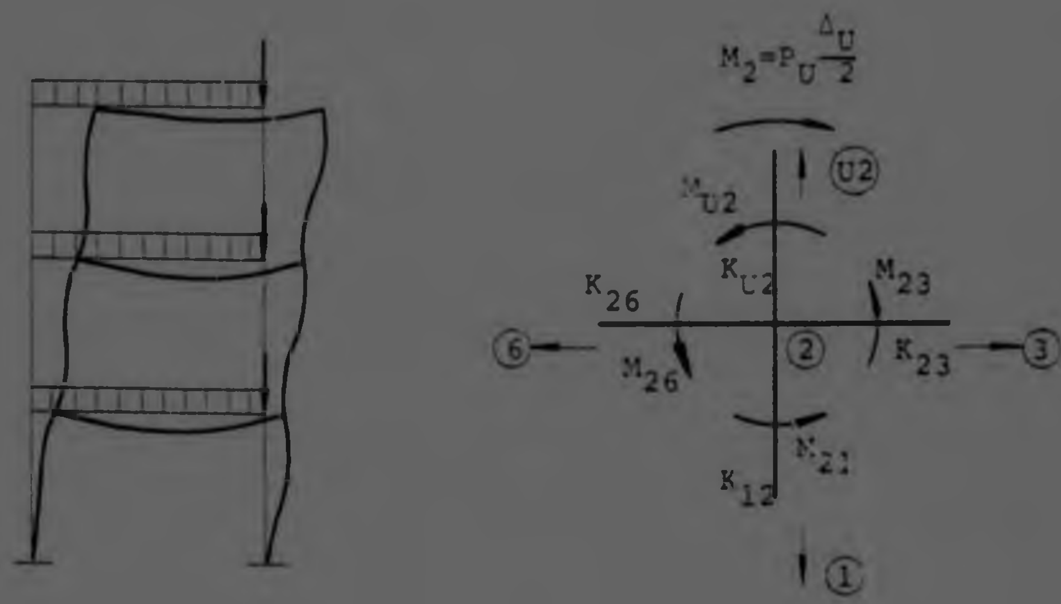

FIGURE 66: P-Δ moments due to vertical load

The procedure to obtain the magnified moment, mag M, is demonstrated for joint 2 of the subassemblage relevant to the case of vertical loading (Figure 25).

Moment equilibrium at joint 2 requires:

$$M_2 = M_{23} + M_{26} + M_{21} + M_{U2}$$

The total joint stiffness ΣK is defined as

$$\Sigma K_2 = K_{12} + K_{23} + K_{26} + K_{U2}$$

For the beam-end moment M_{23} follows,

1st step

$$M_{23} = \frac{K_{23}}{\Sigma K_2} M_2$$

At the same time, the upper column attracts the moment

$$M_{U2} = \frac{K_{U2}}{\Sigma K_2} M_2$$

This moment will again be distributed and causes a further moment increment for M_{23}.

2nd step

$$M_{23} = \frac{K_{23}}{\Sigma K_2} (M_2 + M_{U2}) = \frac{K_{23}}{\Sigma K_2} M_2 \left(1+\frac{K_{U2}}{\Sigma K_2}\right)$$

The moment M_{U2}, when distributed, will also induce a moment in the upper column, which equals

$$M'_{U2} = \frac{K_{U2}}{\Sigma K_2} M_{U2}$$

If M'_{U2} is distributed, M_{23} is further increased to

3rd step

$$M_{23} = \frac{K_{23}}{\Sigma K_2} M_2 \left(1+\frac{K_{U2}}{\Sigma K_2}\right) + \frac{K_{23}}{\Sigma K_2} M'_{U2}$$

$$M_{23} = \frac{K_{23}}{\Sigma K_2} M_2 \left(1+\frac{K_{U2}}{\Sigma K_2}\right) + \frac{K_{23}}{\Sigma K_2} \frac{K_{U2}}{\Sigma K_2} \frac{K_{U2} M_2}{\Sigma K_2}$$

$$= \frac{K_{23}}{\Sigma K_2} M_2 \left[1+\frac{K_{U2}}{\Sigma K_2} + \frac{K_{U2}^2}{(\Sigma K_2)^2}\right]$$

Similarly, for the (r + 1st) step follows.

(r + 1st)step

$$M_{23} = \frac{K_{23}}{\Sigma K_2} M_2 \left[1+\frac{K_{U2}}{\Sigma K_2} + \frac{K_{U2}^2}{(\Sigma K_2)^2} + \frac{K_{U2}^3}{(\Sigma K_2)^3} \cdots \frac{K_{U2}^r}{(\Sigma K_2)^r}\right]$$

Hence, instead of applying the joint moment M_2 to a subassemblage which should exclude the upper column a magnified moment may be considered in conjunction with the full subassemblage of Figure 25. It is sufficiently accurate to include the first three terms in the brackets, i.e.

$$m_{eq} M_2 = M_2 \left[1 + \frac{K_{U2}}{\Sigma K} + \frac{K_{U2}^2}{(\Sigma K)^2}\right] \qquad |EQN. 48|$$

The value in brackets has been abbreviated to z_2.
A magnified moment such as in Equation 48 can occur for joints 1 to 6 of the core-module. The stiffness ratios for the various joints take the form as given in Equations 49a to 49f.

Joint 1

$$\frac{K_{L1}}{\Sigma K_1} = \frac{\frac{1}{6}\beta_2 K_{L1} S_{L1} (1+C_{L1})}{K_{14}+K_{B1}+\frac{1}{6}K_{12}S_{12}(1+C_{12})+\frac{1}{6}\beta_2 K_{L1}S_{L1}(1+C_{L1})} \qquad |EQN.49a|$$

Joint 2

$$\frac{K_{U2}}{\Sigma K_2} = \frac{\frac{1}{6}\beta_3 K_{U2} S_{U2} (1+C_{U2})}{K_{23}+K_{26}+\frac{1}{6}\beta_3 K_{U2}S_{U2}(1+C_{U2})+\frac{1}{6}K_{12}S_{12}(1+C_{12})} \qquad |EQN.49b|$$

Joint 3

$$\frac{K_{U3}}{\Sigma K_3} = \frac{\frac{1}{6}\beta_3\ K_{U3}\ S_{U3}\ (1+C_{U3})}{K_{23}+K_{35}+\frac{1}{6}\beta_3 K_{U3}S_{U3}(1+C_{U3})+\frac{1}{6}K_{34}S_{34}(1+C_{34})} \quad |\text{EQN.49c}|$$

Joint 4

$$\frac{K_{L4}}{\Sigma K_4} = \frac{\frac{1}{6}\beta_2\ K_{L4}\ S_{L4}\ (1+C_{L4})}{K_{14}+K_{B4}+\frac{1}{6}K_{34}S_{34}(1+C_{34})+\frac{1}{6}\beta_2 K_{L4}S_{L4}(1+C_{L4})} \quad |\text{EQN.49d}|$$

Joint 5

$$\frac{K_{U5}}{\Sigma K_5} = \frac{\frac{1}{6}\beta_3\ K_{U5}\ S_{U5}\ (1+C_{U5})}{K_{35}+K_{B5}+\frac{1}{6}\beta_3 K_{U5}S_{U5}(1+C_{U5})+\frac{1}{6}K_{L5}S_{L5}(1+C_{L5})} \quad |\text{EQN.49e}|$$

Joint 6

$$\frac{K_{U6}}{\Sigma K_6} = \frac{\frac{1}{6}\beta_3\ K_{U6}\ S_{U6}\ (1+C_{U6})}{K_{26}+K_{B6}+\frac{1}{6}\beta_3 K_{U6}S_{U6}(1+C_{U6})+\frac{1}{6}K_{L6}S_{L6}(1+C_{L6})} \quad |\text{EQN.49f}|$$

In Equations 49a to 49f, the stiffnesses are related to double-curvature conditions for the beams and columns. In addition, axial forces have been taken into account for the column members by incorporating the relevant stability functions S and C. The meaning of the correlation factors β_2 and β_3 has been explained in section 4.2.4 of the thesis.

APPENDIX II/1

SLOPE-DEFLECTION METHOD APPLIED TO SUBASSEMBLAGE - BUCKLING ANALYSIS

Initially the principles of the slope-deflection method are applied to the case of conventional buckling. Referring to Figure 25 for the general subassemblage and loading and to Figure 36 for the deformed shape, the member moments can be derived as follows applying Equation 14:

$$M_{12} = EK_{12}S_{12}\left[\Theta_1+C_{12}\Theta_2-(1+C_{12})\frac{\Delta}{L_{12}}\right] +M_{F12}$$

$$M_{21} = EK_{12}S_{12}\left[\Theta_2+C_{12}\Theta_1-(1+C_{12})\frac{\Delta}{L_{12}}\right] +M_{F21}$$

$$M_{23} = EK_{23}S_{23}(\Theta_2+C_{23}\Theta_3) +M_{F23}$$

$$M_{32} = EK_{23}S_{23}(\Theta_3+C_{23}\Theta_2) +M_{F32}$$

$$M_{43} = EK_{34}S_{34}\left[\Theta_4+C_{34}\Theta_3-(1+C_{34})\frac{\Delta}{L_{34}}\right] +M_{F43}$$

$$M_{34} = EK_{34}S_{34}\left[\Theta_3+C_{34}\Theta_4-(1+C_{34})\frac{\Delta}{L_{34}}\right] +M_{F34}$$

$$M_{35} = EK_{35}S_{23}(\Theta_3+C_{23}\Theta_5) +M_{F35}$$

$$M_{53} = EK_{35}S_{23}(\Theta_5+C_{23}\Theta_3) +M_{F53}$$

$$M_{62} = EK_{26}S_{23}(\Theta_6+C_{23}\Theta_2) +M_{F62}$$

$$M_{26} = EK_{26}S_{23}(\Theta_2+C_{23}\Theta_6) +M_{F26}$$

In a conventional buckling analysis the applied loads are generally concentrated at the joints and, consequently, the fixed-end moments are equal to zero. The member-end moments M_m in Figure 36 are as follows for the buckling case:

Bottom storeys (M_{m1}) :

$$M_{m1} = F_1 \Theta_1$$

Upper storeys (M_{m1}) :

$$M_{m1} = E\left(\frac{6I_{B1}}{L_{26}}+\frac{4I_{14}}{L_{23}}\right)\Theta_1 + E\,\frac{2I_{14}}{L_{23}}\Theta_4 + F_1\left(N_1 - O_1^2\;\frac{\frac{1}{6}F_1}{\frac{1}{6}F_1 N_1 + E\Sigma K_{B1}}\right)\Theta_1$$

$$M_{m2} = F_2\left(N_2 - O_2^2\;\frac{\frac{1}{6}F_2}{\frac{1}{6}F_2 N_2 + E\Sigma K_{B2}}\right)\Theta_2$$

$$M_{m3} = F_3\left(N_3 - O_3^2\;\frac{\frac{1}{6}F_3}{\frac{1}{6}F_3 N_3 + E\Sigma K_{B3}}\right)\Theta_3$$

Bottom storeys (M_{m4}) :

$$M_{m4} = F_4\;\Theta_4$$

Upper storeys (M_{m4}) :

$$M_{m4} = E\left(\frac{6I_{B4}}{L_{35}}+\frac{4I_{14}}{L_{23}}\right)\Theta_4 + E\,\frac{2I_{14}}{L_{23}}\Theta_1 + F_4\left(N_4 - O_4^2\;\frac{\frac{1}{6}F_4}{\frac{1}{6}F_4 N_4 + E\Sigma K_{B4}}\right)\Theta_4$$

$$M_{m5} = 6EK_{B5}\Theta_5 + F_{U5}\left(N_{U5} - O^2_{U5}\,\frac{\frac{1}{6}F_{U5}}{\frac{1}{6}F_{U5}N_{U5} + E\Sigma K_{BU5}}\right)\Theta_5$$

$$+ F_{L5}\left(N_{L5} - O^2_{L5}\,\frac{\frac{1}{6}F_{L5}}{\frac{1}{6}F_{L5}N_{L5} + E\Sigma K_{BL5}}\right)\Theta_5$$

$$M_{m6} = 6EK_{B6}\Theta_6 + F_{U6}\left(N_{U6} - O^2_{U6}\,\frac{\frac{1}{6}F_{U6}}{\frac{1}{6}F_{U6}N_{U6} + E\Sigma K_{BU6}}\right)\Theta_6$$

$$+ F_{L6}\left(N_{L6} - O^2_{L6}\,\frac{\frac{1}{6}F_{L6}}{\frac{1}{6}F_{L6}N_{L6} + E\Sigma K_{BL6}}\right)\Theta_6$$

It is now possible to formulate the equilibrium equations for the six joints of the core-module.

<u>Joint 1</u>

$$M_{12} + M_{m1} + M_1 = 0$$

<u>Joint 2</u>

$$M_{21} + M_{23} + M_{26} + M_{m2} + M_2 = 0$$

<u>Joint 3</u>

$$M_{32} + M_{34} + M_{35} + M_{m3} + M_3 = 0$$

<u>Joint 4</u>

$$M_{43} + M_{m4} + M_4 = 0$$

Joint 5

$$M_{53} + M_{m5} + M_5 = 0$$

Joint 6

$$M_{62} + M_{m6} + M_6 = 0$$

The moments M_1 to M_6, which may represent moments due to applied loading, are zero for the buckling analysis.

In addition to the six joint equations, one sway-equilibrium equation can be formulated for the core-module. This equation is obtained from the upper section of the sway subassemblage as shown in Figure 67.

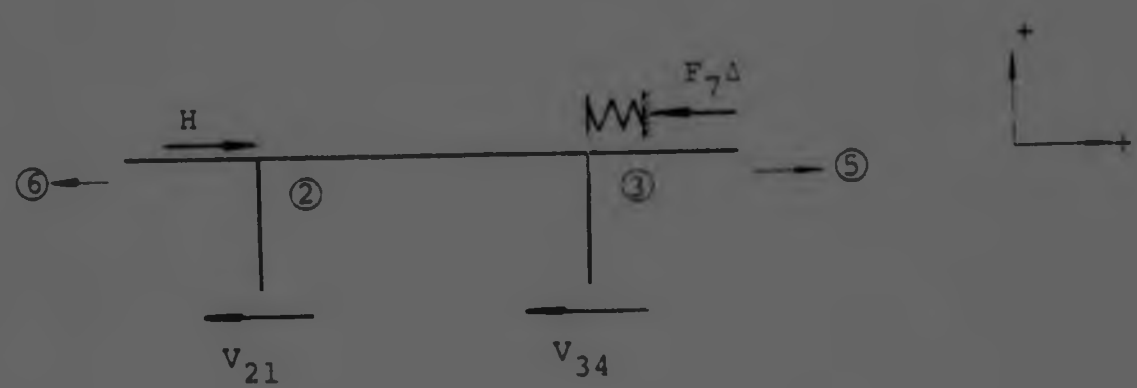

FIGURE 67: Horizontal equilibrium

From $\Sigma H = 0$ follows,

$$-V_{21} - V_{34} - F_7\Delta + H = 0$$

Replacing the shear forces by moments using the relationship given in Equation 16 results in

$$- \frac{EK_{12}}{L^2_{12}} S^2_{12} \ (1-C^2_{12}\ )\Delta + \frac{EK_{12}}{L_{12}} S_{12} \ (1+C_{12})(\Theta_1+\Theta_2)$$

$$+ \frac{M_{F12}+M_{F21}}{L_{12}} - V_{210} - \frac{EK_{34}}{L^2_{34}} S^2_{34} \ (1-C^2_{34})\Delta + \frac{EK_{34}}{L_{34}} S_{34}$$

$$(1+C_{34})(\Theta_3+\Theta_4) + \frac{M_{F34}+M_{F43}}{L_{34}} - V_{340} - F_7\Delta + H = 0$$

For the buckling analysis, where only vertical loads are considered and where beam loads are distributed to the joints, the terms including fixed-end moments, the shear forces V_{210}, V_{340} and the applied horizontal load H are taken as zero.

The six joint equations and the sway-equilibrium equation are given in matrix form in Table 1 of this thesis.

The following abbreviations have been introduced:

$$SC_{23} = \frac{K_{23}}{L_{23}} S_{23} \ (1+C_{23})$$

$$SC_{12} = \frac{K_{12}}{L_{12}} S_{12} \ (1+C_{12})$$

$$SC_{34} = \frac{K_{34}}{L_{34}} S_{34} \ (1+C_{34})$$

$$SC_{122} = \frac{K_{12}}{L^2_{12}} S^2_{12} \ (1-C^2_{12}\ ) \ L_{34}$$

$$SC_{342} = \frac{K_{34}}{L^2_{34}} \; S^2_{34} \; (1-C^2_{34}) \; L_{34}$$

$$SC_{U2} = K_{34} \; S_{U2} \; (1+C_{U2})$$

$$SC_{U3} = K_{34} \; S_{U3} \; (1+C_{U3})$$

$$SC_{L1} = K_{34} \; S_{L1} \; (1+C_{L1})$$

$$SC_{L4} = K_{34} \; S_{L4} \; (1+C_{L4})$$

$$SC_{U5} = K_{34} \; S_{U5} \; (1+C_{U5})$$

$$SC_{L5} = K_{34} \; S_{L5} \; (1+C_{L5})$$

$$SC_{U6} = K_{34} \; S_{U6} \; (1+C_{U6})$$

$$SC_{L6} = K_{34} \; S_{L6} \; (1+C_{L6})$$

$$\bar{F}_2 = \frac{K_{U2}}{K_{34}} = \frac{F_2}{EK_{34}} \qquad \bar{F}_3 = \frac{K_{U3}}{K_{34}} = \frac{F_3}{EK_{34}}$$

$$\bar{F}_{U5} = \frac{K_{U5}}{K_{34}} = \frac{F_{U5}}{EK_{34}} \qquad \bar{F}_{L5} = \frac{K_{L5}}{K_{34}} = \frac{F_{L5}}{EK_{34}}$$

$$\bar{F}_{U6} = \frac{K_{U6}}{K_{34}} = \frac{F_{U6}}{EK_{34}} \qquad \bar{F}_{L6} = \frac{K_{L6}}{K_{34}} = \frac{F_{L6}}{EK_{34}}$$

Upper storeys :

$$\bar{F}_1 = \frac{K_{L1}}{K_{34}} = \frac{F_1}{EK_{34}} \qquad \bar{F}_4 = \frac{K_{L4}}{K_{34}} = \frac{F_4}{EK_{34}}$$

Bottom storeys :

$$\bar{F}_1 = \frac{K_{S1}}{EK_{34}} = \frac{F_1}{EK_{34}} \qquad \bar{F}_4 = \frac{K_{S4}}{EK_{34}} = \frac{F_4}{EK_{34}}$$

N and O-functions :

$$NO_1 = \bar{F}_1\ K_{34} \left(N_1 - O_1^2 \ \frac{\frac{1}{6}\bar{F}_1 K_{34}}{\frac{1}{6}\bar{F}_1 K_{34} N_1 + \Sigma K_{B1}} \right)$$

$$NO_2 = \bar{F}_2\ K_{34} \left(N_2 - O_2^2 \ \frac{\frac{1}{6}\bar{F}_2 K_{34}}{\frac{1}{6}\bar{F}_2 K_{34} N_2 + \Sigma K_{B2}} \right)$$

$$NO_3 = \bar{F}_3\ K_{34} \left(N_3 - O_3^2 \ \frac{\frac{1}{6}\bar{F}_3 K_{34}}{\frac{1}{6}\bar{F}_3 K_{34} N_3 + \Sigma K_{B3}} \right)$$

$$NO_4 = \bar{F}_4\ K_{34} \left(N_4 - O_4^2 \ \frac{\frac{1}{6}\bar{F}_4 K_{34}}{\frac{1}{6}\bar{F}_4 K_{34} N_4 + \Sigma K_{B4}} \right)$$

$$NO_{U5} = \bar{F}_{U5} K_{34} \left(N_{U5} - O_{U5}^2 \ \frac{\frac{1}{6}\bar{F}_{U5} K_{34}}{\frac{1}{6}\bar{F}_{U5} K_{34} N_{U5} + \Sigma K_{BU5}} \right)$$

$$NO_{L5} = \bar{\bar{F}}_{L5}K_{34}\left(N_{L5} - O^{2}_{L5}\ \frac{\frac{1}{6}\bar{\bar{F}}_{L5}K_{34}}{\frac{1}{6}\bar{\bar{F}}_{L5}K_{34}\bar{N}_{L5} + \Sigma K_{BL5}}\right)$$

$$NO_{U6} = \bar{\bar{F}}_{U6}K_{34}\left(N_{U6} - O^{2}_{U6}\ \frac{\frac{1}{6}\bar{\bar{F}}_{U6}K_{34}}{\frac{1}{6}\bar{\bar{F}}_{U6}K_{34}N_{U6} + \Sigma K_{BU6}}\right)$$

$$NO_{L6} = \bar{\bar{F}}_{L6}K_{34}\left(N_{L6} - O^{2}_{L6}\ \frac{\frac{1}{6}\bar{\bar{F}}_{L6}K_{34}}{\frac{1}{6}\bar{\bar{F}}_{L6}K_{34}N_{L6} + \Sigma K_{BL6}}\right)$$

APPENDIX II/2

SLOPE - DEFLECTION METHOD APPLIED TO SUBASSEMBLAGE - LOAD ANALYSIS

For the load analysis, the fixed-end moments M_F and the shear forces V_O need to be considered. They can be expressed as follows for a member A - B shown in Figure 34:

$$M_{FAB} = - EKS\ (\gamma_A + C\gamma_B) \qquad |\text{EQN. 50a}|$$

and

$$M_{FBA} = EKS\ (\gamma_A + C\gamma_B) \qquad |\text{EQN. 50b}|$$

where γ_A and γ_B represent the end rotations of the member A - B when simply supported and subjected to the given loading. Expressions for γ_A and γ_B can be found in the standard literature. Two common cases relevant to the loading conditions investigated in this research are given below.

Uniformly distributed loading of intensity q:

$$\gamma_A = -\gamma_B = \frac{qL}{P}\left(\frac{1}{m}\tan\frac{m}{2} - \frac{1}{2}\right) \qquad |\text{EQN. 51}|$$

symmetrical dual-point load of magnitude U :

$$\gamma_A = -\gamma_B = \frac{U}{P}\left(\frac{\cos\ n\frac{m}{2}}{\cos\frac{m}{2}} - 1\right) \qquad |\text{EQN. 52}|$$

where P is the axial member force and m is obtained from Equation 15c.
For zero axial forces P, the expressions in Equations 50a and 50b reduce to the fixed-end moments of the basic slope-deflection method applicable to a first-order analysis.

For a member A - B, the simply supported shear forces V_O corresponding to the same two load cases are as follows:

Uniformly distributed loading of intensity q :

$$V_{ABO} = - V_{BAO} = \frac{qL}{2}$$

symmetrical dual-point load of size U:

$$V_{ABO} = - V_{BAO} = U$$

<u>Vertical loading</u>

For the analysis of vertical loading the member-end moments of the core-module are identical to the moments formulated for the buckling analysis (see preceding appendix II/1). However, the member moments M_m in Figure 36 should include the possible fixed-end moments as follows:

Bottom storeys (M_{m1}) :

$$M_{m1} = F_1\ \theta_1$$

Upper storeys (M_{m1}) :

$$M_{m1}+M_1 = E\left(\frac{4I_{B1}}{L_{26}}+\frac{4I_{14}}{L_{23}}\right)\theta_1 + E\ \frac{2I_{14}}{L_{23}}\ \theta_4$$

$$+ F_1\ S_{L1}\ (1+C_{L1})\left(\beta_2\theta_1 - \beta_1\ \frac{\Delta}{L_{34}}\ \frac{L_{L1}}{L_{34}}\right) + M_{FB1} + M_{F14}$$

$$- P_{L1}\ \frac{\Delta}{2}\ \beta_1\ \ z_1\ \frac{L^2_{L1}}{L^2_{12}}$$

$$M_{m2}+M_{m2} = F_2S_{U2}(1+C_{U2})\left(\Theta_2\beta_3-\beta\frac{\Delta}{L_{34}}\frac{L_{U2}}{L_{34}}\right)-P_2\frac{\Delta}{2}\beta z_2\frac{L_{U2}^2}{L_{12}^2}$$

$$M_{m3}+M_3 = F_3S_{U3}(1+C_{U3})\left(\Theta_3\beta_3-\beta\frac{\Delta}{L_{34}}\frac{L_{U3}}{L_{34}}\right)-P_3\frac{\Delta}{2}\beta z_3\frac{L_{U3}^2}{L_{34}^2}$$

Bottom storeys (M_{m4}) :

$$M_{m4} = F_4\ \Theta_4$$

Upper storeys (M_{m4}) :

$$M_{m4}+M_4 = E\left(\frac{4I_{B4}}{L_{35}}+\frac{4I_{14}}{L_{23}}\right)\Theta_4 + E\frac{2I_{14}}{L_{23}}\Theta_1 + F_4S_{L4}(1+C_{L4})$$

$$\left(\beta_2\Theta_4-\beta_1\frac{\Delta}{L_{34}}\frac{L_{L4}}{L_{34}}\right)+M_{FB4}+M_{F14}-P_{L4}\frac{\Delta}{2}\beta_1 z_4\frac{L_{L4}^2}{L_{34}^2}$$

$$M_{m5}+M_5 = \left[F_{U5}S_{U5}(1+C_{U5})\beta_3+F_{L5}S_{L5}(1+C_{L5})\beta_2+4EK_{B5}\right]\Theta_5$$

$$-\left[F_{U5}S_{U5}(1+C_{U5})\beta\frac{L_{U3}}{L_{34}}+F_{L5}S_{L5}(1+C_{L5})\right]\frac{\Delta}{L_{34}}$$

$$-P_5\frac{\Delta}{2}\beta z_5\frac{L_{U2}^2}{L_{34}^2}-\beta_5 M_{F32}$$

$$M_{m6}+M_6 = \left[F_{U6}S_{U6}(1-C_{U6})\beta_3+F_{L6}S_{L6}(1+C_{L6})\beta_2+4EK_{B6}\right]\Theta_6$$

$$-\left[F_{U6}\ \ldots\ _{U6})\beta\frac{L_{U2}}{L_{34}}+F_{L6}S_{L6}(1+C_{L6})\right]\frac{\Delta}{L_{34}}$$

$$-P_6\frac{\Delta}{2}\beta z_6\frac{L_{U2}^2}{L_{34}^2}-\beta_6 M_{F32}$$

The correlation factors β, β_1, β_2 and β_3 have been explained in sections 4.2.3 and 4.2.4 of the thesis.

With the above moments, the seven inhomogeneous equations of Table 2 can be developed by using the six joint equations and the sway-equilibrium equation already formulated for the buckling anaysis. The load vector L_{VV} contains terms referring to vertical loading.

Horizontal loading

In contrast to the analysis for vertical loading, the moments M_m and the applied joint moments of Figure 36 assume the following form for the case of horizontal loading. The subassemblage of Figure 31 is applicable.

$$M_{m1} = 0$$

$$M_{m2}+M_2 = - M_{AP2} - P_2 \frac{\Delta}{2} \beta \frac{L_{U2}^2}{L_{12}^2}$$

$$M_{m3}+M_3 = - M_{AP3} - P_3 \frac{\Delta}{2} \beta \frac{L_{U3}^2}{L_{34}^2}$$

$$M_{m4} = 0$$

$$M_{m5} = 0$$

$$M_{m6} = 0$$

The sway correlation factor β has been derived in section 4.2.3 of this thesis.
Using the member-end moments already formulated for the buckling analysis (Appendix II/1), it is now possible to develop the six joint equations and the sway-equilibrium

equation which appear in matrix format in Table 3. The load vector L_{VH} contains terms relationg to horizontal loading.

Axial member forces

Axial member forces for the load analysis are established by satisfying horizontal and vertical equilibrium at the various joints of the relevant subassemblages. This is demonstrated below .

Joint 2

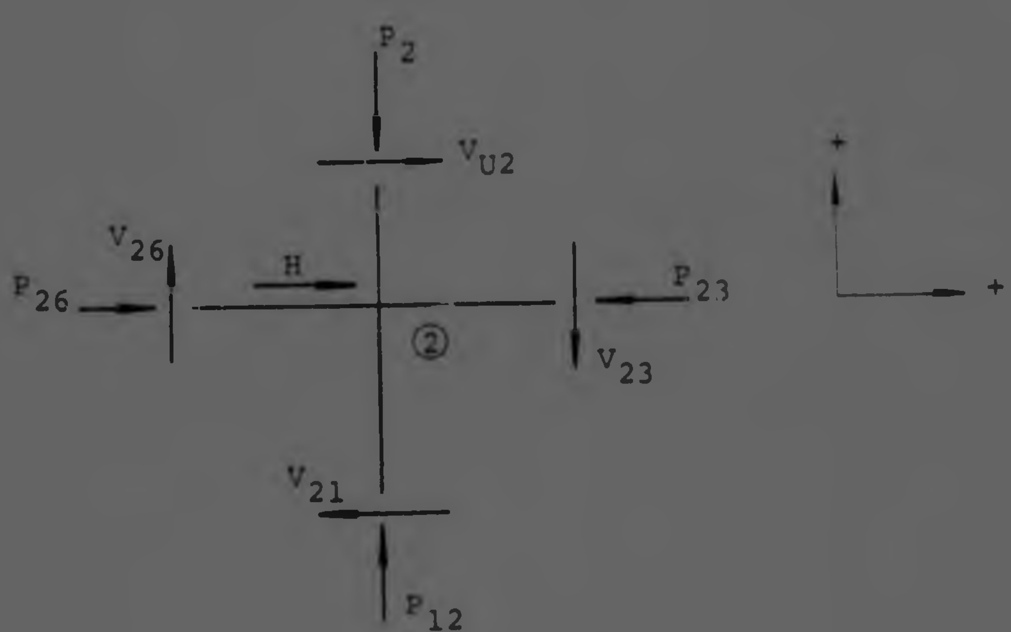

Vertical equilibrium : $P_{12} + V_{26} - V_{23} - P_2 = 0$

Horizontal equilibrium: $H - V_{21} - P_{23} + V_{U2} + P_{26} = 0$

Joint 3

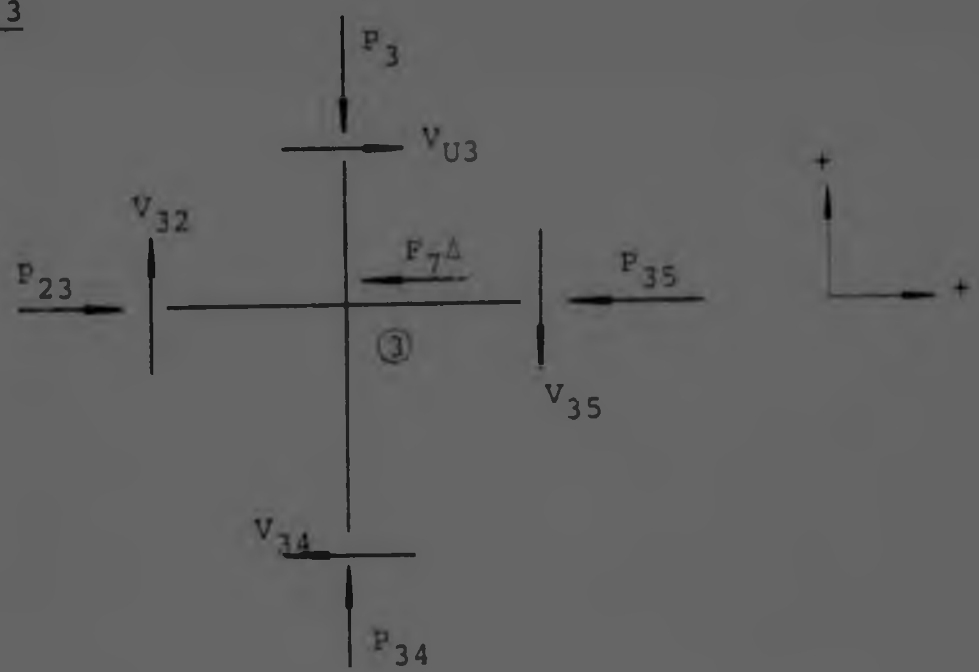

Vertical equilibrium : $V_{32} - V_{35} - P_3 + P_{34} = 0$

Horizontal equilibrium: $P_{23} - P_{35} - F_7 = 0$

Joint 6

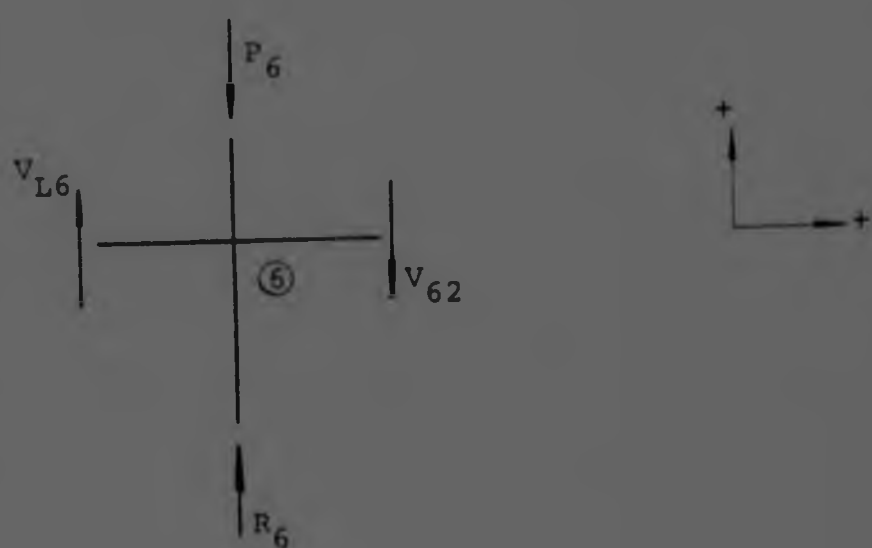

Vertical equilibrium : $R_6 + V_{L6} - P_6 - V_{62} = 0$

Joint 5

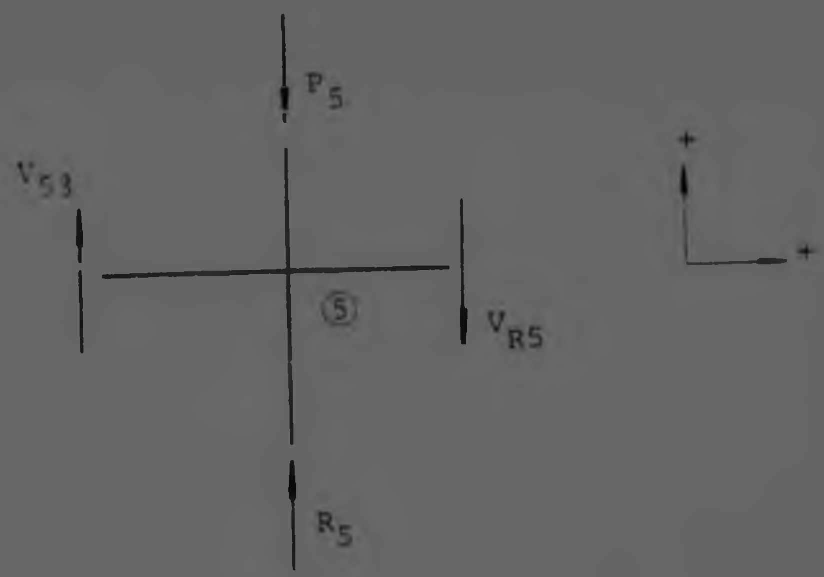

Vertical equilibrium : $R_5 + V_{53} - V_{R5} - P_5 = 0$

In the calculation of axial forces two independent cases are considered, i.e. intermediate storeys of multi-storey frames and single-storey frames or top-most storeys of multi-storey frames.

For intermediate storeys the axial forces in the beams are assumed to be negligible. This leaves the column forces to be considered. They are determined from vertical equilibrium at the various joints of the subassemblage.

$$P_{12} = P_2 + V_{23} - V_{26}$$

$$P_{34} = P_3 + V_{35} - V_{32}$$

$$R_5 = P_5 + V_{R5} - V_{53} \simeq \bar{P}_5 - V_{53}$$

$$R_6 = P_6 - V_{L6} - V_{62} \simeq \bar{P}_6 - V_{62}$$

<u>Joint 5</u>

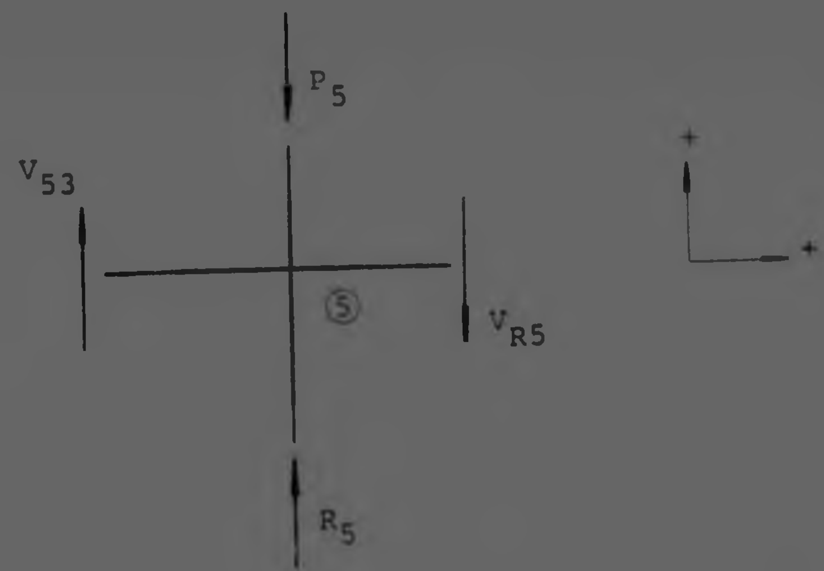

Vertical equilibrium : $R_5 + V_{53} - V_{R5} - P_5 = 0$

In the calculation of axial forces two independent cases are considered, i.e. intermediate storeys of multi-storey frames and single-storey frames or top-most storeys of multi-storey frames.

For intermediate storeys the axial forces in the beams are assumed to be negligible. This leaves the column forces to be considered. They are determined from vertical equilibrium at the various joints of the subassemblage.

$$P_{12} = P_2 + V_{23} - V_{26}$$

$$P_{34} = P_3 + V_{35} - V_{32}$$

$$R_5 = P_5 + V_{R5} - V_{53} \simeq \bar{P}_5 - V_{53}$$

$$R_6 = P_6 - V_{L6} - V_{62} \simeq \bar{P}_6 - V_{62}$$

Since exact expressions will not be available for the terms V_{R5} and V_{L6}, these will be approximated and added to the axial loads P_5 and P_6 from the upper storey. The total load $\bar{P}_5$ and $\bar{P}_6$ will then be applied to the core-module as an external load.

For top-most storeys and single-storey structures the axial forces in the beams at level 6 - 2 - 3 - 5 will be included. To simplify matters, the axial forces in beams 2 - 6 and 3 - 5 will be set equal to P_{23}, the force in the beam between joints 2 and 3. Hence, for analysis purposes, P_{35} and P_{26} are initially taken as zero. On this basis P_{23} is calculated and subsequently equated to P_{35} and P_{26}. In this case, effectively only P_{23} appears as an unknown. The force P_{23} follows from the horizontal equilibrium equation at joint 2. The term V_{U2} is zero for top-most storeys and simple portal frames, i.e.

$$P_{23} = H - V_{21}$$

If the shear forces V are substituted into the above expressions for the axial member forces, the axial force matrix of Table 4 is obtained.

APPENDIX III

" SYMMETRY - BUCKLING "

In order to obtain the stiffness matrix $\bar{C}$ for the case of "Symmetry - Buckling", the member-end moments are required in their incremental form such as given in Equation 31, incorporating the differentiated stability functions of Equations 33a and 33b. For the core-module of Figure 25 follows :

Infinitesimal member moments

$$\delta M_{12} = EK_{12}S_{12}\left[\delta\Theta_1+C_{12}\delta\Theta_2-(1+C_{12})\frac{\delta\Delta}{L_{12}}\right]+\left\{EK_{12}S_{12}\Theta_2C'_{12}\right.$$

$$-EK_{12}S_{12}C'_{12}\frac{\Delta}{L_{12}}+EK_{12}S'_{12}\left[\Theta_1+C_{12}\Theta_2-(1+C_{12})\frac{\Delta}{L_{12}}\right]$$

$$\left.+M'_{F12}\right\}\delta P_{12}$$

$$\delta M_{21} = EK_{12}S_{12}\left[\delta\Theta_2+C_{12}\delta\Theta_1-(1+C_{12})\frac{\delta\Delta}{L_{12}}\right]+\left\{EK_{12}S_{12}\Theta_1C'_{12}\right.$$

$$-EK_{12}S_{12}C'_{12}\frac{\Delta}{L_{12}}+EK_{12}S'_{12}\left[\Theta_2+C_{12}\Theta_1-(1+C_{12})\frac{\Delta}{L_{12}}\right]$$

$$\left.+M'_{F21}\right\}\delta P_{12}$$

$$\delta M_{23} = EK_{23}S_{23}(\delta\Theta_2+C_{23}\delta\Theta_3)+\left[EK_{23}S_{23}\Theta_3C'_{23}\right.$$

$$\left.+EK_{23}S'_{23}(\Theta_2+C_{23}\Theta_3)+M'_{F23}\right]\delta P_{23}$$

$$\delta M_{32} = EK_{23}S_{23}(\delta\Theta_3+C_{23}\delta C_2)+\Big[EK_{23}S_{23}\Theta_2C'_{23}$$

$$+EK_{23}S'_{23}(\Theta_3+C_{23}\Theta_2)+M'_{F32}\Big]\ \delta P_{23}$$

$$\delta M_{43} = EK_{34}S_{34}\left[\delta\Theta_4+C_{34}\delta\Theta_3-(1+C_{34})\frac{\delta\Delta}{L_{34}}\right]+\Big\{EK_{34}S_{34}\Theta_3C'_{34}$$

$$-EK_{34}S_{34}C'_{34}\ \frac{\Delta}{L_{34}}+EK_{34}S'_{34}\left[\Theta_4+C_{34}\Theta_3-(1+C_{34})\frac{\Delta}{L_{34}}\right]$$

$$+M'_{F43}\Big\}\delta P_{34}$$

$$\delta M_{34} = EK_{34}S_{34}\left[\delta\Theta_3+C_{34}\delta\Theta_4-(1+C_{34})\frac{\delta\Delta}{L_{34}}\right]+\Big\{EK_{34}S_{34}\Theta_4C'_{34}$$

$$-EK_{34}S_{34}C'_{34}\ \frac{\Delta}{L_{34}}+EK_{34}S'_{34}\left[\Theta_3+C_{34}\Theta_4-(1+C_{34})\frac{\Delta}{L_{34}}\right]$$

$$+M'_{F34}\Big\}\delta P_{34}$$

Assuming P_{35} and P_{26} to be equal to P_{23} and thus approximating S_{35} and S_{26} to S_{23}, C_{35} and C_{26} to C_{23} and, similarly, equating the first derivatives it follows, that

$$\delta M_{35} = EK_{35}S_{23}(\delta\Theta_3+C_{23}\delta\Theta_5)+\Big[EK_{35}S_{23}\Theta_5C'_{23}$$

$$+EK_{35}S'_{23}(\Theta_3+C_{23}\Theta_5)+M'_{F35}\Big]\ \delta P_{23}$$

$$\delta M_{53} = EK_{35}S_{23}(\delta\Theta_5+C_{23}\delta\Theta_3)+\Big[EK_{35}S_{23}\Theta_3C'_{23}$$

$$+EK_{35}S'_{23}(\Theta_5+C_{23}\Theta_3)+M'_{F53}\Big]\ \delta P_{23}$$

$$\delta M_{62} = EK_{26}S_{23}(\delta\Theta_6 + C_{23}\delta\Theta_2) + \Big[EK_{26}S_{23}\Theta_2 C_{23}'$$

$$+ EK_{26}S_{23}'(\Theta_6 + C_{23}\Theta_2) + M_{F62}'\Big]\delta P_{23}$$

$$\delta M_{26} = EK_{26}S_{23}(\delta\Theta_2 + C_{23}\delta\Theta_6) + \Big[EK_{26}S_{23}\Theta_6 C_{23}'$$

$$+ EK_{26}S_{23}'(\Theta_2 + C_{23}\Theta_\epsilon) + M_{F26}'\Big]\delta P_{23}$$

Differentiated fixed-end moments M_F'

The infinitesimal fixed-end moments M_F' which appear as part of the member moments, can be obtained from Equations 50a and 50b by differentiation with respect to the axial member force P.

$$\frac{dM_{FAB}}{dP} = M_{FAB}' = EK\Big[S(\gamma_A' + C\gamma_B' + C'\gamma_B) + S'(\gamma_A + C\gamma_B)\Big] \quad |EQN.53|$$

and $M_{FBA}' = - M_{FAB}'$

The differentiated terms γ_A' and γ_B' can be derived from the basic expressions in Equations 51 and 52.

Uniformly distributed loading of intensity q :

$$\frac{d\gamma_A}{dm}\frac{dm}{dP} = \gamma_A' = \frac{qL}{2P^2}\left(1 + \frac{1}{1+\cos m} - \frac{3}{m}\tan\frac{m}{2}\right) \quad |EQN.54|$$

and $\gamma_B' = - \gamma_A'$

Symmetrical dual-point load of magnitude U :

$$\frac{d\gamma_A}{dm}\,\frac{dm}{dP}=\gamma_A'=\frac{U}{2P^2}\left[\frac{\cos\frac{\eta}{2}m}{2\cos\frac{m}{2}}\left(4+\eta m\tan\frac{\eta}{2}m-m\tan\frac{m}{2}\right)-2\right] \qquad |\text{EQN. }55|$$

and $\quad \gamma_B' = -\gamma_A'$

The term m has been defined in Equation 15c.

<u>Incremental member moments δM_m</u>

Referring to Figure 36, the differentiated moments δM_m are simplified as follows, using the stability functions N and O. The N, O-functions are exclusively concerned with elastic buckling.

Bottom storeys (δM_{m1}) :

$$\delta M_{m1} = F_1\delta\theta_1$$

Upper storeys (δM_{m1}) :

$$\delta M_{m1} = E\left[\left(\frac{6I_{B1}}{L_{26}}+\frac{4I_{14}}{L_{23}}\right)\delta\theta_1+\frac{2I_{14}}{L_{14}}\,\delta\theta_4\right.$$

$$\left.+\frac{I_{L1}}{L_{L1}}\left(N_1-O_1^2\;\frac{\frac{I_{L1}}{6L_{L1}}}{\frac{I_{L1}}{6L_{L1}}N_1+\Sigma K_{B2}}\right)\delta\theta_1\right]$$

$$\delta M_{m2} = \frac{EI_{U2}}{L_{U2}}\left(N_2 - O_2^2 \frac{\frac{I_{U2}}{6L_{U2}}}{\frac{I_{U2}}{6L_{U2}} N_2 + \Sigma K_{B2}}\right)\delta\Theta_2$$

$$\delta M_{m3} = \frac{EI_{U3}}{L_{U3}}\left(N_3 - O_3^2 \frac{\frac{I_{U3}}{6L_{U3}}}{\frac{I_{U3}}{6L_{U3}} N_3 + \Sigma K_{B3}}\right)\delta\Theta_3$$

Bottom storeys (δM_{m4}) :

$$\delta M_{m4} = F_4 \delta\Theta_4$$

Upper storeys (δM_{m4}) :

$$\delta M_{m4} = E\left[\left(\frac{6I_{B4}}{L_{35}} + \frac{4I_{14}}{L_{23}}\right)\delta\Theta_4 + \frac{2I_{14}}{L_{23}}\,\delta\Theta_1\right.$$

$$\left. + \frac{I_{L4}}{L_{L4}}\left(N_4 - O_4^2 \frac{\frac{I_{L4}}{6L_{L4}}}{\frac{I_{L4}}{6L_{L4}} N_4 + \Sigma K_{B4}}\right)\delta\Theta_4\right]$$

$$\delta M_{m5} = E\left[6K_{B5} + \frac{I_{U5}}{L_{U5}}\left(N_{U5} - O_{U5}^2 \frac{\frac{I_{U5}}{6L_{U5}}}{\frac{I_{U5}}{6L_{U5}} N_{U5} + \Sigma K_{BU5}}\right)\delta\Theta_5\right.$$

$$\left. + \frac{I_{L5}}{L_{L5}}\left(N_{L5} - O_{L5}^2 \frac{\frac{I_{L5}}{6L_{L5}}}{\frac{I_{L5}}{6L_{L5}} N_{L5} + \Sigma K_{BL5}}\right)\delta\Theta_5\right]$$

$$\delta M_{m6} = E\left[6K_{B6} + \frac{I_{U6}}{L_{U6}}\left(N_{U6} - O_{U6}^{2}\,\frac{\frac{I_{U6}}{6L_{U6}}}{\frac{I_{U6}}{6L_{U6}}\,N_{U6} + 2K_{BU6}}\right)\delta\Theta_{6}\right.$$

$$\left. + \frac{I_{L6}}{L_{L6}}\left(N_{L6} - O_{L6}^{2}\,\frac{\frac{I_{L6}}{6L_{L6}}}{\frac{I_{L6}}{6L_{L6}}\,N_{L6} + 2K_{BL6}}\right)\delta\Theta_{6}\right]$$

The stability functions N and O in δM_m should also be used in their differentiated form in conjunction with the primary rotations Θ. However, since other simplifications have been made in regard to the far-end conditions of the ancillary columns, it is believed that the differentials of the N and O-functions would unduly increase the complexity of the problem without any significant gain in accuracy.

Joint equations

With the differentiated member-end moments known, it is possible to formulate the joint equations as follows:

Joint 1

$$\delta M_{m1} + \delta M_{12} = 0$$

Substituting the moments M_{m1} and M_{12}, this equation becomes

$$\delta M_{m1} + EK_{12}S_{12}\left[\delta\Theta_{1} + C_{12}\delta\Theta_{2} - (1+C_{12})\frac{\delta\Delta}{L_{12}}\right] + \alpha_{1}\delta P_{12} = 0$$

The factor α_1 represents all terms containing the incremental change δP_{12}.

ıt 2

$$\delta M_{m2} + \delta M_{21} + \delta M_{23} + \delta M_{26} = 0$$

$$\delta M_{m2} + EK_{12} S_{12} \left[\delta\Theta_2 + C_{12}\delta\Theta_1 - (1+C_{12}) \frac{\delta\Delta}{L_{12}} \right] + \alpha_2\, \delta P_{12}$$

$$+ EK_{23} S_{23} (\delta\Theta_2 + C_{23}\delta\Theta_3) + \alpha_3 \delta P_{23} + EK_{26} S_{23} (\delta\Theta_2 + C_{23}\delta\Theta_6) = 0$$

The factor α_2 represents all terms containing the incremental change δP_{12} and α_3 represents all terms containing δP_{23}.

Joint 3

$$\delta M_{m3} + \delta M_{32} + \delta M_{34} + \delta M_{35} = 0$$

$$\delta M_{m3} + EK_{23} S_{23} (\delta\Theta_3 + C_{23}\delta\Theta_2) + \alpha_4 \delta P_{23} + EK_{34} S_{34}$$

$$\left[\delta\Theta_3 + C_{34}\delta\Theta_4 - (1+C_{34}) \frac{\delta\Delta}{L_{34}} \right] + \alpha_5 \delta P_{34} + EK_{35} S_{23}$$

$$(\delta\Theta_3 + C_{23}\delta\Theta_5) = 0$$

The factors α_4 and α_5 represent all terms containing δP_{23} and δP_{34} respectively.

Joint 4

$$\delta M_{m4} + \delta M_{43} = 0$$

$$\delta M_{m4} + EK_{34}S_{34}\left[\delta\Theta_4 + C_{34}\delta\Theta_3 - (1+C_{34})\frac{\delta\Delta}{L_{34}}\right] + \alpha_6\delta P_{34} = 0$$

The factor α_6 represents all terms containing δP_{34}.

Joint 5

$$\delta M_{m5} + \delta M_{53} = 0$$

$$\delta M_{m5} + EK_{35}S_{23}(\delta\Theta_5 + C_{23}\delta\Theta_3) + \alpha_{10}\delta P_{23} = 0$$

The coefficient α_{10} combines all terms containing δP_{23}.

Joint 6

$$\delta M_{m6} + \delta M_{62} = 0$$

$$\delta M_{m6} + EK_{26}S_{23}(\delta\Theta_6 + C_{23}\delta\Theta_2) + \alpha_{11}\delta P_{23} = 0$$

The coefficient α_{11} combines all terms containing δP_{23}.

In the equations for joints 5 and 6 it has been assumed that the stability functions pertaining to beams 2 - 6 and 3 - 5 are equal to those of member 2 - 3 and that the incremental force change for all beam members is δP_{23}.

The displacement equation

Referring to Figure 67, the sway-equilibrium equation for the incremental force changes takes the following form for the case of "Symmetrical Buckling" :

$$-\delta V_{21} - \delta V_{34} - F_7\delta\Delta = 0$$

This equation can be expanded by substituting the terms δV as given in Equation 32. This leads to the following incremental version of the sway equation :

$$-\frac{EK_{12}}{L_{12}^2}\left[S_{12}^2(1-C_{12}^2)\delta\Delta\right]+\frac{EK_{12}}{L_{12}}S_{12}(\delta\Theta_1+\delta\Theta_2)(1+C_{12})-\alpha_7\delta P_{12}$$

$$-\frac{EK_{34}}{L_{34}^2}\left[S_{34}^2(1-C_{34}^2)\delta\Delta\right]+\frac{EK_{34}}{L_{34}}S_{34}(\delta\Theta_3+\delta\Theta_4)(1+C_{34})-\alpha_9\delta P_{34}$$

$$-F_7\delta\Delta = 0$$

where α_7 combines all terms containing δP_{12} and α_9 represents all terms containing δP_{34}.

Incremental axial force changes δP

In order to obtain the homogeneous set of equations given in Equation 29, it is necessary to express all incremental force changes δP by rotations $\delta\Theta$ and the sway change $\delta\Delta$. This is achieved by considering horizontal and vertical equilibrium at the various joints of the structure. The same assumptions as for the calculation of the axial forces due to applied loading are retained (Appendix II). In addition, the axial force changes δR_5 and δR_6 are taken as zero. This is justified because other simplifications have already been made in regard to the ancillary columns

adjoining nodes 5 and 6 of the core-module.
If the subassemblage is infinitesimally displaced in a general way, all axial beam forces will undergo incremental changes. In line with previous assumptions, axial beam forces are taken as zero except for the top storeys of multi-storey frames and for single-storey frames. In these instances a good approximation of the real behaviour is obtained by assigning initially the entire force change in the beams to beam 2 - 3. Subsequently, the change of force in the other beam members is equated to δP_{23}.

Joint 2

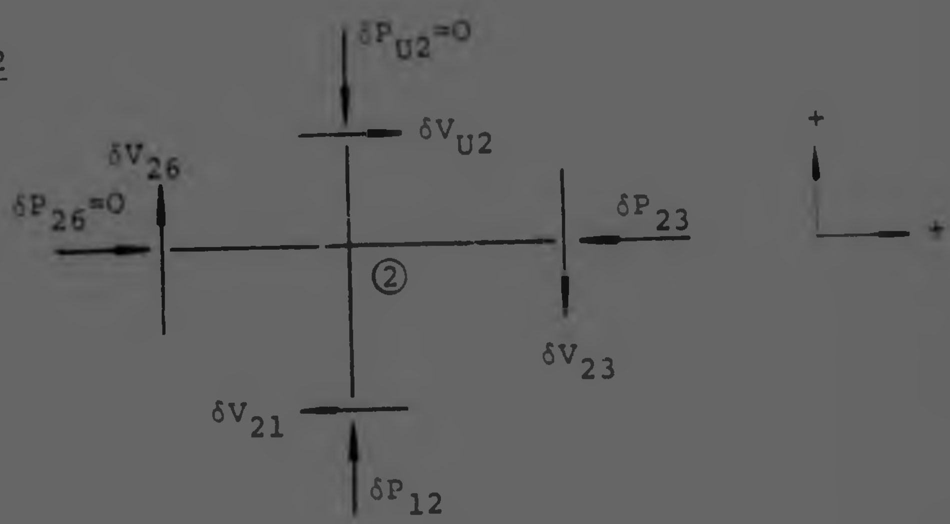

Vertical equilibrium : $\delta P_{12} - \delta V_{23} + \delta V_{26} = 0$

Horizontal equilibrium : $-\delta V_{21} - \delta P_{23} + \delta V_{U2} + \delta P_{26} = 0$

Because of the assumptions made above, the latter equation reduces, for cases in which the axial forces in the beams matter, to

$$-\delta V_{21} - \delta P_{23} = 0$$

The two significant equations can be expanded as follows, substituting the general expressions for δV :

$$\delta P_{12}+\left[\frac{EK_{23}}{L_{23}}\, S_{23}(\delta\Theta_2+\delta\Theta_3)(1+C_{23})\right]-\frac{EK_{26}}{L_{26}}\left[S_{23}(\delta\Theta_2+\delta\Theta_6)\right.$$

$$\left.(1+C_{23})\right]+\alpha_8\delta P_{23}=0$$

and

$$-\frac{EK_{12}}{L_{12}}\left[S_{12}^2(1-C_{12}^2)\delta\Delta\right]+\frac{EK_{12}}{L_{12}}\, S_{12}(\delta\Theta_1+\delta\Theta_2)(1+C_{12})-\alpha_7\delta P_{12}$$

$$-\delta P_{23}=0$$

Substituting δP_{12} from the first equation into the second equation results in the following expression for δP_{23}:

$$\delta P_{23}(1-\alpha_7\alpha_8) = -\frac{EK_{12}}{L_{12}}\left[S_{12}^2(1-C_{12}^2)\delta\Delta\right]+\frac{EK_{12}}{L_{12}}\, S_{12}(\delta\Theta_1+\delta\Theta_2)$$

$$(1+C_{12})-\alpha_7\left\{-\frac{EK_{23}}{L_{23}}\left[S_{23}(\delta\Theta_2+\delta\Theta_3)(1+C_{23})\right]\right.$$

$$\left.+\frac{EK_{26}}{L_{26}}\left[S_{23}(\delta\Theta_2+\delta\Theta_6)(1+C_{23})\right]\right\} \qquad |\text{EQN. } 56|$$

Back-substituting δP_{23} into the above expression gives the final equation for δP_{12}:

$$\delta P_{12} = -\frac{EK_{23}}{L_{23}}\left[S_{23}\ (\delta\Theta_2+\delta\Theta_3)(1+C_{23})\right]+\frac{EK_{26}}{L_{26}}\left[S_{23}(\delta\Theta_2+\delta\Theta_6)\right.$$

$$\left.(1+C_{23})\right]-\frac{\alpha_8}{1-\alpha_7\alpha_8}\left\{-\frac{EK_{12}}{L_{12}^2}\left[S_{12}^2(1-C_{12}^2)\delta\Delta\right]+\frac{EK_{12}}{L_{12}}\, S_{12}\right.$$

$$(\delta\Theta_1+\delta\Theta_2)(1+C_{12})-\alpha_7\left\{-\frac{EK_{23}}{L_{23}}\left[S_{23}(\delta\Theta_2+\delta\Theta_3)(1+C_{23})\right]\right.$$

$$\left.\left.+\frac{EK_{26}}{L_{26}}\left[S_{23}(\delta\Theta_2+\delta\Theta_6)(1+C_{23})\right]\right\}\right\} \qquad |\text{EQN. } 57|$$

The remaining axial force change δP_{34} is obtained by considering vertical equilibrium at joint 3.

Joint 3

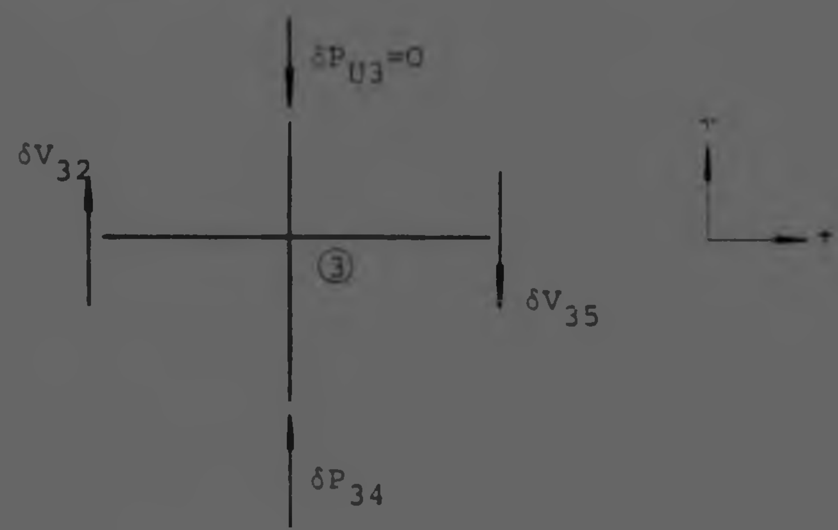

The infinitesimal force change in the upper column is set equal to zero. Since some substantial adjustments have already been made in regard to the conditions at the remote end of the member, this further simplification is of minor importance.

Vertical equilibrium : $\delta P_{34} + \delta V_{32} - \delta V_{35} = 0$

If the shear forces δV are substituted

$$\delta P_{34} - \frac{EK_{23}}{L_{23}}\left[S_{23}(\delta\Theta_2+\delta\Theta_3)(1+C_{23})\right] + \frac{EK_{35}}{L_{35}}\left[S_{23}(\delta\Theta_3+\delta\Theta_5)\right.$$

$$\left.(1+C_{23})\right] - \alpha_{12}\delta P_{23} = 0$$

The coefficient α_{12} combines all terms containing δP_{23}.

Substituting the previously found expression for δP_{23} gives the final equation for δP_{34}.

$$\delta P_{34} = \frac{EK_{23}}{L_{23}}\left[S_{23}(\delta\Theta_2+\delta\Theta_3)(1+C_{23})\right] - \frac{EK_{35}}{L_{35}}\left[S_{23}(\delta\Theta_3+\delta\Theta_5)\right.$$

$$\left.(1+C_{23})\right] + \frac{\alpha_{12}}{1-\alpha_7\alpha_8}\left\{-\frac{EK_{12}}{L_{12}^2}\left[S_{12}^{*}(1-C_{12}^{*})\delta\Delta\right]\right.$$

$$+\frac{EK_{12}}{L_{12}}S_{12}(\delta\Theta_1+\delta\Theta_2)(1+C_{12})-\alpha_7\left\{-\frac{EK_{23}}{L_{23}}\left[S_{23}\right.\right.$$

$$\left.\left.\left.(\delta\Theta_2+\delta\Theta_3)(1+C_{23})\right]+\frac{EK_{26}}{L_{26}}\left[S_{23}(\delta\Theta_2+\delta\Theta_6)(1+C_{23})\right]\right\}\right\}$$

|EQN. 58|

With δP_{23}, δP_{12} and δP_{34} calculated in this manner and setting δP_{35} and δP_{26} equal to δP_{23}, it is now possible to substitute these incremental axial force changes into the six joint equations and the one sway equation. As a result, the required system of homogeneous linear equations is obtained which is presented in Table 5. The stiffness matrix $\bar{C}$ of Table 5 is used to calculate the elastic buckling load for the special case of "Symmetry - Buckling".

APPENDIX IV/1

LOAD ANALYSIS FOR "SYMMETRY - BUCKLING" - DIFFERENTIAL EQUATION METHOD

With reference to Figures 41 and 42, the differential equation method is first applied to the case of dual-point loading.

Rotational restraints

Using the stability functions of the slope-deflection method, the elastic rotational restraints F_3, F_4 and F_5 can be expressed as follows :

$$F_3 = \bar{F}_3 \, EK_{34} \, S_{U3} \, (1+C_{U3}) \, \beta_3$$

Bottom storeys (F_4) :

$$F_4 = \bar{F}_4 \, EK_{34}$$

Upper storeys (F_4) :

$$F_4 = EK_{34} \left[2 \, \frac{\dfrac{I_{14}}{L_{23}} + \dfrac{I_{B4}}{L_{35}}}{K_{34}} + \bar{F}_4 \, S_{L4} \, (1+C_{24}) \, \beta_2 \right]$$

$$F_5 = EK_{34} \left[\bar{F}_{U5} S_{U5} (1+C_{U5}) \beta_3 + \bar{F}_{L5} S_{L5} (1+C_{L5}) \beta_2 + 4 \frac{K_{B5}}{K_{34}} \right]$$

Member moments $M + Py_i$ for the deformed shapes

Member 3 - 4 :

$$M = P_{34}y_2 + H_4x_2 - M_{m4} - \frac{q_{34}x_2^2}{2}$$

Member 3 - 2 :

$$M = V_{32}x_1 - M_{32} + P_{23}y_1 \qquad x_1<\xi L_{23}$$

$$M = P_{23}y_1+V_{32}x_1-M_{32}-U_1(x_1- \xi L_{23}) \qquad x_1>\xi L_{23}$$

Member 3 - 5 :

$$M = \bar{R}_5x_3-M_{m5}-M_5+P_{23}y_3 \qquad x_3<\xi L_{35}$$

$$M = \bar{R}_5x_3-M_{m5}-M_5-U_3(x_3- \xi L_{35})+P_{23}y_3 \qquad (1-\xi)L_{35}>x_3<\xi L_{35}$$

$$M = \bar{R}_5x_3-M_{m5}-M_5-U_3(2x_3-L_{35})+P_{23}y_3 \qquad x_3>(1-\xi)L_{35}$$

These moments are used in differential equations such as given in Equation 34. The differential equations, which have solutions of the kind presented in Equation 35, result in the following expressions:

Member 3 - 4 :

$$y_2 = C_1\sin\frac{m_{34}x_2}{L_{34}} + C_2\cos\frac{m_{34}x_2}{L_{34}} + a_3-b_3x_2 + c_3x_2^2$$

Member 3 - 5 :

$$y_{31} = C_3\sin\frac{m_{35}x_3}{L_{35}} + C\cos\frac{m_{35}x_3}{L_{35}} + a_6 - b_6x_3$$

$$y_{32} = C_5\sin\frac{m_{35}x_3}{L_{35}} + C_6\cos\frac{m_{35}x_3}{L_{35}} + a_7 - b_7x_3$$

$$y_{33} = C_7\sin\frac{m_{35}x_3}{L_{35}} + C_8\cos\frac{m_{35}x_3}{L_{35}} + a_8 - b_8x_3$$

Member 3 - 2 :

$$y_{11} = C_9 \sin \frac{m_{23}x_1}{L_{23}} + C_{10} \cos \frac{m_{23}x_1}{L_{23}} + a_4 - b_4 x_1$$

$$y_{12} = C_{11} \sin \frac{m_{23}x_1}{L_{23}} + C_{12} \cos \frac{m_{23}x_1}{L_{23}} + a_5 - b_5 x_1$$

The first derivatives are also required :

Member 3 - 4 :

$$y_2' = C_1 \frac{m_{34}}{L_{34}} \cos \frac{m_{34}x_2}{L_{34}} - C_2 \frac{m_{34}}{L_{34}} \sin \frac{m_{34}x_2}{L_{34}} - b_3 + 2c_3 x_2$$

Member 3 - 5 :

$$y_{31}' = C_3 \frac{m_{35}}{L_{35}} \cos \frac{m_{35}x_3}{L_{35}} - C_4 \frac{m_{35}}{L_{35}} \sin \frac{m_{35}x_3}{L_{35}} - b_6$$

$$y_{32}' = C_5 \frac{m_{35}}{L_{35}} \cos \frac{m_{35}x_3}{L_{35}} - C_6 \frac{m_{35}}{L_{35}} \sin \frac{m_{35}x_3}{L_{35}} - b_7$$

$$y_{33}' = C_7 \frac{m_{35}}{L_{35}} \cos \frac{m_{35}x_3}{L_{35}} - C_8 \frac{m_{35}}{L_{35}} \sin \frac{m_{35}x_3}{L_{35}} - b_8$$

Member 3 - 2 :

$$y_{11}' = C_9 \frac{m_{23}}{L_{23}} \cos \frac{m_{23}x_1}{L_{23}} - C_{10} \frac{m_{23}}{L_{23}} \sin \frac{m_{23}x_1}{L_{23}} - b_4$$

$$y_{12}' = C_{11} \frac{m_{23}}{L_{23}} \cos \frac{m_{23}x_1}{L_{23}} - C_{12} \frac{m_{23}}{L_{23}} \sin \frac{m_{23}x_1}{L_{23}} - b_5$$

The constants of integration $C_1 \ldots C_{12}$ have to be determined from boundary and continuity conditions.

The variables a, b and c have the following meaning:

$$a_3 = \frac{M_{34}}{P_{34}} - \frac{2c_3L_{34}^2}{m_{34}^2}$$

$$a_4 = \frac{M_{32}}{P_{23}}$$

$$a_5 = \frac{M_{32}-U_1\xi L_{35}}{P_{23}}$$

$$a_6 = \frac{M_{m5}+M_5}{P_{23}}$$

$$a_7 = \frac{M_{m5}+M_5-U_3\xi L_{35}}{P_{23}}$$

$$a_8 = \frac{M_{m5}+M_5-U_3L_{35}}{P_{23}}$$

$$b_3 = \frac{H_4}{P_{34}}$$

$$b_4 = \frac{V_{32}}{P_{23}}$$

$$b_5 = \frac{V_{32}-U_1}{P_{23}} = 0$$

$$b_6 = \frac{\bar{R}_5}{P_{23}} = b_7 = b_8$$

$$c_3 = \frac{q_{34}}{2P_{34}}$$

$$V_{32} = P_{34} - P_3 - \bar{R}_5 + 2U_1$$

The variables a, b and c have the following meaning:

$$a_3 = \frac{M_{34}}{P_{34}} - \frac{2c_3L_{34}^2}{m_{34}^2}$$

$$a_4 = \frac{M_{32}}{P_{23}}$$

$$a_5 = \frac{M_{32}-U_1\xi L_{35}}{P_{23}}$$

$$a_6 = \frac{M_{m5}+M_5}{P_{23}}$$

$$a_7 = \frac{M_{m5}+M_5-U_3\xi L_{35}}{P_{23}}$$

$$a_8 = \frac{M_{m5}+M_5-U_3L_{35}}{P_{23}}$$

$$b_3 = \frac{H_4}{P_{34}}$$

$$b_4 = \frac{V_{32}}{P_{23}}$$

$$b_5 = \frac{V_{32}-U_1}{P_{23}} = 0$$

$$b_6 = \frac{\overline{R}_5}{P_{23}} = b_7 = b_8$$

$$c_3 = \frac{q_{34}}{2P_{34}}$$

$$V_{32} = P_{34} - P_3 - \overline{R}_5 + 2U_1$$

The axial force parameters have been defined as follows:

$$m_{34} = L_{34}\sqrt{\frac{P_{34}}{EI_{34}}}$$

$$m_{23} = L_{23}\sqrt{\frac{P_{23}}{EI_{23}}}$$

$$m_{35} = L_{35}\sqrt{\frac{P_{23}}{EI_{35}}}$$

Boundary and continuity conditions

Member 3 - 4 :

1. $x_2 = 0$; $y_2 = 0$
2. $x_2 = L_{34}$; $y_2 = 0$

Member 3 - 5 :

3. $x_3 = 0$; $y_{31} = 0$
4. $x_3 = L_{35}$; $y_{33} = 0$
5. $x_3 = L_{35}$ and $x_2 = L_{34}$; $y'_{33} = -y'_2$
6. $x_3 = \xi L_{35}$; $y_{31} = y_{32}$
7. $x_3 = L_{35}(1-\xi)$; $y_{32} = y_{33}$
8. $x_3 = \xi L_{35}$; $y'_{32} = y'_{31}$
9. $x_3 = L_{35}(1-\xi)$; $y'_{32} = y'_{33}$

Member 3 - 2 :

10. $x_1 = 0$; $y_1 = 0$

11. $x_1 = \frac{L_{23}}{2}$; $y'_{12} = 0$

12. $x_1 = \xi L_{23}$; $y_{11} = y_{12}$

13. $x_1 = \xi L_{23}$; $y'_{11} = y'_{12}$

14. $x_1 = 0$ and $x_2 = L_{34}$; $y'_{11} = -y'_2$

It is now possible to solve for the various constants of integration using the relevant boundary or continuity condition .

Condition 1 :

$$C_2 = - a_3$$

Condition 2 :

$$C_1 = \frac{1}{\sin m_{34}} \left[a_3(\cos m_{34}-1) + b_3L_{34} - c_3L_{34}^2 \right]$$

Condition 14 :

$$C_9 = \frac{L_{23}}{m_{23}} \left\{ a_3 \left[- \frac{m_{34}}{L_{34}} \text{cotan } m_{34} \ (\cos m_{34}-1) - \frac{m_{34}}{L_{34}} \sin m_{34} \right] + b_3 \ (1-m_{34} \text{ cotan } m_{34}) - c_3L_{34} \ (2+m_{34} \text{ cotan } m_{34}) + b_4 \right\}$$

Condition 11 :

$$C_{11} = \frac{L_{23}}{m_{23} \text{ cotan } \frac{m_{23}}{2}} \left(C_{12} \frac{m_{23}}{L_{23}} \sin \frac{m_{23}}{2} + b_5 \right)$$

Condition 10 :

$$C_{10} = - a_4$$

Condition 12 :

$$C_{11} = \frac{1}{\sin m_{23}\xi}\,(C_9 \sin m_{23}\xi + C_{10} \cos m_{23}\xi + a_4 - b_4\xi L_{23}$$

$$- C_{12} \cos m_{23}\xi - a_5 + b_5\xi L_{23})$$

Equating conditions 11 and 12 and solving for C_{12} gives

$$C_{12} = \frac{1}{\tan \frac{m_{23}}{2} + \operatorname{cotan} m_{23}\xi}\left\{\frac{1}{\sin m_{23}\xi}\left[C_9 \sin m_{23}\xi\right.\right.$$

$$\left.\left. + a_4(1-\cos m_{23}\xi) - b_4\xi L_{23} - a_5\right]\right\}$$

Eventually, from condition 13 the final Equation 36a is obtained. In order to solve this equation for H_4 the coefficients a, b, c need to be expressed as functions of H_4, P_{12}, P_{34} or $\bar{R}_5$.

The axial forces P_{12}, P_{34} and $\bar{R}_5$ are taken from the solution of Equation 23 for loading equal to the elastic buckling load. The outstanding terms in parameters a, b and c are evaluated from the following moment expressions:

$$M_{43} = M_{m4}$$

$$M_{34} = H_4 L_{34} - \frac{q_{34}L_{34}^2}{2} - M_{43} = H_4 L_{34} - \frac{q_{34}L_{34}^2}{2} - M_{m4}$$

$$M_{35} = -\bar{R}_5 L_{35} + M_{m5} + M_5 + U_3 L_{35}$$

$$M_{32} = M_{34} + M_{m3} + M_3 + U_3 L_{35} - \bar{R}_5 L_{35} + M_5 + M_{m5}$$

$$M_{23} = M_{32}$$

$$M_m = U_1 \xi L_{23} - \frac{M_{32} + M_{23}}{2}$$

The required solutions are obtained by expressing M_{m3}, M_{m4} and M_{m5} as functions of H_4, P_{12}, P_{34} or $\overline{R}_5$. This is accomplished by using the relationship between the elastic rotational restraints, member-end tangents and moments as follows:

$$M_{m3} = F_3 \; y'_{11}(x_1=0) = F_3 \left(C_9 \frac{m_{23}}{L_{23}} - b_4 \right) \qquad |\text{EQN. 59a}|$$

$$M_{m4} = F_4 \; y'_2 \; (x_2=0) = F_4 \left(C_1 \frac{m_{34}}{L_{34}} - b_3 \right) \qquad |\text{EQN. 59b}|$$

$$M_{m5} = F_5 \; y'_{31}(x_3=0) = F_5 \left(C_3 \frac{m_{35}}{L_{35}} - b_6 \right) \qquad |\text{EQN. 59c}|$$

Using C_1 from condition 2 and substituting $M_{34} = H_4L_{34} - \frac{q_{34}L_{34}^2}{2} - M_{m4}$ into Equation 59b leads to

$$M_{m4} = F_4 \frac{\varepsilon_2}{\varepsilon_1} \qquad |\text{EQN. 60}|$$

in which,

$$\varepsilon_1 = 1 - \frac{F_4 m_{34}(\cos m_{34} - 1)}{L_{34}P_{34}\sin m_{34}}$$

and

$$\varepsilon_2 = F_4 \left[\frac{H_4}{P_{34}} \left(\frac{m_{34}}{\sin m_{34}} - 1 \right) - \frac{m_{34}q_{34}L_{34}}{2P_{34} \sin m_{34}} - \frac{q_{34}EI_{34}}{P_{34}^2} \frac{(\cos m_{34} - 1)m_{34}}{L_{34} \sin m_{34}} \right]$$

Similarly, M_{m3} is derived by using C_9 from condition 14 and M_{m4} from Equation .0. Equation 59a then results in

$$M_{m3} = F_3(M_{m4}\ \varepsilon_3 + \varepsilon_4) \qquad |\text{EQN. } 61|$$

in which,

$$\varepsilon_3 = \frac{m_{34}}{P_{34}L_{34}}\left[-\sin m_{34} - \cot an\ m_{34}\ (\cos m_{34} - 1)\right]$$

and

$$\varepsilon_4 = \frac{H_4}{P_{34}}(1 - m_{34}\ \cot an\ m_{34}) - \frac{q_{34}L_{34}}{P_{34}}\left[1 - \frac{m_{34}}{2}\cot an\ m_{34} - \frac{\sin m_{34}}{m_{34}} - \frac{\cot an\ m_{34}}{m_{34}}(\cos m_{34} - 1)\right]$$

The derivation of M_{m5} is rather tedious since further constants of integration, i.e. C_4, C_5, C_6, C_7 and C_8 need to be calculated in order to obtain C_3 for Equation 59c. Some intermediate results are given below.

Condition 6 :

$$C_3 = \frac{-a_6 + b_6\xi L_{35} - b_7\xi L_{35} + a_7}{\sin m_{35}\xi} - C_4\ \cot an\ m_{35}\xi + C_5 + C_6 \cot an\ m_{35}\xi$$

Condition 3 :

$$C_4 = -\ a_6$$

Conditions 4 & 5 :

$$C_8 = \frac{1}{\tan m_{35} + \cot an\ m_{35}}\left[\frac{b_8L_{35} - a_8}{\sin m_{35}} - \frac{L_{35}}{m_{35}\cos m_{35}}\left(\frac{-C_1}{L_{34}}m_{34}\cos m_{34} + \frac{C_2}{L_{34}}m_{34}\sin m_{34} + b_3 - 2c_3L_{34} + b_8\right)\right]$$

Condition 4 :

$$C_7 = \frac{b_8 L_{35} - a_8}{\sin m_{35}} - C_8 \text{ cotan } m_{35}$$

Conditions 7 & 9 :

$$C_6 - C_8 = \frac{1}{\tan m_{35}(1-\xi) + \text{cotan } m_{35}(1-\xi)}$$

$$\left[\frac{a_8 - a_7 + b_7 L_{35}(1-\xi)}{\sin m_{35}(1-\xi)} - \frac{(b_7 - b_8) L_{35}}{m_{35} \cos m_{35}(1-\xi)} \right]$$

Condition 7 :

$$C_5 = C_7 + (C_8 - C_6) \text{cotan } m_{35}(1-\xi)$$

$$+ \frac{a_8 - a_7 + b_7 L_{35}(1-\xi) - b_8 L_{35}(1-\xi)}{\sin m_{35}(1-\xi)}$$

Using these constants of integration, C_3 can be reduced to a function of C_8 which in turn can be substituted from conditions 4 & 5. Subsequently, after some manipulation, M_{m5} can be determined as in Equation 62.

$$M_{m5} = F_5 \frac{\varepsilon_5}{\varepsilon_6} \qquad |\text{EQN. } 62|$$

where,

$$\varepsilon_6 = 1 + \frac{F_5 m_{35}}{P_{23} L_{35} \sin m_{35}} \left(1 + \frac{\text{cotan } m_{35}\xi - \text{cotan } m_{35}}{\tan m_{35} + \text{cotan } m_{35}} \right.$$

$$\left. - \text{ cotan } m_{35}\xi \sin m_{35} \right)$$

and

$$\epsilon_5 = -\frac{U_3 \xi m_{35}}{P_{23} \sin m_{35}\xi} + \frac{M_5 m_{35}}{P_{23} L_{35}} \text{cotan } m_{35}\xi + \frac{b_8 L_{35} - \frac{M_5 - U_3 L_{35}}{P_{23}}}{\sin m_{35}}$$

$$\frac{m_{35}}{L_{35}} \left(1 + \frac{\text{cotan } m_{35}\xi - \text{cotan } m_{35}}{\tan m_{35} + \text{cotan } m_{35}}\right) - \frac{U_3 m_{35}(1-\xi)}{P_{23} \sin m_{35}(1-\xi)}$$

$$\left[1 + \frac{\text{cotan } m_{35} - \text{cotan } m_{35}(1-\xi)}{\tan m_{35}(1-\xi) + \text{cotan } m_{35}(1-\xi)}\right]$$

$$+ \frac{\text{cotan } m_{35}\xi - \text{cotan } m_{35}}{\cos m_{35}(\tan m_{35} + \text{cotan } m_{35})} \left(C_1 \frac{m_{34}}{L_{34}} \cos m_{34}\right.$$

$$\left. - C_2 \frac{m_{34}}{L_{34}} \sin m_{34} - b_3 + 2c_3 L_{34} - b_8\right) - b_8$$

Hence, in successive steps M_{m4}, M_{m3} and M_{m5} can be determined in that order for a trial value of H_4. Subsequently, the moments M_{43}, M_{34}, M_{32}, M_{23} and M_{35} are calculated so that the variables a, b and c can be solved and substituted into Equation 36a. A solution for H_4 is found when Equation 36a is satisfied.

Dual-point load and zero axial beam forces

If the stiffness reduction in the beam members is neglected Equation 36b is obtained. Compared with the previous case, the following adjustments are required. All other terms remain unchanged or are irrelevant.

$$a_4 = M_{32}$$

$$b_4 = V_{32} = U_1$$

$$C_9 = a_3\left[-\frac{m_{34}}{L_{34}} \text{ cotan } m_{34}(\cos m_{34}-1) - \frac{m_{34}}{L_{34}} \sin m_{34}\right]$$

$$+b_3(1-m_{34} \text{ cotan } m_{34})-c_3L_{34}(2-m_{34} \text{ cotan } m_{34})$$

$$C_{11} = \frac{b_4}{2}\,\frac{L_{23}^2}{4} - a_4\frac{L_{23}}{2} + U_1\,\frac{L_{23}^2}{2}\,(\xi - \tfrac{1}{4})$$

$$M_5 = \frac{F_5}{EI_{35}}\,\frac{\varepsilon_5}{\varepsilon_6}$$

where,

$$\varepsilon_6 = 1 + \frac{F_5L_{35}}{EI_{35}}$$

and

$$\varepsilon_5 = \bar{R}_5\,\frac{L_{35}^2}{2} - M_5L_{35}+M_4\varepsilon_3+\varepsilon_4+ \frac{U_3}{2}\left[L_{35}^2(\xi^2-1)\right]$$

<u>Uniformly distributed beam loading</u>

The following results are obtained when the dual-point loadings on the beams are replaced by a uniformly distributed loading.

<u>Member moments $M + Py_1$</u>

Member 3 - 4 :

$$M = P_{34}y_2 - H_4x_2 - M_{m4} - \frac{q_{34}x_2^2}{2}$$

Member 3 - 2 :

$$M = P_{23}y_1 - V_{32}x_1 - M_{32} - \frac{q_{23}x_1^2}{2}$$

Member 3 - 5 :

$$M = P_{23}y_3 + \bar{R}_5 x_3 - M_{m5} - M_5 - \frac{q_{35}x_3^2}{2}$$

The differential equations of the type as in Equation 34 have the following solutions :

Member 3 - 4 :

$$y_2 = C_1 \sin m_{34} \frac{x_2}{L_{34}} + C_2 \cos m_{34} \frac{x_2}{L_{34}} + a_3 - b_3 x_2 + c_3 x_2^2$$

Member 3 - 5 :

$$y_3 = C_3 \sin m_{35} \frac{x_3}{L_{35}} + C_4 \cos m_{35} \frac{x_3}{L_{35}} + a_6 - b_6 x_3 + c_6 x_3^2$$

Member 3 - 2 :

$$y_1 = C_5 \sin m_{23} \frac{x_1}{L_{23}} + C_6 \cos m_{23} \frac{x_1}{L_{23}} + a_4 - b_4 x_1 + c_4 x_1^2$$

<u>Variables a, b, c</u>

$$a_3 = \frac{M_{m4}}{P_{34}} - \frac{2c_3 L_{34}^2}{m_{34}^2}$$

$$a_4 = \frac{M_{32}}{P_{23}} - \frac{2c_4 L_{23}^2}{m_{23}^2}$$

$$a_6 = \frac{M_{m5}+M_5}{P_{23}} - \frac{2c_6 L_{23}^2}{m_{23}^2}$$

$$b_3 = \frac{H_4}{P_{34}}$$

$$b_4 = \frac{V_{32}}{P_{23}}$$

$$b_6 = \frac{\bar{R}_5}{P_{23}}$$

$$c_3 = \frac{q_{34}L_{34}}{2P_{34}L_{34}}$$

$$c_4 = \frac{q_{23}L_{23}}{2P_{23}L_{23}}$$

$$c_6 = \frac{q_{35}L_{35}}{2P_{23}L_{35}}$$

$$V_{32} = P_{34} - P_3 - \bar{R}_5 + q_{35}L_{35} - \frac{q_{23}L_{23}}{2}$$

Constants of integration

$$C_1 = \frac{1}{\sin m_{34}}\left[a_3(\cos m_{34} - 1) + b_3L_{34} - c_3L_{34}^2\right]$$

$$C_2 = -a_3$$

$$C_5 = \frac{L_{23}}{m_{23}}\left\{a_3\left[-\frac{m_{34}}{L_{34}}\text{ cotan } m_{34}(\cos m_{34} - 1) - \frac{m_{34}}{L_{34}}\sin m_{34}\right]\right.$$

$$\left. + b_3(1 - m_{34}\text{ cotan } m_{34}) - c_3L_{34}(2 + m_{34}\text{ cotan } m_{34}) + b_4\right\}$$

$$C_6 = -a_4 \qquad\qquad C_4 = -a_6$$

$$C_3 = \frac{b_6L_{35} - a_6 - c_6L_{35}^2}{\sin m_{35}} - C_4\text{ cotan } m_{35}$$

From the condition that $y_1 = 0$ for $x_1 = \frac{L_{23}}{2}$

Equation 37a is derived by substituting the various constants of integration.

The following relationships are essential for the parameters a, b and c which appear in some form in Equation 37a.

$$M_{43} = M_{m4}$$

$$M_{34} = H_4 L_{34} - \frac{q_{34} L_{34}^2}{2} - M_{43} = H_4 L_{34} - \frac{q_{34} L_{34}^2}{2} - M_{m4}$$

$$M_{32} = M_{34} + M_{m3} + M_3 + \frac{q_{35} L_{35}^2}{2} - \bar{R}_5 L_{35} + M_{m5} + M_5$$

$$M_{23} = M_{32}$$

$$M_{mi} = \frac{q_{23} L_{23}^2}{8} - \frac{M_{32} + M_{23}}{2}$$

$$M_{m4} = F_4 \frac{\varepsilon_2}{\varepsilon_1}$$

$$M_{m3} = F_3 \; (M_{m4} \varepsilon_3 + \varepsilon_4)$$

$$M_{m5} = F_5 \frac{\varepsilon_5}{\varepsilon_6}$$

The factors ε_1, ε_2, ε_3 and ε_4 are exactly the same as for the case of dual-point loading. However, ε_5 and ε_6 are defined as follows :

$$\varepsilon_6 = 1 + \frac{m_{35}}{P_{23} L_{35} \sin m_{35}} (1 - \cos m_{35})$$

and

$$\varepsilon_5 = \frac{m_{35}}{L_{35} \sin m_{35}} \left[b_6 L_{35} - c_6 L_{35}^2 + \left(\frac{M_5}{P_{23}} - \frac{2 c_6 L_{23}^2}{m_{23}^2} \right) (\cos m_{35} - 1) \right] - b_6$$

<u>Uniformly distributed load and zero axial beam forces</u>

The following values assume a new meaning compared with the preceding case :

$$a_4 = M_{32}$$

$$b_4 = V_{32} = P_{34}-P_3-\overline{R}_5+q_{35}L_{35} = \frac{q_{23}L_{23}}{2}$$

$$c_4 = \frac{q_{23}L_{23}}{2L_{23}}$$

$$c_6 = 0$$

$$C_5 = -C_1 \frac{m_{34}}{L_{34}} \cos m_{34}+C_2 \frac{m_{34}}{L_{34}} \sin m_{34}+b_3-2c_3L_{34}$$

$$M_{m5} = \frac{F_5L_{35}}{EI_{35}} \frac{\overline{R}_5 \frac{L_{35}}{6} - \frac{q_{35}L_{35}^2}{24} -M_5}{1 + \frac{F_5L_{35}}{2EI_{35}}}$$

These expressions are relevant for Equation 37b.

The special case of a two-bay frame, as shown in Figure 68, requires some modifications. These are given for the case of uniformly distributed beam loading.

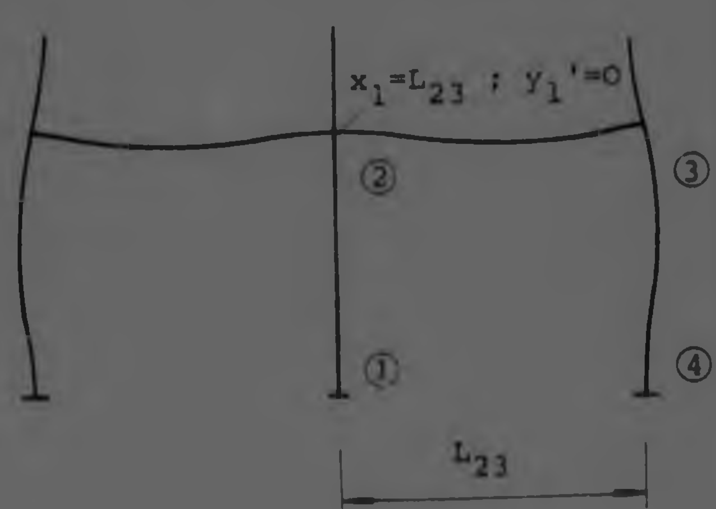

FIGURE 68: Two - bay frame

Equation 37a is modified to

$$C_5 \frac{m_{23}}{L_{23}} \cos m_{23} - C_6 \frac{m_{23}}{L_{23}} \sin m_{23} - b_4 + 2c_4 L_{23} = 0 \qquad |\text{EQN.63a}|$$

and Equation 37b to

$$C_5 + \left(c_4 \frac{L_{23}^3}{3} + a_4 L_{23} - b_4 \frac{L_{23}^2}{2} \right) \frac{1}{EI_{23}} = 0 \qquad |\text{EQN.63b}|$$

The bending moment M_{23}, in this case, is

$$M_{23} = q_{23} \frac{L_{23}^2}{2} - M_{32}$$

LOAD ANALYSIS FOR "SYMMETRY - BUCKLING" - MOMENT DISTRIBUTION FOR JOINTS 4 AND 5

Joint 4

With reference to Figure 43, the following moment needs to be distributed at joint 4 :

$$\text{ad } M_{F4} = \beta_8 M_{F32} + \beta_9 M_{F35}$$

The distribution procedure is based on distribution coefficients μ which incorporate the beam stiffnesses and the stiffness of the column members as obtained from the slope-deflection method.

$$\mu_{43} = \frac{1}{2}\;\frac{SC_{34}L_{34}\frac{1}{6}}{\frac{SC_{34}L_{34}}{6} + \frac{I_{14}}{L_{23}} + \frac{I_{B4}}{L_{35}} + \frac{I_{L4}}{L_{L4}}\,\frac{SC_{L4}}{6K_{34}}\,\beta_2}$$

$$\mu_{34} = \frac{1}{2}\;\frac{SC_{34}L_{34}\frac{1}{6}}{\frac{K_{23}}{2} + K_{35} + \frac{SC_{34}L_{34}}{6} + \overline{F}_3\,\frac{SC_{U3}}{6}\,\beta_3}$$

$$\mu_{32} = \frac{1}{4}\;\frac{K_{23}}{\frac{K_{23}}{2} + K_{35} + \frac{SC_{34}L_{34}}{6} + \overline{F}_3\,\frac{SC_{U3}}{6}\,\beta_3}$$

$$\mu_{53} = \frac{1}{2}\;\frac{K_{35}}{K_{35} + K_{B5} + \overline{F}_{U5}\,\frac{SC_{U5}}{6}\,\beta_3 + \overline{F}_{L5}\,\frac{SC_{L5}}{6}}$$

$$\mu_{35} = \frac{1}{2}\;\frac{K_{35}}{K_{35} + K_{B5} + \frac{SC_{34}L_{34}}{6} + \overline{F}_3\,\frac{SC_{U3}}{6}\,\beta_3}$$

The various terms SC, $\bar{F}_3$, $\bar{F}_{U5}$ and $\bar{F}_{L5}$ have been explained in Appendix II/1. The additional moments can then be found as in Equations 64a - 64d and Equation 38.

$$\text{ad } M_{43} = \text{ad } M_{F4}\mu_{43}\,(2-\mu_{34}) \qquad |\text{EQN. 64a}|$$

$$\text{ad } M_{34} = \text{ad } M_{F4}\mu_{43}\,(1-2\mu_{34}) \qquad |\text{EQN. 64b}|$$

$$\text{ad } M_{35} = \text{ad } M_{F4}\mu_{43}\,(2-\mu_{53}) \qquad |\text{EQN. 64c}|$$

$$\text{ad } M_{53} = \text{ad } M_{F4}\mu_{43}\mu_{35}\,(1-2\mu_{53}) \qquad |\text{EQN. 64d}|$$

<u>Joint 5</u>

The same procedure is adopted for a loading applied to the right of joint 5 as shown in Figure 69 :

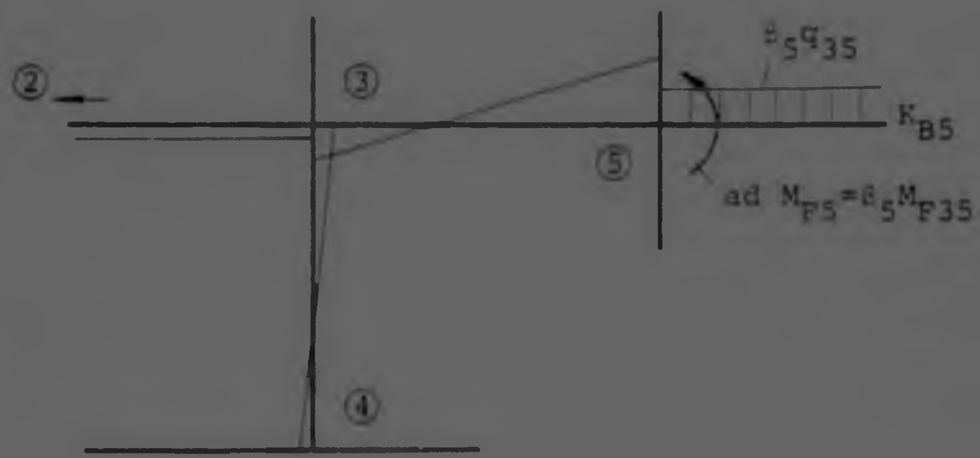

FIGURE 69: Additional loading at joint 5

The first iteration step of the technique developed by Kani[115] results in the moments given in Equations 65a to 65e.

$$\text{ad } M_{53} = \text{ad } M_{F5}\mu_{53}\,(2-\mu_{35}) \qquad |\text{EQN. } 65a|$$

$$\text{ad } M_{35} = \text{ad } M_{F5}\mu_{53}\,(1-2\mu_{35}) \qquad |\text{EQN. } 65b|$$

$$\text{ad } M_{34} = \text{ad } M_{F5}\mu_{53}\,(2-\mu_{43}) \qquad |\text{EQN. } 65c|$$

$$\text{ad } M_{43} = \text{ad } M_{F5}\mu_{53}\mu_{34}\,(1-2\mu_{43}) \qquad |\text{EQN. } 65d|$$

$$\text{ad } M_{32} = 2 \text{ ad } M_{F5}\mu_{53}\mu_{32} \qquad |\text{EQN. } 65e|$$

These moments have to be added to the bending moments obtained from the analysis of the subassemblage excluding loadings to the right of joint 5 and on the beams adjoining node 4 The above values apply to a completely symmetrical structure in regard to geometry and loading.

APPENDIX V

"LIMITING SLENDERNESS RATIO" FOR SUBASSEMBLAGE

Equation 40 is derived from the compression stress of the section by using the following relationships:

$$A = \frac{I}{r^2}$$

$$\lambda = \frac{L}{r}$$

$$P = \frac{m^2EI}{L^2}$$

where P is the axial member force.

The stress f_{max} in Figure 47 becomes:

$$f_{max} = \frac{P}{A} + \frac{My}{I}$$

$$f_{max} = \frac{m^2Er^2}{L^2} + \frac{M}{P}\frac{Em^2y}{L^2}$$

$$f_{max} = E\left(\frac{m^2}{\lambda^2} + \frac{M}{P}\frac{m^2}{L}\frac{y}{r}\frac{1}{\lambda}\right)$$

Dividing by E and multiplying by λ^2 leads to a quadratic equation, the solution of which is given in Equation 40. The dimension y is the distance from the centre of gravity of the section to the extreme fibre.

Referring to Equations 40, 41, 46a and 46b the "limiting slenderness ratio" λ_ℓ is found for the various critical sections indicated in Figure 46a. All values have been expressed in terms of the column member between joints 3 and 4.

The beams are assumed to be of uniform depth, d_B. The suffix (mi) refers to the centre of the relevant beam.

First-yield in beams

Beam 2 - 3 :

$$\lambda_{\ell 34} = \frac{M_{23}}{f_{PB}} \frac{d_B}{d_{34}} \frac{L_{34}}{I_{23}} \frac{d_{34}}{2r_{34}}$$

$$\lambda_{\ell 34} = \frac{M_{32}}{f_{PB}} \frac{d_B}{d_{34}} \frac{L_{34}}{I_{23}} \frac{d_{34}}{2r_{34}}$$

$$\lambda_{\ell 34} = \frac{M_{mi}}{f_{PB}} \frac{d_B}{d_{34}} \frac{L_{34}}{I_{23}} \frac{d_{34}}{2r_{34}}$$

Beam 3 - 5 :

$$\lambda_{\ell 34} = \frac{M_{35}}{f_{PB}} \frac{d_B}{d_{34}} \frac{L_{34}}{I_{35}} \frac{d_{34}}{2r_{34}}$$

$$\lambda_{\ell 34} = \frac{M_{53}}{f_{PB}} \frac{d_B}{d_{34}} \frac{L_{34}}{I_{35}} \frac{d_{34}}{2r_{34}}$$

$$\lambda_{\ell 34} = \frac{M_{mi}}{f_{PB}} \frac{d_B}{d_{34}} \frac{L_{34}}{I_{35}} \frac{d_{34}}{2r_{34}}$$

Beam 2 - 6 :

$$\lambda_{\ell 34} = \frac{M_{26}}{f_{PB}} \frac{d_B}{d_{34}} \frac{L_{34}}{I_{26}} \frac{d_{34}}{2r_{34}}$$

$$\lambda_{\ell 34} = \frac{M_{62}}{f_{PB}} \frac{d_B}{d_{34}} \frac{L_{34}}{I_{26}} \frac{d_{34}}{2r_{34}}$$

$$\lambda_{\ell 34} = \frac{M_{mi}}{f_{PB}} \frac{d_B}{d_{34}} \frac{L_{34}}{I_{26}} \frac{d_{34}}{2r_{34}}$$

<u>First-yield in columns</u>

Column 3 - 4 :

$$\lambda_{\ell 34} = \frac{d_{34}}{2r_{34}} \frac{M_{43}}{I_{34}} \frac{L_{34}}{f_{PC}} \left[\frac{1}{2} + \frac{1}{2}\sqrt{1 + \frac{4 f_{PC} P_{34} I_{31}}{\left(\frac{d_{34}}{2r_{34}} - M_{43}\right)^2}} \right]$$

$$\lambda_{\ell 34} = \frac{d_{34}}{2r_{34}} \frac{M_{34}}{I_{34}} \frac{L_{34}}{f_{PC}} \left[\frac{1}{2} + \frac{1}{2}\sqrt{1 + \frac{4 f_{PC} P_{34} I_{34}}{\left(\frac{d_{34}}{2r_{34}} M_{43}\right)^2}} \right]$$

Column 1 - 2 :

$$\lambda_{\ell 34} = \frac{d_{12}}{2r_{34}} \frac{M_{12}}{I_{12}} \frac{L_{34}}{f_{PC}} \left[\frac{1}{2} + \frac{1}{2}\sqrt{1 + \frac{4 f_{PC} P_{12} I_{12}}{\left(\frac{d_{12}}{2r_{12}} M_{12}\right)^2}} \right]$$

$$\lambda_{\ell 34} = \frac{d_{12}}{2r_{34}} \frac{M_{21}}{I_{12}} \frac{L_{34}}{f_{PC}} \left[\frac{1}{2} + \frac{1}{2}\sqrt{1 + \frac{4 f_{PC} P_{12} I_{12}}{\left(\frac{d_{12}}{2r_{12}} M_{21}\right)^2}} \right]$$

In many cases the term under the square root may be approximated to 1,0.

APPENDIX VI/1

SAMPLE DESIGN GRAPHS

GRAPHS A : ELASTIC BUCKLING LOAD P_O

GRAPH A1

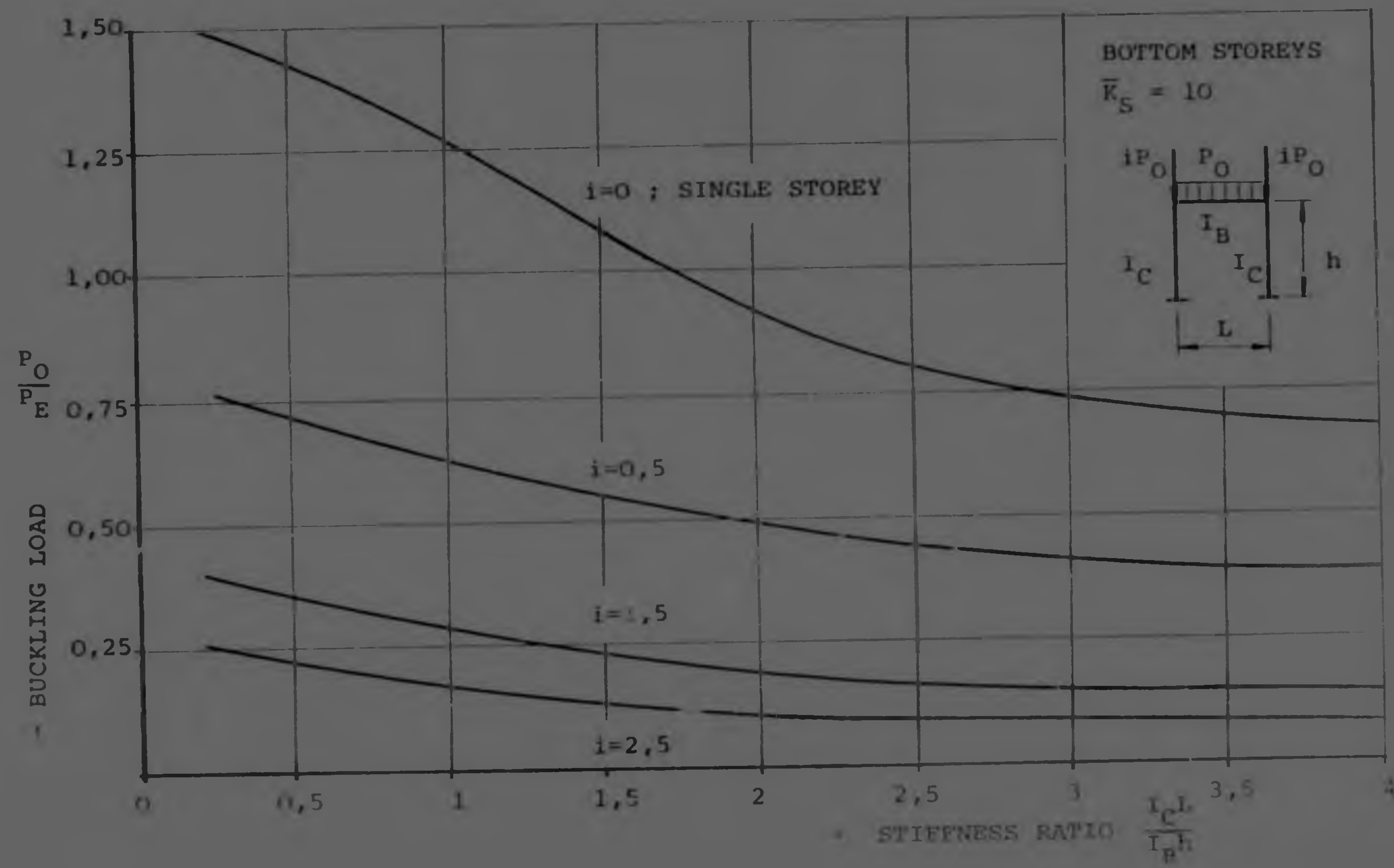
BOTTOM STOREYS
$\overline{K}_S = 10$
iP_O
P_O
iP_O
I_B
I_C
I_C
h
L
i=0 ; SINGLE STOREY
i=0,5
i=1,5
i=2,5
1,50
1,25
1,00
0,75
0,50
0,25
$\frac{P_O}{P_E}$ - BUCKLING LOAD
0
0,5
1
1,5
2
2,5
3
3,5
4
- STIFFNESS RATIO $\frac{I_C L}{I_B h}$

GRAPH A2

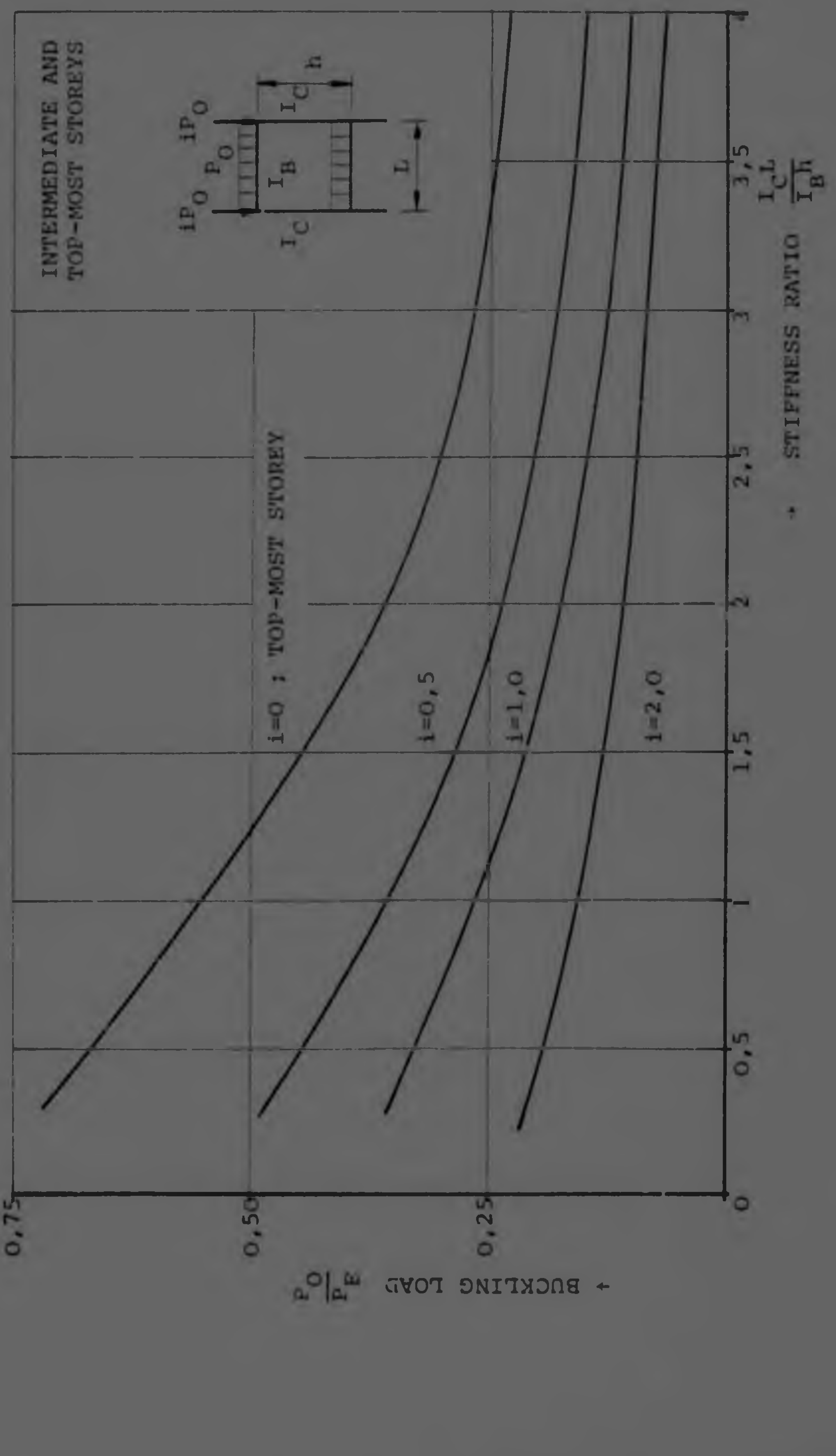
INTERMEDIATE AND TOP-MOST STOREYS
iP_O P_O iP_O
I_C I_B I_C h
L
i=0 ; TOP-MOST STOREY
i=0,5
i=1,0
i=2,0
0 0,5 1 1,5 2 2,5 3 3,5 4
0,75 0,50 0,25
→ STIFFNESS RATIO $\frac{I_C L}{I_B h}$
→ BUCKLING LOAD $\frac{P_O}{P_E}$

APPENDIX VI/2

SAMPLE DESIGN GRAPHS

GRAPHS B : "LIMITING SLENDERNESS RATIO" λ_ℓ AND REDUCTION FACTOR α

For all values from Graphs B first-yield may be assumed to occur in a beam member, except for single-storey portal frames and top-most storeys in multi-storey frames, where first-yield may either occur in a beam or in a column. In this instance, the largest value for λ_ℓ after the application of both adjustment factors, is relevant. The value for α is directly applicable, provided $f_p \approx 240$ MPa.

Adjustment factors for λ_ℓ

First-yield in beam:

$$\frac{240}{f_{PC}} \quad \frac{f_{PC}}{f_{PB}} \quad \frac{I_C}{I_B} \quad \frac{d_B}{d_C} \quad \frac{d_C}{2r_C}$$

First-yield in column:

$$\frac{240}{f_{PC}} \quad \frac{d_C}{2r_C}$$

GRAPH B1

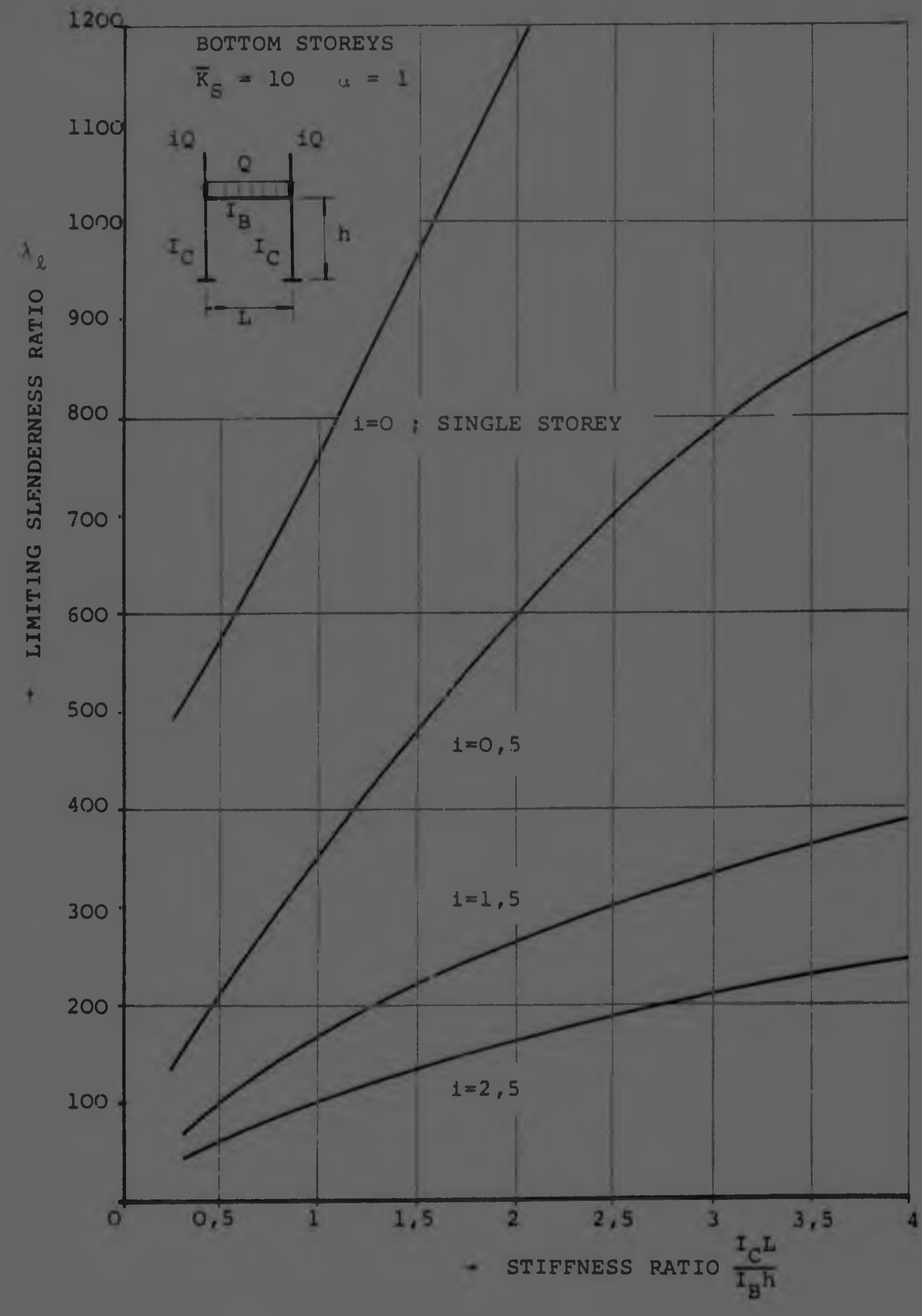
BOTTOM STOREYS
$\bar{K}_S = 10 \quad \alpha = 1$
iQ
iQ
Q
I_B
I_C
I_C
h
L
λ_ℓ
LIMITING SLENDERNESS RATIO
1200
1100
1000
900
800
700
600
500
400
300
200
100
i=0 ; SINGLE STOREY
i=0,5
i=1,5
i=2,5
0
0,5
1
1,5
2
2,5
3
3,5
4
STIFFNESS RATIO $\frac{I_C L}{I_B h}$

GRAPH B2

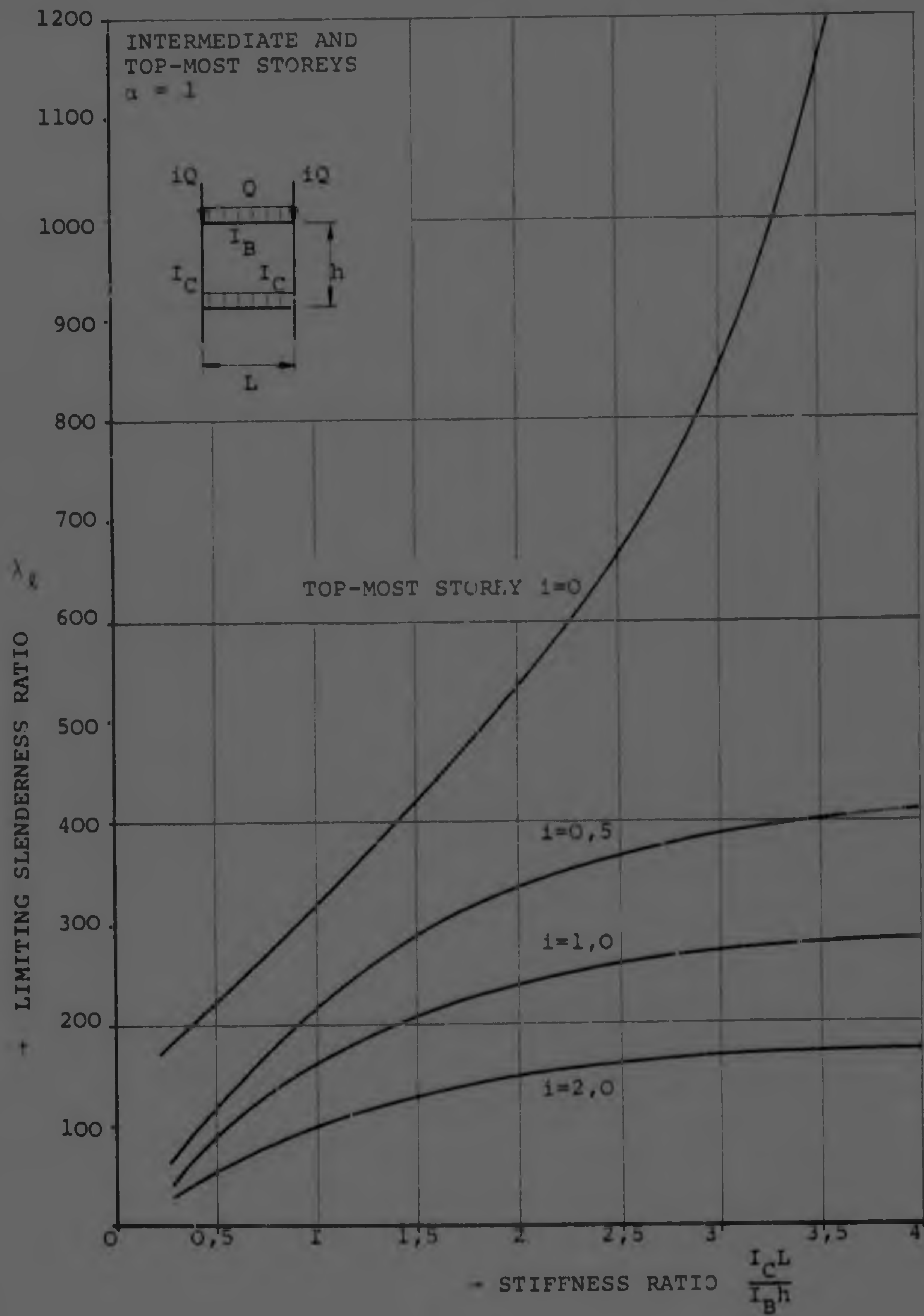
INTERMEDIATE AND
TOP-MOST STOREYS
α = 1
iQ
Q
iQ
I_B
I_C
I_C
h
L
TOP-MOST STOREY i=0
i=0,5
i=1,0
i=2,0
λ_ℓ
LIMITING SLENDERNESS RATIO
1200
1100
1000
900
800
700
600
500
400
300
200
100
0
0,5
1
1,5
2
2,5
3
3,5
4
STIFFNESS RATIO $\frac{I_C L}{I_B h}$

GRAPH B3

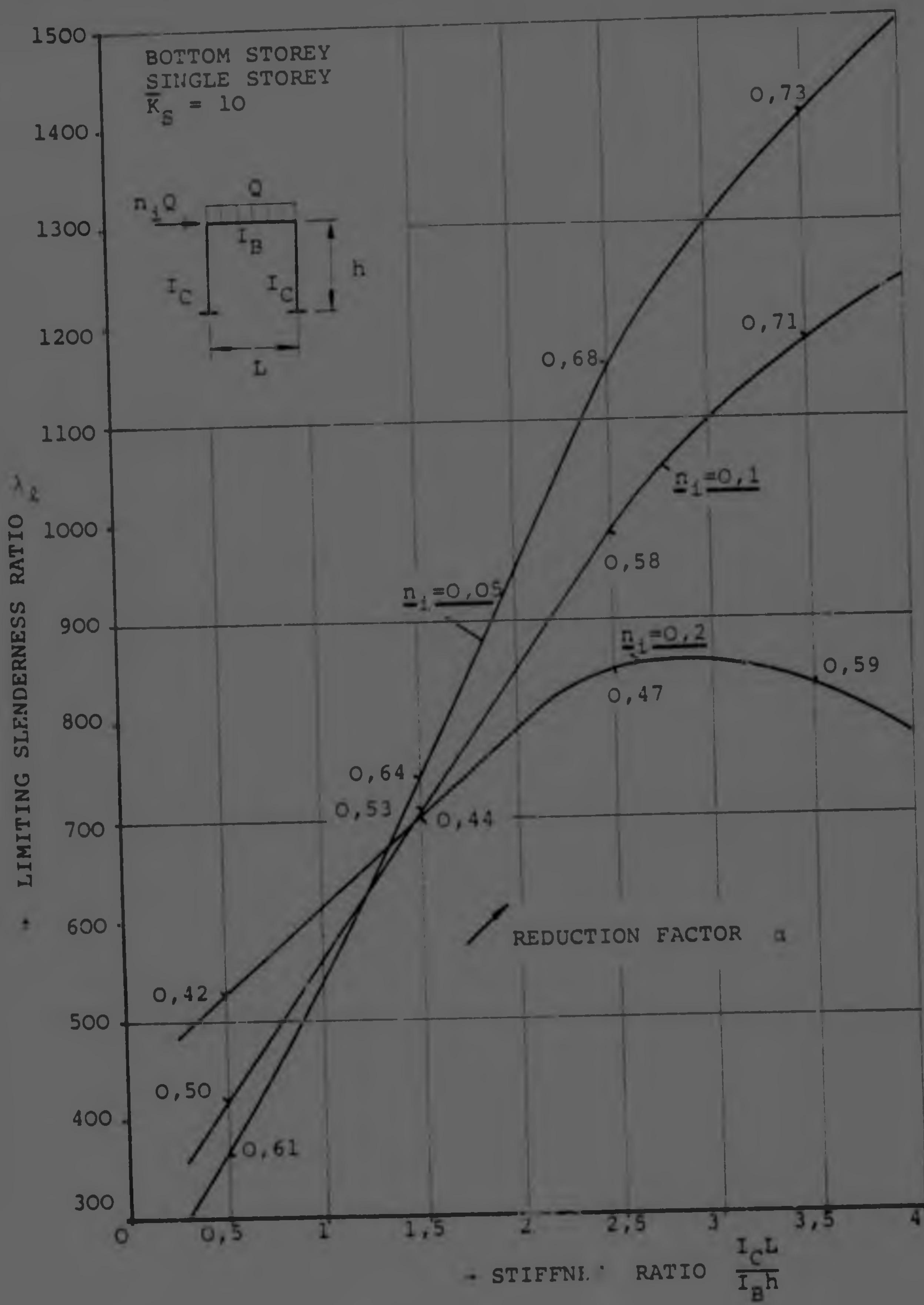
BOTTOM STOREY
SINGLE STOREY
$\overline{K}_S$ = 10
$n_i Q$
Q
I_B
I_C
I_C
h
L
LIMITING SLENDERNESS RATIO λ_ℓ
1500
1400
1300
1200
1100
1000
900
800
700
600
500
400
300
0
0,5
1
1,5
2
2,5
3
3,5
4
STIFFNE RATIO $\frac{I_C L}{I_B h}$
0,73
0,71
0,68
n_i=0,1
0,58
n_i=0,05
n_i=0,2
0,59
0,47
0,64
0,53
0,44
REDUCTION FACTOR α
0,42
0,50
0,61

GRAPH B4

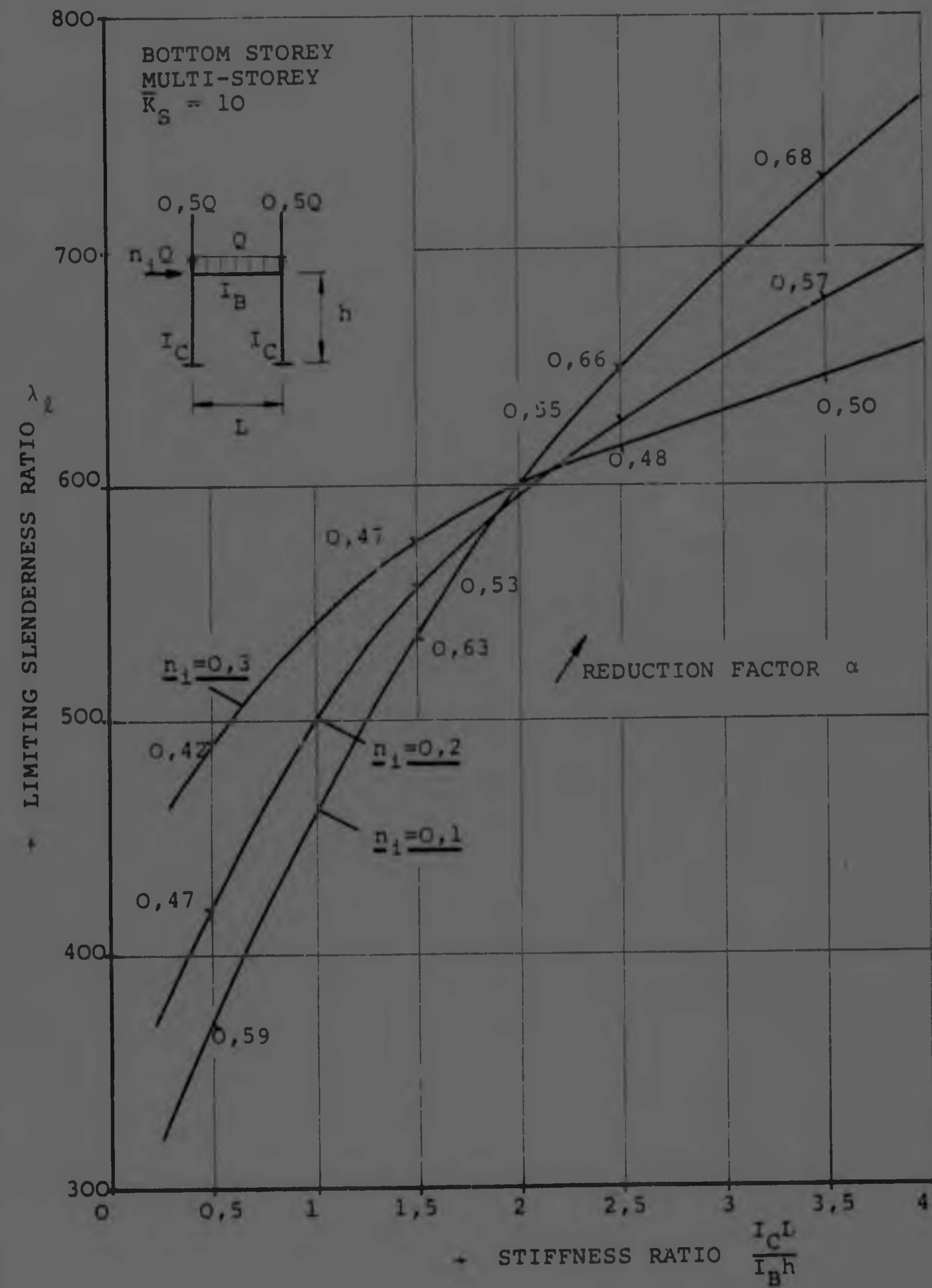
BOTTOM STOREY
MULTI-STOREY
$\bar{K}_S = 10$
0,5Q
0,5Q
Q
n_iQ
I_B
I_C
I_C
h
L
LIMITING SLENDERNESS RATIO λ_ℓ
STIFFNESS RATIO $\frac{I_C L}{I_B h}$
REDUCTION FACTOR α
n_i=0,3
n_i=0,2
n_i=0,1
0,68
0,57
0,66
0,55
0,50
0,48
0,47
0,53
0,63
0,42
0,47
0,59
800
700
600
500
400
300
0
0,5
1
1,5
2
2,5
3
3,5
4

GRAPH B5

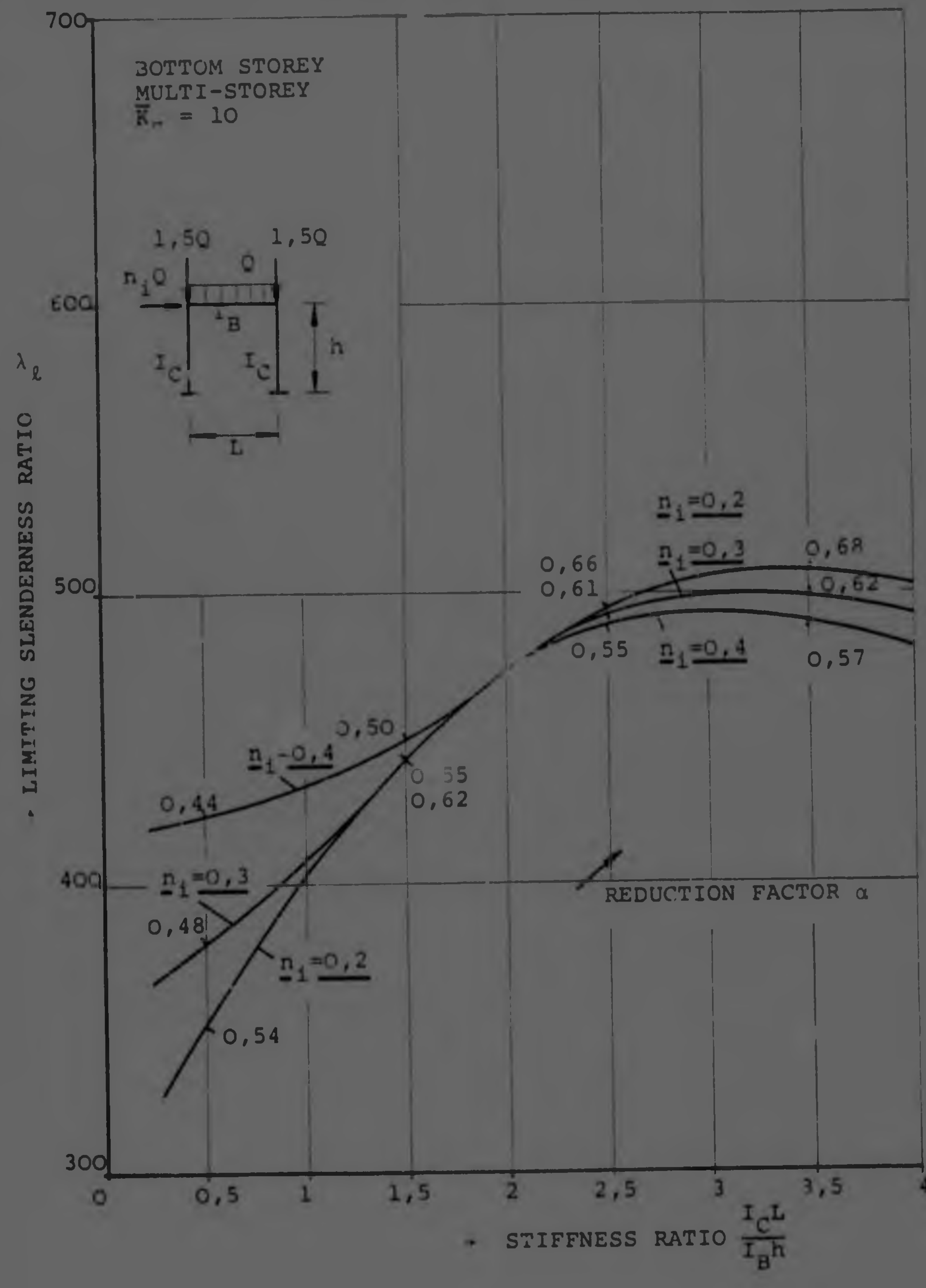
BOTTOM STOREY
MULTI-STOREY
$\overline{K}_c$ = 10
1,5Q
1,5Q
Q
n_iQ
I_B
I_C
I_C
h
L
LIMITING SLENDERNESS RATIO λ_ℓ
700
600
500
400
300
n_i=0,2
n_i=0,3
n_i=0,4
0,66
0,61
0,55
0,68
0,62
0,57
0,50
n_i=0,4
0,55
0,62
0,44
n_i=0,3
0,48
n_i=0,2
0,54
REDUCTION FACTOR α
0
0,5
1
1,5
2
2,5
3
3,5
4
STIFFNESS RATIO $\frac{I_C L}{I_B h}$

GRAPH B6

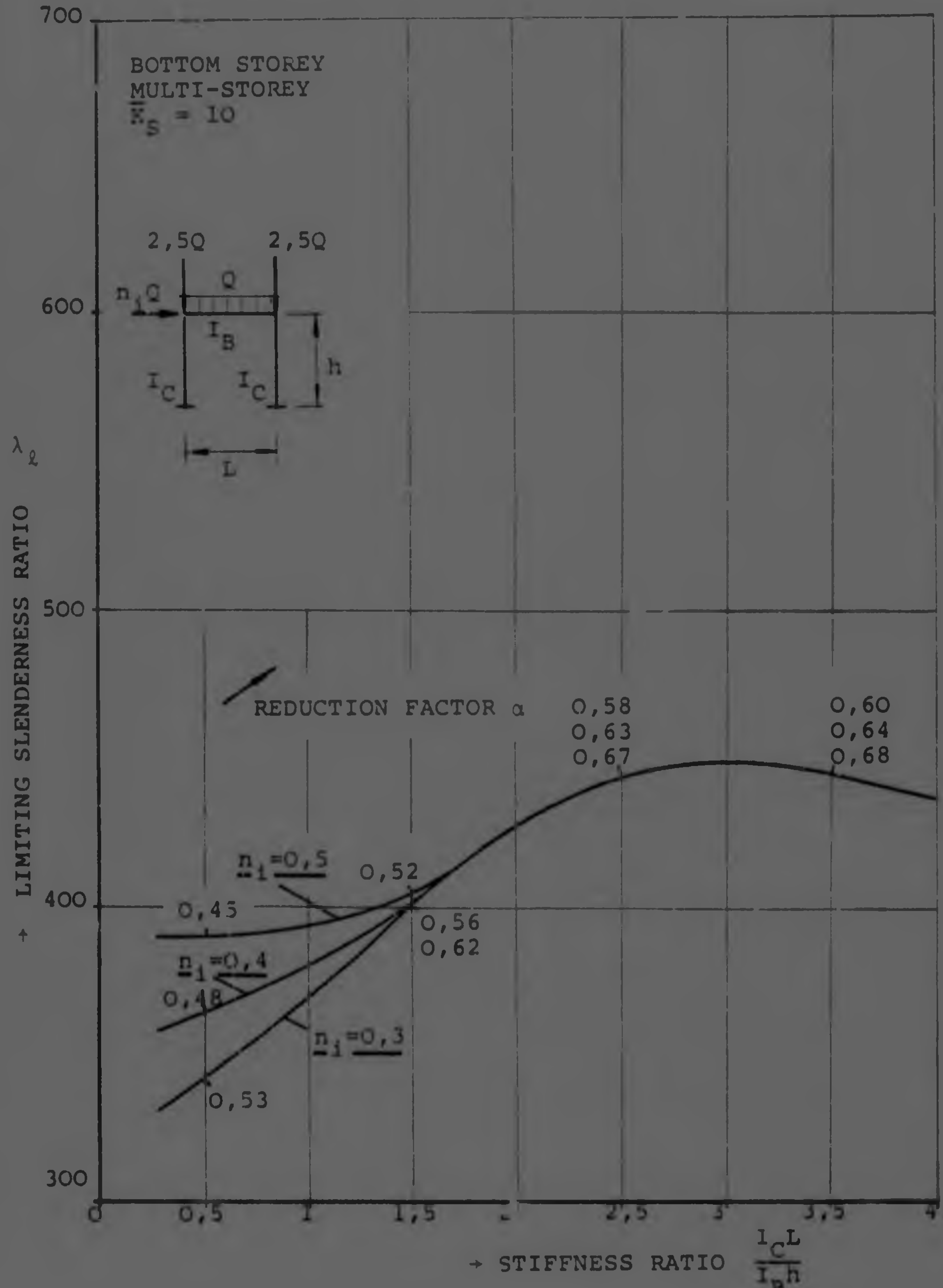
BOTTOM STOREY
MULTI-STOREY
$\bar{K}_S$ = 10
2,5Q
2,5Q
Q
n_iQ
I_B
I_C
I_C
h
L
700
600
500
400
300
λ_ℓ
↑ LIMITING SLENDERNESS RATIO
REDUCTION FACTOR α
0,58
0,63
0,67
0,60
0,64
0,68
n_i=0,5
0,52
0,45
0,56
0,62
n_i=0,4
0,48
n_i=0,3
0,53
0
0,5
1
1,5
2
2,5
3
3,5
4
→ STIFFNESS RATIO $\frac{I_C L}{I_B h}$

GRAPH B7

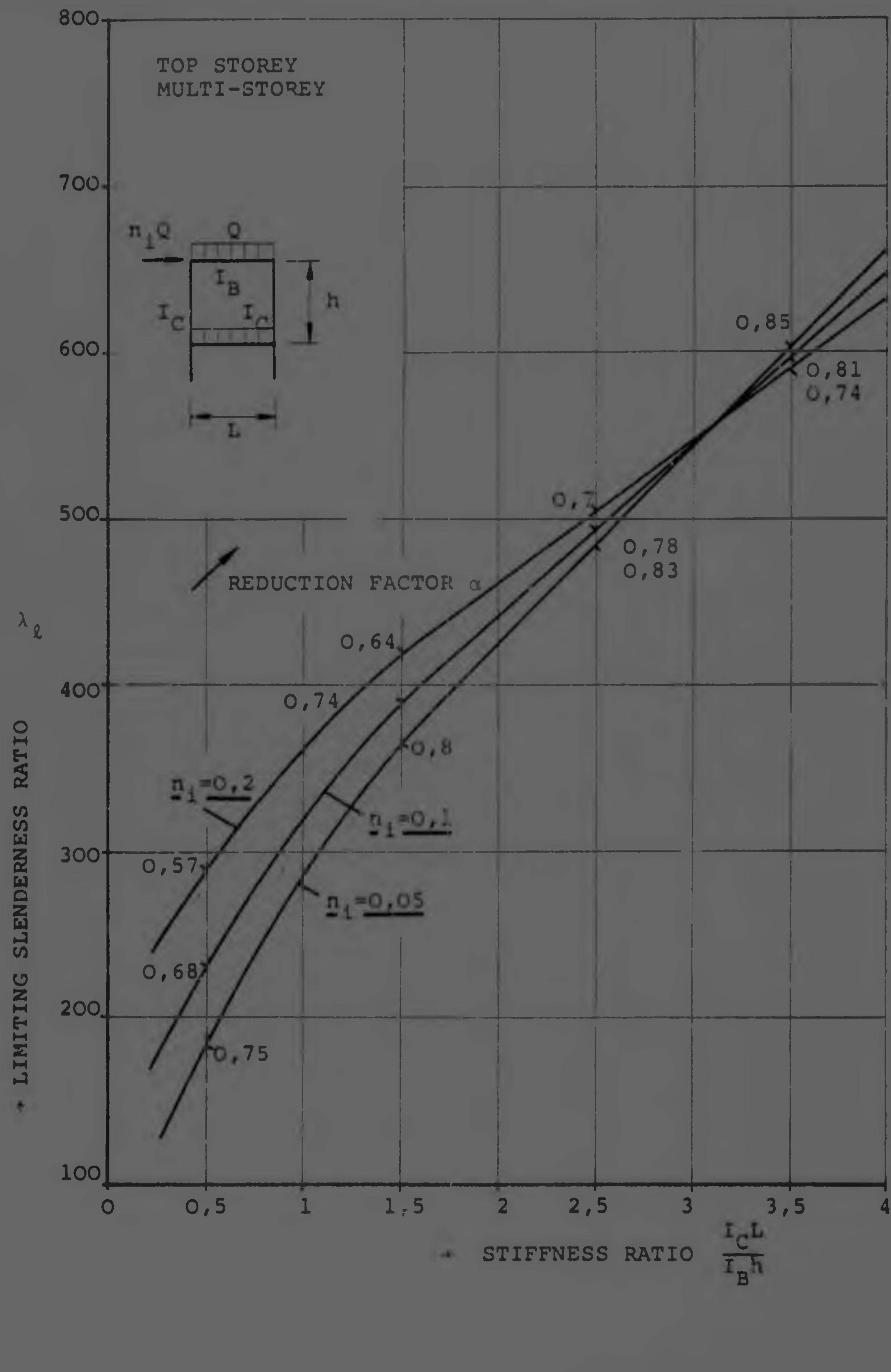

TOP STOREY
MULTI-STOREY
$n_i Q$
Q
I_B
I_C
I_C
h
L
REDUCTION FACTOR α
λ_ℓ
LIMITING SLENDERNESS RATIO
STIFFNESS RATIO $\frac{I_C L}{I_B h}$
n_i=0,2
n_i=0,1
n_i=0,05
0,57
0,68
0,75
0,74
0,64
0,8
0,7
0,78
0,83
0,85
0,81
0,74
800
700
600
500
400
300
200
100
0
0,5
1
1,5
2
2,5
3
3,5
4

GRAPH B8

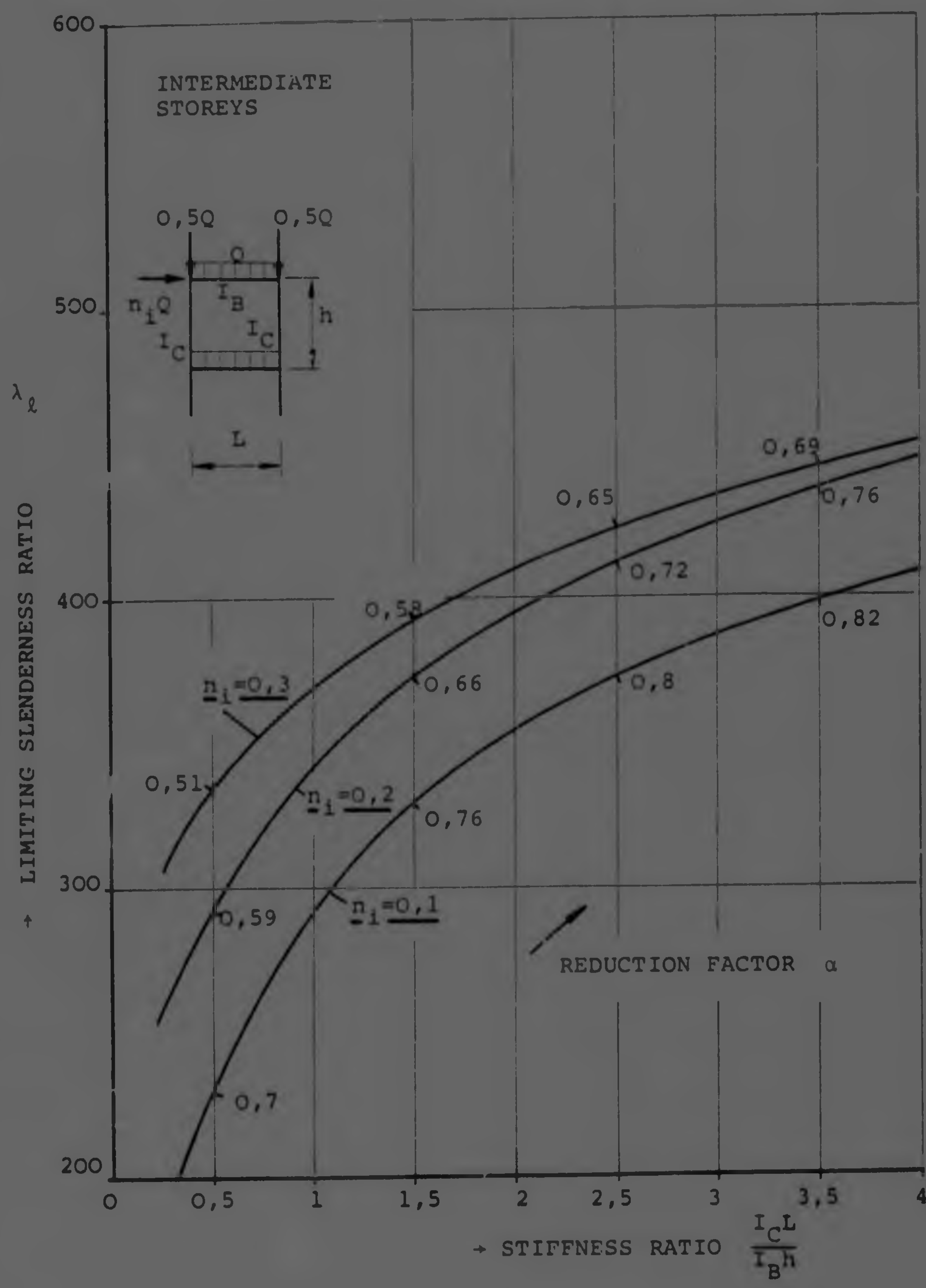

INTERMEDIATE STOREYS
0,5Q
0,5Q
Q
$n_i Q$
I_B
I_C
I_C
h
L
600
500
400
300
200
λ_ℓ
LIMITING SLENDERNESS RATIO
0
0,5
1
1,5
2
2,5
3
3,5
4
STIFFNESS RATIO $\frac{I_C L}{I_B h}$
$n_i = 0,3$
$n_i = 0,2$
$n_i = 0,1$
0,51
0,58
0,65
0,69
0,59
0,66
0,72
0,76
0,7
0,76
0,8
0,82
REDUCTION FACTOR α

GRAPH B9

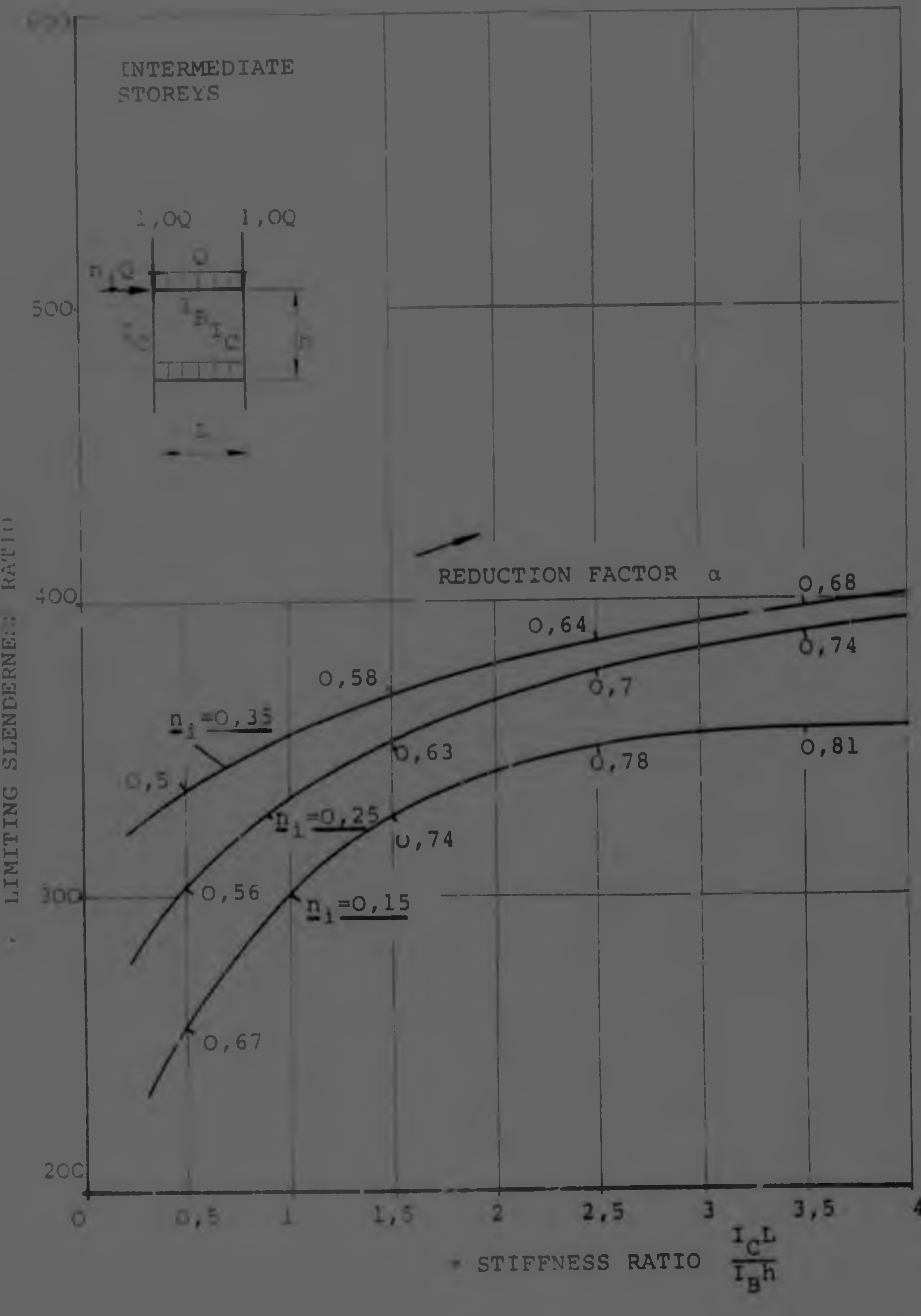
INTERMEDIATE STOREYS
1,0Q
1,0Q
$n_i Q$
Q
I_B
I_C
I_C
h
L
REDUCTION FACTOR α
0,68
0,64
0,74
0,58
0,7
n_i=0,35
0,63
0,81
0,5
0,78
n_i=0,25
0,74
0,56
n_i=0,15
0,67
LIMITING SLENDERNESS RATIO
200
300
400
500
600
0
0,5
1
1,5
2
2,5
3
3,5
4
STIFFNESS RATIO $\frac{I_C L}{I_B h}$

GRAPH B10

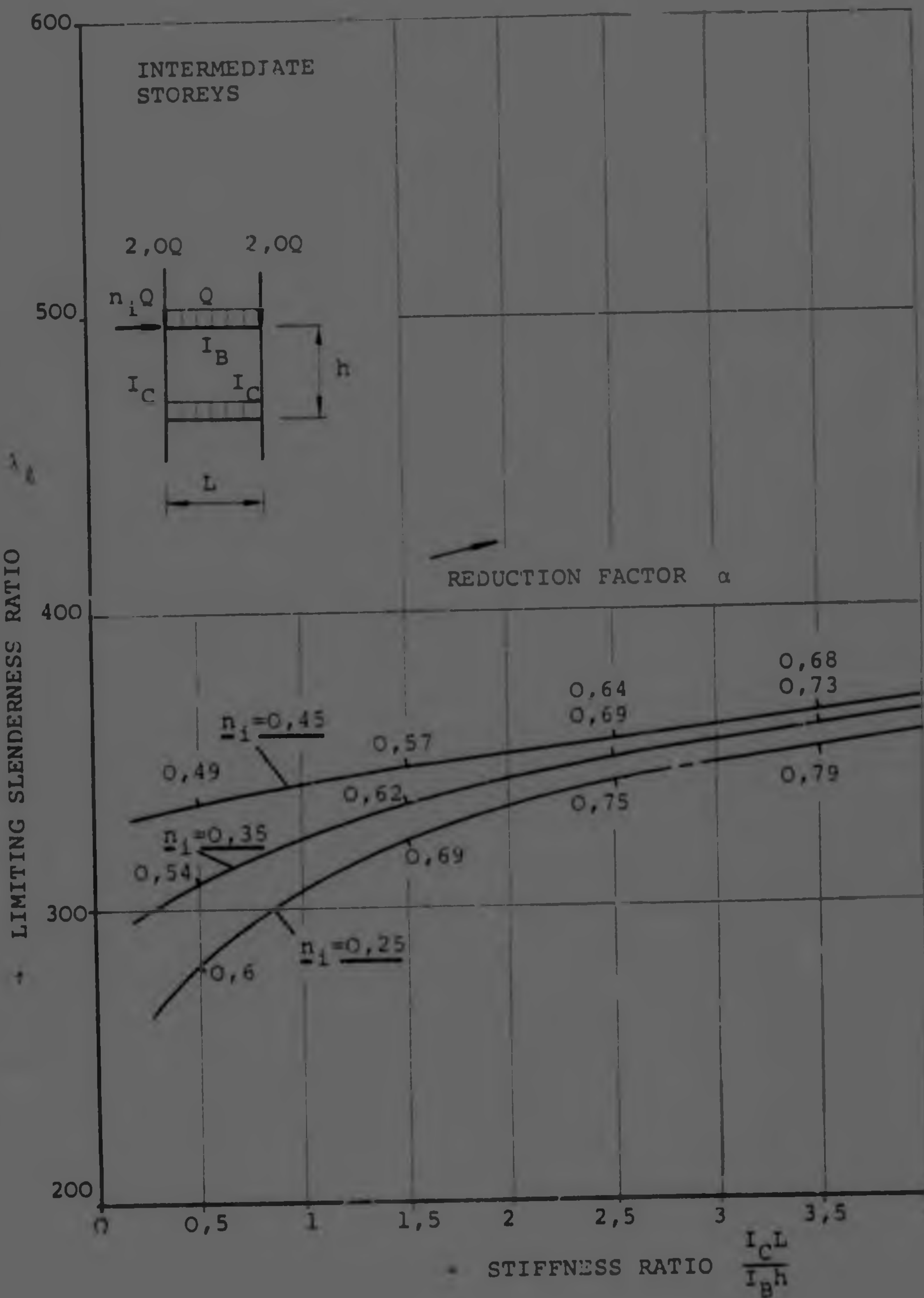
INTERMEDIATE STOREYS
2,0Q
2,0Q
n_iQ
Q
I_B
I_C
I_C
h
L
REDUCTION FACTOR α
n_i=0,45
n_i=0,35
n_i=0,25
0,49
0,57
0,64
0,69
0,68
0,73
0,62
0,75
0,79
0,54
0,69
0,6
LIMITING SLENDERNESS RATIO
600
500
400
300
200
0
0,5
1
1,5
2
2,5
3
3,5
4
STIFFNESS RATIO $\frac{I_C L}{I_B h}$

LIST OF REFERENCES

1. Rankine, W J M — Useful Rules and Tables London, 1866

2. Merchant, W — "The Failure Load of Rigid Jointed Frameworks as influenced by Stability" The Structural Engineer, Vol.32,1954, pp.185-190

3. Wood, R H — "Effective Lengths of Columns in Multi-Storey Buildings", Building Research Establishment (BRE)- Current Paper, CP 85/74, 1974

4. Lu, L W — "Inelastic Buckling of Steel Frames" Journal of the Structural Division American Society of Civil Engineers (ASCE), Vol.91, No ST6, 1965, pp.185-214

5. ECCS — European Recommendations for Steel Constructions, Vol.II, Recommendations, European Convention for Constructional Steelwork (ECCS), 1976

6. ECCS — Manual on the Stability of Steel Structures by the Committee 8 of the European Convention for Constructional Steelwork (ECCS), 1976

7. BSI — Draft Standard Specification for the Structural use of Steelwork in Buildings, British Standards Institution (BSI), London, 1977

8. AISC — Specification for the Design, Fabrication and Erection of Structural Steel in Buildings, American Institute of Steel Construction (AISC), N.York, 1978

9. SAA — Steel Structures Code, AS 1250 Standards Association of Australia (SAA), Sidney, Australia, 1975

10. CSA — Steel Structures for Buildings - Limit State Design, Standard No CSA S16.1,1974, Canadian Standards Association (CSA), Rexdale, Ontario, Canada, 1974

11.	Oxfort, J	"Ueber die Begrenzung der Traglast eines Statisch Unbestimmten Biegesteifen Tragwerks aus Baustahl durch das Instabilwerden des Gleichgewichtes", Stahlbau, Vol.30,1961, p.45
12.	Oxfort, J	"Die Verfahren zur Stabilitaetsberechnung Statisch Unbestimmter Biegesteifer Stahlstabwerke, verglichen an einem Untersuchungsbeispiel", Stahlbau, Vol.32, 1963,p.42
13.	Chu, K H Pabacius, A	"Elastic and Inelastic Buckling of Portal Frames", Journal of the Engin. Mechanics Division, ASCE, Vol.90, No.EM5, 1964, pp.221-249
14.	Moses, F	"Inelastic Frame Buckling", Journal of the Structural Division ASCE, Vol.90, No.ST6, 1964, pp.105-121
15.	Yura, J A Galambos, T V	"The Ultimate Strength of Single-Storey Frames", Fritz Engineering Laboratory Report, No.273.18, Lehigh University, Bethlehem,Pa., 1964.
16.	Adams, P F	"Load Deformation Relationships for Simple Frames", Fritz Engineering Laboratory Report, No.273.21, Lehigh University, Bethlehem,Pa.,1964
17.	Grierson, D E	"Computer-Based Methods for the Plastic Design of Multi-Storey Building Frames", Rapport interne de la Commision 5, CECM, May, 1975
18.	Massonnet, C	"The European Recommendations (ECCS) on the Plastic Design of Steel Frames", Acier-Stahl-Steel, No.4, 1976, pp.146-153
19.	Horne, M R Morris, L J	"Optimum Design of Multi-Storey Rigid Frames", Chapter 14 of the book by Gallagher, R H and Zienkiewicz, O C, Optimum Structural Design, J Wiley & Sons, N.York,1973
20.	Emkin, L Z Litle, W A	"Plastic Design of Multi-Storey Steel Frames by Computer", Journal of the Structural Division, ASCE, Vol.96, No.ST11, 1970, pp.2373-2388

21. Emkin, L Z; Litle, W A — "Storey-wise Plastic Design for Multi-Storey Steel Frames", Journal of the Structural Division, ASCE, Vol.98, No.ST11, 1972, pp.327-345

22. Tranberg, W; Swannell, P; Meek, J L — "Frame Collapse Using Tangent Stiffness", Journal of the Structural Division, ASCE, Vol.102, No.ST3, 1976, pp.659-675

23. Horne, M R — Discussion of "The Stability of Tall Buildings" by Wood, R H, Proceedings, Institution of Civil Engineers (ICE), Vol.12,1959,pp.502-507

24. Horne, M R — "Instability and the Plastic Theory of Structures", Transactions, Engineering Institution of Canada, Vol.4, No.2, 1960, pp.31-43

25. Medland, I C — "Strain-Hardening and the Collapse Load of Steel Frameworks", Ph.D. Thesis, University of Manchester,1963

26. Horne, M R; Medland, I C — "The Collapse Load of Steel Frameworks, allowing for the Effects of Strain-Hardening", Proceedings, ICE, Vol.33, 1966, pp.381-402

27. Davies, M J — "Frame Instability and Strain-Hardening in Plastic Theory", Journal of the Structural Division ASCE, Vol.92, No.ST3, 1966, pp.1-15

28. Parikh, B P — "Elastic-Plastic Analysis and Design of Unbraced Multi-Storey Steel Frames", Fritz Engineering Laboratory Report, No.273.44, Lehigh University, Bethlehem, Pa., 1966

29. Davies, J M — "The Response of Plane Frameworks to Static and Variable Repeated Loading in the Elastic-Plastic Range", The Structural Engineer, Vol.44, 1966, pp.277-283

30. Korn, A; Galambos, T V — "Behaviour of Elastic-Plastic Frames", Journal of the Structural Division, ASCE, Vol.94,No.ST5,1968, pp.1 [illegible] 41

31. McNamee, B M; Lu, L W — "Inelastic Multi-Storey Frame Buckling", Journal of the Structural Division, ASCE, Vol.98, No.ST7, 1972, pp.1613-1631

32. Wood, R H — "The Stability of Tall Buildings", Proceedings, ICE, Vol.11,1958, pp.69-102

33. Driscoll, G C; Armacost, J O; Hansell, W L — "Plastic Design of Multi-Storey Frames by Computer", Journal of the Structural Division, ASCE, Vol.96, No.ST1, 1970, pp.17-33

34. Majid, K I — Non-Linear Structural Matrix Methods of Analysis and Design, Butterworth, London, 1972

35. Jennings, A; Majid, K — "An Elastic-Plastic Analysis by Computer for Framed Structures Loaded up to Collapse", The Structural Engineer, Vol.43,No.12, 1965, pp.[illegible]-412

36. Majid, K I; Anderson, D — "Elastic-Plastic Design of Sway Frames by Computer", Proceedings, ICE, Vol.41, 1968,pp.705-729

37. Cheong-Siat-Moy, F — "Automatic Plastic Analysis and Design of High Rise Steel Structures", Ph.D. Thesis, University of Sydney, 1974

38. Cohn, M Z; Franchi A — "Structural Plasticity Computer System:Strupl", Journal of the Structural Division, ASCE, Vol.105, No.ST4, 1979, pp.789-804

39. Driscoll, G C; et al — "Plastic Design of Multi-Storey Frames - Lecture Notes", Fritz Engineering Laboratory Report, No.273.20, Lehigh University, Bethlehem, Pa., 1965

40. Ojalvo, M; Lu, L W — "Analysis of Frames Loaded into the Plastic Range", Journal of the Engineering Mechanics Division, ASCE, Vol.87-8, No.EM4, 1961, pp.35-47

41. Daniels, J H; Lu, L W — "Plastic Subassemblage Analysis for Unbraced Frames", Journal of the Structural Division, ASCE, Vol.98, No.ST8, 1972, pp.1769-1788

42. Levi, V; Driscoll, G C; Lu, L W — "Analysis of Restrained Columns permitted to Sway", Journal of the Structural Division, ASCE, Vol.93, No.ST1, 1967, pp.87-108

43. Cheong-Siat-Moy, F — "Inelastic Sway Buckling of Multi-Storey Frames", Journal of the Structural Division, ASCE, Vol.102. No.ST1, 1976, pp.65-75

44. Cheong-Siat-Moy, F — "Multi-Storey Frame Design Using Storey Stiffness Concept", Journal of the Structural Division, ASCE, Vol.102, No.ST6, 1976, pp.1197-1212

45. Galambos, T V — Structural Members and Frames, Prentice-Hall Inc., Englewood Cliffs, N.Jersey, 1968

46. Massonnet, C E — "European Approaches to P-Δ Method of Design", Journal of the Structural Division, ASCE, Vol.104, ST1, 1978, pp.193-198

47. Strnad, M; Pirner, M — "Static and Dynamic Full-Scale Tests on a Portal Frame Structure", The Structural Engineer, Vol.56B, No.3, 1978, pp.45-52

48. Bryan, E.R. — The Stressed Skin Design of Buildings Crossby Lockwood Staples, London, 1972

49. Strnad, M — "Interaction of the Sheeting and the Portal Frames in Light Steel Halls", Stavebni informacni stredisko, Praha, 1975

50. Davies, J M — "The Plastic Collapse of Framed Structures Clad with Corrugated Steel Sheeting", Proceedings, ICE, Vol.55, Pt.2, 1973, pp.23-42

51. Bryan, E R — "Wand-, Dach- und Deckenscheiben im Stahlhochbau", Der Bauingenieur, Vol.50, No.9, 1975, p.341

52. Bryan, E R — "Stressed Skin Design and Construction: A State of Art Report", The Structural Engineer, No.9, Vol.54, 1976, pp.347-351

53. Davies, J M — "Calculation of Steel Diaphragm Behaviour", Journal of the Structural Division, ASCE, Vol.102, No.ST7, 1976, pp.1411-1430

54. ECCS — European Recommendations for the Stressed Skin Design of Steel Structures, No.19, ECCS, XVII·77-IE, 1977

55. Wood, R H; Roberts, E H — "A Graphical Method of Predicting Side-Sway in the Design of Multi-Storey Buildings", BRE-Current Paper, CP53/75, 1975

56. Goldberg, J E — "Buckling of One-Storey Frames and Buildings", Transactions, ASCE, Vol.126, Pt.II, 1961, pp.482-515

57. Salem, A H — "Frame Instability in the Plastic Range", Ph.D. Thesis, Manchester University, 1958

58. Low, M W — "Some Model Tests in Multi-Storey Rigid Steel Frames", Proceedings, ICE, Vol.13, 1959, pp.287-298

59. Ligtenberg, F K — "Stability and Plastic Design (1 and 2)", Heron, No.3., Delft, The Netherlands, 1965

60. AISC — Specification for the Design, Fabrication and Erection of Structural Steel for Buildings, AISC, N.York, 1969

61. Wood, B R; Beaulieu, D; Adams, P F — "Column Design by P-Δ Method", Journal of the Structural Division, ASCE, Vol.102, No.ST2, 1976, pp.411-427

62. Wood, B R; Beaulieu, D; Adams, P F — "Further Aspects of Column Design by P-Δ Method", Journal of the Structural Division, ASCE, Vol.102, No.ST3, 1976, pp.487-500

63. Cheong-Siat-Moy, F — "Results of Recent Frame Stability Studies with Reference to AS1250 Code Provisions", Proceedings, 2nd Conference on Steel Development Australian Institute of Steel Construction, Melbourne, Austr., 1977

64. Cheong-Siat-Moy, F — "Control of Deflections in Unbraced Steel Frames", Proceedings, ICE, Part 2, Paper No.7718, 1974, pp.619-634

65. Liapunov, S — "Ultimate Strength of Multi-Storey Steel Rigid Frames", _Journal of the Structural Division_, ASCE, Vol.100, No.ST8, 1974, pp.1643-1655

66. Cheong-Siat-Moy, F — "Strength of Steel Frames under Gravity Loads", _Journal of the Structural Division_, ASCE, Vol.103, No.ST6, 1977, pp.1223-1235

67. Cheong-Siat-Moy, F — "Sway Buckling and Design of Unbraced Steel Frames", _Fritz Engineering Laboratory Report_, No.396.1, Lehigh University, Bethlehem, Pa. 1976

68. Lu, L W et al — "Strength and Drift Characteristics of Steel Frames", _Journal of the Structural Division_, ASCE, Vol.103, No.ST11, 1977, pp.2225-2241

69. MacGregor, J G; Hage, S E — "Stability Analysis and Design of Concrete Frames", _Journal of the Structural Division_, ASCE, Vol.103, No.ST10, 1977, pp.1953-1970

70. Cheong-Siat-Moy, F — "Frame Design without using Effective Column Length", _Journal of the Structural Division_, ASCE, Vol.104, No.ST1, 1978, pp.23-33

71. Daniels, J H et al — "Frame Stability and Design of Columns in Unbraced Multi-Storey Steel Frames", _Fritz Engineering Laboratory Report_, No.375.2, Lehigh University, Bethlehem, Pa., 1975

72. Ramirez, D R — "The Effect of Beam Yielding on the Stability of Columns - An Experimental Study", Ph.D.Thesis, University of Texas, Austin, Texas, 1975

73. Kuhn, G R — "An Appraisal of the Effective Length Alignment Charts", M.Sc.Thesis, Arizona State University, Tempe, Arizona, 1976

74. Kuhn, G R; Lundgren, H — "An Appraisal of the Effective Length Alignment Charts", _Proceedings_, Colloquium on Stability of Structures under Static and Dynamic Loads, SSRC Meeting, Washington, ASCE, 1977, pp.212-242

75. Johnston, B G (Ed) — Guide to Stability Design Criteria for Metal Structures, 3rd Ed., J Wiley & Sons, Inc., N.York,1976

76. Johnston, B G — "Third SSRC Guide with Column Design Applications", Journal of the Structural Division, ASCE, Vol.103, No.ST7, 1977, pp.1359-1375

77. Lind, N C — "Simple Illustrations of Frame Instability", Journal of the Structural Division, ASCE, Vol.103, No.ST1, 1977, pp.1-8

78. Grier, W G — Essays on the Effective Length of Frame of Columns, Jackson Publications, Kingston, Ontario, Canada, 1966

79. Cheong-Siat-Moy,F — "Consideration of Secondary Effects in Frame Design", Journal of the Structural Division, ASCE, Vol.103, No.ST10, 1977, pp.2005-2010

80. Cheong-Siat-Moy,F — "Stiffness Design of Unbraced Steel Frames", Engineering Journal, AISC, Vol.13, No.1, 1976, pp.8-10

81. van der Woude, F; Johnston, B G; Zweig, A — Discussion on "Frame Design without using Effective Column Length" Journal of the Structural Division, ASCE, Vol.104, No.ST11, 1978, pp.1809-1814

82. Yura, J A — "The Effective Length of Columns in Unbraced Frames", Engineering Journal, AISC, Vol.8, No.2, 1971, pp.37-42

83. Disque, R O — "Inelastic K-Factor for Column Design", Engineering Journal, AISC, Vol.10, No.2, 1972, pp.33-35

84. Iffland, J S B — "High Rise Building Column Design", Journal of the Structural Division, ASCE, Vol.104, No.ST9, 1978, pp.1469-1482

85. Rosenblueth, E — "Slenderness Effects in Buildings", Journal of the Structural Division, ASCE, Vol.91, ST1, 1967, pp.229-252

86. Goldberg, J E — "Approximate Methods for Stability and Frequency Analysis of Tall Buildings", Proceedings, Conferencia Regional Sobre Edificios de Altura, Spain, Sept.17-19,1973, pp.123-146

87. Stevens, L K — "Elastic Stability of Practical Multi-Storey Frames", Proceedings, ICE, Vol.36, 1967. pp.99-117

88. Anderson, D — "Simple Calculation of Elastic Critical Loads for Unbraced, Multi-Storey Steel Frames", The Structural Engineer, Vol.58A, No.8, 1980, pp.243-245

89. Young, B W — "Proposals for Steel Column Design in the new Bridge Code", Cambridge University Report, Department of Engineering, July, 1970

90. Allen, D — "The Merchant-Rankine Approach to Member Stability", Journal of the Structural Division, ASCE, Vol.104, No.ST12, 1978, pp.1909-1914

91. Bjorhovde, R; Galambos, T V; Ravindra, M K — "LRFD Criteria for Steel Beam - Columns", Journal of the Structural Division, ASCE, Vol.104, No.ST9, 1978, pp.1371-1386

92. Wood, R H — "A New Approach to Column Design" BRE-Report (28) YH2 (A3f),1973

93. Yu, C K; Tall, L — "A 515 Steel Beam - Columns", IABSE Publication (31-II), 1971

94. Bjorhovde, R; Tall, L — "Development of Multiple Column Curves", Proceedings, CRC/ECCS/JCRC/IABSE Joint Colloquium on Column Strength, CTICM, Paris, Nov.1972

95. Bjorhovde, R; Tall, L — "Maximum Column Strength and the Multiple Column Curve Concept", Fritz Engineering Laboratory Report, No.337.29, Lehigh University, Bethlehem, Pa., Oct.1971

96. Bjorhovde, R — "Deterministic and Probabilistic Approaches to the Strength of Steel Columns", Ph.D. Thesis, Lehigh University, Bethlehem,Pa., 1972

97.	Scholz, H	"Symmetrical and Antisymmetrical Buckling of Unbraced Frames", The Civil Engineer in South Africa, Vol.21, No.1, Johannesburg, 1979, pp.3-9
98.	Gaylord, E Gaylord, C	Design of Steel Structures, 2nd Ed., McGraw-Hill, N.York, 1972
99.	ASCE Subcommittee No.31	"Wind Bracing in Steel Buildings" Transactions, ASCE, Vol.105,1940, pp.1713-1738
100.	Lothar, J	Advanced Design in Structural Steel, Prentice-Hall, Englewood Cliffs, N.Jersey, 1960
101.	Norris, C H Wilbur, J B	Elementary Structure Analysis, McGraw-Hill, N.York, 1960
102.	Sutherland, H Bowman, H L	Structural Theory, J Wiley & Sons, N.York, 1950
103.	Hauf, H D Pfisterer, H A	Design of Steel Buildings, J Wiley & Sons, N.York, 1949
104.	Chwalla, E	"Die Stabilitaet Lotrecht Belasteter Rechteckrahmen", Bauingenieur, Vol.19, 1938, pp.69-72
105.	Masur, E F Chang, I C Donnell, L H	"Stability of Frames in the Presence of Primary Bending Moments" Journal of the Engineering Mechanics Division, ASCE, Vol.87, No.EM4, 1961, pp.19-34
106.	Lu, L W	"Stability of Frames under Primary Bending Moments", Journal of the Structural Division, ASCE, Vol.89, No.ST3, 1965, pp.35-62
107.	Avram, C N	"The Problem of Partial Restraint in Elastic Soil", Buletinul, Comunicarilov Stiintifice si Tehnice, Vol.1, Romania, 1956
108.	Tsytovitch, N A	Mehanika Gruntov, Stroyisdat, Moscow, 1951
109.	Hirschfeld, K	Baustatik, 2nd Ed., Springer, Berlin, 1965

110. Zahmel, D — "Naeherungsweise Berechnung der Knicklaengen von Stockwerkrahmen" Stahlbau, Vol.24, No.4,1955, p.89

111. Schinzle, M — "Verkantung des Starren Rechteckfundamentes unter Momentenbeanspruchung", Bautechnik, Vol.42, 1965, pp.58-64

112. Galambos, T V — "Influence of Partial Base Fixity on Frame Stability", Transactions, ASCE, Vol.126, Pt.2, 1961, p.929

113. CCA — Handbook on the Unified Code for Structural Concrete (CP 110:1972), CCA, London, 1972, p.24

114. Masur E F — "Post-Buckling Strength of Redundant Trusses", Transactions, ASCE, Vol.119, 1954, p.699

115. Kani, G — Die Berechnung Mehrstoeckiger Rahmen, 11th Ed., Verlag Konrad Wittwer, Stuttgart, 1965

116. Horne, M R — "Elastic-Plastic Failure Loads of Plane Frames", Proceedings, Royal Society of Engineers,London, Series A, Vol.274, 1963, p.343

117. Fey, F — "Approximate Second-Order Analysis of Reinforced Concrete Frames" (in German), Bauingenieur, Berlin, Germany, June, 1966

118. MacGregor J G — "Theme II - Simple Design Procedures for Concrete Columns", Introductory Report, 1974 Quebec Symposium on Design and Safety of Reinforced Concrete Compression Members, IABSE, Zuerich

119. Parme A L — "Capacity of Restrained Eccentrically Loaded Long Columns", Special Publication SP13, Symposium on Reinforced Concrete Columns, ACI, Detroit, Michigan, 1966, pp.355-360

120. Korn, A — "The Elastic-Plastic Behaviour of Multi-Storey, Unbraced Planar Frames", D.Sc.Thesis, Washington University, St.Louis, Mo., 1967

121. Ketter, R L; Kaminsky, E L; Beedle, L S — "Plastic Deformations of Wide-Flange Beam - Columns", Transactions, ASCE, Vol.120, 1955, pp.1028-1061